



UNIVERSITY OF TRENTO
Department of
Cellular, Computational and Integrative Biology (CIBIO)

International PhD Program in Biomolecular Sciences

XXXI Cycle

**Precursor miRNAs are locally processed
to regulate growth cone steering**

Tutor

Prof. Dr. Marie-Laure Baudet
CIBIO - University of Trento

PhD thesis of

Eloina Corradi
CIBIO - University of Trento

ACADEMIC YEAR 2017/2018

International PhD Program in Biomolecular Sciences

Department of Cellular, Computational and Integrative Biology (CIBIO),
University of Trento

Declaration of authorship

I, Eloina Corradi, confirm that this is my own work and the use of all material from other sources have been properly and fully acknowledged.

Corradi Eloina

A chi mi dá l'energia e la forza per esplorare sempre nuovi territori

*“The brain is a world consisting of a number of unexplored continents
and great stretches of unknown territory.”*

Santiago Ramon y Cajal

Preface

This thesis has been developed during the three-year Doctoral program of the International PhD Program in Biomolecular Sciences, Department of Cellular, Computational and Integrative Biology (CIBIO) of the University of Trento.

Most of the work has been carried out at CIBIO (Trento) in the Giovanni Armenise-Harvard laboratory of axonal neurobiology, Advance Imaging and Model Organism facilities, under the supervision of Prof. Marie-Laure Baudet. Furthermore, I spent four months (January 2018 - May 2018) at the Department of Physiology, Development and Neuroscience of the Cambridge University (UK) for a collaboration with Prof. Christine Holt, supported by an Erasmus+ Travel grant.

The presented research has been financed by Marie Curie Career Integration (618969 GUIDANCE-miR), G. Armenise-Harvard Foundation Career, and MIUR SIR (RBSI144NZ 4) grants (to Marie-Laure Baudet).

Some *ex vivo* and the *in vivo* FRAP were acquired with a spinning disc confocal microscope (HH lab, Cambridge University, UK), IHC on P0 mice sections at the confocal microscope at the Institute for biomedicine (EURAC, Bolzano, Italy), polysome profiling experiments were run in collaboration with Dr. Gabriella Viero (FBK, Trento, Italy).

Most of data present in this manuscript are preprinted in BioRxiv (470393; doi: 10.1101/470393), where I am the first author, with the title “Precursor miRNAs are trafficked along axons associated with vesicles and locally processed to regulate growth cone steering” (Corradi et al., 2018). Part of the text of the BioRxiv preprinted has been reported in this thesis. Some data in the thesis are not published yet, and part of them published in Cell Reports two years ago (Bellon et al., 2017). My specific contributions to the 2017 publication are outlined in Appendix A.

Trento, January 2019

Eloina Corradi

Acknowledgments

I would like to thank Prof. Marie-Laure Baudet for giving me the opportunity to work on such an amazing project, for the stimulating scientific discussions, for helping me growing as a scientist. In the past four years, she has guided me through my PhD encouraging me to explore new ideas, to solve problems with different strategies, to progressively become independent.

Many thanks to all the lab members, who during these years have been supporting me with discussions and troubleshooting, teaching me techniques, keeping a warm and nice working environment and collaborating in the current thesis project. In particular, I would like to thank Archana Iyer, for teaching me the LCM and organoculture, and for IHC on Dicer; Irene dalla Costa, Michela Rocuzzo and Antoneta Gavoci for the work on molecular beacon and pre-miRNA trafficking; Stephanie Strohbuecker for the prediction analysis on miR-181-5p target and for proof reading of the thesis; Simone Bridi for the collapse assay and teaching me electroporation. I will never forget those happy moments we shared good news together, those hard times in which closeness and support were not lacking.

Many gratitude also to Prof. Christine Holt for hosting me in her lab in Cambridge for four months, making me breath the extremely stimulating international environment, giving me the opportunity to discuss and present my work. I consider her a model for all women in science. I would also acknowledge her lab members, and in particular to Julie Qiaojin Lin and Hovy Wong, for teaching me the FRAP technique, the brain exposure preparation and for all the time spent together. I am glad to have been part of the team for a while.

Thanks to the collaborators on all projects I have participated in. It has been a pleasure working with all of them. Thanks to Gabriella Viero and Marta Marchioretto for the polysome profiling experiments (FBK, TN), to Alexandros Lavdas and Andrew A. Hicks for the access at the confocal microscope at the Institute for Biomedicine (EURAC, BZ), to Natalia Koralewska and Ania Kurzynska for the ongoing research on inhibitors of pre-miRNAs (Institute of Bioorganic Chemistry, Poznan, Poland) and to the external supervisors Prof. Robert Hindges and Prof. Antonella Riccio, who spent part of their time to read and review this thesis.

Last but not least my special gratitude goes to my husband Walter and our incoming little boy. For supporting and giving me the energy to carry on this project and to look at the future with hope and motivation.

Contents

Abbreviations	ix
Abstract	xi
1 Introduction	1
1.1 Brain wiring and axon guidance	2
1.2 The growth cone	2
1.2.1 Growth cone function and structure	2
1.2.2 Cytoskeletal dynamics: growth cone engine	4
1.2.3 Microtubules isoforms	6
1.2.4 Growth cone collapse	8
1.2.5 Guidance cues	8
1.3 Signal transduction	12
1.3.1 Semaphorin 3A signal transduction	13
1.3.2 Complexity of the response	15
1.4 Local translation	16
1.4.1 Local translation functions	18
1.4.2 Local translation regulation	18
1.5 MicroRNAs	21
1.5.1 miRNA biogenesis	21
1.5.2 miRNA structure and mechanism of action	22
1.5.3 Mechanisms of regulation of mature miRNAs	24
1.6 miRNAs in brain wiring	24
1.6.1 miRNAs in axon guidance	25
1.6.2 Compartmentalized activation of miRNAs	26
1.7 Retinal Ganglion Cells as a cellular model	28
1.7.1 From the retina to the brain: the RGCs' journey	28
1.7.2 Retinotectal pathway	30
1.7.3 Guidance cues along <i>Xenopus laevis</i> retinotectal pathway	31
1.8 <i>Xenopus laevis</i> as model organism	32
2 Project aims	35
3 Material and methods	37
3.1 (FLAG-HA ₂)-Dicer mice	37
3.1.1 Mice genotyping	38
3.1.2 Immunohistochemistry on mice sections (IHC)	40
3.2 <i>Xenopus laevis</i>	41
3.2.1 Microinjection	42
3.2.2 Electroporation	42

3.2.3	RGC culture	43
3.2.4	RGC axonal sample collection	44
3.2.5	Axonal transfection	45
3.2.6	Axonal stimulation	45
3.2.7	Collapse assay	46
3.2.8	Fluorescence Recovery After Photo-bleaching (FRAP)	46
3.2.9	Live imaging: pre-miR trafficking	47
3.3	Molecular Biology: from RNA extraction to RT-(q)PCR	47
3.3.1	RNA extraction	47
3.3.2	Quantity, quality and purity of the RNA axonal samples	48
3.3.3	RNA retrotranscription	48
3.3.4	PCR and gel visualization	49
3.3.5	RT-qPCR	50
3.4	Plasmids	50
3.4.1	Wild type 3'UTR and mutated fragments amplification	50
3.4.2	Joining the mutated fragments and amplicon purification	51
3.4.3	Plasmid digestion and ligation	51
3.4.4	Transformation and colonies screening	52
3.4.5	Q5 site-direct mutagenesis kit (NEB)	52
3.4.6	Plasmid sequencing and mutagenesis assessment	52
3.5	Data analysis and statistics	53
3.5.1	RT-qPCR	53
3.5.2	FRAP analysis	54
3.5.3	Live imaging analysis: pre-miR trafficking	54
3.5.4	MSD analysis	55
3.6	Bioinformatics prediction, data analysis and tools	56
3.6.1	Software and Algorithms	56
3.6.2	Pre-miRNA candidate selection and validation	56
3.6.3	miR-181 target prediction and candidate selection	57
4	Dicer and pre-miRNAs in axons	59
4.1	Dicer presence in mice RGC axons	59
4.1.1	Dicer detection in P0 mice RGC axons at the superior colliculus	61
4.2	Pre-miRNA detection in <i>Xenopus laevis</i> RGC axons	64
4.3	miR-181 family: focus on pre-miR-181a-1 and pre-miR-181a-2	67
4.3.1	Pre-miR-181a-1 is more abundant in axons than pre-miR-181a-2	68
4.4	Conclusions	69
5	Pre-miR-181a-1 is actively transported on vesicles along axons	71
5.1	Molecular beacon (MB): tool for live imaging of endogenous molecules	72
5.2	Pre-miR-181a-1 trafficked along axons	74
5.3	Endogenous pre-miR-181a-1 is actively transported toward the growth cones	76
5.4	Endogenous pre-miR-181a-1 is transported on vesicles	78
5.5	Conclusions	81

6	Pre-miR-181a-1/a-2 local maturation in <i>Xenopus laevis</i> RGC axons upon Sema3A stimulation	83
6.1	Isolated axons preparation	83
6.2	qPCR: assessment of pre-miRNA processing	84
6.2.1	U6 as normalizer in axonal samples	87
6.3	Pre-miR-181a-1/a-2 maturation in RGC axons upon cue exposure	89
6.3.1	Sema3A stimulation	90
6.3.2	Slit2 stimulation	92
6.4	Conclusions	92
7	Newly generated miRNAs are important for growth cone steering <i>ex vivo</i>	93
7.1	MO design and validation	94
7.2	Axonal block of NGmiRNAs	95
7.2.1	Growth cone responsiveness to Sema3A is impaired when blocking NGmiRNAs	98
7.3	Conclusions	98
8	NGmiRNAs silence locally translated transcripts	99
8.1	Investigation of local axonal translation: polysome profiling	99
8.2	Investigation of local axonal translation: a candidate-driven approach	102
8.2.1	miR-181-5p candidate selection	102
8.3	Fluorescence recovery after photobleaching (FRAP) with Venus construct	104
8.3.1	Venus plasmids cloning	105
8.3.2	FRAP control: β -Actin	109
8.3.3	TUBB3 is locally translated in axons and inhibited by Sema3A ex- posure	110
8.3.4	Sema3A inhibition of TUBB3 axonal translation is mediated by NG- miRNAs	110
8.3.5	TUBB3 local translation regulation by NGmiRNAs <i>in vivo</i>	113
8.3.6	APP is locally translated in axons and inhibited by Sema3A exposure	114
8.3.7	THBS1 is not translated in axons	115
8.4	Conclusions	117
9	General discussion	119
9.1	Different pre-miRNAs and miRNAs distribution in subcellular compartments	119
9.2	Subcompartmentalization of miRNA biogenesis	121
9.2.1	Pre-miRNAs versus miRNAs	121
9.3	Delocalization of miRNA biogenesis by pre-miRNAs trafficking	123
9.3.1	miRNAs are transported actively to the growth cone	123
9.3.2	miRNAs are transported to the growth cone on vesicles	123
9.4	Basal translation	124
9.4.1	Basal local protein translation of TUBB3 is silenced by Sema3A- induced NGmiRNAs	125
9.5	Impact of the study	126

10 Summary and future perspectives	127
10.1 Future perspectives	128
A miR-182 regulates Slit2-mediated axon guidance by modulating Cofilin-1 LPS	131
A.1 My contributions in the paper	132
A.2 Conclusions	138
B Primers, oligos and reagents table	139
C Recipes and reagent preparation	143
C.1 IHC	143
C.2 Organoculture	143
Bibliography	145
List of Tables	162
List of Figures	164

Abbreviations

ACTB	β -Actin
Ago 2	Protein argonaute-2
APP	Amyloid beta precursor protein
BSA	Bovine serum albumine
CAM	Cell adhesion molecule
cAMP	Cyclic adenosine monophosphate
C domain	Central domain
Ch	Chromosome
CHX	Cycloheximide (translational blocker)
CNS	Central nervous system
co-MO	Control morpholino
CRMP	Collapsin-response mediator protein
DRG	Dorsal root ganglion
E13	Embryonic day 13
ECM	Extra cellular matrix
Endo	Endogenous
Exo	Exogenous
FRAP	Fluorescence recovery after photobleaching
GAP	GTPase-activating protein
GCL	Ganglion cell layer
GDP	Guanosine diphosphate
GEF	Guanidine exchange factor
GTP	Guanosine triphosphate
H4	Histone H4
HF	High fidelity
HIGS	Heat inactivated goat serum
IHC	Immunohistochemistry
LE/Ly	Late endosome/Lysosome
LCM	Laser capture microdissection
LGN	Lateral geniculate nucleus
LPS	Local protein synthesis
MAP2	Microtubule-associated protein 2
MB	Molecular beacon
miRNA	micro RNA
MO	Morpholino
MRE	miRNA Responsive Element
mRFP	Monomeric red fluorescent protein
mRNA	messenger RNA
MS222	Tricaine methanesulfonate
MSD	Mean square displacement

Abbreviations

MT	Microtubule
MVB	Multi vesicular bodies
NGF	Nerve growth factor
NGmiRNAs	Newly generated miRNAs
NGS	Normal goat serum
NMD	Nonsense-mediated mRNA Decay
OE-PCR	Overlapping extension PCR
OC	Optic chiasm
ON	Optic nerve
ONH	Optic nerve head
OT	Optic tract
P0	Post-natal day zero
PBS	phosphate buffered saline
PFA	Paraformaldehyde
PLL	Poly-L-Lysine
Pre-miRNA	Precursors miRNA
Pri-miRNA	Primary miRNA
pSILAC	pulsed stable isotope labeling of amino acids in cell culture
PSF	Antibiotic-Antimycotic (penicillin, streptomycin, Amphotericin B)
RBP	RNA binding protein
RF	Retrograde Flow
RFU	Relative fluorescence unit
RGC	Retinal ganglion cell
RIN	RNA integrity number
RISC	RNA induced silencing complex
RTK	Receptor tyrosine kinase
RTP	Receptor tyrosine phosphatase
RT-PCR	Reverse transcription PCR
RT-qPCR	Real time quantitative PCR
SC	Superior colliculus
SEM	Standard error mean
Sema3A	Semaphorin 3A
TAE	Tris-acetate-EDTA
TBE	Tris-borate-EDTA
TF	Transcription factor
THBS1	Thrombospondin 1
TRAP	Translating ribosome affinity purification
TUBB3	Tubulin beta 3 class III
UTR	Untranslated region
VEGF	Vascular endothelial growth factor

Abstract

During the development of the nervous system, axons grow and generate a complex network of interconnected neurons. To establish these connections, the tip of the growing axon, the growth cone, is guided by chemotropic cues en route to its target with exquisite precision. Axons must sometimes navigate a significant distance before reaching their final destination. As an alternative to energy-expensive protein transport from distant cell bodies, seminal studies have revealed that growth cones rely on local mRNA translation to generate certain proteins acutely on demand. These cue-induced newly synthesized proteins contribute to fuel growth cone steering.

Several groups reported the presence of Dicer at growth cones, and I observe the presence of endogenous Dicer in RGC axons of FLAG-HA₂-Dicer transgenic mice. These observations raise the intriguing possibility that not only proteins but also miRNAs could be produced locally in this compartment. In my work, I have therefore explored whether miRNA biogenesis occurs locally within growth cone and if this is important for growth cone steering, using *Xenopus laevis* retinal ganglion cell (RGC) axons as a model.

Specific precursor microRNAs (pre-miRNAs) are detected in pure *Xenopus* RGC axonal preparations by miRNA-seq and PCR, and endogenous pre-miR-181a-1 is actively trafficked to distal axons by hitchhiking on vesicles. Upon exposure to Sema3A, but not Slit-2, pre-miR-181a-1/a-2 are processed within axons by Dicer into newly generated miRNAs (NGmiRNAs). In contrast, pre-miR-182 remains unprocessed upon Sema3A exposure, highlighting a mechanism that is not only cue-, but also pre-miRNA molecule-specific. Inhibiting NGmiRNAs in axons abolishes growth cone responsiveness to cues *ex vivo*. miRNAs are thus locally produced and these newly generated miRNAs mediate cue-induced growth cone steering.

To deepen mechanistic insights, I assess whether newly generated miRNAs silence the translation of specific mRNAs in response to cues using FRAP analysis with a Venus reporter. I observe that APP and TUBB3 are locally translated in axons in basal conditions and that are both silenced in response to Sema3A. I uncover that this cue-induced silencing of TUBB3 is mediated by newly generated miRNAs specifically in axons *ex vivo* and *in vivo*.

Taken together, these results indicate that newly generated miRNAs gate cue-induced silencing of a specific subset of mRNAs in time and space, thereby regulating growth cone behavior. Local biogenesis of miRNAs in axons constitute an important additional regulatory layer in the complex mechanism of axon targeting.

1 Introduction

The aim of this thesis is to identify and to characterize specific microRNAs (miRNAs), that are newly generated at the growth cone level, and that play a key role in axon guidance by regulating specific messenger RNAs (mRNA) during axonal steering and outgrowth. The biological context investigated in this project is brain wiring (Section 1.1), the process ensuring the formation of complex networks of neurons during development, from cell fate specification, to cell migration, axon pathfinding, target selection, and synaptogenesis. During this process each growing neuron extends its axon in a complex environment and is guided by its dynamics tip, called growth cone, which senses the surrounding signals (Section 1.2). These signals, or chemotropic cues, can attract or repel axons, by inducing a modulation of the cytoskeleton in the growth cone (Section 1.3).

Axon guidance is finely regulated and the axons reach their destination with a high degree of precision. The regulation of specific mRNAs at the growth cone level is suspected to play a crucial role in axon pathfinding (Section 1.4). However, the identity of key regulatory players of mRNA translation and their mode of action at the growth cone are largely unknown. A possible interesting class of molecules, which influence the stability and regulate the translation of specific target mRNAs in a temporal and spatial specific way, are small regulatory non-coding RNAs, such as miRNAs (Section 1.5 and Section 1.6). Using retinal ganglion cells (RGC) as a cellular model the role of miRNAs in axon guidance was investigated (Section 1.7).

The molecular mechanisms which underlie brain wiring are of particular interest because some hereditary neurological disorders are caused by mutations in axon guidance receptors (Van Battum et al., 2015), and some guidance molecules play roles in adult nervous system recovery after injury (Yaron, Zheng, 2007). Thus, identification and characterization of molecules involved in axon guidance could have an important clinical impact. Moreover, miRNAs have been shown to be deregulated in many pathological conditions (Vicente et al., 2016; Boese et al., 2016) and thus the modulation of miRNAs levels is considered as a possible therapeutic target. Indeed, it is possible to restore the correct level of these small non coding RNAs either through an exogenous delivery of miRNAs (miRNA mimics) or by blocking miRNAs using antisense matching oligos (antimiRs) (Rupaimoole, Slack, 2017). Since miRNAs are emerging as potential therapeutic tools (Lambert et al., 2015; Nagaraj et al., 2015), increased knowledge on miRNAs' mode of action and maturation may be useful for developing specific clinical therapies.

Last but not least, the answers to questions such as “How do neurons form a functional network?”, “Which regulatory molecules are involved in this process?”, “How is the complexity of brain wiring regulated in terms of signaling pathway transduction?” have not only implications for neuronal development, but also for neuronal regeneration in adult.

To ease the notation, a series of abbreviations will be used throughout the entire text of this thesis. The corresponding full names, which they refer to, are reported into the list of abbreviation (page ix).

1.1 Brain wiring and axon guidance

The most appropriate word to describe the mammalian brain is “complexity”. The brain controls bodily movements, posture and balance, interprets the world around us using input from the sensory organs and regulates our body’s decision accordingly, represents the memory of what we have learned and allows us to elaborate information and to plan actions. The organ that manages all these activities is composed by approximately 100 billion neurons, each of which forms in average about 10,000 synaptic connections (Bullmore et al., 2009) or even more (e.g. about 200,000 synapses in rodent cerebellum Purkinje cells (Korbo et al., 1993; Hansel, Linden, 2000)). These numbers indicate the brain’s structural complexity, which is especially impressive considering that the formation of its precise and specific neural connections are highly regulated at the molecular level.

Brain wiring, the process in which axons grow and form connections during nervous system development, is finely regulated and indeed errors in the formation of neuronal connections have impacting effects. Abnormal brain wiring is a pathogenic mechanism in schizophrenia (Heuvel van den, Kahn, 2011) and has also been linked to autism spectrum disorders (Roine et al., 2015).

Studying early embryonic developmental stages enables to follow the journey of the very first axons and hence allows to investigate brain connectivity at stages with lower complexity than that found in adult individuals (Pelt van et al., 1994). The first axons are called “pioneers” and grow in a largely axon-free environment. The “follower” axons extend along pre-existing axonal tracts and arrive later at their target destination (Chédotal, Richards, 2010). The followers find their pathway by fasciculating with the first axons, pioneers, in contrast, are finely guided to their correct destination by environmental cues (Raper, Mason, 2010).

1.2 The growth cone

The tips of the growing axons are called “growth cones”. The growth cones sense the environmental cues and respond to these attractant or repellent specific signals, moving towards the indicated direction.

The first qualitative description of growth cone dates back to 1890, when S.R. Cajal studied the nervous system of fixed chick embryos (Cajal, 1890). Therein he described growth cones as “conical forms with amoeboid movements”. In 1910, R.G. Harrison observed growth cones moving in live tissue in real time (Harrison, 1910), while C.C. Speidel observed *in vivo* growth cones of sensory axons in a growing frog’s tail in 1941 (Speidel, 1941). Over the years, this structure at the end of elongating axons has captured the attention of many researchers, who have tried to better describe both the growth cone and axon guidance mechanisms using different animal models and increasingly advanced microscopy techniques.

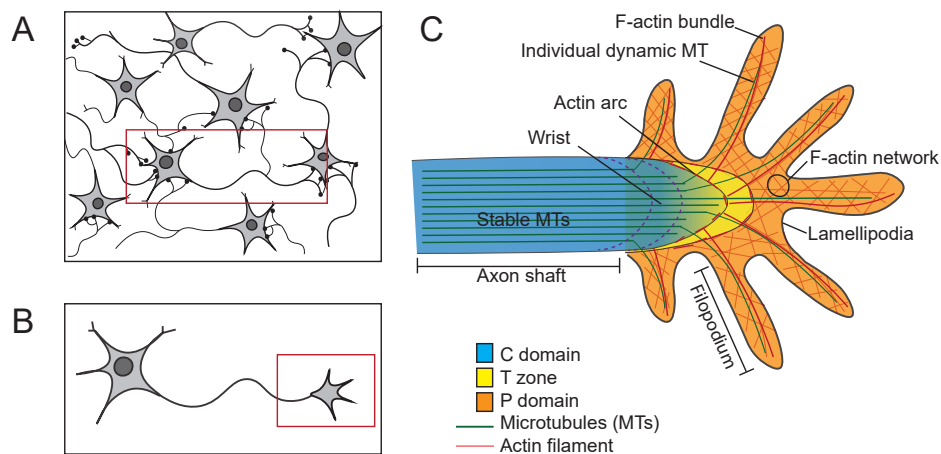
1.2.1 Growth cone function and structure

The growth cone is the highly dynamic distal tip of an axon, it is the central information processing component during axon guidance processes allowing neurons to reach their final

destination with impressive accuracy. It is “fan-shaped” to probe the environment around it continuously by extending and retracting its protrusions (Dent et al., 2011).

While pathfinding, the growth cone first decides on its direction based on the sensed surrounding signals, followed by its movement along the chosen path utilizing its cytoskeletal components. Actin filaments and microtubules are the cytoskeletal components of the growth cone. Both are polarized polymers since they have a “plus end” growing part on which new components are added, and a “minus end” where depolymerization occurs. In particular, actin filaments are helical polymers composed of actin globular monomers. Microtubules are formed by alpha/beta tubulin dimers assembled in a head-to-tail configuration (Dent, Gertler, 2003). These polarized structures are highly dynamic and their specific distribution within the growth cone confers the right conformation and structure to achieve motility (Section 1.2.2).

Figure 1.1: Growth cone structure



The growth cones domains and structure (A) Complex network of neurons formed during brain wiring process. (B) Detail of a single neuron. The red box highlights the position of the growth cone. (C) The growth cone is organized in filopodia and lamellipodia, it can be separated into three domains based on the cytoskeleton distribution (C, T and P). Figure drawn by the Author, information from (Lowery, Van Vactor, 2009; Geraldo, Gordon-Weeks, 2009).

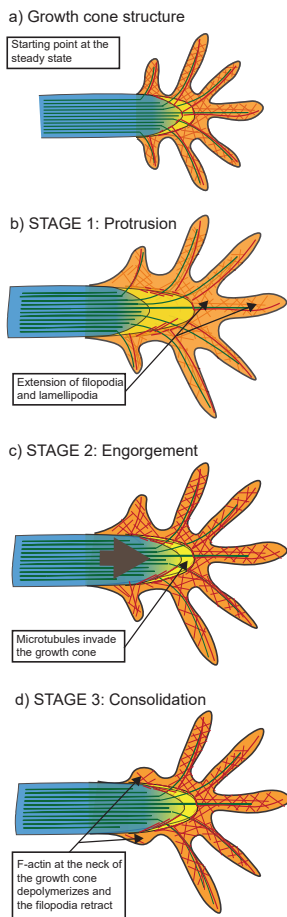
According to the distribution of actin and microtubules the growth cone can be divided in three domains (Figure 1.1). The peripheral (P) domain contains filopodia, comprised of bundled actin filaments and individual dynamic microtubule, and lamellipodia, consisting of a network of branched F-actin filaments. The filopodia are the sensory protrusions and lamellipodia are the sheets of membrane separating the filopodia finger-like structures one from the others. Then there is the central (C) domain, which is constituted of stable bundled microtubules that enter the growth cone from the axon shaft. The interface between the P and C domain is called transition (T) zone, where contractile structures

(actin arcs) lie perpendicular to filopodia (Lowery, Van Vactor, 2009). Growth cones from all the different species analyzed so far are organized into these three domains (P, C and T) and contain filopodia and lamellipodia (Dent, Gertler, 2003).

The growth cone is a complex machinery and it may be compared to a car traveling in a big city with many crossing streets: only following specific pathways allows the car to reach its correct final destination. After having depicted the growth cone structure above, the following sections will describe the engine of this particular machine, the road on which it moves and grows and, finally, the road signs along the pathway that indicate the correct directions to reach the specific final destination.

1.2.2 Cytoskeletal dynamics: growth cone engine

Figure 1.2: Stage of growth cone progression.



Reworked from (Lowery, Van Vactor, 2009).

All the growth cone movements (turning, protrusion, progression, and retraction) depend on how actin and microtubule components are organized: the cytoskeleton represents the engine allowing axon motility. The first observation and description of growth cone movements dates from 1986 (Goldberg, Burmeister, 1986). In this work the morphological changes observed during axon outgrowth are presented. Three consecutive stages form new axon segments: protrusion, engorgement, and consolidation (Figure 1.2).

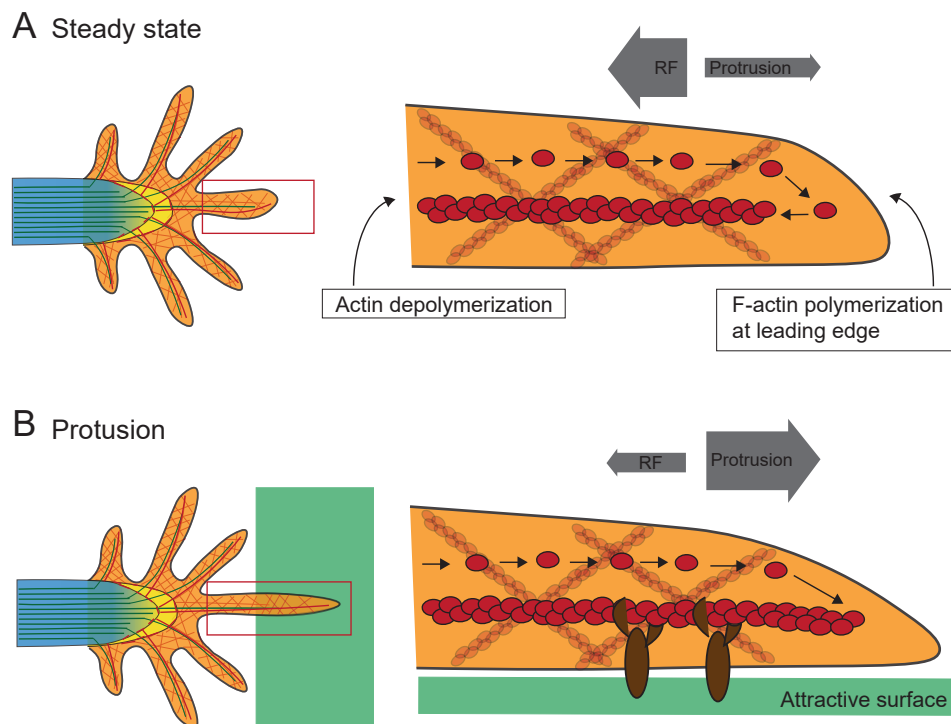
Protrusion is the stage of growth cone progression in which both filopodia and lamellipodia extend. During engorgement the F-actin arcs are reoriented, microtubules invade the growth cone, the C domain moves forward, and is finally fixed. Consolidation refers to the step in which actin filaments at the neck of the growth cone depolarize and this proximal part assume a cylindrical conformation. By repeating these three stages many times axons elongate (Dent, Gertler, 2003).

The assembly of actin filaments at the leading edge allows growth cone progression and its dynamic behavior in general. The continuous recycling of actin monomers, which move from the center to the leading edge of the growth cone, results in a back movement of the entire actin filament: this phenomenon is known as actin filament retrograde flow (RF) (Figure 1.3). The unbalance between F-actin retrograde flow (RF) and actin polymerization at the filopodia tips determines the protrusion or retraction of the growth cone (Challacombe et al., 1996). The RF is enhanced by the polymerization of actin at the leading edge and antagonized by the contraction of the motor protein myosin II in the T zone. Myosin II contraction causes the deformation of the F-actin bundles, pushing the filaments forward and in this

way enhancing the polymerization at the tips (Lowery, Van Vactor, 2009). In summary, protrusion is enhanced either by actin polymerization or by increasing myosin contraction. Conversely retraction or collapse are caused by reducing actin polymerization, increasing depolymerization or reducing myosin II contraction.

This dynamic process is translated into a movement when growth cone receptors bind to an adhesive substrate, creating a mechanical link between receptors and F-actin flow (Figure 1.3). This interaction acts as an anchor blocking the RF of actin filament, advancing the protrusion, ultimately leading to axonal elongation (following the morphological changes described above).

Figure 1.3: Growth cone advance



Model of growth cone advance In growth cone filopodia actin is dynamic, with continuous disassembly of actin monomers at the center of the growth cone and polymerization at the leading edge. This process determines the retrograde flow (RF) of actin filament. (A) In the steady state there is a balance between polymerization and depolymerization, the growth cone does not advance and the retrograde flow is higher than the protrusion (as indicated by the gray arrows above the picture). (B) When the filopodia contact an attractive surface an interaction between the growth cone and adhesive molecules is stabilized. By blocking the retrograde flow with physical binding protrusion occurs. Polymerization at the leading edge continues, the back movement of actin filament is blocked, hence the growth cone is able to advance. Figure drawn by the Author, information from (Gomez, Letourneau, 2014; Nichol et al., 2016).

The actin filaments are cytoskeletal components that maintain the growth cone's shape and that play an essential role in axon guidance (Dent, Gertler, 2003), but microtubules also play a role in this process. By inducing alternately actin or microtubules depolymerization, Yamada and colleagues concluded that actin is essential in correct axonal outgrowth and microtubules (MTs) are fundamental for maintaining proper axon structure (Yamada et al., 1970; Wessells et al., 1971). Subsequent studies underlined that microtubules not only have a maintenance role, but also play an active role during the early steps of growth cone steering and protrusion through their entrance into the filopodia in the P zone (Sabry et al., 1991; Tanaka, Kirschner, 1991).

Moreover, MTs movements are also important during engorgement: the interactions of MTs with the actin network and actin arcs in the C domain is necessary to have a functional outgrowth. The disruption of the actin arc is translated into failure of MT consolidation during axon outgrowth, causing abnormalities in the C domain during progression (Schaefer et al., 2008). Asymmetrical protrusion determines steering instead of growth cone elongation in the same direction. In particular, axons can turn through depolarization of actin and destabilization of microtubules in one direction, and actin polymerization and microtubules stabilization in the opposite side. In conclusion, both the cytoskeletal components themselves and their interactions are important for the proper function of growth cone motility.

1.2.3 Microtubules isoforms

As aforementioned, microtubules are key part of the growth cone engine (Section 1.2.2), they are composed by alpha/beta tubulin dimers assembled in a head-to-tail configuration (Dent, Gertler, 2003), and have a fast growing end (the “plus” end) (Akhmanova, Steinmetz, 2008). Microtubule polymers undergo to a stochastic switch between growing (polymerization) and shortening phases (depolymerization) (Gordon-Weeks, 2004). These phases are known as catastrophes and rescues, and the continuing switch between the two is called dynamic instability (Gordon-Weeks, 2004). The dynamic instability of microtubules is essential for many cellular processes as cell division, motility, and differentiation (Horio, Murata, 2014). These cellular processes rely on the dynamic rearrangement of alpha/beta tubulins, the building blocks of microtubules. The regulation in isoforms composition and post translational modifications (PTMs) of the tubulin building blocks are mechanisms to control microtubules dynamic (Verhey, Gaertig, 2007; Hammond et al., 2008).

Indeed, different tubulin isoforms exists. In vertebrates there are six isoforms for both α and β -tubulin which are conserved (Joshi, Cleveland, 1990); specifically in human the variety increased and eight isotypes for both α and β -tubulin are reported (Leandro-García et al., 2010). Tubulin superfamily is highly heterogeneous, some isotypes are ubiquitously expressed, but others are enriched in particular cells or predominantly involved in specific mechanisms (McKean et al., 2001). For example in mice, out of the six β -tubulin isotypes, four are found specifically in brain and they are differently expressed during development (Denoulet et al., 1986). High expression of TUBB2A, TUBB2B, TUBB3, and TUBB4 has been also reported in human brain (Leandro-García et al., 2010). The different tissue distribution of those isoforms, as well as their deregulation in pathological contexts (Leandro-García et al., 2010), suggest important and specific roles for each tubulin isotype.

Brain malformations have been observed in patient harboring TUBA1A mutations; mutations in both TUBB2B or TUBA1A have been associated with lissencephaly and polymicrogyria; and deletion of TUBA8 in mice caused polymicrogyria, brain anomalies, and optic nerve hypoplasia (Liu, Dwyer, 2014). Moreover, TUBB2B and TUBB3 mutations have been associated with axon-guidance defects and disorders, such as congenital fibrosis of the extra-ocular muscles (CFEOM) (Tischfield et al., 2010; Cederquist et al., 2012).

1.2.3.1 Tubulin beta isoform III (TUBB3)

Tubulin beta isoform III (TUBB3) is primarily expressed in neurons and it is the only isotype enriched specifically in these cells (Katsetos et al., 2003). TUBB3 exerts roles in neurogenesis and axon guidance maintenance (Poirier et al., 2010; Tischfield et al., 2010). Tischfield and colleagues identified eight different mutations of TUBB3 in human causing ocular motility disorder (CFEOM3) (Tischfield et al., 2010). Axon guidance defects were observed in human harboring TUBB3 mutation through magnetic resonance imaging (MRI) of the intracranial motor nerves. In particular, the authors observed aberrantly innervated muscles by the oculomotor nerve: the lateral rectus muscle was innervated by the oculomotor nerve instead of abducens nerve causing ocular motility restrictions and/or aberrant eyelid elevation (Tischfield et al., 2010). Moreover, in order to better characterized the most common human TUBB3 mutation (R262C), they created a knock-in disease mouse. *Tubb3*^{R262C/R262C} mice showed defects in commissural axons and cranial nerves guidance. At E18.5 aberrant fiber projections at the midline were observed, as well as thinner or absent midline crossing of anterior commissural axons compare to WT. At E11.5-E12 cranial nerves guidance defects were observed by neurofilament staining. Finally, a failure of the correct muscles innervation by the oculomotor nerve was showed in *Tubb3* mutated mice. Those data collected from both human harboring different TUBB3 mutations and from *Tubb3*^{R262C/R262C} mice, strongly support a central role of TUBB3 in axon guidance mechanisms.

Other six different mutations in TUBB3 genes were reported (Poirier et al., 2010). All patients harboring one of this mutation show cortical disorganization and axonal abnormalities caused by neuronal migration and differentiation defects. Moreover, MRI of TUBB3-mutated patients revealed various aberrant phenotype in cortical and gyral organization and tractography studies on the corticospinal tract showed misorientation of the pyramidal fibers, and the presence of misprojecting cortical neurons.

Both those two clinical studies strongly supported a critical role played by TUBB3 during axon guidance. Moreover, TUBB3 expression peak during brain development, from axon guidance to maturation stages, and its levels decrease in adult central nervous system (CNS) (Jiang, Oblinger, 1992). This observation further support a TUBB3 involvement in nervous system development. Interestingly, TUBB3 mRNA has been observed and locally translated only in embryonic sensory axons, but not in adult axons, where the axonal presence of this isoform relies on transport of the protein from the soma (Gumy et al., 2011).

Among the different tubulin isoforms, TUBB3 is enriched in the dynamic portion of microtubules and *in vitro* data suggest a specific role in microtubule polymerization dynamics (Panda et al., 1994). Recent *in vitro* and *in vivo* experiments show that dorsal root

ganglia in *Tubb3*^{-/-} mice have a decreased in both microtubules dynamicity and neurite outgrowth rate (Latremoliere et al., 2018).

Even if TUBB3 functions are not yet fully uncovered, several evidences pointing to a neuronal specific role exerted by modulation of microtubules dynamic in neurogenesis and in development during axon guidance.

1.2.4 Growth cone collapse

A drastic rearrangement of cytoskeletal components happens during growth cone collapse. During growth cone collapse the actin filaments and microtubules present in filopodia depolymerize (Fawcett, 1993) and microtubules move rapidly into the growth cone central domain (Dent et al., 2011). During this event, axons may retract to the point that also cytoskeletal component inside axon, and not only growth cone, start to depolymerize (Fawcett, 1993). This growth cone behavior occurs *in vivo* during pathfinding, and *ex vivo* by exposure to repulsive stimuli (Section 1.2.5).

Growth cone collapse *in vivo* has been observed in *C. elegans* as a mechanism to maintain a single terminal growth cone instead of multiple (Knobel et al., 1999) and in leech embryos as a mechanism to avoid axonal progression (Wolszon et al., 1994). However, the *in vivo* roles of this drastic event has not been fully characterized yet, because *in vivo* multiple signals are integrated simultaneously and the complexity of growth cone behavior is elevated (Gallo, Letourneau, 2004). Carol Mason and Lynda Erskine have proposed that the rarely observed *in vivo* events of collapse are due to particular situation in which there is less conflicts among different stimuli (Mason, Erskine, 2000).

However, the read out of collapse *ex vivo* is much simpler than the *in vivo*, since one stimulus at the time can be studied and the shape of isolated growth cones can be monitored, defined and described. For example, retinal ganglion cell (RGC) growth cones in culture are considered collapsed if no filopodia are present, or if there are only two or fewer filopodia each shorter than 10 μm (Campbell et al., 2001). Considering the simple read-out of the *ex vivo* response, the growth cone collapse has become a standard assay. Indeed, it has been largely used as assay for different neuronal cell types (Wahl et al., 2000; Campbell et al., 2001; Deglincerti et al., 2015; Bellon et al., 2017). It has been applied mainly to study growth cone responsiveness to different stimuli, but recently also in the context of axonal degeneration studies (Unsain et al., 2018). In this thesis work, the growth collapse assay has been used to investigate the impact of non-coding RNAs (ncRNAs) on proper axonal response to external stimuli.

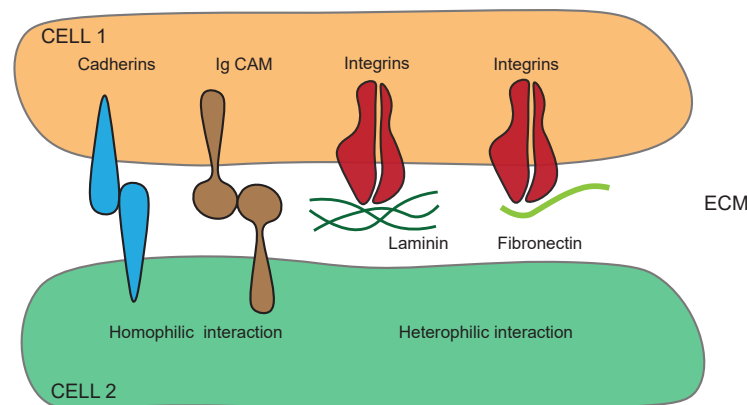
1.2.5 Guidance cues

What has been described so far refers to growth cone structure and motility: the bodywork and the engine of the car which is guiding axons during pathfinding. What is missing to this description is the road on which axons are moving and the road signs that indicate the direction. Growth cone filopodia probe the surrounding environment, and according to the cues sensed, they orient themselves and hence determine axonal pathfinding. Both road and road signs exert a role in guiding the growth cone by attraction or repulsion, and they act respectively as long-range and short-range cues (Figure 1.5).

1.2.5.1 The road: short range cues

The growth cone road is composed by adhesive and anti-adhesive molecules, which induce contact attraction or repulsion by interacting with growth cone components. The contact attractive mechanism is mediated both by molecules presented on the surface of neighboring cells and by molecules embedded into the extracellular matrix (ECM) (Lowery, Van Vactor, 2009).

Figure 1.4: Major families of cell-adhesion molecules (CAMs)



Major families of cell-adhesion molecules (CAMs) The “road” on which the growth cone (CELL 1) moves is represented by CELL 2 and the extracellular matrix (ECM) components (laminin and fibronectin). The interactions between CELL 1 and the road are mediated by CAMs (cadherins, IgCAM, and integrin) on the growth cone surface. Figure drawn by the Author, information from (Tessier-Lavigne, Goodman, 1996; Pollerberg et al., 2013).

Neighboring cells expose some Cell Adhesion Molecules (CAMs) that are recognized by the growth cone. In particular, there are two families of CAMs that act as attractive guidance molecules during axonal pathfinding: the immunoglobulin (Ig) and cadherin superfamilies (Tessier-Lavigne, Goodman, 1996; Maness, Schachner, 2007).

Among the guidance molecules embedded into the ECM there are fibronectin and laminin, both acting as attractive cues through their interaction with the growth cone. All the guidance molecules exposed either on the surface of neighboring cells or in the ECM interact with the growth cone through other cell adhesive molecules. The interaction can be homophilic, such the one between a cadherin and another cadherin, or heterophilic, such as the one between integrin on the growth cone and ECM proteins (Figure 1.4).

Besides these attractive signals there are also repulsion mechanisms that “avoid the exit of the car from the road”, causing arrest or collapse of the growth cone. The “guard rail” of the axonal pathfinding are Eph ligands, transmembrane semaphorins and some ECM components (e.g. tenascin) (Tessier-Lavigne, Goodman, 1996). Ephrins are membrane-bound ligands and their receptors are tyrosine kinases of the Eph family (Cheng et al., 1995). There are two classes of these guidance molecules: ephrin-A and ephrin-B. The first is anchored at the membrane and binds EphA receptor, the second has a transmembrane domain and binds to EphB receptors (Wilkinson, 2001).

1.2.5.2 The road signs: long range cues

Aside from the contact-mediated signals there are diffusible molecules which may act as chemorepellent or chemoattractive cues. Among these molecules are highly conserved families of guidance molecules: Netrins, Slits, and Semaphorins (Dickson, 2002).

Netrin is a diffusible cue that is able to give rise to both effects, repellent and attractive, dependent on the receptor on the growth cone (Hedgecock et al., 1990). Slits are large secreted proteins that interact with the Roundabout (Robo) family of receptors. Normally Slit acts as repellent causing growth cone collapse, however it can also have a positive effect by stimulating axon branching (Dickson, 2002). Semaphorins have both transmembrane and secreted isoforms and their signal is mediated by multimeric receptor complexes which include a plexin protein (Tamagnone et al., 1999). Semaphorins are divided into eight classes according to their structure; the forms from 3 to 7 are found in vertebrates (Raper, 2000).

Table 1.1: Guidance cue and receptors

Guidance cues	Receptors	References
Conserved families of guidance molecules		
Netrins	DCC/Frazzled	(Dickson, 2002)
Slits	Robo	(Dickson, 2002)
Ephrin A (EphA)	EphA	(Dickson, 2002)
Ephrin B (EphB)	EphB	(Dickson, 2002)
Semaphorins	Plexin Neuropilin	(Dickson, 2002)
Morphogens		
Wnt	Frizzled Ryk	(Zou, 2004)
SHH	Boc	(Okada et al., 2006)
BMP	BmprIa (ALK3) BmprIb (ALK6)	(Liu et al., 2003)
Growth factors		
BDNF	TrkB	(Tuttle, O'Leary, 1998)
NGF	TrkA	(Tuttle, O'Leary, 1998)
Neurotransmitters		
Glutamate	NMDA	(Dalva et al., 2000)
ECM protein and CAMs		
Laminin	Integrin	(Tessier-Lavigne, Goodman, 1996)
Fibronectin	Integrin	(Tessier-Lavigne, Goodman, 1996)
IgCAM	IgCAM	(Tessier-Lavigne, Goodman, 1996)
Cadherin	Cadherin	(Tessier-Lavigne, Goodman, 1996)

Ryk, Tyrosine-protein kinase RYK; SHH, Sonic hedgehog protein; Boc, Brother of CDO; BMP, Bone morphogenetic protein; BDNF, Brain-derived neurotrophic factor; NGF, Beta-nerve growth factor; TrkA/B, High affinity nerve growth factor receptor A/B; NMDA, Glutamate receptor ionotropic; IgCAM, cell adhesion molecule of the immunoglobulin superfamily.

Moreover, there are experimental evidences also for the role of growth factors in axon guidance. For example, the injection of nerve growth factor (NGF) into neonatal rodent brains causes aberrant growth of peripheral sympathetic axons (Menesini et al., 1978), and experiments in *Xenopus* show that a gradient of brain-derived neurotrophic factor (BDNF) attracts growth cones of cultured spinal neurons (Song, Poo, 1999). Additionally, neurotransmitters may play a role in axon guidance. In fact, at increasing concentrations of glutamate, dendritic outgrowth rates were reduced (Mattson et al., 1988). A list of the main guidance cue molecules and their receptor is reported in Table 1.1.

A graphical summary of the guidance cues is reported in Figure 1.5. It is a schematic and simplified view of guidance cues complexity. In the real world growth cones have to integrate many signals simultaneously and, as previously mentioned, the response of attraction or repulsion is not an intrinsic property of a cue, but depends on the specific receptors present at the growth cone, on the levels of second messengers such as cyclic adenosine monophosphate (cAMP), on the crosstalk with other cues, adding complexity to the schema (Section 1.3.2). Moreover, guidance cue expression levels are themselves finely regulated by other molecules, adding even more complexity to the schema. For example, the transcription factor (TF) *Irx4* regulates the expression of *Slit1*, and a misexpression of *Irx4* causes a reduction of *Slit* levels, resulting in axon fasciculation defects (Butler, Tear, 2007).

Staying with the analogy of the car, the framework is now completed: car bodywork, engine, street and road signs have been described. How are road signs integrated and translated into engine ignition and movement of car body? The interactions between guidance cues and growth cone receptors are translated into cytoskeletal reorganization and consequently into growth cone motility via signal transduction processes.

1.3 Signal transduction

Signal transduction in growth cone occurs when a guidance cue activates a specific receptor on the surface of the growing axon. Receptors trigger a signaling cascade inside the cell, eliciting a response. Growth cone guidance cues, lead at the end of the biochemical chain of events to the modulation of cytoskeletal components and the regulation of structure and motility of the growing axon (Hall, 1998).

Some growth cone surface receptors have an intracellular domain: Robo, DCC, Plexin and Ephrin (Table 1.1). The binding of a guidance cue with these type of receptors directly promotes the enzymatic activity of the intracellular domain (Strittmatter, Fishman, 1991).

Intracellular domains are sufficient to amplify the signal, to drive attraction or repulsion according to the cues (Bashaw, Goodman, 1999). The enzymatic activities of the receptors are either tyrosine kinases (RTKs) or tyrosine phosphatases (RTPs). Receptors without an intracellular domain promote the signaling cascade by recruiting other RTKs. For example, cell adhesion molecules (CAMs) have a binding site on Fibroblast Growth Factor Receptor (FGFR) and trigger a signaling cascade through the phosphorylation of growth cone protein through FGFR activity (Williams et al., 1994).

Direct or indirect activation of enzymatic phosphorylation and dephosphorylation, is the key step in signal transduction in axon guidance.

The GTPase family, family of hydrolase enzymes that can bind and hydrolyze guano-

sine triphosphate (GTP), acts as a key node in signal transduction in growth cone. In fact, they integrate the upstream signal triggered by the guidance cue, and coordinate the downstream cascade, leading to the ultimate cytoskeletal rearrangement (Dickson, 2002). RhoA, Rac1 and Cdc42 are important members of the Rho guanosine triphosphates (Rho GTPase) family. They are involved in different actin rearrangement events. Indeed actomyosin contraction, F-actin disassembly and F-actin polymerization are the final effects of their signaling cascade.

Rho GTPases are in turn regulated by effector molecules such as Guanidine Exchange Factors (GEFs) and GTPase-Activating Proteins (GAPs), which activate and inactivate Rho GTPase, respectively. In particular, GAPs lead to hydrolysis of GTP to GDP, whereas GEFs stimulate the release of guanosine diphosphate (GDP) to allow binding of guanosine triphosphate (GTP). A schematic representation of signal transduction in growth cone is shown in Figure 1.6.

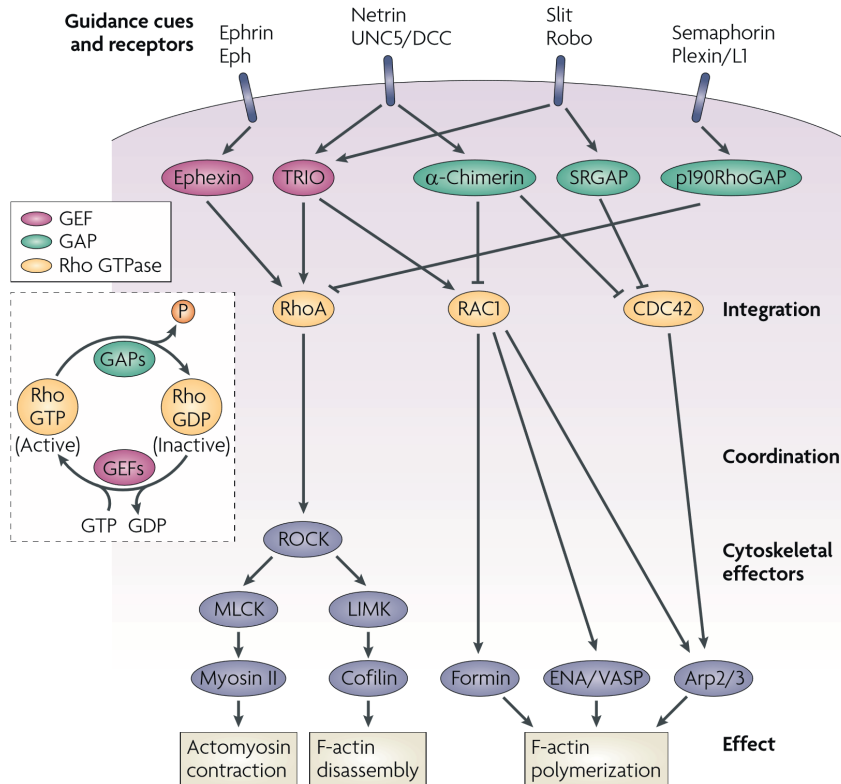
Among the final effectors are Cofilin, Arps and Ena/Vasp. Cofilin is an actin binding protein which depolymerizes F-actin filaments, releasing G-actin monomers. A similar function is played by SCG10 on microtubules (Gorovoy et al., 2005). Arps promotes branching of actin filament and Arp2/3 inhibition has been shown to lead to a reduction of filopodia number and F-actin content in the growth cone (Lanier, Gertler, 2000). Ena/Vasp proteins are anticapping agents that promote actin filaments growth at the leading edge (Lebrand et al., 2004).

1.3.1 Sema3A signal transduction

Sema3A is a secreted protein promoting dendrite development and acting as a repellent cue during axon guidance (Koropouli, Kolodkin, 2014). *In vitro*, Sema3A induces a collapse response, in which filopodia and lamellipodia in the growth cone retract. This change in growth cone morphology is due to both cytoskeletal dynamic modulation (Campbell et al., 2001) and endocytosis of the growth cone membrane (Dang et al., 2012; Carcea et al., 2010). Endocytotic events are needed for Sema3A internalization and thus promotion of the signal transduction (Carcea et al., 2010), but also for reducing the growth cone surface and the number of adhesion molecules embedded into to external membrane (Tojima, Kamiguchi, 2015). A decrease in focal adhesion points contributes in growth cone retraction upon Sema3A exposure.

Sema3A receptor complex is formed by Neuropilin-1 (NP1) and Plexin-A (PlexA) (Takahashi et al., 1999). NP1 is a multifunctional cell surface receptor interacting with both Sema3A and the vascular endothelial growth factor (VEGF) exerting different roles during the development of various tissues. Intriguingly, using knock in and conditional NP1 null mice model, it has been shown that in endothelial cells the VEGF-NP1 signaling is involved in angiogenesis, while the signal cascade activated by Sema-NP1 is not required in vascular development, but it exerts its function specifically during axonal pathfinding events (Gu et al., 2003). NP1 has an high affinity for Sema3A and it represents the binding partner of the repellent cue, while PlexA has an intracellular domain which starts the signal transduction upon Sema3A stimulation (Takahashi et al., 1999; Rohm et al., 2000). Indeed, PlexA has an highly conserved GTPase-activating (GAP) cytoplasmic domain able to interact with several small Rho GTPases. Rho GTPases are involved in guidance cue signal transduction and different receptors use specific cytoplasmic signaling mechanisms

Figure 1.6: Signal transduction



Signal transduction in growth cone Guidance cues, reported in the upper part of the Figure, interact with specific receptors. GEFs and GAPs mediated the response by phosphorylation or dephosphorylation of Rho GTPase family members (RhoA, Rac1 and Cdc42). Some cytoskeletal effectors are reported in the blue circles. The final effects, reported in the gray boxes in the bottom part of the Figure, are all modulations of cytoskeletal components. Cytoskeletal regulation means growth cone motility. Arp 2/3, Actin-Related Protein; ENA/VASP, Enabled/vasolidator-stimulated phosphoprotein; LIMK, LIM domain kinase; MLCK, myosin light chain kinase; ROCK, Rho kinase; SRGAP, slit-robo GAP; UNC5, uncoordinated protein 5. Figure from (Lowery, Van Vactor, 2009).

upon cue recognition (Toyofuku et al., 2005). In dorsal root ganglia (DRG) neurons and spinal motor neurons, Rac-GTP of the Rho GTPases family is required in Sema3A signal transduction cascade (Jin, Strittmatter, 1997; Turner et al., 2004). While in a pull-down assays of HEK 293T cells lysate, Plexin-A1 has been shown to interact with Rnd1 and RhoD, others Rho-related protein with GTPase activity (Zanata et al., 2002).

Guanine nucleotide exchange factors (GEFs) are proteins able to activate Rho GTPases by stimulating the release of guanosine diphosphate (GDP) to allow binding of guanosine triphosphate (GTP) (Figure 1.6). When Neuropilin-1 is present, FERM domain-containing guanine nucleotide exchange factor (GEF) FARP2 associates with Plexin-A1. Upon Sema3A exposure and NP1 binding, FARP2 dissociates from PlexA, gets activated and FARP2 Rac-GEF activity leads to Rnd1 recruitment to Plexin-A1 and downregula-

tion of R-Ras (Toyofuku et al., 2005). After activation of Rho GTPases and guanine nucleotide exchange factors, a phosphorylation cascade mediates downstream to *Sema3A* the modulation of some effectors, and the final regulation of cytoskeletal dynamics. Collapsin-response-mediator protein (CRMP), a microtubules associated protein, plays a crucial role in *Sema3A*/*NP1*/*PlexA* signal pathway (Schmidt, Strittmatter, 2007). Rho is activated during *Sema3A* signal cascade, and it phosphorylates CRMP-2 (Schmidt, Strittmatter, 2007). CRMP-2 binds to microtubule (MT) to stabilize them, but upon phosphorylation it dissociates promoting MT depolymerization (Fukata et al., 2002). Moreover, also glycogen synthase kinase-3 β (GSK-3 β) phosphorylates CRMP-2 and, through CRMP-2 inactivation, it regulates neuronal polarity (Yoshimura et al., 2005). Intriguingly, impairment in GSK-3 β phosphorylation affects *Sema3A* response in neuronal and non-neuronal cells (Eickholt et al., 2002).

Plexin-based signaling mediated by *Sema3A* exerts an important function in axon guidance events, and even if some factors involved in the signal cascade have been discovered, the entire pathway of this cue is still largely unknown. Moreover, *Sema3A*-*NP1* can interact with different Plexins resulting in a different signal cascade. For example, in cortical neurons, *Sema3A*-*NP1* forms a complex with *PlexinA4* controlling the basal dendritic arborization in V cortical layer (Tran et al., 2009).

1.3.2 Complexity of the response

Even if the players of growth cone signal transduction have been elucidated in the previous sections, it is not possible to list guidance cues and their effect. In fact, guidance molecules have not an intrinsic attractive or repulsive nature, their effect depends on the receptors expressed on the growth cone surface. In order to highlight the complexity of the response, in this section examples of single cues that give rise to different effects are described.

For example, *Netrins* are able to act as chemorepulsive agents for cells expressing *Unc-5* receptor, whereas they behave as a chemoattractive factor for neurons expressing *DCC*-type receptors (Colamarino, Tessier-Lavigne, 1995). Moreover, there are cases in which *DCC* receptor also mediates a repulsive effect upon *Netrin* binding. This depends on the intracellular levels of cAMP (Ming et al., 1997). When high level of cAMP are present *Netrin* acts as an attractant to spinal and retinal axons, probably because its levels favor actin polymerization reactions. On the other hand when cAMP levels are low, *Netrin* works as a repellent (Song et al., 1997; Nishiyama et al., 2003). Noteworthy, while axons are growing, they get older and more mature step by step and this aging process affects cAMP levels (Shewan et al., 2002). Therefore, since *Netrin-1* acts differently on axons according to the cAMP levels, it induces a different response depending on the maturation state of the growing axon. *Netrin* is only one such example, but also other guidance cues, such as *Sema3A* and *NGF*, are modulated by the level of a cyclic nucleotide (Song et al., 1998; Piper et al., 2007; Nangle, Keast, 2011). In particular, *Sema3A* acts as a repellent in both parasympathetic and sympathetic neurons, but its activity inducing collapse is mediated respectively by cAMP and cGMP (Nangle, Keast, 2011).

Alternative splicing further increases the complexity of axon guidance in nervous system wiring. Indeed, two functionally antagonistic isoforms of *Robo3* exist, which arise through alternative splicing. These two *Robo3* isoforms cause opposite responses upon *Slit* interaction. *Robo3.1* silences *Slit* repulsion, whereas *Robo3.2* favors *Slit* repulsion (Chen et al.,

2008).

Another general process that allow us to understand the complexity of the signal transduction in growth cones is adaptation, a process that may be subdivided in desensitization and resensitization. The response of a signal depends on the expressed receptors, hence by internalization or degradation of specific receptors desensitization occurs. This step is followed by a slower process called resensitization in which new proteins are synthesized to counteract the previous step (Piper et al., 2005).

This complexity of the response suggests that a specific and localized regulation may happens at the growth cone level to finely control all these mechanisms.

1.4 Local translation

By deepening the understanding of growth cone signal transduction cascades and out-growth mechanisms, another level of regulation must be introduced: local translation. The first evidences of a local translation of mRNA in neuronal axons came from UV absorption and electron micrographic experiments showing the presence of RNA and ribosomes in embryonic neuronal cells (Hughes, 1955; Tennyson, 1970). By electron microscopy, ribosome presence was observed also in dendrites (Steward, Levy, 1982). For years those data were largely debated, but from late 1990s other evidences of ribosomes in axons of different invertebrates start to accumulate (Van et al., 1997; Davis et al., 1992; Sheller, Bittner, 1992) and in 1998, ribosomes in vertebrates axonal sub-compartment were first observed, together with the β -actin transcript (Bassell et al., 1998).

mRNAs and rRNA was shown to be localized in axons of cultured hippocampal neurons (Craig, Banker, 1994) and in RNA granules translocated in living neurons (Knowles et al., 1996). Some years later, Holt and colleagues, established a link between guidance cues and local mRNA synthesis (Campbell, Holt, 2001). In fact they observed that RGC growth cones were unable to respond to Netrin-1 and Sema3A gradients upon local translation inhibition, demonstrating that local changes in protein synthesis can be caused by guidance cue molecules.

The first studies focused on single mRNA molecule, but more recent works have reported a screening of axonal mRNA obtained using high-throughput approaches (Willis et al., 2007; Taylor et al., 2009; Zivraj et al., 2010; Andreassi et al., 2010). Of particular interest for the project, considering that the study was conducted using the same model used in this thesis, is the article of Zivraj and colleagues in which a mRNA screening was performed in *Xenopus laevis* RGC growth cones at two different developmental stages (Zivraj et al., 2010). They observed that the majority of the growth cone mRNAs are functionally involved in protein synthesis and translation, and in metabolic activities. By comparing axon and growth cone mRNA profiling, they discovered the following functional categories specifically enriched in growth cones: cytoskeletal/motor (23%), protein synthesis and translation (15%) and transmembrane surface receptors (15%). Moreover, in the same paper, the authors showed that the growth cone mRNAs increase in number and diversify more in older neurons compare to stages in which the growth cone is nearer to the soma (e.g. 958 transcripts in old growth cones versus 286 in the young ones).

Neurons are polarized cells, and the roles of different sub-compartments are defined by the local translation of specific proteins (Martin, Ephrussi, 2009). Indeed, the newly syn-

thesized proteins in dendrites and axons, confer their specialized and sub-compartmentalized role in neurons. Moreover, through this spatial regulation distant parts of neurons are independent from the soma, e.g. growth cones autonomously react to environmental guidance cues (Lin, Holt, 2008). In 2009 Hengst and colleagues found that the mRNA of Par3, a cytoskeleton regulator, is localized into developing axons, and its local translation is triggered by two different guidance cues NGF and netrin-1. Upon Par3 mRNA ablation from axons the outgrowth-promoting effect of NGF is abolished (Hengst et al., 2009). It is noteworthy that some attractive guidance cues regulate the localized translation of mRNA encoding cytoskeletal proteins (e.g. Netrin-1, NGF, BDNF stimulate axonal protein synthesis of cytoskeletal constituents) and in this way they are controlling the growth cone's progress (Leung et al., 2006; Hengst et al., 2009). An opposite effect mediated via a similar mechanism is performed by some repellent signals, such as Sema3A and Slit-2, which regulate respectively RhoA or Cofilin local proteins synthesis and therefore enhancing the cytoskeletal component disassembly (Wu et al., 2005; Piper et al., 2006). In particular, the mRNA of RhoA, a small guanosine triphosphatase (GTPase) regulating focal adhesion and actin cytoskeleton, localizes in axons. Upon Sema3A exposure, RhoA is locally translated in axons, modulating the cytoskeleton and mediating Sema-3A collapse (Wu et al., 2005). Recently, it has been shown that Sema3A induces a burst in axonal translation and mediates the phosphorylation of the translation initiators factors eIF2 α , up-regulating the local protein synthesis (LPS) of a specific subset of 75 mRNAs (Cagnetta et al., 2018).

It has been shown *in vivo* that β -actin mRNA molecules docked at the branching sites in RGC axons are locally translated in "hotspots" (Wong et al., 2017) and recent high-throughput studies screened the translational state of axons (Shigeoka et al., 2016; Cagnetta et al., 2018; Bernabo et al., 2017). The translational state in *Xenopus* RGC axons has been studied by upon different guidance cue exposure (Cagnetta et al., 2018). While through polysome profiling in mice, changing in the axonal translational state in spinal muscular atrophy has been assessed (Bernabo et al., 2017). Moreover, the locally translated mRNA in RGC axons were studied using Ribotag mice *in vivo* through TRAP (translating ribosome affinity purification) (Shigeoka et al., 2016). The Ribotag mice were obtained by crossing a mice line with an HA tag on the 60S subunit ribosomal protein L22 (RPL22) (Sanz et al., 2009) with a Pax6-alpha-Cre mouse (Marquardt et al., 2001). In this way, Cre was transiently expressed in the neural progenitors in the peripheral retinal primordium inducing the HA-RPL22 expression specifically in RGCs (Shigeoka et al., 2016). Therefore, affinity purification of the translating ribosomes (axon-TRAP) on dissected Ribotag mice superior colliculus (SC) samples allows the translational profiling of the distal compartment of RGC axons *in vivo*. Using the Ribotag mice line, the authors observed that the population of locally translated mRNAs includes ribosomal and mitochondria mRNAs involved in axon maintenance, and that the translational state changes according to the developmental stage and still change in mature axons. Functional Gene Ontology (GO) enrichment analysis show "ribosome and translation" as the most-enriched axonal category (Shigeoka et al., 2016) and similar GO results were obtained in *Xenopus* RGC axons (Cagnetta et al., 2018). In a recent preprinted paper, it has been shown that those locally translated ribosomal subunits get directly incorporated into the axonal ribosomes remodeling the axonal translational state during branching (Shigeoka et al., 2018).

Even if not in the most abundant GO categories, several locally translated proteins belong to the metabolic mitochondrial pathways (Shigeoka et al., 2016; Cagnetta et al.,

2018). Intriguingly, in mice adult axons terminal mitochondrion-linked mRNAs locally translated increase, although it represents only the 5% of the total proteins synthesized at the axonal RGC level (Shigeoka et al., 2016). These observations support the idea that a subset of locally translated proteins is involved in the maintenance of mitochondrial functions. It is also of interest to note that, the translation of some mitochondrial related mRNAs occurs on endosomes in closed proximity of mitochondria themselves, resulting important for mitochondrial integrity and axon maintenance (Cioni et al., 2018). There is a close relationship between mitochondria and local translation. Indeed, not only some mitochondrial mRNAs get locally translated in axons, but the local translation itself is fueled by mitochondria and not by glycolysis during synaptic plasticity (Rangaraju et al., 2019).

Axonal ribosomes and single mRNAs were observed in the late 1990s. After the development of the high-throughput screening approaches, it has been possible to study firstly the vast repertoire of axonal mRNAs and subsequently the subset of molecules translated into axons by combining pulsed stable isotope labeling of amino acids in cell culture (pSILAC) or translating ribosome affinity purification (TRAP) with RNAseq (Shigeoka et al., 2016; Cagnetta et al., 2018). This made it possible to study the changes in axonal protein expression during development, in response to external stimuli and in a pathological context.

1.4.1 Local translation functions

The axonal protein synthesis exert different functions including the regulation of steering, branching, synaptogenesis, and survival/axonal maintenance (Cioni et al., 2018). A list of the known functions of local translation in axons, and associated transcripts has been reported in Table 1.2. Apart from the chemotropic response to guidance cues other biological functions are influenced by local translation of specific transcripts. For example, local translation is involved in retrograde signaling: signals from the growth cone to the nucleus are translated locally, ultimately regulating gene transcription in the end (Ben-Yaakov et al., 2012; Cox et al., 2008). Other transcripts regulate axon elongation and branching (Kundel et al., 2009; Thelen et al., 2012).

Local translation of axonal mRNAs regulates several intra-cellular pathways, among them are the local production of receptors involved in axon guidance, of ribosome components, of cytoskeletal components residing inside growth cone and also of proteins involved in retrograde signaling (Figure 1.7).

1.4.2 Local translation regulation

Neuronal subcompartments rely on local protein synthesis (LPS) to maintain their peculiar morphology. However, many different mRNAs are present at the axonal level, and only a subset of them are locally translation upon demand. This gives rise to the question: “How is a specific population of mRNAs selected to be translated in time and space among the total pool of neuronal mRNAs?”. The answer to this question is still largely unknown.

A mechanism regulating the translome state is indeed the control of the transcriptome state (Cioni et al., 2018). For example, at the branching state of RGC axons, there is a switch in transcriptome and translome from the elongation to the branching/pruning

Table 1.2: Roles of local axonal mRNA translation

Functions of local translation	Associated transcript
Chemotropic response to guidance cues	RhoA, β -Actin, Cofilin
axon elongation	PAR-3, β -Thymosin, ATP5G1, COXIV, ALCAM
axon branching	β -Catenin, β -Actin
axon maintenance	IMPA1, Lamin-B, ATP5G1, COXIV, Cpg15
axon/neurite regeneration	RPL4, Importin β , RanBP1
retrograde signaling: neuronal survival	CREB, STAT3
retrograde signaling: tissue patterning	Smad 1/5/8
synapse formation	CEBP-1, α -Tubulin, Sensorin

Abbreviations: RhoA, Transforming protein RhoA; PAR-3, Partitioning defective 3 homolog; ATP5G1, ATP synthase subunit 9; COXIV, cytochrome c oxidase IV; ALCAM, CD166 antigen, cell adhesion molecule; IMPA1, Inositol monophosphatase 1; Cpg15, Neuritin; RPL4, 60S ribosomal protein L4; RanBP1, Ran-specific GTPase-activating protein; CREB, Cyclic AMP-responsive element-binding protein; STAT3, Signal transducer and activator of transcription; Smad, Mothers against decapentaplegic homolog 1/5/8; CEBP-1, member of the C/EBP class of bZip factors, effectors of the *C. elegans* DLK-1 cascade. Table updated from (Deglincerti, Jaffrey, 2012)

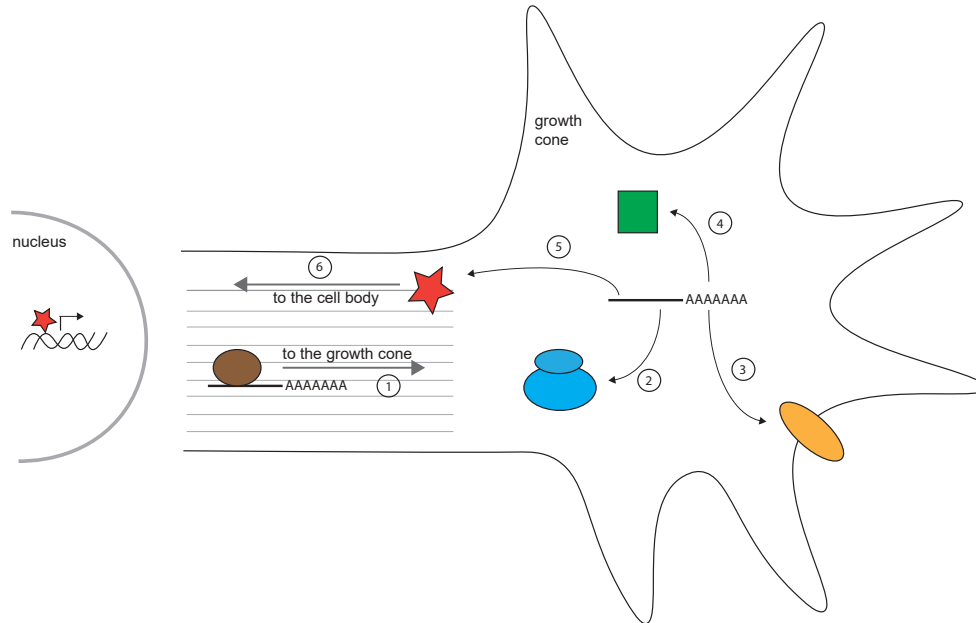
stages (Shigeoka et al., 2016). The neuronal transcriptome state can also be changed by epigenetic modifications at the DNA or histone protein levels induced by extracellular cues (Riccio, 2010).

Neuronal mRNAs population is vast and diverse, and the specific localization at the axonal level contributes in the selection of which mRNAs undergo to local translation in that specific subcompartment (Riccio et al., 2018). Different mechanism has been shown to be link with selectively translocation of neuronal mRNAs to the axonal periphery. The important role of regulatory elements in 3' untranslated region (3'UTR) mediating the for mRNAs localization has been observed in different organisms and cell types (Kislauskis, Singer, 1992) and the 3'UTR region contributes in the selection and translocation of mRNAs towards the axons (Andreassi, Riccio, 2009). Specific localization elements and motifs are of different lenght in nucleotides have been identified in mammalian 3'UTR and are necessary and sufficient for a subcellular localization in neurons (Andreassi, Riccio, 2009).

However, considering the vast population of axonal mRNAs (Zivraj et al., 2010), the spatiotemporal regulation of RNA localization in axons does not entirely explain the selectivity of local protein synthesis. Indeed the regulation of the transcriptome axonal state is unable to explain why at the same developmental stage, with identical mRNAs repertoire, only specific mRNAs are differentially regulated upon different stimuli (Cagnetta et al., 2018). Clearly, a part from regulation of the transcriptome state, other regulatory mechanism must ensure the selectivity in what is translated.

mTOR regulates the phosphorylation of many target proteins, including a binding protein of the elongation initiation factor 4E (eIF4EBP), eIF4EBP phosphorylation leads to

Figure 1.7: Local translation of axonal mRNA



Intra-cellular pathways utilizing local translation of axonal mRNA mRNAs are transported from the nucleus to the growth cone (1). mRNA transcripts in the growth cone can be used as part of the ribosome (2), can be translated into receptors and transmembrane proteins (3), into proteins with specific roles inside the growth cone (4) or into regulatory proteins (5) which are retrogradely transported to the cell body, exerting their function inside the nucleus as transcription factors (6). Figure drawn by the Author, reworked from (Deglincerti, Jaffrey, 2012).

a release of its inhibition toward the elongation initiation factor 4E (eIF4E), inducing the protein synthesis. Therefore, mTOR is a translational activator and it has been recently reported that mTOR is locally translated in axons upon injury to induce a burst in protein synthesis at the injury site (Terenzio et al., 2018). Nevertheless, how the local protein synthesis is induced and regulated in axons by external stimuli, guidance cue, development, injury and regeneration, is still largely unknown (Riccio, 2018).

RNA binding proteins (RBPs) are a class of regulatory molecule, which interact with different mRNAs determining their localization, but also regulating their local translation. Many examples of RBP are reported to regulate the local protein synthesis (LPS) in axons (Hornberg, Holt, 2013; Jung et al., 2012). An example of an RBP mediating in axon mRNA trafficking, but also mRNAs translation is SFPQ (splicing factor proline and glutamine rich). SFPQ mediates the axonal trafficking of *lmb2* and *Bcl-w* mRNAs and it was found to co-localize with ribosomes near to mitochondria in the axonal compartment (Cosker et al., 2016). In general, at the axonal level RBPs can act both as translational repressors

and activators of different mRNAs targets. Some RBPs play a role in axonal guidance processes by regulating the axonal translation of specific mRNAs in response to cue. In *Xenopus* ZBP1 regulates β -actin translation in response to Netrin-1 (Leung et al., 2006) and BDNF (Yao et al., 2006), mediating growth cone turning. Another RBP playing a role in axon guidance is FMRP (Fragile X mental retardation protein 1 homolog). In hippocampal neurons, a knockdown of FMRP reduces the collapse response of growth cones to Sema3A due to deregulation of MAP1B (Microtubule-associated protein 1B) translation in axons (Li et al., 2009).

RBPs are not the only molecules involved in axonal mRNA regulation. Non-coding RNAs (ncRNAs), and among them micro-RNAs (miRNAs), are another important population of regulatory molecules on which I focused my thesis research (Section 1.5). Intriguingly, it has been shown that RBPs and miRNAs can cooperate for the silencing of the target mRNA or compete each other for binding sites on the target (Krol et al., 2010). Therefore, both RBPs and miRNAs modulating the translation of specific transcripts during axon guidance (Iyer et al., 2014).

1.5 MicroRNAs

MicroRNAs (miRNA) are a class of small regulatory non-coding RNAs. Their length range between 18 and 25 nucleotides and they influence the stability of messenger RNAs (mRNAs) through a direct interaction, regulating the translation of the target mRNA in a temporal and spatial specific way (Ha, Kim, 2014; Bartel, 2018). Considering their locally regulation properties, these molecules might play a relevant role in axon guidance.

In this Section it will be elucidated miRNA structure, biogenesis, mechanism of action and of regulation, and what is know so far in literature about the role of these regulatory molecules in axon guidance.

1.5.1 miRNA biogenesis

In animals miRNAs genes are transcribed by RNA polymerase II in the nucleus as a RNA stem-looped structure of ≈ 100 nucleotides (Figure 1.8). The transcription gives rise to a long transcript, called pri-miRNA, that presents a 5' cap and a 3' poly A tail and that appears to be non-coding (Lee et al., 2002).

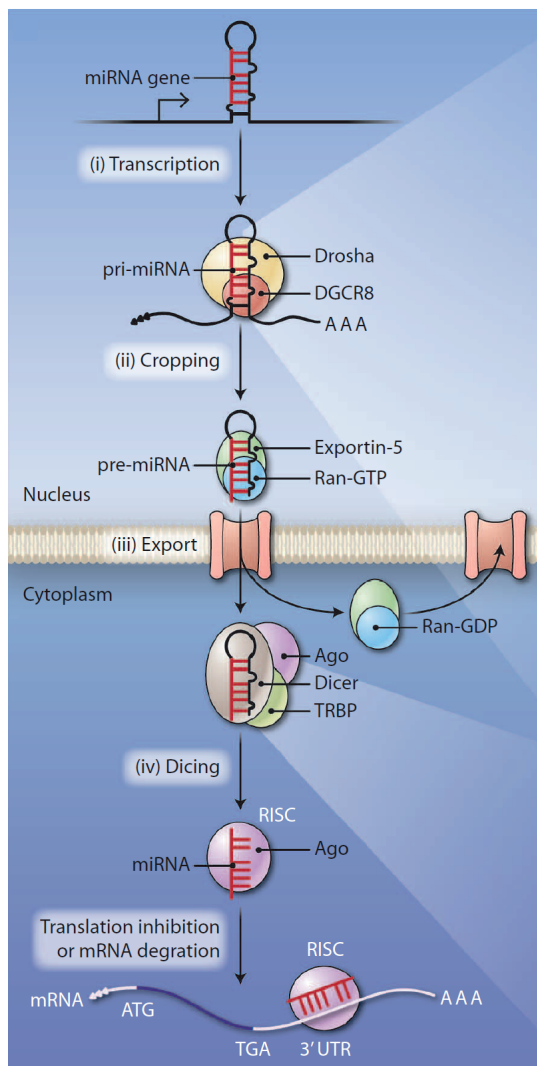
Most human miRNAs are genomically isolated, but there are also several miRNAs that are found in clusters which are transcribed and expressed coordinately (Cai et al., 2004), but all contain secondary structures organized in stem-loops which are recognized by RNase processors (Bartel, 2018). Pri-miRNAs are processed by a ribo-nucleic complex containing RNase III Drosha and the cofactor Pasha (DGCR8) in the nucleus, resulting in miRNA precursors (pre-miRNAs). A common characteristic of RNase III enzymes is that dsRNA cleavage introduces a 2 nt 3' overhang at the cleavage site (Lee et al., 2003). Pre-miRNAs have a length of around 70 nucleotides and contain a stem-loop. These precursors are exported into the cytoplasm, where the maturation is completed.

The protein Exportin-5 (Exp5) forms a transport complex with GTP binding nuclear protein (RANGTP) and a pre-miRNA. It is important to notice that as in the case of Drosha, Exp5 binding is dependent on RNA structure but independent of sequence. The Exp5/Ran-GTP heterodimer binds small RNAs with a terminal RNA stem of more than

16 bp and a short, 3' overhang; i.e., precisely the structure of pre-miRNAs (Gwizdek et al., 2001; Lund et al., 2004).

Once the pre-miRNA reaches the cytoplasm the ribonuclease Dicer, another RNase III, recognizes the 3'-ends generated by Drosha and cleaves the pre-miRNA, near the terminal loop, to produce a miRNA-5p:miRNA-3p having 2-nt 3' overhangs at both ends. The mature and active miRNA is one of the two filaments of the duplex and is about 22 nucleotides long (Starega-Roslan et al., 2011).

Figure 1.8: miRNA biogenesis



Taken from (Hata, Lieberman, 2015).

Dicer cooperates with other proteins: members of the argonaute (AGO) family and HIV-1 transactivation response (TAR) RNA-binding protein (TRBP) (Chendrimada et al., 2005). After Dicer cleavage, the RNA duplex is loaded into the Ago2 protein, which retains the mature miRNA and associates with cofactors of the GW182/TNRC6 family to form the RNA-induced silencing complex (RISC) (Hata, Lieberman, 2015).

A small subset of miRNAs (less than 1%), undergo a non-canonical maturation pathway. An example is miR-451, whose maturation requires Ago2, but not Dicer activity (Cifuentes et al., 2010).

1.5.2 miRNA structure and mechanism of action

miRNAs were first described in 1993 in *C.elegans*, where they were found as non-coding regulatory small RNAs involved in developmental and differentiation processes (Wightman et al., 1993). After this discovery, many other miRNAs have been identified in viruses, plants and animals. Now, about 500 canonical miRNAs have been identified in human genome (Bartel, 2018).

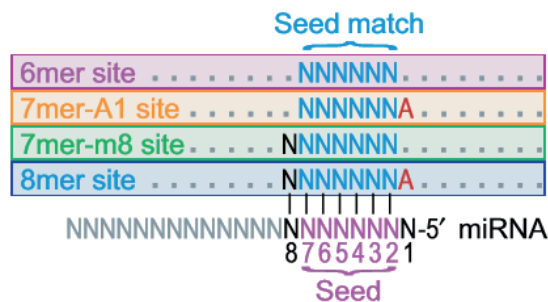
The function of the large majority of miRNAs remains unclear, nevertheless it is known that specific miRNAs play important roles in the regulation of apoptosis and cell proliferation in fruit flies, neuronal asymmetry in *C. elegans*, and hematopoietic differentiation in humans (Bartel, 2004). *C.elegans* has been the first organism in which miRNAs have been

studied, hence there are well characterized miRNAs in this model. For example, miRNAs *lin-4* and *let-7* regulate the timing of larval development in *C.elegans* by down-regulating the expression of specific target mRNAs (Reinhart et al., 2000).

Transition between different developmental stages are not only regulated in *C.elegans* by specific miRNAs expression. Probably in all vertebrate, included in human, miRNAs are expressed in a developmentally regulated or tissue-specific manner (Lagos-Quintana et al., 2002).

In any case, in order to exert its action, the mature miRNA is loaded on a ribonucleic complex called RISC (RNA Induced Silencing Complex). Loaded on RISC, the miRNA binds to a target mRNA sequence and temporally represses translation, or cleaves the target if a perfect complementarity is present (He, Hannon, 2004). The silencing mechanism via a complete degradation of the target is present mostly in plants, although exceptional cases are also present in mammals; for example, in mouse miRNA-196 mediates the degradation of *Hox8* mRNA (Yekta et al., 2004).

Figure 1.9: miRNAs seed sequence



Schematic miRNA seed-matched sites The seed sequence or seed region is a conserved sequence which is mostly situated at positions 2-7 from the 5' miRNA end. The “seed sequence” is perfectly complementary to the target. Taken from (Baek et al., 2008).

Generally in animals, miRNAs bind in a non-perfect complementary way to the 3' untranslated region (UTR) of the target mRNAs blocking the translation. Through this mechanism, miRNAs regulate the translation 60%-90% of protein-coding genes (Bartel, 2018). An individual miRNA is able to target up to a few hundred different mRNAs and is therefore able to regulate the expression of multiple and diverse proteins involved in a biological process (He, Hannon, 2004).

The miRNAs seed sequence is the region recognizing the 3'UTR of the target (Figure 1.9). Seeds have different names (e.g. 7 mer, 8 mer) depending on the number of nucleotides binding to the mRNA. The regions in the 3'UTR complementarity to the seed sequences are also known as miRNAs responsive element (MREs). As aforementioned the 3'UTR regulatory region is critical for of mRNAs translocation to axons and translation in this subcellular compartment (Andreassi, Riccio, 2009). Intriguingly, a recent preprinted paper reported that 3'UTR in sympathetic neuron axons can be cleaved by a

complex containing both Ago2 and HuD RBP (Andreassi et al., 2019). The cleavage leads to the formation of different axonal isoforms in the 3'UTR regulatory region, which in turn provides new regulatory layer of axonal local protein (Andreassi et al., 2019). This observation open new possible mechanisms also for miRNAs regulation considering the localization of MREs.

1.5.3 Mechanisms of regulation of mature miRNAs

The quantity of a specific miRNA species inside a cell depends on the rate of the biogenesis of mature forms, but also on the degradation process. Considering that miRNAs specifically regulate in time and space their targets, it is fundamental to consider how miRNAs levels are controlled inside a cell.

miRNAs are one of the more stable RNA forms, however when these molecules are implicated in the regulation of developmental stages or in critical tissue growth steps, their expression changes quickly suggesting specific regulation of miRNA stability (Rüegger, Großhans, 2012). An example of rapid turnover of miRNA expression is the miR-183/96/182 cluster, miR-204, and miR-211, in mouse neuronal cells in dark adaptation of retinal neurons (Krol et al., 2010). Those miRNAs were downregulated during dark adaptation in 3 hours due to rapid turnover, while upon return to light their levels in retinal neurons increased after only 30 minutes by an increase in the pri-miRNAs transcriptions levels (Krol et al., 2010). Considering the dynamism and the rate at which axon guidance progresses, it is important to address issues of miRNA stability and availability when investigating the role of miRNAs during brain wiring.

The enzymatic mechanisms leading to miRNAs degradation remains largely unknown (though they probably depend on exoribonucleases activity), however some examples of possible factors contributing to miRNA stability have been identified. The 3' end of many miRNAs may harbor some modifications, which either stabilize or destabilize the molecule. In particular RNA adenylation has been implicated to increase miRNA stability (Katoh et al., 2009), whereas uridylation likely inhibits miRNAs activity (Jones et al., 2009).

Besides nucleotide additions to the mature miRNA sequences, there are also internal sequences that affect the stability of the small non-coding RNA. In addition to the previously described effect of AU rich elements to increase mRNA turnover (Chen, Shyu, 1995), it was recently shown that miRNAs with a high density of AU and UA dinucleotide have the shortest half lives in primary human neuronal cells (Sethi, Lukiw, 2009), suggesting another mechanism regulating miRNA stability. In addition to the examples presented so far, also RNA-binding proteins are involved in regulating the stability of miRNAs (e.g. GW182 stabilizes miRNAs through binding to Ago proteins) (Yao et al., 2012).

Last but not least, miRNA abundance may also be regulated by other non-coding RNAs (ncRNAs). Indeed, some miRNAs bind through complementarity to ncRNAs, which act as sponges sequestering specific miRNAs and thus reducing their total amount (Ebert, Sharp, 2010).

1.6 miRNAs in brain wiring

Local translation plays a vital role in axon guidance processes (Section 1.4) . Translation of specific mRNA may in turn be regulated by miRNAs precisely in a temporal and spatial

manner (Section 1.5). miRNAs are therefore key developmental regulators, especially during the development of the nervous system, when numerous miRNAs are enriched or expressed with extreme precision (Hsieh, 2012; Zou et al., 2013). Following are presented the miRNAs' role in brain wiring and miRNAs' cellular compartmentalization.

1.6.1 miRNAs in axon guidance

miRNAs are involved in different aspects of the axon guidance. Some miRNAs play a role in long-range guidance, others are implicated in fasciculation and yet others in axon targeting (Iyer et al., 2014). miRNAs influence the navigation of the growing axons toward the target cell directly or indirectly: they can either regulate the transcriptome of the growing axon controlling the expression of receptors on its surface, or they might affect expression of cues in the target cell.

The first indication of miRNAs role in axon guidance mechanisms came from the research of Pinter and Hindges. Using a conditional deletion approach in mice, they observed aberrant axon pathfinding of retinal ganglion cells (RGCs) in homozygous Dicer mutants (Pinter, Hindges, 2010). In wild type mice RGC axons project out of the retina, cross the chiasm, and reach the target regions in brain (superior colliculus and lateral geniculate nucleus, details in Section 1.7.2). In Dicer depleted mutated mice a strong phenotype was observed at the optic chiasm, where many RGC axons fail in crossing the midline and aberrantly extending ipsilaterally or into the ventral diencephalon (Pinter, Hindges, 2010). This work demonstrates the essential role of Dicer, and therefore of miRNA function, in controlling proper RGC axonal projections into brain, and it represents the first evidence of a key role of miRNAs as regulatory molecules in axon guidance.

Fasciculation is the mechanism by which follower axons extend themselves along the pioneer axon path through axon-axon interaction. Some evidence suggest that miRNAs may also be involved in this aspect of axon guidance. Dicer mutants in zebrafish show defasciculation of some axonal tracts (Giraldez et al., 2005) and depletion of Dicer in mice also causes a defasciculation phenotype of RGC (Pinter, Hindges, 2010).

In other studies, by knocking-out specific miRNAs, the role of these small non-coding regulative molecules in axonal projections has been further investigated. For example, miR-9 depletion, in a miR-9-2/3 double knockout mouse model led to misrouting of thalamocortical (TCAs) and corticofugal axon (CFAs) tracts (Shibata et al., 2011). In following years Lin-4 (miR-125) was reported to regulate long-range guidance, specifically the axonal projection of anterior ventral microtubule (AVM) neurons in *C.elegans* (Zou et al., 2012) (Table 1.3).

At the end of their journey, growing axons reach and innervate their target. miR-124, for example, ensures the correct stalling of RGCs at their target the optic tectum in *Xenopus laevis* (Baudet et al., 2012) (Table 1.3). The molecular mechanism at the basis of this regulatory process is an inhibition of CoREST, at the right time and place, which modulates RGC axonal response to Semaphorin 3A. BDNF promotes RGCs axonal branching within the target region in the brain, and it induces the upregulation of miR-132 in retinal cultures (Marler et al., 2014). miR-132 targets p250GAP, a Rho family GTPase-activating protein, and through the inhibition of its target miR-132 acts downstream of BDNF promoting branching (Marler et al., 2014). Han and collaborators have presented miR-30b as regulator of axonal outgrowth in RGCs by inhibition of Semaphorin 3A expression

Table 1.3: miRNAs involve in axon guidance

miRNA	mRNA target	Species	Neuron type	miRNA effect on	Reference
lin-4	LIN-14	C.elegans	AVM	long-range cue	(Zou et al., 2012)
miR-124	CoREST	X.laevis	RGC	targeting	(Baudet et al., 2012)
miR-134	Xlimk1	X.laevis	Spinal	cue response	(Han et al., 2011)
miR-132	p250GAP	chick, mouse	RGC	cue response	(Marler et al., 2014)
miR-30b	Sema3a	X.laevis	RGC	outgrowth	(Han et al., 2015)
			RGC	apoptosis	(Han et al., 2015)
miR-182	Cofilin	X.laevis	RGC	targeting	(Bellon et al., 2017)

Abbreviations: CoREST, REST corepressor; Xlimk1, LIM domain kinase 1; AVM, Anterior Ventral Microtubule; LOF, Loss Of Function; lin-4, miR-125; RGC, Retinal Ganglion Cells. Updated from (Iyer et al., 2014).

(Han et al., 2015). Loss of miR-182 in *Xenopus laevis* RGC axons leads to targeting defects *in vivo* and a failure of these axons to respond to Slit-2 (Bellon et al., 2017). miR-182 silences Cofilin-1 in basal conditions and its repression is relieved upon Slit-2 stimulation (Bellon et al., 2017) (Table 1.3).

Some recent studies have performed a screening of axonal miRNAs applying different profiling techniques (Natera-Naranjo et al., 2010; Zhang et al., 2013; Sasaki et al., 2014; Hancock et al., 2014; Bellon et al., 2017). The miRNAs that have been identified, the methods used, the cellular and the animal models utilized, have been summarized in Table 1.4.

1.6.2 Compartmentalized activation of miRNAs

Recent evidence highlighted the compartmentalization of miRNA expression within cells. However, not only the miRNAs themselves were proposed to locate to specific subcellular compartment but also the enzymes mediating their final maturation step, Dicer.

In 2005 Dicer and RISC components were shown to be present in somatodendritic parts of large neurons in adult mouse brain (Lugli et al., 2005) and numerous studies have reported the presence of Dicer within mammalian growth cones (Hengst et al., 2006; Zhang et al., 2013; Aschrafi et al., 2008; Vargas et al., 2016; Kim et al., 2015; Gershoni Emek et al., 2018; Hancock et al., 2014). Hengst and colleagues demonstrated that Dicer and other protein involved in RNA interference are present at the growth cone level of cultured dorsal root ganglion (DRG) cells in rat (Hengst et al., 2006). Intriguingly, selective local inhibition of RhoA mRNA expression at the growth cone affects normal collapse behavior in response to Sema3A, underlining a possible role of local regulation by RNA interference (Hengst et al., 2006). The role of Dicer at different developmental retinal stages have been highlighted by several experiments in which the enzyme mediated the miRNAs maturation was deleted (Reh, Hindges, 2018). Dicer deletion causes a spectra of aberrant retinal phenotypes, included in RGCs (Iida et al., 2011; Georgi, Reh, 2010) and RGC axons projection (Pinter, Hindges, 2010). Dicer presence and function in neuronal subcompartment leads to the possibility of a local pre-miRNAs processing.

Table 1.4: miRNAs found enriched in axons and growth cone profiling during axonal development

miRNA	Species	Neuron type	Methods used
(Natera-Naranjo et al., 2010)			
let-7c, miR-125b, miR-103, miR-127, miR-15b, miR-16b, miR-185, miR-204, miR-221b, miR-23a, miR-23b, miR-24, miR-26a, miR-320, miR-329, miR-382, miR-541	Rat	SCG	Microarray and RT-qPCR
(Zhang et al., 2013)			
miR-18a, miR-19a, miR-92	Rat	Cortical	RT-qPCR
(Sasaki et al., 2014)			
miR-181a-1b, miR-361, miR-532b, miR-685, miR-709, miR-720	Mouse	Cortical	Multiplex RT-qPCR
(Hancock et al., 2014)			
let-7-e, miR-106a, miR-125a-5p, miR-132b, miR-138, miR-17, miR-182, miR-191, miR-19b, miR-24, miR-29a, miR-30b, miR-30c, miR-328, miR-342-3p, miR-384-5p, miR-434-3p, miR-484, miR-495, miR-680	Mouse	DRG	RT-qPCR

Data reported in the Table are re-elaborated from (Iyer et al., 2014).

The first miRNA precursor observed in a specific subcellular compartment has been pre-miR-134 (Bicker et al., 2013). In dendrites of hippocampal neurons, locally enriched pre-miR-134 may be a local source of the mature form of the corresponding miRNA, involved in brain plasticity and synaptic protein synthesis. In 2018 the same research group demonstrated that the dendritic accumulation of pre-miR-134 is tightly regulated with BDNF promoting and NMDA blocking its accumulation. Furthermore, synthetic miR-134 is able to rescue BDNF-dependent dendritogenesis when pre-miR-134 trafficking is reduced. (Zampa et al., 2018). Precursors of miRNA are not only present in dendrites but also in axons (Kim et al., 2015; Aschrafi et al., 2008, 2012). Pre-miR-338, for example, reaches distal neurons as part of the ribonucleoprotein complex and associates with axonal mitochondria in superior cervical ganglion (SCG) neurons (Vargas et al., 2016).

Several lines of evidence have now accumulated and point to Dicer and pre-miRNA localization in dendrites and in axons. Nonetheless, so far, a single study published in 2017 showed pre-miRNA processing in neuronal subcompartments. In particular, local uncaging of glutamate activates Dicer which in turn leads to the production of mature miR-181 through local pre-miRNA processing in dendrites (Sambandan et al., 2017).

1.7 Retinal Ganglion Cells as a cellular model

So far, the axon guidance process has been presented, giving particularly importance to the local protein synthesis (LPS) in axons and to miRNAs molecules as possible key regulators in this mechanism. This section will introduce the cellular model I used to study the role of newly generated miRNAs (NGmiRNAs) in brain wiring: the Retinal Ganglion Cells (RGCs). These particular cells connecting the retina to the brain are the only type of neurons projecting out of the retina. Those neurons transmit the information from the external world through visual processing to the cognitive part of the brain. RGCs serve as a good model for both axon guidance as well as subcellular compartmentalization. Indeed, RGCs have to navigate several pathfinding events occurring along their path to their final target.

I used two animal models to study miRNAs role in RGC brain wiring: mouse and *Xenopus laevis*. Despite the fact that differences in the global organization of the visual system exist between the two organisms under study, critical decision points during RGC pathfinding persist. Following, the developmental stages corresponding to key steps along the RGC axon's journey will be described in more detail.

1.7.1 From the retina to the brain: the RGCs' journey

The retina is the innermost tissue layer of the eye, it is part of the central nervous system, and it transduces the light from the environment into RGC action potentials, leading to visual perception. The retina is organized in layers, and the inner layer of the retina is the ganglion cell layer (GCL) where RGC bodies are located (Scalia, 1976).

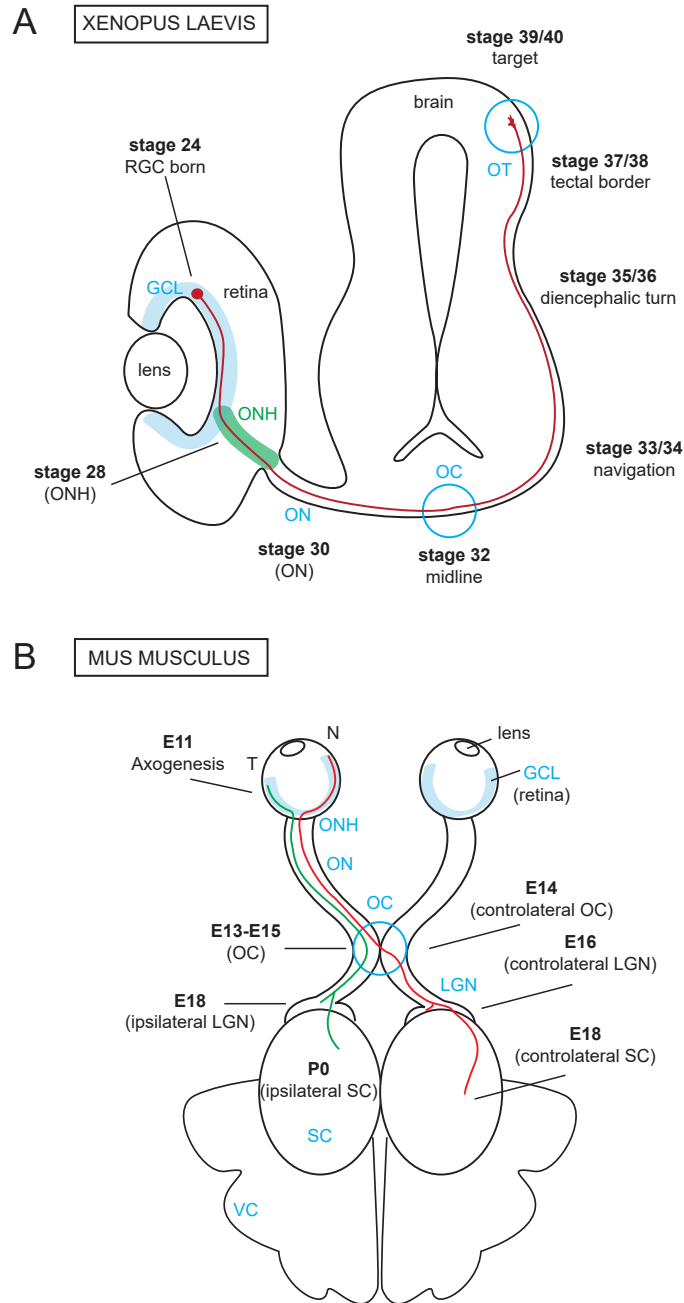
The GCL represents the starting point of the RGCs journey toward the brain, indeed from this layer RGC axogenesis occurs. In *Xenopus*, RGCs are born at stage 26 and RGC axons start extending from the dorsocentral part of the retina around stage 27 (Holt, 1984; Dingwell et al., 2000). In mouse, on the other hand, RGCs are born on embryonic day 11 (E11) (Dräger, 1985; Bovolenta, Mason, 1987).

At stage 28, pioneers *Xenopus* RGC axons grow along the vitreal surface of the retina and then exit through the optic nerve head (ONH) forming the optic nerve (ON). At stage 30 they enter the brain through the ventral diencephalon (McFarlane, Lom, 2012). While in mice, the pioneer axons begin to grow into the diencephalon at stage E12.5 (Erskine et al., 2000), with the first axons arriving at the optic chiasm at stage E13, however they do not cross the midline until stage E14-E15 (Bovolenta, Mason, 1987; Colello, Guillery, 1990).

Xenopus RGC axons cross into the contralateral brain at the optic chiasm at stage 32 (McFarlane, Lom, 2012), thereupon they travel up dorsally till the mid-diencephalon, where they drastically turn caudally at stage 35/36 to reorient themselves towards the tectum, their final target (Dingwell et al., 2000). The tectal border is reached at stage 37/38 (McFarlane, Lom, 2012), and at stage 40 the majority of the pioneers RGC axons have reached their target. There the growth cones undergo dramatic morphological changes, begin to branch and arborize and, at later stages, form synapses with tectal neuron partners (McFarlane, Lom, 2012; Dingwell et al., 2000).

In mice, contralateral axons first reach their target regions (lateral geniculate nucleus, LGN and superior colliculus, SC), from stage E16 onward, while at E16 the ipsilateral

Figure 1.10: RGC journey in *Xenopus laevis* and *Mus musculus* animal model



The RGC journey from the retina to the brain target (A) Cross section of *Xenopus laevis* retina and brain. A single RGC axon projection is depicted from axogenesis to stage 39/40 when axons reach their final target, the optic tectum. The Figure was reworked from (Dingwell et al., 2000). (B) Schematic representation of the visual pathway in the mouse. Contralateral RGCs (red), ipsilateral RGCs (green). The Figure was reworked from (Erskine, Herrera, 2014). Abbreviations: GCL, ganglion cell layer; ONH, optic nerve head; ON, optic nerve; OC, optic chiasm; OT, optic tectum; N, nasal retina; T, temporal retina; LGN, lateral geniculate nucleus; SC, superior colliculus; VC, visual cortex; E11, embryonic day 11; P0, postnatal day 0.

projections are, at this stage, still in the proximal optic tract. The latter only grow into LGN and SC from E18 till birth (Godement et al., 1984). RGC axons invade the SC, branch, and ultimately start forming synapses after birth between P0 and P12, with the peak of axonal branching at P3 (Hindges et al., 2002). All the developmental stages presented are schematized in Figure 1.10.

Xenopus and mouse differ also in the way the topographic map is established in the target region (optic tectum and superior colliculus respectively). In both cases, the RGCs axons arborize in the target region mapping the retina: temporal-nasal (T-N) axis of the retina is mapped along the anterior-posterior (A-P) axis of the target region in the brain, and the dorsal-ventral (D-V) along the lateral-medial (L-M) axis (McLaughlin et al., 2003). However, even if the general map retina-target region is the same in both animal model there are important differences between the two.

In mouse at the superior colliculus the growth cones stop at different position according to the Ephrins levels and start branching from the axon shaft (interstitial branching). In the termination zone (TZ) axons start arborize and the overshooting axon portions get eliminated. A portion of RGCs undergoes to death and refinement occurs within the TZ (McLaughlin et al., 2003). While, in frogs when RGC axons reach the tectum they form branches from the basal part of the growth cone and then from those arbors are formed. In this case there are not overshooting axons to eliminate. Moreover, another difference is that in frogs the tectum expand during RGC axonal projection development, it is still in expansion during the arborization phase, and the termination zone is refined as the tectum enlarged (McLaughlin et al., 2003).

1.7.2 Retinotectal pathway

Several key decision points of axonal pathfinding lie along the retinotectal pathway which are common among different organisms: RGCs move towards the optic nerve head (ONH) and exit the eye, cross the midline at the optic chiasm (OC), recognize the target and innervate it.

After axogenesis in the retinal ganglion cell layer (GCL), RGC axons orient and extend along the ganglion cell fiber layer toward the optic nerve head (ONH) and project out of the retina. The RGC axons exit the eyes forming the optic nerve (ON) and the RGCs axons from the two eyes meet at the optic chiasm (OC) (Dingwell et al., 2000) (Figure 1.10). After a navigation phase, the RGCs reach their target, recognize it, stop there, arborize and form a topographical map. The target regions are the optic tectum (OT) in *Xenopus laevis*, lateral geniculate nucleus (LGN) and superior colliculus (SC) in *Mus musculus* (Figure 1.10).

The optic chiasm is a key point in the axon guidance process. Here, the RGC axons coming from the nasal retina (N) travel to the opposite part of the brain (contralateral axons), while the axons from the temporal retina (T) do not cross the optic chiasm, instead they turn and innervate the same brain hemisphere (ipsilateral axons). The proportion between contralateral and ipsilateral projections vary in different organisms, according to the position of the eyes and the degree of binocular vision overlap (Jeffery, Erskine, 2005). The eyes are positioned frontally in primates, and the number of contralateral and ipsilateral axons is approximately the same. The eyes in mice are positioned more laterally than in primates and the degree of overlap of binocular vision decreases. Therefore, also

the proportion between the two type of projections varies: only 3-5% of RGC axons project ipsilaterally in mice (Dräger, 1985). In *Xenopus* tadpoles the visual fields of the two eyes do not overlap and ipsilateral projections are completely absent during the first developmental stage. They first appear at about stage 54 (Hoskins, Grobstein, 1985).

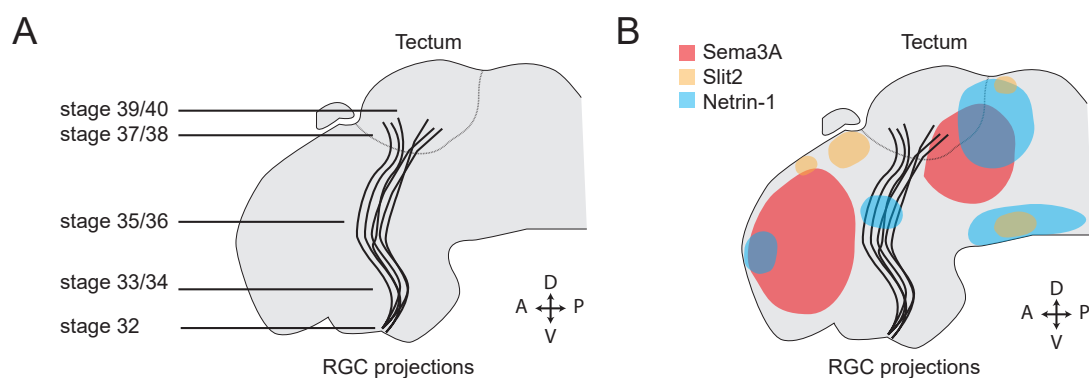
1.7.3 Guidance cues along *Xenopus laevis* retinotectal pathway

During the RGCs journey towards their final target in the brain, many guidance cues are directing the axonal projection along the right path (Section 1.2.5). Following, I have reported the brain localization of the main RGCs guidance cues in *Xenopus* in relationship with the specific developmental stage.

In situ hybridization on whole mount *Xenopus* brain showed that Sema3A is expressed at the anterior boundary of the optic tract where axons bend caudally towards their target at stage 35/36, and in the posterior part of the tectum, reached by RGCs at stage 37/38 (Campbell et al., 2001) (Figure 1.11). Growth cones acquire responsiveness to Sema3A with age: they are not responding at stage 24, while a rapid collapse response occurs at stage 35/36, suggesting a responsive to the cue only at “older” stages (Campbell et al., 2001).

Slit-2 exerts collapse response *ex vivo* on retinal explants from stage 32 onwards (younger axons are not responsive to it), and at stage 40 *in vivo*, it expresses posteriorly and anteriorly at the boundary tectum, confining the RGC projections there (Piper et al., 2006) (Figure 1.11).

Figure 1.11: *Xenopus laevis* stages and guidance cues



Guidance cue distribution along the optic pathway Schematic of RGC optic pathway in the lateral view of *Xenopus laevis* brain. (A) Corresponding stages of RGC projections journey, Figure reworked from (McFarlane, Lom, 2012). (B) Sema3A, Slit2, and Netrin-1 guidance cue distribution along the optic pathway. Figure adapted and reworked from (Wit de, Verhaagen, 2007; Erdogan et al., 2016; Campbell et al., 2001; Piper et al., 2006). Abbreviations: RGC, retinal ganglion cells; D, dorsal; P, posterior; V, ventral; A, anterior.

Netrin-1 at the optic nerve head (ONH) exerts an attractive function (stage 28), however, once RGCs exit the eye the same cue has a repulsive effect (Shewan et al., 2002). Netrin-1 localization within the *Xenopus* brain was studied through *in situ hybridization*: a patch

of its expression was observed at the optic tract in the diencephalon (central light blue circle in Figure 1.11 B), and at the posterior boundary of the tectum (Shewan et al., 2002). This cue, in its repellent function in older stages, helps to confine RGCs superficially to the optic tract (stage 35/36), and inside the tectum (stage 37/38-40), without overshooting, at the target level.

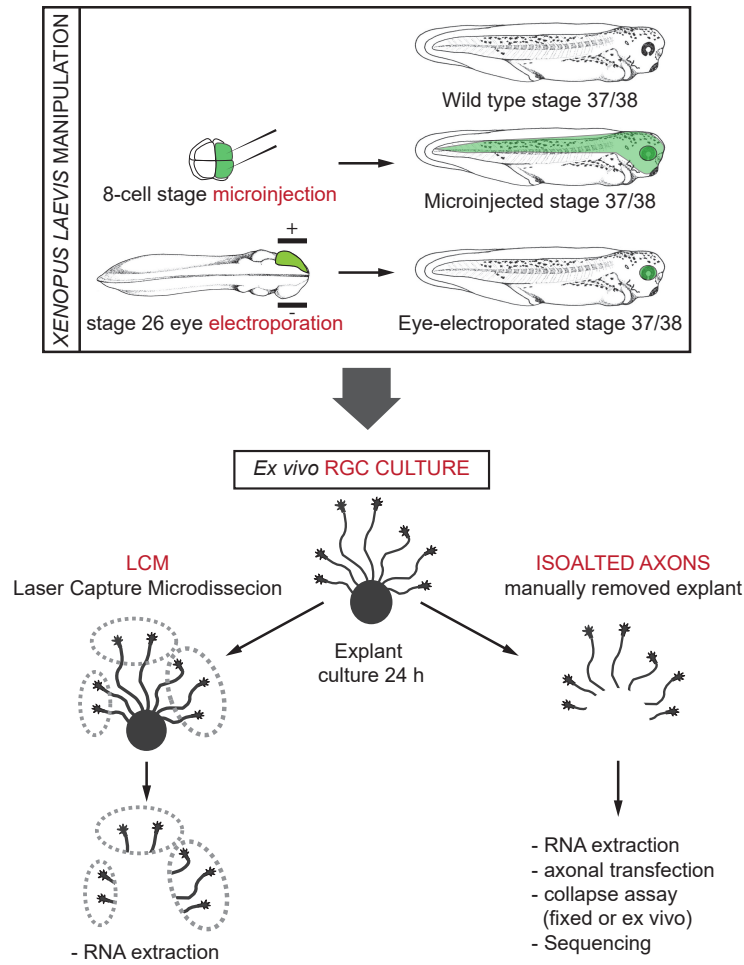
1.8 *Xenopus laevis* as model organism

Xenopus laevis is a model organism largely used in the developmental biology research. Frogs eggs are around 1.2 mm in diameter and all the embryo development occurs *ex utero*, enabling both an easy manipulation and an easy observation of early developmental stages. Moreover, plating the dissected eyes allow *ex vivo* axonal culture, and Retinal Ganglion Cells (RGCs) grow in minimal culture medium, without the external addition of growth factors or hormones (Section 3.2.3). These characteristics make *Xenopus laevis* an invaluable tool for studying brain development and axon guidance both *in vitro* and *in vivo*.

As summarized in Figure 1.12, *Xenopus laevis* were manipulated in different ways. Molecular constructs were introduced by microinjection at the dorsal animal blastomeres of eight-cell-stage (Method Section 3.2.1) or by electroporation in the eye primordial (Method Section 3.2.2). By selecting the microinjection as delivery system, the introduced molecule will be targeting the entire central nervous system (CNS), while by electroporating specifically the eye only the RGC axons will be targeted in the brains, keeping an unmodified surrounding environment in which they can grow.

The axons of the retinal ganglion cells in culture were then collected in different way (Method Section 3.2.4) and axonal RNA was extracted (Method Section 3.3.1). In culture, I also studied axonal responsiveness to different repulsive cues through collapse assay (Method Sections 3.2.6, 3.2.7) or specifically modulated the axonal subcellular compartment, by removing the explant, e.g. the soma contribution, and performed axonal transfection (Section 3.2.5). RGC axons in culture or in their *in vivo* context can be acquired, performing live imaging (Method Sections 3.2.8, 3.2.9).

Figure 1.12: *Xenopus laevis* manipulation



***Xenopus laevis* as animal model** Molecular constructs can be introduced by microinjection at 8-cells stage targeting the entire CNS or by electroporation in the eye primordial for selectively label RGC axons projecting out of the eye (targeted regions shown in green in the grown stage 37/38 embryos). The cultured RGCs axons can then be collected by LCM or after severing the explants for different purpose (listed in the Figure).

2 Project aims

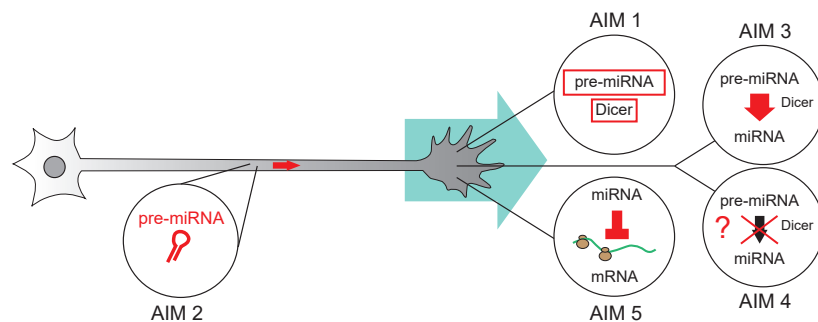
During brain wiring, axons are guided towards the proper target. Errors during this process cause abnormal neuronal connection and brain function abnormalities. Therefore, brain wiring and axon guidance events are finely tune and regulate. During axonal journey, the growth cone senses the surrounding environment and transduces the sensed cues and stimuli into modulation of the cytoskeleton components. The final result of the signal cascade is the growth cone movements (growing, turning, steering) and its pathfinding towards the final destination.

Neurons are highly polarized cells and have to maintain their morphology and to guarantee specific sub-compartmentalized functions. One mechanism to achieve this goal is the translocation of mRNAs at the axonal level, thereby regulating in time and space the proteomic state through local protein synthesis (LPS). How axonal LPS is regulated remains still largely unknown.

Intriguingly, several research groups showed axonal presence of Dicer (Hengst et al., 2006; Zhang et al., 2013; Aschrafi et al., 2008; Vargas et al., 2016; Kim et al., 2015; Gershoni Emek et al., 2018; Hancock et al., 2014), suggesting a possible local processing of pre-miRNAs into their active mature form. Therefore, the aim of this thesis is to investigate this possibility, gaining insights into LPS regulated in axons by newly generated miRNAs (NSmiRNAs).

To achieve this purpose, the following sub-aims have been identified:

Aim1	Investigate the presence of Dicer and pre-miRNAs at the retinal ganglion cell (RGC) axonal level
Aim2	Unravel possible mechanisms of pre-miRNA trafficking towards the growth cone
Aim3	Check for local miRNAs biogenesis occurrence in axons
Aim4	Explore the impact of NGmiRNAs on axons behavior
Aim5	Identify the possible mRNA targets regulated by miRNAs at the axonal level



Molecular mechanisms of axon guidance processes are of particular interest not only for the developmental biologist, but also for the study neurological disorders (Van Battum et al., 2015), and adult nervous system recovery and repair (Yaron, Zheng, 2007). Therefore, the clinical impact could be relevant, also considering that miRNA-based therapy designed to replace or to block specific miRNA in pathological conditions are emerging as new promising therapeutics (Lambert et al., 2015; Nagaraj et al., 2015; Rupaimoole, Slack, 2017). Increasing the knowledge on miRNAs mode of action and maturation could thus be useful for developing new clinical tools based on the targeted delivery and local activation of miRNAs.

3 Material and methods

Two animals models were used during my PhD project to investigate the role of pre-miRNAs in brain wiring: (FLAG-HA₂)-Dicer mice (Section 3.1) and *Xenopus laevis* (Section 3.2). C57BL6 mice with a N-terminal FLAG-HA₂ tagged Dicer (Comazzetto et al., 2014) were used to investigate Dicer localization within retinal ganglion cells (RGCs) optic tract. While *Xenopus laevis*, easier to manipulate and whose RGC axons grow from the eye in a minimum culture medium, was exploited as model system to investigate pre-miRNAs presence and role in axonal compartment. All animal experiments were approved by the University of Trento Ethical Review Committee and by the Italian “Ministero della Salute” both according to the D.Lgs nr.116/92 and with the authorization n1159/2016-PR and n546/2017-PR according to art.31 of D.lgs. 26/2014.

A separate Section has been entirely dedicated to molecular biology techniques (Section 3.3). To study non-coding RNA functions involved in axon guidance processes, several technical challenges from a molecular point of view need to be taken into account: quality and amount of axonal RNA starting material, specificity and efficiency of RT-qPCR assays, molecular manipulation of specific target through axonal transfection, primer design targeting specific gene in a tetraploid organism such as *Xenopus laevis*.

Finally, this Chapter closes describing how data have been analyzed (Section 3.5) and which bioinformatic analysis and tools were run (Section 3.6). List of reagents, primers and oligos (Appendix B) as well as medium recipes (Appendix C) have been reported in separated appendixes to make easier the reading of this Chapter.

3.1 (FLAG-HA₂)-Dicer mice

C57BL6 mice with a N-terminal (FLAG-HA₂) tagged Dicer were generated by Comazzetto et al. in 2014 through loxP recombination (Comazzetto et al., 2014). They created this model in order to study Dicer localization using anti-HA antibody, since specific antibodies against the HA-epitope are available (Comazzetto et al., 2014; Much et al., 2016).

Mice were kindly donated by Donal O’Carroll and were housed in a temperature- and humidity-controlled room, in small cages housing maximum five animals each, at the Department of Cellular, Computational and Integrative Biology (CIBIO, University of Trento). The colony was increased in number and maintained, in accordance with the *Decreto Legislativo 4 marzo 2014, n°26*.

For mice breeding, the Jackson Laboratory guidelines were followed (www.jax.org): C57BL6 mice mating age range from 6-8 weeks to 8-9 months of life, gestation is around 20 days and the weaning was therefore performed after the 21st day of live. Before mating, males were divided in different cages and single males was maintained alone for few days before mating. Male and females were then separated after a week and not return until pups are weaned. In the first two weeks of life of the pups, new metallic tags were applied to the animals ears and sampling for genotyping performed. For genotyping,

small piece of tails were sampling until the first 17 days of the mouse life, where the cartilage of the tail is not yet formed and it can be cut without causing suffering to the animal, while if the sampling occurred later, ear were used instead to minimize animal pain (Hankenson et al., 2008). Tag and sampling for genotyping are services offered by the Model Organism Facility (MOF) at CIBIO, while colony expansion and maintenance, breeding planning, weaning, time point pregnancy and sampling for experiment, are tasks of the users. On the 21st day from birth, the new litters were weaned, separating the new born males and females. After the establishment of an inbred colony, samples collection for the experimental procedures has started.

In (FLAG-HA₂)-Dicer mice, Dicer localization was assessed at two different developmental stages: embryonic day 13.5 (E13.5), when RGCs reach the optic chiasm (Bovolenta, Mason, 1987; Colello, Guillery, 1990), and post-natal day zero (P0) when RGCs start innervating the targets (Hindges et al., 2002). Time point pregnancy is necessary to correctly defined the embryonic stage. Therefore, pregnancies in mice were set up by determining the stage of female estrous cycle, identifying the appropriate time for mating. At that point, two females were placed with a male, and the day after male was separated from females, vaginal plugs were checked as control of mating occurrence, and this time it was considered E0.5 developmental stage. At the embryonic stage of interest, the pregnant dams were euthanized by CO₂ exposure followed by cervical dislocation, pups were removed from the amniotic sac and euthanasia of individual fetuses was induced by decapitation with surgical scissors. P0 mice have been euthanized by decapitation since at this stage they are still resistance to hypoxia and physical methods are recommended to ensure death (Pritchett et al., 2005).

3.1.1 Mice genotyping

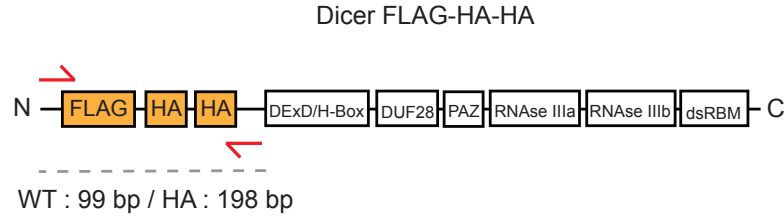
Mice genotyping were performed in order to validate the animal model in different phases of the work: initially during the expansion of the colony, then on samples from the animals used in the experimental procedure, and finally in a phase of refreshment of the genetic background of the inbred mice. A refresh of the transgenic mouse strain is suggested by the Jackson Laboratory guidelines after 5 generation of inbreeding, since spontaneous mutations might arise in the colony of mice. A back-cross with WT mice will genetically refresh the obtained progeny.

Initially for the characterization of the mice model, a phenol-based DNA extraction was performed and samples were sequenced after PCR (Nucleospin Carlo Erba Reagents kit used for PCR gel extraction and Eurofins service for sequencing). However, phenol-based DNA extraction is time consuming, and alkaline lysis was tested as quicker alternative (details on protocols are reported below). The disadvantage of this second procedure is storability since it does not include a step of purification from nuclease and DNA could therefore be degraded during long storage time (Klitschar, Neuhuber, 2000). Hence this protocol was chosen when PCR was run immediately after extraction.

A schematic of Dicer gene carrying a FLAG-HA₂ tag at the N-terminal, with small arrows indicating primers used for genotyping, is reported in Figure 3.1.

Phenol-based DNA extraction Mice small piece of the tail or of the ear were stored at -80°C in 1.5 mL tubes until used. For DNA extraction, disruption of tissue was

Figure 3.1: Dicer schematic



Schematic of FLAG-HA₂-Dicer Red arrows indicate primers used for the genotyping spanning the FLAG-HA₂ region. Dicer is a multidomain protein (represented in the small box along the gene): two conserved catalytic RNase III domains are RIIIA and RIIIB, both helicase (DEXD) and PAZ (Piwi/Argonaute/Zwille) domains, and two double stranded RNA binding domains (DUF28 and dsRBM).

achieved by adding 50 μ L of digestion buffer with proteinase K (Ambion, 0.5 mg/mL final concentration) and by incubating the samples overnight at 55°C gently shaking (400 rpm). The digestion buffer was composed by 50 mM Tris-HCl pH 8.0 (Sigma), 100 mM EDTA pH 8.0 (Sigma), 100 mM NaCl (Sigma), 1% SDS (Sigma) and autoclaved milliQ H₂O to reach the final volume. High temperatures, chaotropic salts contained in the buffer, and detergents (such as SDS) help to denature proteins, which are in this way more exposed to proteinase K cut. Indeed, this is an enzyme which is stable at high temperature, cleaves the peptide bond in proteins thereby digesting contaminant proteins and DNase which might damage the nucleic acid of interest.

The day after, following the tissue disruption, proteinase K (Ambion) was inactivated by sample incubation at 70°C for 5 minutes. The rest of the procedure was carried out on ice. In order to separate nucleic acid from the contaminants a phenol extraction was performed. Basic pH phenol is preferred for DNA sample collection, since ensure DNA stratification into the aqueous phase instead to the organic one (Sambrook, Russell, 2006). Hence, 50 μ L of Phenol:Chloroform:Isoamyl alcohol pH 6.7-8.0 (Invitrogen) were mixed with each sample. After a quick spin of 2 minutes at 15000 rpm the sample stratified into three phases: an upper one containing the aqueous phase with the nucleic acids, an interphase with the denatured proteins and a bottom one, with the phenolic phase containing lipids and proteins enriched in hydrophobic aminoacids in their composition. Therefore, the top phase was collected and transferred to a new tube. To increase the quality of the DNA, another extraction step was performed by adding the same volume of the transferred supernatant of Phenol:Chloroform:Isoamyl alcohol pH 6.7-8.0 (Invitrogen). After another centrifuge, the top phase was transferred.

Finally, DNA was recovered from the aqueous phase by mixing the samples with Sodium Acetate (NaOAc, Sigma) (1:10 of the starting volume, final concentration 0.3 M), and isopropanol (Sigma) in the same volume of the starting one, and kept for 1 hour at -80°C. Then, samples were spun for 30 minutes 13000 rpm at 4°C collecting the DNA in bottom part of the tubes. Supernatant was removed and the pellet was washed with 1 mL 70% ethanol (Sigma). This final washing step was needed for desalting the sample. After ethanol removal, samples were dried and resuspended in 20 μ L TE buffer 1x and incubated

for 15 minutes at 65°C . The concentration of the collected DNA samples were measured by NanoDrop.

NaOH DNA extraction When DNA was directly used as input for PCR without any storage period nor further preparation for sequencing, a quicker procedure was used to extract DNA and check mice genotype. In few hours DNA extraction was obtained by combining alkaline lysis and heating of the sample.

In particular, $50\ \mu\text{L}$ of NaOH 50 mM (Sigma) were added to each sample tube and incubated 1 hour at 95°C gently shaking (400 rpm). After 30 minutes incubation, samples were vigorously vortexed to help homogenization. Tubes were incubated for few minutes at 4°C and $5\ \mu\text{L}$ of 1M Tris-HCl pH 8 (Sigma) were added to the samples for neutralizing the basic solution. If the the alkalinity of the mixture is not decreased, the polymerase enzyme for PCR would be inhibited. Following Tris-HCl addition, samples were mixed and centrifuged at 5000 rpm for 10 min to collect remaining debris at the bottom of the tube. $4\ \mu\text{L}$ of the supernatant were used directly as input for PCR reaction (for details on PCR reaction refer to 3.3.4).

3.1.2 Immunohistochemistry on mice sections (IHC)

Immunohistochemistry (IHC) is a technique which makes possible the study of protein localization exploiting the recognition of specific antigens by fluorescent labeled antibodies.

There are multiple protocols for IHC staining consisting in steps for sample preparation, sectioning and for sample staining. The following sections will present those steps, each of them has been optimized for mice, considering this animal model was never used before in our laboratory. All recipes of buffers and reagent used for IHC, as well as the heat inactivation goat serum (HIGS) preparation are reported in Appendix C.

Sample preparation and sectioning E13.5 whole head and P0 brains dissections were performed in PBS 1x (Gibco) at 4°C to better preserve the tissue. Samples were washed in cold PBS 1x to remove blood residual and fixed in 4% para-formaldehyde (PFA, Life Technologies) overnight with gently shaking at 4°C . After fixation, the samples were washed in 1x PBS (Gibco) three times consecutively, left for 1 hour at 4°C shaking in PBS 1x to remove all the PFA residuals. PFA can give fluorescence background and over-fixation can cause conformational changes of the tissue (Watkins, 1995), hence PFA incubation and washing steps were optimized accordingly.

After fixation the sample were transferred in 30% sucrose (ACS reagent) solution shaking at 4°C until sunk. Sucrose was removed as much as possible (also by absorbing it with a piece of paper), then samples were moved in OCT (Tissue Freezing Medium, Leica) and incubated for 30 minutes, then they were embedded and stored at -80°C until sectioning.

Sectioning was performed using Leica CM 1850 UV cryostat after 1 hour temperature equilibration of the block at -20°C . An equilibration at the cryostat temperature is important for preserving the integrity of the sections during cut. Thickness of sections was fixed at $14\ \mu\text{m}$ and the orientation was selected according to the sample. E13.5 samples were sectioned horizontally, while P0 brain sagittally. Sections were collected on Superfrost Plus Microscope Slides (Thermo Fisher Scientific).

IHC protocol After sectioning, the slides were let dried for 30 minutes, washed twice in PBS 1x (Gibco) for 5 minutes and once in TPBS 1x (0.1% Triton 100x (Fisher Chemical) in PBS) for 10 minutes at room temperature. Antigen retrieval was performed in a preheated steamer for 25 minutes by immersion of the slides in 10 mM sodium citrate buffer pH 6 (ACS reagent). A first set of staining was performed without antigen retrieval step, however adding this high temperature treatment the fluorescence background was reduced and the signal to noise ratio improved.

Slides were cooled in the buffer by leaving them 45 minutes at room temperature. Sections were permeabilized by three consecutive washes of 5 minutes in TPBS. Sections were blocked with 300 μ L 10% HIGS (Gibco) for 2 hours at room temperature. Rabbit anti-HA Y-11 (sc-805, 1:50, Santa Cruz Biotechnology) was used to stain Dicer-HA, mice anti-neurofilament (3A10, 1:500, Developmental Studies Hybridoma Bank, DSHB) was used to track neurons. Primary antibodies were incubated overnight at 4°C in a humidified chamber. After three washing steps in TPBS of 5 minutes each, secondary antibodies Alexa 488 anti-rabbit or 594 (F(ab')₂ fragments) anti-mouse (Life Technologies) were used at 1:1000 and incubated 1 hour at room temperature in the dark. Sections were washed three times in TPBS for 5 minutes each, and counterstained with nuclear marker ToPro (T3605, 1:1000, Molecular probes). The nuclear staining was washed by three steps in TPBS of 5 minutes each, and slides were mounted with 40 μ L ProLong Gold Antifade Mountant without DAPI (Molecular Probes). Slides were stored at room temperature in the darkness and visualize at the confocal Leica TCS SP5 or SP8 microscope within a week.

Imaging Slides were acquired at the confocal Leica TCS SP5 microscope (Figure 4.3, 4.5 A) and confocal Leica SP8 with white light lasers (Figure 4.5 B). All images were acquired through sequential scanning between frames. Format: 1024x1024, speed 100 Hz, line average: 2, frame average: 8. Laser intensity, gain and offset were optimized for best signal to noise ratio and these settings were maintained throughout acquisitions and for all conditions. For Figure 4.5 A, a 40x objective was used and a zoom factor of 3 applied during acquisition. The signal was detected by a photomultiplier tube (PMT) after selecting the emission wavelength range by a monochromator to avoid any possible bleedthrough between channels (Figure 4.4). In particular laser 488 (495-570); laser 543 (565-625); laser 633 (650-790).

For Figure 4.5 B, a 40x objective with a zoom factor of 1.99 was used and a Z-stack of 6-14 μ m depth applied in order to capture the axons projections. Excitation wavelength for the three channels were: 491 nm (Dicer), 590 nm (neurofilament), and 633 nm (To-Pro).

3.2 *Xenopus laevis*

Xenopus laevis embryos were obtained through *in vitro* fertilization and kept at 14°C in 0.1x MMR buffer. The developmental stages were identified according to (Nieuwkoop, Faber, 1994).

3.2.1 Microinjection

Morpholino mixtures were injected into both dorsal animal blastomeres of eight-cell-stage embryos as described previously (Leung, Holt, 2008). Specifically, jelly coat from embryos was manually removed with fine forceps (dejelling). Dejelling was done at the 4-cell stage using dejelling solution for 5 minutes (0.2 M Tris pH 8.8 and 0.2 M DTT in water). Embryos were then washed three times in 0.1x MMR and transferred into an injection dish containing 4% Ficoll (Carl Roth GmbH) prepared in 0.1x MMR to enable them to sink and were aligned such that the dorsal blastomeres faced the glass capillary injection needle (1.0 mm outer diameter (OD) x 0.5 mm internal diameter (ID), Harvard Apparatus). Once embryos reached 8-cell stage 1 nL mixture (described below for all different experiments) were injected using a pressurized microinjector (Picospritzer). Following injection, embryos were transferred to 0.1x MMR and kept at 14°C. At the neurula stage (stage 19), embryos were sorted to check for fluorescence.

The microinjected morpholino mixture composition and concentration is specified in Figure legend and morpholinos sequences reported in Appendix B (Table B.1).

3.2.2 Electroporation

Electroporation is a technique for delivering molecules within cells applying an electric field which leads to cells permeabilization. This delivery system has been optimized for targeting *Xenopus laevis* eye primordia (Falk et al., 2007). The design of specific sylgard chambers, the electrodes and micro-manipulators at a fixed position, permit the correct target of the eye primordia and enable the reproducibility of the electroporation.

Preparing and loading capillaries Borosilicate standard glass capillary with an internal diameter of 0.50 mm (Harvard Apparatus) were fixed in a glass micropipette puller (Narishige, PC-10). A dual heating step of 65°C first and 60°C then were applied. Capillaries were back-filled with 2 µL of the molecule of interest using micro-loader tips (Eppendorf), then fixed in the micromanipulator and open under the microscope with tweezers.

Xenopus laevis eye electroporation Stage 24 embryos were dechorionated and washed once in 0.1x MMR. Electroporation was performed at stage 26 (or stage 28 for the *in vivo* FRAP experiment Figure 8.12). Before electroporation, few embryos were rinsed at a time in 1x MBS and anesthetized in 1x MBS + MS222 (0.2%). The anesthetized embryos were placed into an home-made T shaped electroporation chamber, belly up, as previously described (Falk et al., 2007). The right eye primordia faced the positively charged electrodes towards which the plasmids, negatively charged, were diffusing. The plasmid injection was followed by 8 electric pulses of 50 ms duration, with an interval of 1000 ms between each and the construct was delivered at 18 V (2 pulses only in Figure 8.12). The pressure per square inc (PSI) was set at 40 PSI. After electroporation the embryos were rinsed and kept in 0.1x MMR at 14°C. After 24-48 hours from electroporation, the adequate electroporation of the construct was checked at a fluorescence microscope.

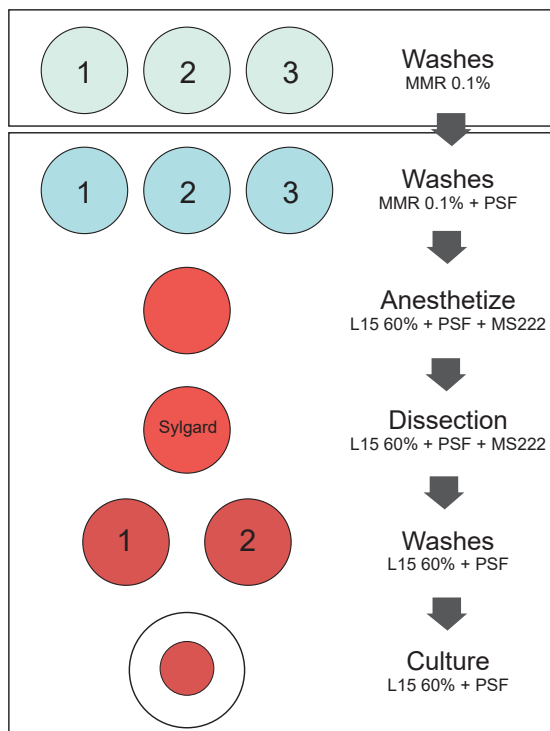
I electroporated different plasmids for my project, and the concentration have been optimized for each experiment. Cloning procedure used to obtain the plasmids is described

in Section 3.4, while composition and concentration of electroporated morpholino cocktail or plasmid mixture is specified in Figure legends.

3.2.3 RGC culture

Retinal Ganglion Cells (RGC) axons can be cultured on different support previously coated. In particular, glass coverslips (Bellco) were used for collapse assay (Figure 6.7), while for all the other experiments glass-bottom dishes (MatTek) were used as support. MatTek dishes are optimized for life imaging and the bottom glass is fixed in the plate allowing an easier manually cut of the explants than any other supports.

Figure 3.2: Organoculture protocol



Glass coverslips (Bellco) or glass-bottom dishes (MatTek) were coated with poly-L-lysine (Sigma, 10 $\mu\text{g}/\text{mL}$ diluted in ddH₂O (double distilled water)) for three hours or overnight at 20°C, washed three times with ddH₂O and dried under the hood for at least 10 minutes. Poly-L-lysine was applied to the glass surface to make it positively charged. This leads to an increase in electrostatic interaction between the glass surface and the laminin, thus improving cell attachment. Afterwards, plates were coated with laminin (Sigma) 10 $\mu\text{g}/\text{mL}$, diluted in L-15 medium 100 % (Gibco), for one hour at room temperature, followed by two washes with 60% L15 cultural medium (diluted in ddH₂O) and 1% Antibiotic-Antimycotic (Thermofisher). Plate coating and culture were done in a sterile environment as well as culture medium preparation (for their recipes refer to Appendix C).

Embryos were washed three times in 0.1% MMR (10x MMR in ddH₂O) before their transfer into the sterile environment of the hood, and before dissection, embryos were washed other three times in 0.1% MMR (10x MMR in ddH₂O and 1% Antibiotic-Antimycotic).

Embryos were then anesthetized with 0.3 mg/mL MS222 (60% L-15 in ddH₂O, 1% Antibiotic-Antimycotic and MS222 (Sigma)). Anesthetized embryos were secured laterally with custom made pins on a sylgard dish. Both eyes (in case of wild type condition or microinjected embryos) or electroporated eyes were dissected, washed twice in 60% L-15, plated on the pre-coated dishes containing culture medium and cultured at -20°C for 24 hours in 60% L-15 and 1% Antibiotic-Antimycotic (different culture time than 24 hours are specified in Figure legend). All steps are graphically summarized in Figure 3.2, in the Figure the color red indicates MS222 presence in the medium.

For each support different volume of PLL, laminin and culture medium were applied (Table 3.1).

Table 3.1: Culture support - PLL, laminin, cultural medium volume

	10 $\mu\text{g}/\text{mL}$ PLL	milliQ washes	10 $\mu\text{g}/\text{mL}$ laminin	L15 60% + PSF
Coverslip	500 μL	1 mL	200 μL	500 μL
MatTek 35 mm	300 μL	500 μL	200 μL	300-200 μL
MatTek 50 mm	1.5 mL	2 mL	1 mL	1.5 mL
RNase free POL	2 mL	2 mL	1 mL	1 mL

3.2.4 RGC axonal sample collection

In order to collect axonal samples different strategies were used: *ex vivo* Laser Capture Microdissection (LCM) and isolated axon. LCM allows a pure axonal preparation but axons should be fixed to be laser-cut and the yield of the RNA extracted is therefore quite low, ranging between 100 to 200 pg/ μL . The manual removal of the explants (isolated axon preparation) enables to have *ex vivo* alive axons for 1.5 hours and by RNA extraction the yield range between 1.5 ng/ μL to 5 ng/ μL , depending on the number of cultured explants and the cut efficiency. I have personally set up this second sample preparation in our lab, obtaining an axonal RNA quality and amount which allow also sequencing analysis.

Laser Capture Microdissection (LCM) 60 dissected eyes from stage 37/38 embryos were cultured on RNase free POL (Polyester) membranes (Leica) with 1 mL 60% L-15 medium (Gibco) for 24 hrs. The following day, cultures were stained with FM-1-43FX dye (Thermo Fisher) for 20 minutes in order to visualize axonal processes and to visualize fibroblasts and cell bodies. Following staining, cultures were fixed in 1% PFA (Life Technologies) for 5 minutes and subjected to ethanol (Sigma) dehydration (25%, 50%, 75%, 90% and 100%) for 1 minute each. Axons were captured using the Leica microdissector LMD6500 and collected in tubes containing lysis buffer RL (Norgen) with -mercaptoethanol (Sigma, 1:100). The settings used were: Magnification: 20X and 40X, Power: 33-38, Aperture: 1, Speed: 16-14, Specimen Balance: 0, Offset:50.

Isolated axons by explants manually removal After 24 hours culture of stage 37/38 RGC axons, the 35 to 50 explants were manually removed. To remove the explants, axons were cut using two pins (0.20 mm) at the stereomicroscope: first the explants were cut by scratching the eye surrounding with short and perpendicular movements, then once dislodged the eye was moved away from the axons. All explants were removed from the plate using a p10 pipette in order to remove as little medium from the plate as possible. The complete experimental procedure was concluded within 1.5 hours after the first cut. Before RNA extraction or axonal stimulation five consecutive washes steps of 300 μL (MatTek 35 mm) or 1 mL (MatTek 50 mm) culture medium were applied.

3.2.5 Axonal transfection

Stage 37/38 explants were cultured in 300 μL L15 60% + PSF (culture medium) on 50 mm MatTek dishes for 24 hours at 20°C. Morpholinos were thawed on ice, incubated at 65°C for 5 minutes to dissolve aggregates, mixed by vortexing and diluted in the culture medium at an intermediate concentration of 6 μM . 110 μL of the prepared dilution were incubated with 1.1 μL of NeuroMag Transfection Reagent (OZ Biosciences) for 20 minutes. During the incubation time, axons were severed from the explants and eyes were removed from the plate. 100 μL of culture medium were removed from the plate and replaced by 100 μL of NeuroMag reagents and morpholino mixtures, obtaining a 2 μM final concentration. The culture dish with the axons was incubated for 15 minutes on the magnetic base (OZ Biosciences) at room temperature following the manufacturer's instructions.

After transfection the plates were incubated for 30 minutes at 20°C, followed by three consecutive washes of 200 μL culture medium without perturbing the axons in the plate. Then, a 10-minute stimulation with 200 ng/ μL Sema3A (R&D System) or PBS (Gibco) was applied. For collapse assay the cultures were fixed as described below (See 3.2.7), while for RNA extraction four more consecutive washing steps with 400 μL 1x PBS (Gibco) each were applied, followed by removal of 1x PBS and addition of the lysis buffer (refer to axonal stimulation (3.2.6) and RNA extraction (3.3.1) for details). The complete experimental procedure was concluded within 1.5 hours after the first cut, a timing that is critical for axonal transfection. Plates were processed in groups of 2 plates each to preserve axonal healthy and respecting the timing of the protocol. The order of the plates were randomized in the different independent experiment.

Axonal transfection morpholino mixtures are reported in Figure legend, and morpholinos sequence are in Appendix B (Table B.1).

3.2.6 Axonal stimulation

Chemotropic cues were resuspended in sterile 0.1% protease-free BSA (Sigma), stored at -80°C, thawed on ice right before dilution preparation and usage. Intermediate dilution of cues were prepared in 1x PBS pH 7.4 (Gibco), to obtain in the culture dish a final concentration of 200 ng/mL. The final cue concentration in MatTek 50 mm dishes containing 1.5 mL medium was obtained by removing 200 μL of culture medium from the plate and replacing with 200 μL of cue intermediate stock at 1500 ng/mL. While, in MatTek 35 mm dishes containing 300 μL , the final concentration was obtained by removing 50 μL of culture medium and replacing with 50 μL of cue intermediate stock at 1200 ng/mL. In controls unstimulated plate, the same volume of culture medium was replaced by 1x PBS pH 7.4 (Gibco).

The appropriate concentration of a given cue was identified through testing each for protein synthesis dependency using a collapse assay on coverslips combined with the translational blocker cyclohexamide (50 μM CHX, Sigma) (Sema3A Figure 6.7; Slit2, (Bellon et al., 2017)). CHX was diluted in 1x PBS pH 7.4 (Gibco) and applied to the dish 2 minutes before cue exposure. In the corresponding negative control dish, in which translation was not block, 50 μL of PBS 1x (Gibco) were added instead of CHX. Each stimuli (Sema3A or Slit2, R&D System) was applied for 10 minutes and later washed out with five consecutive 1x PBS (Gibco) washing steps. At the end of the procedure, axonal health and quantity were quickly checked at the microscope and RNA were extracted.

3.2.7 Collapse assay

Collapse assay is an *ex vivo* test on axons to investigate cue responsiveness (Campbell et al., 2001). Growth cones were considered collapsed when they possessed no filopodia, or two or fewer filopodia each shorter than 10 μm (Campbell et al., 2001). 10-16 explants were cultured per condition in all the independent experiments run.

200 ng/mL human recombinant Sema3A-FC (R&D System), Slit2 (R&D System) or PBS (Gibco, for control) were bathed to explant culture for 10 minutes and then fixed in 2 % paraformaldehyde (PFA, Life Technologies), 7.5 % (wt/vol) sucrose (ACS reagent) diluted in PBS (Gibco) for 30 minutes. After 30 minutes in the fixative solution, three washes steps of 400 μL PBS 1x (Gibco) each were performed. 200 μL PBS 1x were remaining in the plate during the counting at the microscope.

To avoid subjective bias, all collapse analysis was done blind to experimental condition. For isolated axon preparations, axons closer than 100 μm to the cut, as well as explants with less than 50 % of the starting grown axons, were excluded from the count.

3.2.8 Fluorescence Recovery After Photo-bleaching (FRAP)

Ex vivo Electroporated embryos with mRFP and Venus noUTR/Venus-3'UTR of interest were raised until stage 37/38 and culture on 14 mm MatTek dishes. For Figures 8.8, 8.9, 8.9, 8.13, axons were imaged using a PerkinElmer Spinning Disk UltraVIEW ERS, Olympus IX81 inverted spinning disk confocal microscope, 60X UPLSAPO objectives (NA 1.3), with Hamamatsu C11440-22CU camera. The labeled axons were visualized with 561 nm-laser 250 ms exposure time (mRFP) and 488 nm-laser 200 ms exposure time (Venus). The filter setup used for acquisition were: Venus- 525/50; mRFP-445/60, 615/70 dual-band filter; Dichroic-405/488/561/640. Axons were photo-bleached with a 488 nm-laser maximum laser power with the following settings: 60 for PK cycles; 1 for PK step size; 8000 ms for PK spot period; 2 for PK spot cycles; Small for PK spot size; None for PK attenuation. Images for both mRFP and Venus were acquired before photo-bleaching, immediately after photo-bleaching, and then each minute for 10 minutes. Each image was captured with a Z-stack of 0.5 μm and an imaging depth of 2 μm .

For Figure 8.10, the labeled axons were visualized with an inverted TILL Photonics iMIC2, using a UPLSAPO 60x/1.2 water-immersion objective and a AVT Stingray F145B.30 fps as detector. Axons were photo-bleached with a 488 nm-laser 30% laser power with the following settings: dwell time ($\text{ms}/\mu\text{m}^2$) 1; scan line optimum; line overlapping 41%; ROI loop count 1; experiment loop count 10. mRFP and Venus were visualized using an oligochrome Xenon arc lamp epifluorescence. The filter setup used for acquisition were: Venus ex 482/18 and em 525/45; mRFP ex 563/9 and em quadband 446/523/600/677. Images for both mRFP and Venus were acquired before photobleaching, immediately after photobleaching, and then each minute for 10 minutes. Each image was captured with a Z-stack of 0.5 μm and an imaging depth of 3 μm .

In control experiments, the protein synthesis was blocked with 100 μM cyclohexamide (CHX, Sigma), diluted in the cultural medium, and incubated for 30 minutes in the culture dishes before imaging (Wong et al., 2017). In control experiments where eyes were severed from grown axons, explants were manually removed right before each FRAP experiments (Figures 8.9, 8.9, 8.13) or right before axonal transfection (Figure 8.10). In

the stimulated conditions with Sema3A, the cue was added to the cultures immediately after photo-bleaching (post-photobleaching timepoint 0).

In vivo Electroporated embryos with mRFP and Venus noUTR/Venus-TUBB3 3'UTR WT and MRE mutated were raised until stage 40/41 and prepared for live imaging (Wong et al., 2017). In particular, embryos were anesthetized with 0.3 mg/mL MS222 (Sigma) in 1X MMR, placed in a sylgard dish and secured with a custom made pin on their left side part. The part of the brain, contralateral to the electroporated eye, was exposed by removing the epidermis and the skin layers. Then the electroporated eye was removed in order to avoid trafficking from the soma to the RGC axonal compartment (Figure 8.12). Embryos were washed in 0.1 mg/mL MS222 (Sigma) in 1X MMR once and mounted on an oxygenated chamber, obtained by superimposed two Gene Frame (ThermoFisher) on Nunc Permanox slides (ThermoFisher) filled with 0.1 mg/mL MS222 (Sigma) in 1X MMR. Two/three embryos were mounted per chamber and acquired using a PerkinElmer Spinning Disk UltraVIEW ERS, Olympus IX81 inverted spinning disk confocal microscope, 60X UPLSAPO objectives (NA 1.3), with Hamamatsu C11440-22CU camera. Each image was captured with a Z-stack of 0.7 μm and an imaging depth of 7 μm (Figure 8.12).

3.2.9 Live imaging: pre-miR trafficking

Live imaging was performed inverted Leica Dmi8 epifluorescence microscope coupled with a sCMOS monochromatic camera (AndorZyla 4.2 Megapixel) and with a HC PL Apo CS2 63x/1.4 immersion oil objective. The acquisition mode was set to 12-bit grayscale and “low noise” gain mode for fluorescence and “high well capacity” for phase contrast. No binning was applied to the acquisition. Exposure time and light intensity were chosen to optimize the signal to noise ratio, but were always kept invariant for the same batch of analysis. Exposure time was kept as low as possible (100-150 ms). Time-lapses for pre-miR-181a-1 trafficking analysis consisted of 150 to 300 consecutive frames recorded continuously, for a total time of 17 to 44 s, respectively, with a 0.144 s delay between two consecutive frames, while it consisted of 130 frames per channel for co-trafficking with CD63. The distal end of single axons was chosen by the phase for imaging, strictly avoiding bundles, and had to comprise a stereotypical growth cone. The selected axon segment had to be at least 50-100 μm to the growth cone and at least 100 μm far from the soma.

Endogenous pre-miRNA was tracked using a Molecular Beacon (MB) designed and validated by Antoneta Gavoci and Michela Rocuzzo from the lab. MB sequence is reported in Appendix B (Table B.1). Exogenous pre-miR was *in vitro* labeled using Label IT Nucleic Acid Labeling Kit (Mirus) by Irene dalla Costa and Michela Rocuzzo from the lab. In the results Chapter 5 my contribution on this part of the work has been clearly stated.

3.3 Molecular Biology: from RNA extraction to RT-(q)PCR

3.3.1 RNA extraction

Single Cell RNA Purification Kit (Norgen) was used to extract RNA from axonal samples. Culture medium was removed from the cultured axon and 200 μL of the lysis buffer (Buffer

RL, Norgen) mixed with β -mercaptoethanol (Sigma, 1:100) was added to the axonal culture and incubated for 5 minutes. The lysate was transferred in a new tube, 120 μ L of absolute ethanol added and mixed by vortexing for 10 seconds. RNA binding to column and column washing steps were performed following the manufacturer's instruction. RNA was eluted by applying twice 9 μ L Elution Solution to the column, collected in low binding RNase free tubes and stored at -80°C .

Total RNA from eye were extracted using Norgen Total RNA Purification Micro Kit (#35300) following the manufacturer's instructions and running an on-column RNase free-DNaseI treatment (Norgen). For small fraction RNA collection the Split kit (Lexogen) was used, following manufacturer's instruction.

3.3.2 Quantity, quality and purity of the RNA axonal samples

Quantity and quality of the axonal RNA was assessed through Bioanalyser - Agilent RNA 6000 Pico Kit. The kit consists into a chip where a matrix is loaded into the wells providing a platform for high sensitivity microfluidics-based automated RNA electrophoresis. Following manufacturer's instruction 1 μ L of each RNA sample was run on a chip, assessing the RNA integrity number (RIN) and concentration (Figure 6.1). The concentration of the RNA sample obtained from isolated axons range from 1.5 ng/ μ L to 5 ng/ μ L, with a RIN between 6 and 8.

The RIN is computed by an algorithm written by Agilent and evaluates the RNA integrity based on the ratio between the area under the 28S and 18S rRNA peaks of the Bioanalyzer electrophoretic trace. The RIN value ranges from 1 to 10, with 10 corresponding to the least degraded RNA samples and 1 to the completely degraded ones. RNA samples with a RIN below 5 are considered as highly degraded, and not suitable to obtain reliable qPCR data (Fleige et al., 2006). For RNA-seq or microarray experiments a RIN higher than 7 is considered as good threshold for selecting high quality RNA samples (Heumüller-Klug et al., 2015).

Axonal purity was checked by PCR (Section 3.3.4): in a pure axonal sample, β -actin is expected to be present, while Microtubule-associated protein 2 (Map2) and Histone 4 (H4) should be absent. Map2 is normally expressed at the dendrite level, whereas H4 is a nuclear transcript (Bellon et al., 2017).

3.3.3 RNA retrotranscription

RNA from LCM or isolated axons was extracted and retrotranscribed to check pre-miRNAs' presence in an extreme pure axonal preparation by normal PCR (Section 4.2). Pre-miRNAs' maturation was assessed on axonal samples deriving from manual severed explants (isolated axons) exposed to cue before extraction and measuring both pre-miRNA and miRNA levels by RT-qPCR (Section 6.2). Below the amount of RNA retrotranscribed, as well as the cDNA input in the PCR reaction, refer to these two different experimental approaches.

3-5 μ L axonal RNA from LCM or isolated axons, or 10 ng total RNA from eye samples were retrotranscribed with SuperScript IV (Thermofisher) using random hexamers primers (Euroclone) following the manufacturer's instructions. The final 20 μ L reaction were incubated for 10 minutes at 23°C , followed by 10 minutes at 54°C and 10 minutes at 80°C .

Gene specific miRNA retrotranscription was performed with TaqMan MicroRNA Reverse Transcription Kit (Thermofisher) and the TaqMan qPCR assay (Thermofisher) following the manufacturer's instructions. TaqMan retrotranscription reaction cycle: 30 min at 16°C, 30 min at 42°C, and 5 min at 85°C.

In all the retrotranscriptions performed, a no template control was run. This control, in which the enzyme is present, but the template is absent, allow us to investigate the possible contamination in the mix or primer used for the reaction. A no enzyme control is needed to check for genomic contamination. This kind of control was run in all the reactions regarding retrotranscription of eye and brain RNA samples, in which even if a DNase treatment was applied, we wanted to ensure the absence of gDNA in the starting material. For axonal sample collected both by LCM or by the manual removal of the explants, the no enzyme control was not routinely included in the reaction for two reasons. First, because of the limitation in amount in the starting material, and second because genomic contamination in axonal RNA is unlikely to occur and it is indirectly checked by the systematic axonal purity test. Indeed, if MAP2 or H4 were amplified it could be an indication of contamination from cell body and those samples are not consider to be pure and therefore not used for subsequent analysis (for axonal purity test refer to 3.3.2). When the amount of axonal RNA was sufficient a no enzyme control was run for the retrotranscription reaction.

Different amount of RNA samples were retrotranscribed and the cDNA obtained was diluted prior to PCR or qPCR analysis (amount of RNA, dilution factor and input in PCR and RT-qPCR reaction are reported in the Table 3.2).

Table 3.2: RNA input and cDNA dilutions

Sample	RNA input *	Dilution factor	cDNA input in 10 μL
Eye	2 μL	1:3 (1:10)	1-2 μL
Isolated ax	2.5 μL	1:3 (1:10)	2-2.5 μL
Ax LCM	4 μL	1:2	3.5 μL
RGC LCM	4 μL	1:2	3.5 μL

* The minimal amount of 1 ng RNA input was always respected, and no more than 10 ng (10 ng for eye samples) were used as input in the retrotranscription, as indicated in the manufacturer's instructions.

3.3.4 PCR and gel visualization

2 μL 1:3-1:10 diluted cDNA (from isolated axon preparation, dilution depending on the amount of starting material), or 3-4 μL undiluted cDNA (from LCM axonal collection) were used as input for GoTaq G2HotStart Polymerase (Promega) PCR reaction following manufacturer's instruction. For mice genotyping, a small piece of tail was collected post-mortem, DNA was extracted by alkaline lysis and heating of the sample (Section 3.1.1) and 4 μL of the supernatant were used directly as input for PCR reaction. The general PCR cycle used was: 95°C for 3 minutes for enzyme activation, following by 35 cycles of 90°C for 30 seconds, annealing temperature (Ta) for 30 seconds, 72°C for 30 seconds, and

a final extension of 5 minutes at 72°C. Primers list and annealing temperature used are reported in the Appendix (Table B.1).

The entire reaction volume (20 µL) was loaded in a 2 % TAE (Euroclone) or 3 % TBE (ThermoFisher) agarose gel (Sigma Aldrich), run at 5.5 V/cm for 1 hour on an electrophoretic apparatus (BioRad) and visualized with UVITec Alliance LD2. The DNA was stained with Clear Sight DNA Stain (Bioatlas).

3.3.5 RT-qPCR

Pre-miRNA expression levels were investigated using Power SYBR Green PCR Master Mix (x2) (Applied Biosystem) and 0.25 µL of each 10 µM primer (all primers sequence and annealing temperature used are reported in Table B.1). qPCR cycling were run on BioRad CFX96 as following: 10 minutes at 95°C for denaturation, 35 cycles of 10 seconds at 95°C (denaturation), 35 seconds at the specific annealing temperature. A melting curve (65°C to 95°C increasing by 0.5°C each 5 seconds) was run at the end of the cycle to assess amplicon specificity.

For miRNA amplification, TaqMan Universal Master Mix II (ThermoFisher) was used with the following TaqMan MicroRNA Assay (4427975 or 4440886): miR-181a-5p (ID: 000480); miR-181a-1-3p (ID: 004367-mat); miR-181a-2-3p (ID:005555-mat); miR-182 (ID: 000597) and snU6 (ID: 001973). qPCR cycling were run on BioRad CFX96 following manufacturer's instructions.

3.4 Plasmids

The plasmids pCS2+Venus, pCS2+Venus+ACTB 3'UTR and pCS2+mRFP were provided by Christine Holt (Department of Physiology, Development and Neuroscience, University of Cambridge, UK). pCS2+mRFP were used as counterstain to trace axons after photobleaching, while the Venus construct was used to investigate local translation of specific candidates of interest through FRAP experiments. pCS2+Venus was used as control (no UTR), changes in axonal translation were assessed with pCS2+Venus+3'UTR wild type and pCS2+Venus+3'UTR whole miR-181 MRE(s) had been mutated for the following selected candidates: TUBB3 chL (Xelaev18022595m.g), APP chL (Xelaev18011533m.g), and THBS1 chL (Xelaev18042667m.g). The 3'UTR were cloned into the pCS2 Venus plasmid between monomeric Venus coding sequence and polyA signal.

3.4.1 Wild type 3'UTR and mutated fragments amplification

Total mRNA from stage 37/38 eyes was extracted with Total RNA Purification Micro Kit (Norgen) and reverse transcribed with SuperScript III First-Strand Synthesis System (ThermoFisher) using 50 µM Oligo(dT) primers (Euroclone). 150 ng cDNA were used in input in normal PCR reaction with Q5 High-Fidelity DNA Polymerase 2x Master mix (NEB). For each fragment to be amplified, two 50 µL reactions were run with 1 µL a pre-mixed forward and reverse primers 10 µM. Mutated fragments were amplified using primers containing the MRE mutation at the 3' or 5' end. PCR cycling conditions were: 2 minutes at 98°C for denaturation, 35 cycles of 10 seconds at 98°C (denaturation), 30 seconds at specific annealing temperature (T_{an}), extension at 73°C with different time

accordingly to the amplicon length, 2 min at 72°C for the final extension. Primers used for 3' UTR amplification with each specific annealing temperature (T_{an}) are reported in Appendix B (Table B.1).

3.4.2 Joining the mutated fragments and amplicon purification

The mutated fragment after gel extraction and purification (QIAquick Gel Extraction Kit, Qiagen) were joint through overlapping-extension PCR (OE-PCR). In particular, purified equimolar concentration (0.15 pmol) of each fragment were incubated with Q5 high fidelity 2x master mix (NEB) in absence of primers in a 40 μ L reaction volume applying the following PCR program: 2 minutes at 98°C for denaturation, 15 cycles of 10 seconds at 98°C (denaturation), a cool-down step of 20 second from 65°C to 55°C, and a final step of extension of 1 minute at 72°C. With this reaction cycle the mutated fragments annealed to each other and worked as long primers for the PCR reaction. After the 15 cycles, 1 μ L of the external forward (10 μ M) and reverse primers (10 μ M) was added and other 20 PCR cycles were run to amplifying the joint fragments. For all the candidates, the general PCR setting remained as just described, a part from the annealing temperature which were optimized for each gene (App: 66°C; Thbs1: 60°C; Tubb3: 65°C) and a final extension of 2 minutes at 72°C were applied. App gene has 1 miR-181 MRE, Tubb3 gene has 2 MREs, and Thbs1 has 3 MREs. Two out of the three MRE in THBS1 were mutated through OE-PCR, while the third site, close to the 5' end of the amplicon was inserted by Q5 mutagenesis kit (NEB), described below.

Wild type 3'UTR amplicons and OE-PCR products were purified on column with QIAquick PCR Purification Kit (Qiagen) following manufacturer's instructions and 2 μ g were digested for 1 hour at 37°C with 2 μ L SnaBI (NEB), 2 μ L XbaI (NEB) enzymes, 8 μ L CutSmart buffer (NEB), in a 80 μ L volume volume. After digestions, the fragments were run on TAE 0.5 x 1.8% agarose gel (Sigma-Aldrich), bands were cut out and purified with QIAquick Gel Extraction Kit (Qiagen), and quantified at the NanoDrop.

3.4.3 Plasmid digestion and ligation

10 μ g pCS2+Venus plasmid were digested first with 5 μ L XbaI (NEB) in 100 μ L final volume, using 10x CutSmart as buffer (NEB), for 1 hour at 37°C. Then, the first enzyme was inactivated with 20 minutes at 65°C and afterwards the second cut was performed incubating the plasmid for 1 hour at 37°C with 8 μ L SnaBI (NEB) in a 150 μ L final volume, adding 5 μ L of CutSmart (NEB). Sequential digestion increased the cut efficiency, decreasing the background of the transformation. Following manufacturer's instruction a 30 minutes incubation with Alkaline Phosphatase (CIP, NEB) enzyme was carried at 37°C. Proper digestion was assessed on a TAE 0.5 x 1.8% agarose gel (Sigma-Aldrich), the band was cut out and purified with QIAquick Gel Extraction Kit (Qiagen) following manual instructions. For the ligation step, 50 ng of the digested and purified vector were incubated with the insert of interest (mutated or wild type 3'UTR) in a 1:3 molar ratio, 2 μ L of T4 DNA Ligase Buffer (NEB) and 1 μ L T4 DNA Ligase (NEB) in a final 20 μ L reaction volume. The mix was incubated at 16°C overnight, heat-inactivated for 10 minutes at 65°C.

3.4.4 Transformation and colonies screening

The ligated plasmid and insert was chilled on ice and 1 μL were used in the transformation reaction with 25 μL high-efficiency NEB 5-alpha Competent *E. coli* cells (C2987, NEB). Cells were kept on ice for 30 minutes without mixing, followed by a heat shock at 42°C for 30 seconds. After 2 minutes on ice 100 μL SOC media (NEB) were added to the cells and the vial was shaken vigorously (250 rpm) at 37°C for 60 minutes. After 1 hour, 100 μL of transformed cells were plated on pre-warmed selection plate (Ampicillin, Sigma) and grown at 37°C overnight. A negative control plate with cells transformed with vector only was used as reference. The day after, from the plates of interest, 20 colonies were picked and grown overnight in 15 mL LB (Fisher BioReagents) with 100 $\mu\text{g}/\text{mL}$ Ampicillin (Sigma). Plasmid extraction was performed with QIAprep Spin Miniprep Kit (Qiagen) following the manual instructions and a first screening was performed through digestion at 37°C for 1 hour of the obtained plasmids (5 μL plasmid, mixed with 10x CutSmart buffer (NEB) in a 30 μL final volume). Different combination of endonuclease (NEB) was used accordingly to the 3'UTR (APP: Hind III HF and XbaI; THBS1: Hind III HF; TUBB3: Hind III HF) (Figure 8.5). The plasmids found positive in the first screening were sequenced. After confirming by sequencing the occurrence of the correct transformation, cells were grown overnight shaking (250 rpm) at 37°C and plasmid purified using QIAfilter Plasmid Midi Kit (Qiagen).

3.4.5 Q5 site-direct mutagenesis kit (NEB)

Thbs1 contains a miR-181 MRE in the initial portion of the 3'UTR and it was not possible to mutate it by OE-PCR. Indeed, considering the vicinity of the MRE to the 5' end of the 3' UTR, it was not possible to design a forward primer for OE-PCR which allows both amplification of the 3'UTR and the introduction of the mutated MRE. Hence, once I mutated 2 out of the 3 MREs of the plasmid, the third mutation was inserted using Q5 site-direct mutagenesis kit (NEB) and two specific primers design with NEBaseChanger online tool (NEBaseChanger.neb.com). Primers sequences are reported in Appendix B (Table B.1). Mutagenesis reaction was performed following manufacturer's instruction, using 25 ng of input plasmid, 1.25 μL of each primer (at 10 μM), in a final PCR reaction volume of 25 μL . 1 μL of the reaction product was then mix by pipetting with 5 μL KLD buffer (NEB) and 1 μL KLD enzyme mix, in a 10 μL final reaction volume and incubated 5 minutes at room temperature. 2.5 μL of this reaction was used to transformed 5 μL competent cells (C2987, NEB) as described above.

3.4.6 Plasmid sequencing and mutagenesis assessment

The correct insertion of the 3'UTR of interest into pCS2-Venus plasmids was checked by sequencing. The occurrence of miR-181 MRE mutagenesis was examined, paying attention in not having inserted new MREs in the mutated region. Mutated MREs were kept at the same length of the wild type in order to not disrupt the 3'UTR structure and the introduction of new MREs created by the insertion of the mutation was checked by BLAST in miRBase and avoided in the final construct. In particular, the reverse complement of all the possible combination of new 7 mer created by the insertion of the mutation were searched by sequence in miRBase (<http://www.mirbase.org/search.shtml>) using SSearch

method and an E-value cut-off of 2000. All the output alignments were checked and if there were matching to the seed sequence (2-8 position) to any miRNAs, the absence of that specific miRNA in RGC axonal sequencing data (Bellon et al., 2017) was verified.

3.5 Data analysis and statistics

All data were analyzed with Prism (GraphPad 6 or 7) and all experiments were performed in at least three independent biological replicates. A batch of embryos from different fertilized frog was considered as an independent biological replicate. For all tests, the significance level was $\alpha = 0.05$. * $p < 0.05$, ** $p < 0.01$, *** $p < 0.001$, **** $p < 0.0001$, ns: non-significant. Exact number of replicates, tests used and statistics are reported in Figure legend.

3.5.1 RT-qPCR

For RT-qPCR quantitative analysis, cycle threshold (Ct) were defined with CFX96 BioRad software v3.1, as mean of three technical replicates per sample. All technical replicates have a standard deviation smaller than 0.35. All Ct values are smaller than 35. Amplification efficiency of the new designed primers (pre-miR-181a-1/a-2 and pre-miR-182) were investigated with standard curves independently from the actual experiments (Figure 6.3). To calculate miRNA or pre-miRNA differential expression, ΔCt method (Schmittgen et al., 2008) was applied as follows:

$$2^{-\Delta Ct} = 2^{-(Ct_{miR_x} - Ct_{U6})} \quad (3.1)$$

Each experiment was run for at least three different independent biological samples. T-test (if data were normally distributed) or Mann-Whitney test (for non-parametric data) were computed on the ΔCt mean comparing stimulated and unstimulated axonal samples or morphants and controls.

Standard curve Serial 1:2 dilutions were prepared starting from eye cDNAs 400 ng. The dilutions were run on BioRad CFX96 with the same amplification program described in the previous paragraph. The efficiency of an assay should be 90-105%. The efficiency of the reaction is calculated from the slope of the standard curve using the following formula:

$$E = 10^{\frac{-1}{\text{slope}}} \quad (3.2)$$

Efficiency is normally expressed as a percentage.

$$\% \text{ Efficiency} = (E - 1) \times 100\% \quad (3.3)$$

An efficiency of 100% means that the amount of the PCR product will perfectly double at each cycle ($E = 2$).

$$\% \text{ Efficiency} = (2 - 1) \times 100\% \quad (3.4)$$

Efficiency was evaluated for the new designed pre-miRNAs primer. Another important parameter is the regression coefficient R^2 . R-squared is a statistical measure of how close the data are to the fitted regression line, R^2 should be > 0.980 .

Moreover, replicates should give similar C_t values, assessed by evaluating C_t mean standard deviation. We set 0.35 as threshold, to be specific, when C_t mean standard deviation in a triplicate is > 0.35 the entire sample was removed.

Normalizer stability To investigate the normalizer stability in our samples, the $2^{(-Ct)}$ was calculated (Schmittgen et al., 2008), Box 6. A t-test was then computed on the potential internal control $2^{(-Ct)}$ values, statistically comparing axons stimulated (cue) vs unstimulated (PBS). The internal control was considered as stable in the dataset when the internal control gene did not vary under the experimental conditions.

3.5.2 FRAP analysis

The mean intensity of the Venus signal normalized per growth cone area was measured with Volocity 64x software (Figures 8.8, 8.9, 8.12, 8.13) or Image J (Figure 8.10), by manually tracing the terminal of RGC axons on the sum of the z-stack for that specific timepoint. During acquisition growth cones saturated for Venus signal were excluded. mRFP signal was used as reference to trace the axons. The background intensity was measured for the same area in proximity to the growth cone of interest and removed from the axonal Venus signal. From the background-corrected fluorescence intensity at each timepoint (F) the fluorescence signal after photobleaching (F_0) was removed and normalized to the fluorescence signal pre-photobleaching (F_P):

$$FRAP = \frac{(F - F_0)}{F_P} \quad (3.5)$$

Collapsed axons were removed from the analysis, considering the massive reduction of growth cone area, the mean intensity of the fluorescence signal could induce in a final misinterpretation of the data (Cagnetta et al., 2018). FRAP data were reported as curves of the recovered fluorescence signal in a 10-minute timeframe. The different curves were described by fitting the data with a nonlinear model (one-phase decay option in Prism) and differences between conditions were analyzed for statistical significance with an extra sum-of-square F test (Wong et al., 2017). Each axon acquired belongs to different explant, hence different embryos and each experiment was repeated at least three independent times. To avoid technical biases, the order of processing of the stimulation conditions with Sema3A, MO and co-MO samples, or wt and mutated were randomized both in term of organoculture and acquisition.

3.5.3 Live imaging analysis: pre-miR trafficking

Movies were mapped back onto kymographs of the live pre-miR-181a-1, MB or CD63 movement using ImageJ. The image processing software FIJI, plugin KymoReslicedWide FIJI/ImageJ plugin was used to generate kymographs from time-lapse movies, because of its high accuracy in detecting particle trajectories. For pre-miR-181a-1 trafficking studies, the specific macro tsp050706.txt for FIJI/imageJ software (author: J. Rietdorf FMI Basel + A. Seitz EMBL Heidelberg) was used, once the kymograph was obtained, to extrapolate from the tracked traces information about velocity and spatial directionality of the particles. The plugin was custom modified to also obtain particle directionality. Puncta's velocity was calculated by considering the average speed of its segmental components.

For co-trafficking analysis, the two kymographs (MB and CD63-eGFP puncta) were merged on and artificial color assigned using FIJI. Overlapping trace were considered as co-transported puncta when CD63 trace overlapped over the entire trajectory of the MB trace.

Endogenous and exogenous kymograph analysis were performed by Antoneta Gavoci, while CD63 co-trafficking analysis were computed by Irene dalla Costa. In the results Chapter 5 my contribution on this part of the work has been clearly stated.

3.5.4 MSD analysis

Region of interest (ROI) containing a segment from a single axon but not its growth cone was selected. Trajectories of single cy3-particles were recovered with Fiji/ImageJ using TrackMate plugin for automated single-particle tracking (Tinevez et al., 2017). To discriminate trajectories of particle that underwent directed motion from nonspecific noise and immobile objects, we selected trajectories based on their total displacement (minimum of 2.9 μm) and duration (80 consecutive frames). For each recovered trajectory, the mean square displacement (MSD) was calculated as follows:

$$MSD(\tau) = \langle (x(t + \tau) - x(t))^2 + (y(t + \tau) - y(t))^2 \rangle \quad (3.6)$$

where x and y are the coordinates of the particle along the axon, t and τ are the absolute and lag times, respectively, and the brackets represent the time average. This calculation was performed for $\approx 25\%$ of the total time of the trajectory (Ruthardt et al., 2011).

The MSD data were fitted with an anomalous diffusion model (Otero et al., 2014):

$$MSD = A\tau^\alpha + B \quad (3.7)$$

where A depends on the motion properties of the particle, B is the residual MSD, and the coefficient α is an indication of the particle motion-type (Otero et al., 2014). Trajectories were classified as actively driven ($\alpha > 1.5$), diffusive ($0.9 < \alpha < 1.1$) or confined ($\alpha < 0.5$) (Otero et al., 2014). Diffusion coefficient D was calculated for those particles moved only by diffusion ($0.9 < \alpha < 1.1$):

$$D = \frac{MSD}{qt} \quad (3.8)$$

where t is time in seconds of the frames analysed and q is a constant depending on the dimension of the fitting model ($q = 2 * dim = 4$). Equation (3.8) can be rewritten as:

$$t = \frac{MSD}{4D} = \frac{\langle r^2 \rangle}{4D} \quad (3.9)$$

where t is time in second, and r is the displacement length in μm . For computing the time that pre-miR particles would taken to travel along axons driven only by diffusion, we considered that the distance from *Xenopus laevis* RGC cell bodies to the tip of axons is 500 μm (Turner-Bridger et al., 2018).

Endogenous and exogenous MSD analysis were performed by Michela Rocuzzo, while I computed the diffusion coefficient calculation. In the results Chapter 5 my contribution on this part of the work has been clearly stated.

3.6 Bioinformatics prediction, data analysis and tools

3.6.1 Software and Algorithms

Different software and algorithms were used throughout this thesis project (Table 3.3) and mentioned in the Method Sections when adopted.

Table 3.3: Software and Algorithms

Analysis and prediction		
Name	Version, reference or link	Used for
GraphPad PRISM	version 6 or 7	All stat analysis
Fiji	ImageJ 1.52e Jave1.8.0 172	Imaging analysis
Volocity	6.3 Perkin Elmer	Imaging analysis
Xenbase	www.xenbase.org	<i>Xenopus laevis</i> BLAST, check for primers and MB off-targets
TargetScan	version 6	Target prediction
Reactome	www.reactome.org	Reactome pathway selection
miRBase	www.mirbase.org	Check for MRE sequence
CFX Manager	(BioRad) version 3.1	RT-qPCR analysis
Primers design		
Name	Version, reference or link	Used for
NCBI Blast	www.ncbi.nlm.nih.gov/tools/primer-blast/	For all primer design
Oligo Calc	http://biotools.nubic.northwestern.edu/OligoCalc.html	Check for primer dimers
Oligo Analyzer	https://eu.idtdna.com/calc/analyzer	Check for primer dimers and self complementarity
Reverse complement	http://reverse-complement.com/	Check reverse primers

For primer design the NCBI Primer-Blast tool was utilized, giving as input the *Xenopus laevis* sequence of interest to be amplified. The best primer pairs proposed by the software, were then screened for probability of self-complementarity and primer dimers formation using Oligo Calc and Oligo Analyzer (Table 3.3). Two or three primer pairs remaining promising because of low levels of predicted self-complementarity and dimerization, were finally screened with XenBase Blast for possible off-targets in *Xenopus laevis*. The complementarity of reverse primers were checked after running “Reverse complement” tool.

For molecular beacon (MB) Blast the reverse complement of the MB was blasted (www.xenbase.org) to check for possible off-targets in *Xenopus laevis*. The blast tool “blastn-DNA query to DNA database” was used, selecting as database “*Xenopus laevis* J-strain 9.1 Genome” and as E value cut off 10 (Table 5.1).

3.6.2 Pre-miRNA candidate selection and validation

Axonal pre-miRNAs candidates were selected from the published sequencing data (GEO accession number: GSE86883; (Bellon et al., 2017)). The sequencing was performed on Illumina MiSeq with a library preparation specific for short RNAs (TruSeq Small RNA Library Preparation Kit, Illumina), and the two libraries yielded 7.8 and 10.8 million reads.

Candidate pre-miRNAs were identified by reads spanning the loop sequence of the pre-miRNA in addition to the -5p and -3p mature miRNA isoforms. The sequencing data were

mapped to the available *Xenopus tropicalis*, *Xenopus laevis* and *Danio rerio* pre-miRNA sequences present in miRBase v21 (Bellon et al., 2017). For the pre-miRNAs candidate selection all sequences were required to perfectly match to *Xenopus laevis*. To achieve this aim all the reference sequences used in the mapping contained in miRBase v21 were blasted against the J-strain 9.2 Genome in Xenbase, using the default settings (E value 0.1, BLOSUM62 matrix), checking perfect match between reads and organism.

The axonal presence of three candidates were then validated by PCR (Section 3.3.4) on pure axons collected by LCM (Section 3.2.4).

3.6.3 miR-181 target prediction and candidate selection

miR-181a-5p targets were predicted among the axonal RNA (identified by sequencing of an isolated pure axonal sample derived from 50 cultured explants). I personally cultured RGC axons, manually severed the 50 explants and extract the axonal RNA and checked for its purity. All the bioinformatics analysis on the sequenced data and the identification of the predicted targets was run by Stephanie Strohbuecker. Afterwards, I followed up the analysis by integrating the bioinformatic work, selecting specific Reactome pathways of interest and with a literature research to narrow down to the three final selected candidates.

A minimal amount of information to describe the bioinformatic analysis is reported in the following paragraph, while the complete Table of the prediction analysis is reported as Table 1 (bioRxiv 470393; doi: <https://doi.org/10.1101/470393>). The ranked putative targets of the axon guidance Reactome pathway (R-HSA-422475) and integrin cell surface interaction Reactome pathway (R-HSA-216083), are reported in this thesis in Table 8.1.

Identification of axonal RNA 10 ng of axonal RNA collected from isolated axons and SPRI beads (Beckman Coulter) purified were used as input for the Ovation SoLo RNA-Seq System, Custom AnyDeplete (NuGEN) and sequenced using NextSeq 500 - MID, paired-end 80 nt approach (Illumina) at the EMBL Genomics Core facility (Heidelberg, Germany). Using the AnyDeplete system *Xenopus laevis* rRNA sequences identified through the ncbi nucleotide and the SILVA databases were removed. After ensuring raw sequence read quality with FastQC, reads were trimmed using Trimmomatic according to the Ovation SoLo RNA-Seq System instructions. Additionally, we removed adapter sequences and reads shorter than 40 bp. Trimmed reads were mapped with HISAT2, using default settings apart from `-rna-strandness FR`, to the *Xenopus laevis* genome (version 9.1) with an added rRNA contig and subsequently sorted using samtools.

Using a custom *Xenopus laevis* transcriptome annotation, reads mapping to genes were quantified with FeatureCounts. The expression levels for each gene were calculated using the `rpkm()` function from the edgeR package. We identified genes as axonally present if they were detectable at or above 1 FPKM.

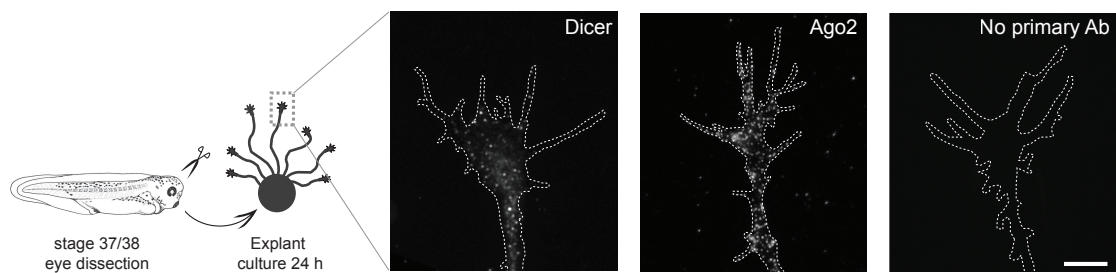
miR-181 target prediction with TargetScan *Xenopus laevis* miR-181a targets were predicted using custom scripts (TargetScan 6) with custom annotated *Xenopus laevis* 3'UTR sequences. All predicted human and mouse miR-181a targets, including those with poorly conserved target sites but removing non-canonical ones, were downloaded from TargetScanHuman 7.1 and TargetScanMouse 7.1, respectively. Identification of candidates axonally present predicted miR-181a-5p *Xenopus laevis* targets with an annotated

3'UTR of at least 50 bp length were screened using their human orthologs ncbi entrez IDs against the following Reactome (Fabregat et al., 2015) pathways of interest: axon guidance pathway (R-HSA-422475) and integrin cell surface interactions pathway (R-HSA-216083). In addition, we filtered the obtained predicted miR-181a-5p targets for those that are within the top 20 % of predicted targets and are also predicted to be targeted by miR-181-5p in human or mouse.

4 Dicer and pre-miRNAs in axons

Numerous studies have reported the presence of Dicer within mammalian growth cones by immunofluorescence in culture (Hengst et al., 2006; Zhang et al., 2013; Aschrafi et al., 2008; Vargas et al., 2016; Kim et al., 2015; Gershoni Emek et al., 2018; Hancock et al., 2014) but whether Dicer is also detected in lower vertebrates such as *Xenopus laevis* was investigated for the first time by Archana Iyer in our laboratory. She observed a distribution of Dicer but also of Ago2 in retinal ganglion cell (RGC) axons in this species (Figure 4.1).

Figure 4.1: Dicer and Ago2 in *Xenopus laevis* growth cone



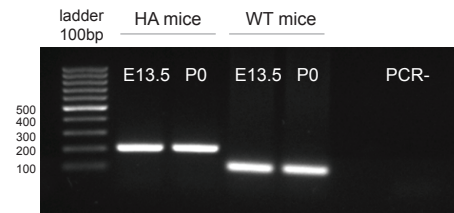
***Xenopus laevis* immunohistochemistry (IHC)** Representative cultured stage 37/38 *Xenopus laevis* RGC growth cones stained with anti-Dicer and anti-Ago2 antibodies, where a clear punctate Dicer- and Ago2-immunoreactive signal was observed. No primary antibody (Ab): negative control. Scale bar: 10 μm .

This observation was an important starting point for my thesis project, opening many questions such as: "Is Dicer really in RGC axons? Or is it an artifact of anti-Dicer immunoreactivity?", "Why is Dicer at the axonal level in RGC?", "Are pre-miRNAs present even in this axonal compartment?".

These questions are addressed in this Chapter, in which data on Dicer localization in RGC axons using (FLAG-HA₂)-Dicer mice model (Section 4.1), as well as pre-miRNA axonal localization in *Xenopus laevis* RGC (Section 4.2) are presented.

4.1 Dicer presence in mice RGC axons

Dicer is widely distributed in growth cones from many different neuronal cell types and species suggesting an important and universal local role for Dicer in this compartment. Considering that there are concerns about the specificity of anti-Dicer antibody (Cormazetto et al., 2014), I confirmed *bona fide* expression of Dicer within axons using an endogenously epitope tagged (FLAG-HA₂)-Dicer knock-in mouse allele, investigating Dicer

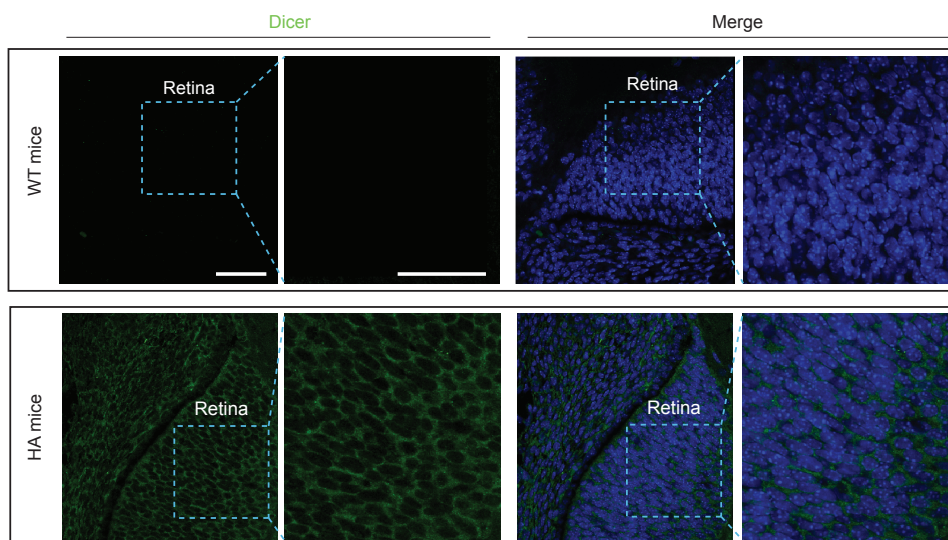
Figure 4.2: FLAG-HA₂-Dicer mice genotyping

Genotyping PCR Representative gel of mice genotyping. PCR amplification of the region overlapping the FLAG-HA₂ epitope of Dicer tagged gene. Abbreviations: WT, wild type; HA, FLAG-HA₂-Dicer; bp, base pair; E13.5, embryonic day 13.5; P0, postnatal day 0.

distribution in RGC axons using anti-HA antibody *in vivo*. I selected the immunohistochemistry (IHC) approach to study Dicer localization, because IHC on sections gives information about the protein localization in its *in vivo* tissue context which is more complex compared to a neuronal cell culture model.

The presence of the epitope (FLAG-HA₂) in the tagged Dicer mice samples used was checked by genotyping (Figure 4.2). Schematic of the Dicer gene structure is shown in the Method Section where the mice model is presented (Section 3.1, Figure 3.1).

Figure 4.3: Cytoplasmic Dicer localization in E13.5 retina

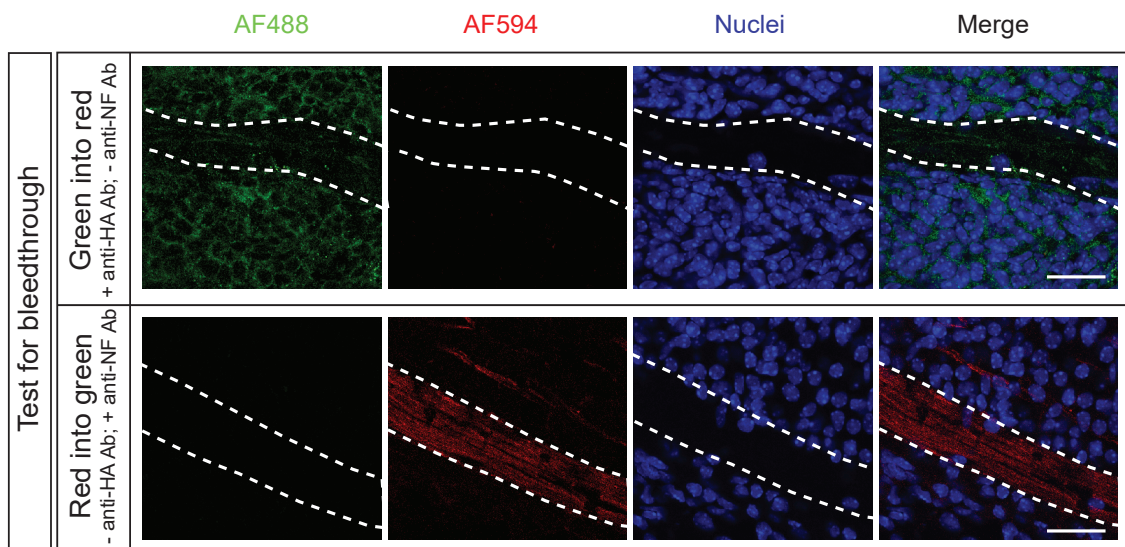


Dicer localization in E13.5 retina Representative mice embryonic day 13.5 (E13.5) retina section stained with anti-HA antibodies to detect (FLAG-HA₂)-Dicer. Note the absence of HA signal in wild type (WT) mice and the cytoplasmic localization of Dicer, as previously reported (Much et al., 2016). Scale bar: 50 μ m.

The endogenous localization of Dicer was studied by an immunohistochemistry (IHC) approach, on fixed sections. Specificity of the anti-HA antibody was confirmed by the absence of signal in WT mice (Figures 4.5, 4.3) and the presence of signal within the cytoplasm of retinal cells, as expected (Much et al., 2016) (Figure 4.3).

To avoid false positive results stemming from bleedthrough between the acquisition channels used for Dicer and neurofilament detection (Dicer, AF 488 green; neurofilament, AF 594 red), the absence of bleedthrough was confirmed at the confocal microscope (Figure 4.4, Method Section 3.1.2).

Figure 4.4: Bleedthrough absence in the imaging settings



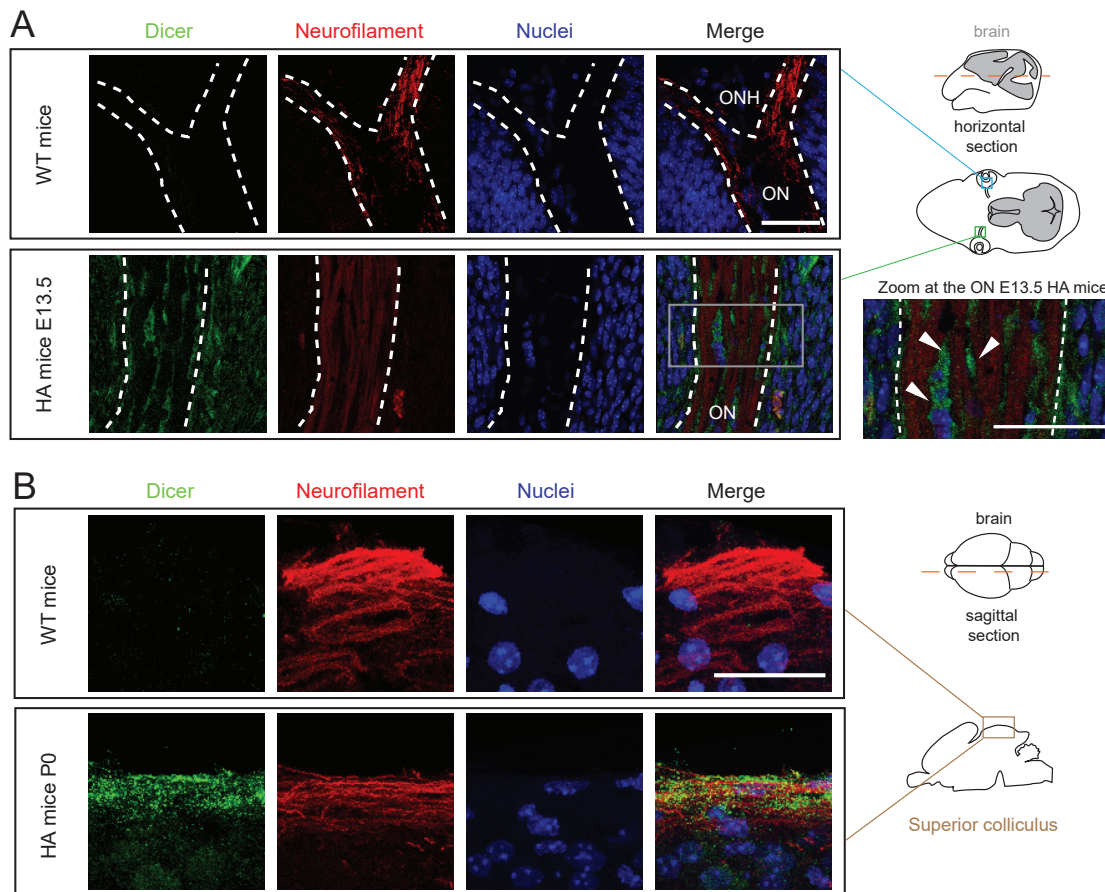
Test for bleedthrough E13.5 optic nerve immunostaining. Green into red bleedthrough was checked by using anti-HA antibody only, without immunostaining for neurofilament (AF 594). Red into green bleedthrough was checked by using anti-NF only, without immunostaining for Dicer (AF 488). Dashed white lines delineate the optic nerve. Abbreviations: AF 488, Alexa Fluor 488 nm; AF 594, Alexa Fluor 594 nm; Ab, antibody; NF, neurofilament. Scale bar: 30 μm .

4.1.1 Dicer detection in P0 mice RGC axons at the superior colliculus

At E13.5, when RGC axons are reaching the chiasm (Bovolenta, Mason, 1987; Colello, Guillery, 1990), Dicer was not detected in axons marked with anti-neurofilament antibody but appeared in cells within the optic nerve head (Figure 4.5 A, arrowheads). The optic nerve (ON) is composed by retinal ganglion cells axons, glial cells and blood vessels (Salazar et al., 2018). In the ON, the vast majority of nuclei belong to astrocytes and they are organized in glial columns within the optic nerve tract closed to the optic nerve head (Tehrani et al., 2018). At E13.5 Dicer signal surrounds the nuclear staining in the ON (Figure 4.5 A, arrowheads), suggesting a localization within astrocytes.

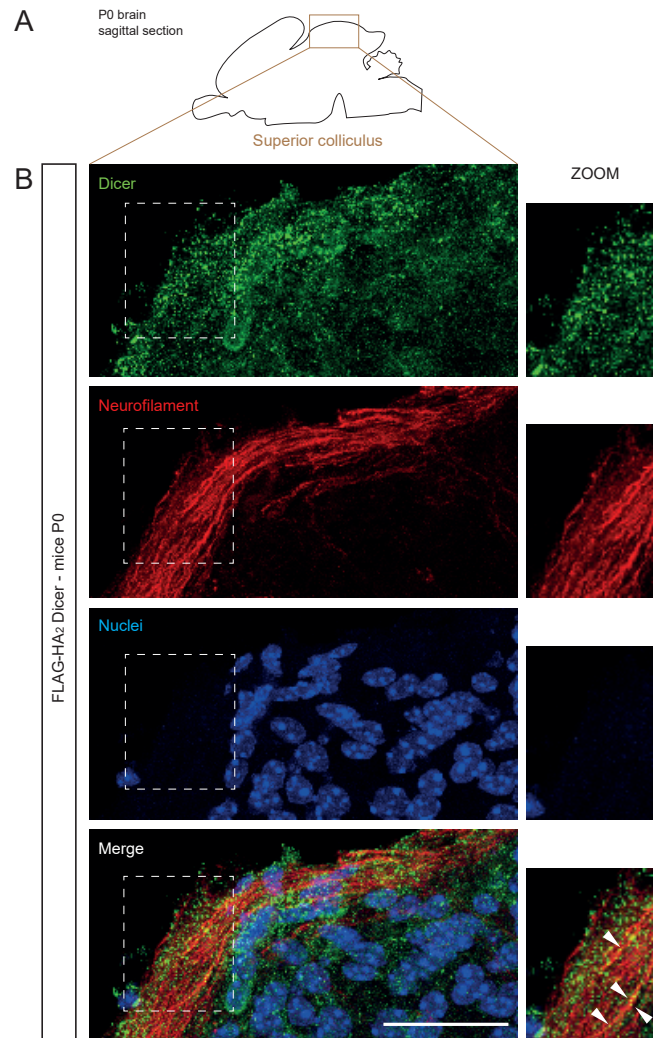
By P0, Dicer was detected within RGC axons where HA- and axonal neurofilament-associated signals clearly co-localized (Figure 4.5 B, 4.6). At this stage, axons start innervating their target centers, the superior colliculus and lateral geniculate nucleus (Hindges et al., 2002).

Figure 4.5: Dicer localization in E13.5 and P0 mice



Dicer localization in P0 superior colliculus (A) Representative E13.5 mice brain cross-section (dashed red line in the schematic) comprising the optic nerve (ON) stained with anti-neurofilament and anti-HA antibodies to detect RGC axons and (FLAG-HA₂)-Dicer, respectively. Note the absence of HA signal in wild type (WT) mice. The white dashed delineates the ON. Zoom of the triple stained ON (right panel): Dicer signal is detected inside ON cells surrounding axon bundles but not in axons per se (arrowheads). (B) Representative P0 superior colliculus (sagittal sectioning of P0 brains along the dashed red line in the schematic) stained with anti-neurofilament and anti-HA antibodies to detect RGC axons and (FLAG-HA₂)-Dicer, respectively. Note the absence of HA signal in wild type (WT) mice and the presence of Dicer within neurofilament-marked RGC axons. Abbreviations: WT, wild type; HA, (FLAG-HA₂)-Dicer; E13.5, embryonic day 13.5; P0, post-natal day 0; ONH, optic nerve head; ON, optic nerve. Scale bar: 30 μ m.

Figure 4.6: Dicer localization in P0 mice



Dicer localization (A) Schematic of P0 superior colliculus sagittal sectioning. The box indicates the region of interest. (B) Representative P0 superior colliculus stained with anti-neurofilament and anti-HA antibodies to detect RGC axons and (FLAG-HA₂)-Dicer, respectively. Dashed white box indicates the region zoomed in panel C. (C) Zoom of the triple stained P0 superior colliculus in a free nuclei region: Dicer signal is detected inside axons (arrowheads). Abbreviations: HA, (FLAG-HA₂)-Dicer; P0, post-natal day 0. Scale bar: 30 μ m.

This strongly suggests that Dicer, and by extension newly generated miRNAs, may act within RGC axons during the process of axon targeting but not during the earlier period of axon pathfinding. Overall, these results indicate the presence of Dicer within mammalian axons *in vivo* during a specific developmental window.

4.2 Pre-miRNA detection in *Xenopus laevis* RGC axons

The presence of Dicer at the growth cone suggests that miRNAs may be locally produced within this compartment. If this were the case, inactive hairpin precursor forms of miRNAs should be detectable in axons and growth cones. Axonal pre-miRNAs candidates were selected from the published sequencing data (GEO accession number: GSE86883), (Bellon et al., 2017). The criteria followed for the selection was identifying reads spanning not just the -5p and -3p mature forms but also the loop sequence of pre-miRNA. The more reads mapping the entire loop the higher the chance to have the corresponding pre-miRNA in the axonal sample (Figure 4.7, Method 3.6.2).

Figure 4.7: List of candidate axonal pre-miRNAs

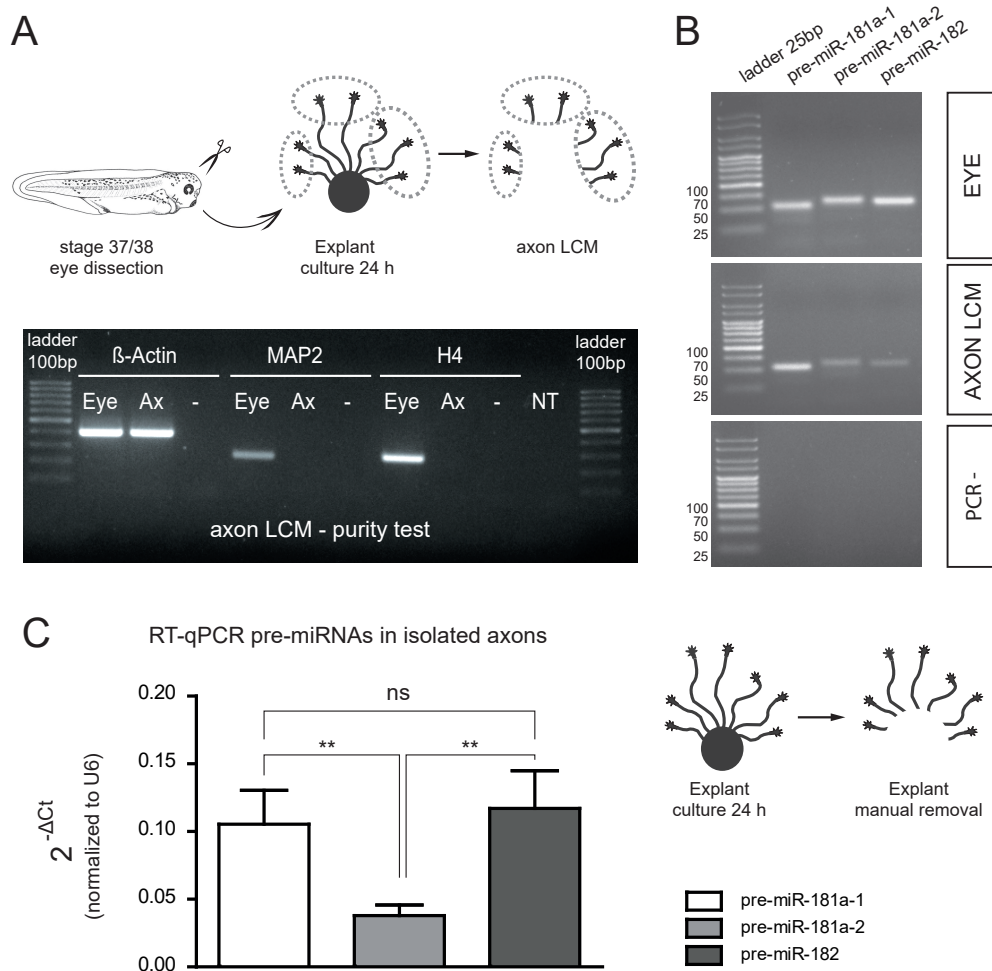
dre-let-7b	dre-mir-10b-2	dre-mir-124-2	dre-mir-124-5	dre-mir-128-1	dre-mir-139	dre-mir-25	dre-mir-26a-1	dre-mir-454b	dre-mir-455-1
dre-mir-726	xla-mir-1306	xla-mir-133a	xla-mir-133b	xla-mir-133d	xla-mir-142	xla-mir-15c	xla-mir-18	xla-mir-194	xla-mir-19b
xla-mir-1b	xla-mir-20	xla-mir-205	xla-mir-223	xla-mir-23a	xla-mir-24b	xla-mir-363	xla-mir-427	xla-mir-428	xla-mir-703
xla-mir-92a-1	xla-mir-92a-2	xtr-let-7a	xtr-let-7b	xtr-let-7c	xtr-let-7e-1	xtr-let-7e-2	xtr-let-7f	xtr-let-7g	xtr-let-7i
xtr-mir-100	xtr-mir-101a-1	xtr-mir-101a-2	xtr-mir-103-1	xtr-mir-103-2	xtr-mir-106	xtr-mir-107	xtr-mir-10a	xtr-mir-10c	xtr-mir-122
xtr-mir-124	xtr-mir-125a	xtr-mir-125b-1	xtr-mir-125b-2	xtr-mir-126	xtr-mir-128-2	xtr-mir-129-1	xtr-mir-129-2	xtr-mir-130a	xtr-mir-130b
xtr-mir-130c	xtr-mir-132	xtr-mir-133a	xtr-mir-133c	xtr-mir-135-1	xtr-mir-135-2	xtr-mir-137	xtr-mir-138	xtr-mir-139	xtr-mir-140
xtr-mir-143	xtr-mir-144	xtr-mir-145	xtr-mir-146a	xtr-mir-146b	xtr-mir-148a	xtr-mir-148b	xtr-mir-150	xtr-mir-153-1	xtr-mir-153-2
xtr-mir-155	xtr-mir-15a	xtr-mir-15b	xtr-mir-16a	xtr-mir-16b	xtr-mir-16c	xtr-mir-17	xtr-mir-181a-1	xtr-mir-181a-2	xtr-mir-181b-1
xtr-mir-181b-2	xtr-mir-182	xtr-mir-183	xtr-mir-184	xtr-mir-18a	xtr-mir-190	xtr-mir-191	xtr-mir-192	xtr-mir-193	xtr-mir-194-1
xtr-mir-194-2	xtr-mir-196a	xtr-mir-196b	xtr-mir-199a	xtr-mir-199b	xtr-mir-19a	xtr-mir-19b-2	xtr-mir-1a-1	xtr-mir-1a-2	xtr-mir-200a
xtr-mir-200b	xtr-mir-203	xtr-mir-204-1	xtr-mir-204-2	xtr-mir-205a	xtr-mir-205b	xtr-mir-206	xtr-mir-208	xtr-mir-20a	xtr-mir-210
xtr-mir-212	xtr-mir-214	xtr-mir-215	xtr-mir-216	xtr-mir-217	xtr-mir-218-1	xtr-mir-218-2	xtr-mir-2184	xtr-mir-2188	xtr-mir-219
xtr-mir-22	xtr-mir-221	xtr-mir-222	xtr-mir-23a-2	xtr-mir-23b	xtr-mir-24a	xtr-mir-24b	xtr-mir-26-2	xtr-mir-27a	xtr-mir-27b
xtr-mir-27c-1	xtr-mir-29a	xtr-mir-29c	xtr-mir-29d	xtr-mir-301-1	xtr-mir-301-2	xtr-mir-302	xtr-mir-30a	xtr-mir-30b	xtr-mir-30c-1
xtr-mir-30c-2	xtr-mir-30d	xtr-mir-30e	xtr-mir-338-1	xtr-mir-338-2	xtr-mir-33a	xtr-mir-33b	xtr-mir-34a	xtr-mir-34b-3	xtr-mir-363
xtr-mir-365-1	xtr-mir-375	xtr-mir-383	xtr-mir-425	xtr-mir-427-1	xtr-mir-428b	xtr-mir-429	xtr-mir-449a	xtr-mir-449b	xtr-mir-449c
xtr-mir-451 *	xtr-mir-489	xtr-mir-499	xtr-mir-7-1	xtr-mir-7-2	xtr-mir-7-3	xtr-mir-92b	xtr-mir-9-3	xtr-mir-9406	xtr-mir-96
xtr-mir-98	xtr-mir-99	xtr-mir-9a-1	xtr-mir-9a-2	xtr-mir-9b					

■ More than 5 reads spanning the whole loop No reads spanning the loop region
■ Less than 5 reads spanning the whole loop * Dicer independent miRNA biogenesis

List of candidate axonal pre-miRNAs derived from (Bellon et al., 2017). Pre-miRNAs with more than 5 reads mapping to the hairpin loop were considered abundant (highlighted in red).

I screened the sequencing data by first selected those pre-miRNAs with small RNA fragments mapping to the loop region partially or entirely. Reads mapping to the entire loop region were observed for 35 pre-miRNAs, while partially match was observed for other 60 pre-miRNAs. I therefore went through a second round of selection, to assess if those reads partially spanning the loop were real *Xenopus laevis* candidates or not. Since the sequencing data were mapped to the available *Xenopus tropicalis*, *Xenopus laevis* and *Danio rerio* pre-miRNA sequences present in miRBase v21 (Bellon et al., 2017), I investigated if the partial matching was due to differences among organisms or real mismatch with *Xenopus laevis* pre-miRNAs sequence. To do that, I blasted all the reference sequences used in

Figure 4.8: Pre-miRNAs' presence in pure RGC axons



Pre-miRNAs' presence in pure RGC axons collected by LCM (A) RT-PCR performed on RNA extracted from axons collected by LCM (Ax) or from eyes. β -Actin mRNA is present both in eye and axons, while MAP2 and H4 are present only in the eye sample, suggesting the absence of contamination from cell bodies or other cells in LCM axonal samples. 35 PCR cycles were run. (B) RT-PCR performed on RNA extracted from eyes or from LCM isolated axons, confirming the axonal presence of pre-miR-181a-1, pre-miR181a-2 and pre-miR-182. 35 PCR cycles were run. (C) Quantification of pre-miRNA expression levels using the $2^{(-\Delta Ct)}$ method and U6 as normalizer in isolated axons obtained after explant manual removal. Values are mean \pm SEM. Statistics: ** $p < 0.01$. Data were normally distributed (Shapiro-Wilk test). One-way ANOVA followed by Tukey's multiple comparison post-hoc test, $n=7$, each n corresponds to a RT-qPCR experiment on axonal RNA from 40 cultured explants, all n are independent experiments. In each independent experiment embryos are derived from a different fertilized frog. Abbreviations: LCM, laser capture microdissection; Ax, axonal sample; Eye, stage 37/38 eye; -, no template control of the PCR; NT, no template control of the retrotranscription; ns, not significant.

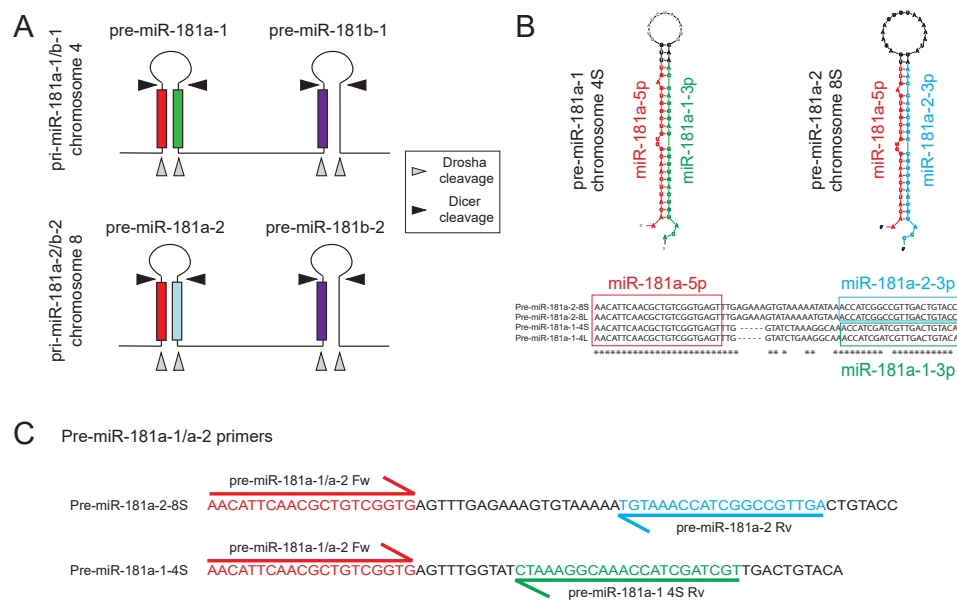
the mapping against the J-strain 9.2 Genome in Xenbase (Method 3.6.2), finding other 7 pre-miRNA candidates perfectly match to *Xenopus laevis*.

Considering the first and the second round of candidates selection I ended up with 42 pre-miRNA candidates with small RNA fragments mapping perfectly to *Xenopus laevis* pre-miRNA hairpin loop region (Figure 4.7). Pre-miRNA-182, pre-miR-181a-1 and pre-miR-181a-2 were amongst the 9 most abundant pre-miRNAs in axon, as determined by the number of mapped reads (Figure 4.7).

To validate the presence of these precursors within axons, I performed PCR from RGC axons derived from stage 37/38 whole eye explant culture and collected axons by laser capture microdissection (LCM) (Methods 3.2.4). This approach yields pure axons, suggested by the presence of beta-actin mRNAs, known to be located in *Xenopus* RGC axons, and the absence of Map2, a dendritic marker, and of nuclear histone H4 from these captured axons (Bellon et al., 2017) (Figure 4.8).

The presence of pre-miR-181a-1, pre-miR181a-2 and pre-miR-182, three of the most abundant pre-miRNAs in axon (Figure 4.7), was confirmed by PCR of in eyes and axons (Figure 4.8, primers sequence used in PCR reported in Figure 4.9 C).

Figure 4.9: Schematic and sequence of pre-miR-181a-1/a-2 locus



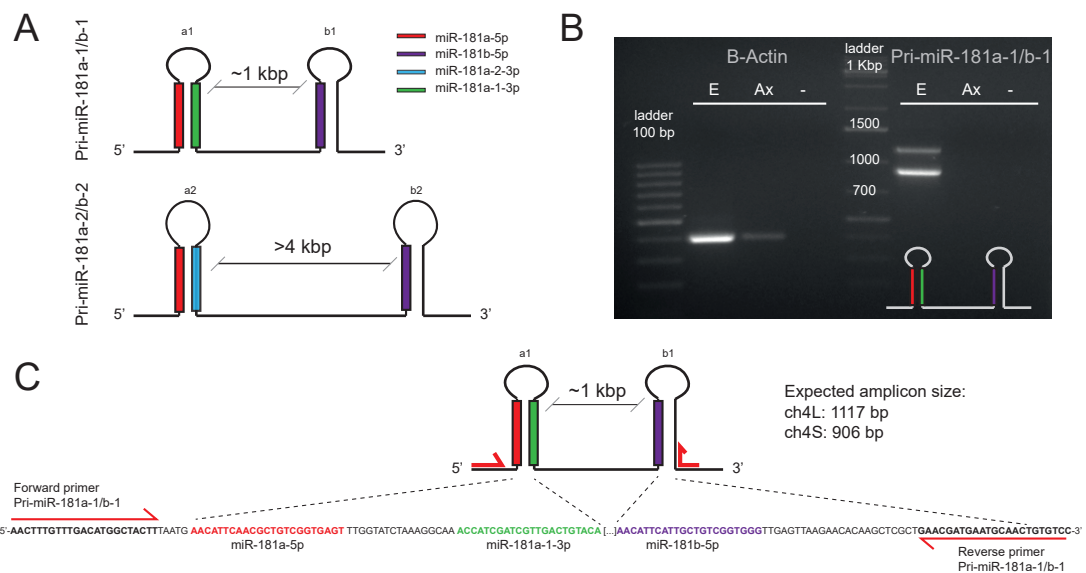
Pri-miR-181a-1/b-1 and a-2/b-2 (A) Schematic representation of pri-miR-181a-1/b-1 on chromosome 4 and of -181a-2/b-2 on chromosome 8. Small gray and black arrowheads indicate Drosha cleavage sites and the black ones Dicer cleavage sites, respectively. Colored boxes show the position of mature miRNAs (red, miR-181a-5p; green, miR-181a-1-3p; light blue, miR-181a-2-3p; purple, miR-181b). (B) Predicted secondary structure (Mfold v3.6) and multiple alignment (MUSCLE v3.8) of the two precursors isoforms, pre-miR-181a-1 (chromosome 4S) and pre-miR-181a-2 (chromosome 8S). (C) Primers sequence of pre-miR-181a-1 and a-2 amplification.

4.3 miR-181 family: focus on pre-miR-181a-1 and pre-miR-181a-2

Pre-miR-181a-1 and pre-miR-181a-2 are derived from two distinct primary transcripts and both give rise to miR-181a-5p and, respectively, to miR-181a-1-3p and miR-181a-2-3p (Figure 4.9). In *Xenopus*, the miR-181 family is composed of miR-181a (-5p and -3p) and miR-181b, while miR-181c and d are unique to mammals (Kos et al., 2016; Wang et al., 2015b).

Interestingly, no reads spanning the loop region of pre-miR-181b-1/b-2 were present in the axonal sequencing data (Figure 4.7), suggesting an absence of those pre-miRNAs in axons and therefore a different distribution of the pre-miRNAs of the same family in different cellular compartment.

Figure 4.10: Pri-miRNA absence in axon



Pri-miRNA absence in axon (A) Schematic representation of pri-miR-181a-1/b-1 and of -181a-2/b-2 highlighting the distance from loop to loop. (B) RT-PCR performed on RNA extracted from eyes or from isolated axons, confirming the eye presence of pri-miR-181a-1/b-1, and its absence in axons. The two bands correspond to the two *Xenopus* isoforms of the two chromosomes, the higher ch 4L, the lower ch 4S. (C) Sequence and schematic of pri-miR-181a-1/b-1. Red arrows indicate the primers position used to amplify pri-miR-181a-1/b-1 in both chromosomes 4L and 4S. Primers are located external to the 3' of the pre-miRNA (forward primer) or overlapping the 5' end of the pre-miRNA and the external region of the stem-loop structure (reverse primer). Abbreviations: Ax, axonal sample; E, stage 37/38 eye; -, no template control of the PCR.

Amplifying pre-miRNA sequence (Figure 4.8, primers in Figure 4.9 C) using normal PCR, could also lead to the amplification of the pri-miRNA if it were present in the sample, since the stem-loop is part of both precursors. I checked absence of pri-miR-

181a-1/b-1 in axonal sample. The pri-miR-181a-1/b-1 amplicon is around 1 kbp long from loop to loop, hence it is easily amplified by normal PCR (Figure 4.10) using primers designed in known regions (e.g. pre-miRNAs stem-loop). Pri-miR-181a-1/b-1 is absent in isolated axonal samples (Figure 4.10), meaning that the products amplified in axons are specifically the endogenous pre-miRNA while in whole eye samples both the precursors will be amplified.

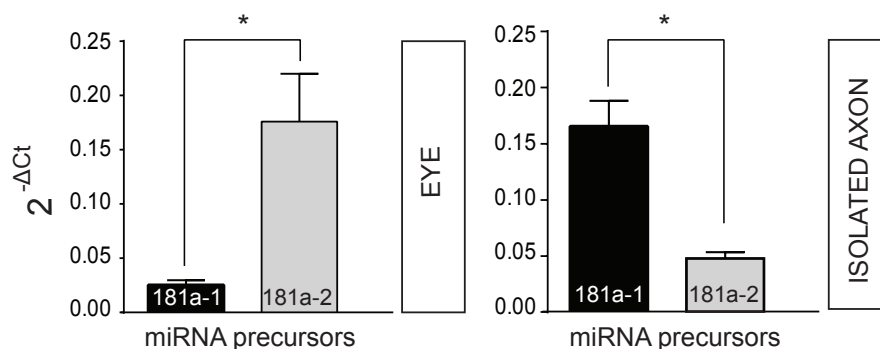
Pre-miR-181a-1/a-2 are identical at the 5' end, sharing the miR-181a-5p mature form, and present a high similarity at the 3' end (Figure 4.9 B). The amplification of this short RNA, with a strong secondary structure and sequence similarity, is technically challenging.

Nevertheless, my primers for pre-miRNAs amplification are able to specifically detect endogenous pre-miRNAs in axonal samples (Figure 4.10).

4.3.1 Pre-miR-181a-1 is more abundant in axons than pre-miR-181a-2

I investigated the relative abundance of the axonal pre-miRNAs and eye precursors by RT-qPCR. The miR-181a-1 precursors were 7.29 ± 1.77 fold significantly less abundant in whole eyes than the miR-181a-2 one. While, pre-miR-181a-1 was 3.65 ± 0.61 fold significantly more abundant in axon than pre-miR-181a-2 (Figure 4.11). Due to limitation in the normalizer (refer to Section 6.2.1) the two different cellular tissues cannot be directly compared, but our observations in the axonal sample indicate that between the two pre-miRNAs of the same family, pre-miR-181a-1 might be preferentially targeted to axons and growth cones (Figure 4.11).

Figure 4.11: miRNAs precursors relative abundance



RT-qPCR on eye and axons. Quantification of the expression levels of miR-181a-1 and miR-181a-2 precursors with the $2^{(-\Delta C_t)}$ method, using U6 as normalizer, in eye or isolated axons. Values are mean \pm SEM. Statistics: * $p < 0.05$. Data were not normally distributed (Shapiro-Wilk test), two-tailed Mann-Whitney test, $n=4$ independent experiments (RNA was collected from 20 eyes or from isolated axons derived from 40 explants for each experiment), in each independent experiment embryos are derived from a different fertilized frog.

4.4 Conclusions

This Chapter opened with some questions on Dicer and pre-miRNAs presence at the RGC axonal level. Taken together, I observed Dicer in *Xenopus laevis* RGC growth cones, as well as in mice RGC at the superior colliculus (SC) at P0, when the axons reach their target region. At earlier developmental stage in mice (E13.5), Dicer was observed inside the optic nerve (ON) and in the retina, but not in the axonal compartment. Glial cells are very abundant inside the ON, and the majority of them are astrocytes (Salazar et al., 2018). Therefore, it is possible that Dicer associated signal is located within within glial cells. A specific glial cell marker should be used to confirm this hypothesis such as GFAP. Nothing is known about Dicer distribution in ON glial cells to the best of my knowledge. It is however interesting to note that neuronal dysfunctions have been observed in various conditional glial cell knock-out Dicer mice model (Tao et al., 2011; Howng et al., 2015; Li et al., 2018), suggesting a role played by Dicer in these cells.

Those results in E13.5 and P0 mice are the first insight into a regulation in Dicer localization in the axonal compartment. This enzyme is indeed present in RGC cell body and not in RGC axons (E13.5) suggesting a specificity in its axonal targeting, and moreover its localization undergoes to a developmental regulation, considering the absence in axon at early stage (E13.5) and its presence in RGC axon at later stages (P0).

From published sequencing data some axonal pre-miRNAs candidates were selected, and three of them validated by PCR on pure LCM axons. Despite miR-181a and miR-181b belonging to the same family and being part of the same pri-miR, their precursors present different distribution in the axonal compartment. Indeed, in RGC axons, pre-miR-181b-1/b-2 are not present (Figure 4.7), and pre-miR-181a-1 is 3.65 fold more abundant than pre-miR-181a-2 (Figure 4.11). This suggests that pre-miR-181a-1 might be preferentially targeted to axons.

In conclusion, both Dicer and pre-miRNAs are detectable at the axonal level, with signs of specificity in their localization to this compartment. Moreover, Dicer sub-localization in RGC axons correlate with specific developmental stages, suggesting a regulation of the timing of its localization.

5 Pre-miR-181a-1 is actively transported on vesicles along axons

The previous Chapter showed axonal localization of Dicer and pre-miRNAs and opened up new challenging questions: “How do pre-miRNAs reach the growth cone?”, “Is their trafficking actively driven or do they reach the growth cone only by diffusion?”, “Does a local processing of pre-miRNAs occur at the axonal level?”. In this Chapter, I contributed in characterizing pre-miRNA trafficking towards the growth cone to unravel potential mechanisms to answer the first two questions while the third question will be addressed in the subsequent Chapter 6.

In order to study pre-miR trafficking, me and colleagues focused on pre-miR-181a-1, because it is the most abundant pre-miRNAs among the ones validated in axons (Figure 4.11).

I have personally been only partially involved in this part of the project and therefore my contribution are specified here. All kymograph analyses (Methods 3.5.3) to track pre-miR-181a-1 in axons were performed by Antoneta Gavoci, my contribution in this part has been to investigate Molecular Beacon (MB) specificity *in silico* (MB Blast, Table 5.1, Method Section 3.6.1) and *ex vivo* in culture by blocking pre-miR-181a-1 maturation. In particular, for the *ex vivo* MB validation, I first proved that the differential small and long RNA extraction allowed us to collect pre-miRNAs separately from pri-miRNAs (Figure 5.3). Second, I ran RT-qPCR on samples in which pre-miR-181a-1 was blocked with a morpholino targeting the Drosha cleavage site (Figure 5.2 B) to check for an effective pre-miR-181a-1 down regulation. Antoneta Gavoci investigated then whether MB was still detectable in the knocked-down pre-miR-181a-1 samples. Moreover, I performed a literature research to categorize puncta velocity, presenting the data accordingly. Indeed, throughout this Chapter we defined stationary puncta as the ones with an average velocity $<0.2 \mu\text{m/s}$. Stationarity at this threshold was applied in *Drosophila melanogaster* neuronal dendrites trafficking studies (Arthur et al., 2015), neuronal dense core vesicles (DCVs) in mice (Knabbe et al., 2018) and recently in mRNA granules trafficking studies in *Xenopus laevis* RGC axon (Leung et al., 2018).

We then divided moving and fast moving puncta respectively in $0.2\text{-}0.5 \mu\text{m/s}$ and $>0.5 \mu\text{m/s}$ (Maday et al., 2014). An average velocity above $0.2 \mu\text{m/s}$ in net transport has been observed in different cellular processes. For example, neurofilaments in axons are translocated at rates that ranged from 0.1 to $>2 \mu\text{m/s}$ (Roy et al., 2000), direct movement of human adenovirus through dynein travel at a speed from 0.2 to $2 \mu\text{m/s}$ (Engelke et al., 2011) and live-cell observation in cultured rat sympathetic neurons show a slow axonal transport of neurofilament proteins with an average transport rate of $0.23 \mu\text{m/s}$ (Wang et al., 2000). Even if slow transport has been observed above $0.2 \mu\text{m/s}$, different studies reported that neuronal transport of vesicles, organelles, proteins, and RNA particles mediated by kinesin and dynein protein family, has a range of velocities from 0.5 to $1 \mu\text{m/s}$

(Hirokawa et al., 2010; Maday et al., 2014).

Apart from this descriptive categories, to further characterize and investigate if what we observed was active or passive trafficking of pre-miR-181a-1, mean square displacement (MSD) analyses were performed by Michela Rocuzzo (Methods 3.5.4). I contributed in fitting the data and calculated the diffusion coefficient D (Methods 3.5.4) for particles with $0.9 < \alpha < 1.1$.

Irene dalla Costa investigated the role of vesicles in mediating pre-miR-181a-1 trafficking along axons through live-imaging using CD63-expressing plasmid and MB to track endogenous pre-miR-181a-1 (Methods 3.5.3). I contributed to her work by doing electroporation, culture and acquisition for some replicates, while she run all kymograph analyses for studying vesicles and pre-miRNAs co-trafficking.

5.1 Molecular beacon (MB): tool for live imaging of endogenous molecules

In order to specifically examine the behavior of pre-miRNAs in living cell, Antoneta Gavoci and Michela Rocuzzo in our lab developed a new approach to track endogenous pre-miRNAs using molecular beacons (MB). MB are single-stranded oligonucleotide probes which fluoresce only when hybridized to their target (Santangelo et al., 2006) (Figure 5.1 A). MB backbone and sequence was carefully designed to maximize the probe's 1) stability, 2) signal-to-noise ratio, and 3) specificity within the cell. Denaturation profiles confirmed the suitable thermodynamic characteristics of our MB design with fluorescence only at temperatures higher than the melting temperature ($T_m = 58\text{ }^{\circ}\text{C}$), and specific signal from the MB at our working temperature ($20\text{-}30\text{ }^{\circ}\text{C}$) only in target presence (Figure 5.1 B).

We first investigated MB specificity with an *in silico* analysis (Methods Section 3.6.1). The MB sequence was blasted against the whole genome to also investigate possible off-targets on ncRNAs and the E value cut off was set at 10 to detect all possible off-targets, even the less probable ones. The MB sequence or part of its sequence was complementary to an additional 9 genomic loci but no corresponding reads were detected in axons by RNA-seq analysis. Therefore, the MB does not match any known *Xenopus laevis* RNA sequence within the axon besides pre-miR-181a-1 (Table 5.1).

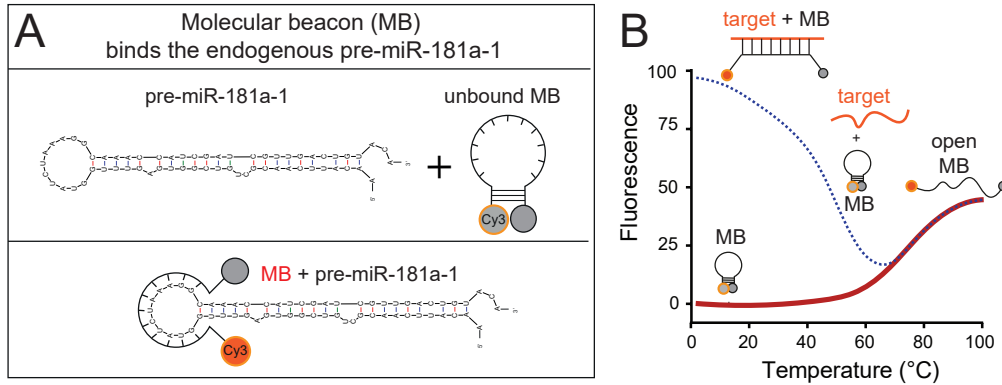
We then tested MB specificity *ex vivo* investigating whether MB is still detectable when endogenous pre-miR-181a-1 is knocked down following microinjection (Figure 5.2 A). Pre-miR-181a-1 knock-down was achieved by microinjecting to 8-cell stage embryos morpholino (MO) designed to block Drosha cleavage. We named this MO pri-miR-MO. After blastomere microinjection with pri-miR-MO (Methods 3.2.1), pre-miR-181a-1 levels were measured by RT-qPCR from the small RNA fraction (Figure 5.2). As aforementioned, primers for pre-miRNAs would also amplify the pri-miRNAs if they were present in the sample. To specifically amplify pre-miRNAs in eye and brain samples an RNA extraction method that allows fractionating long and short RNA species was used (Slit kit Lexogen, Methods 3.3.1). The threshold for the separation of the two fractions is 150 nt: thus, we expect miRNAs and pre-miRNAs in the small fraction, and pri-miRNAs only in the large one. Indeed, in our samples pri-miR-181a-1/b-1 was present only in the large fraction (Figure 5.3). By diving small and large fraction, it was possible to assess the endogenous

Table 5.1: Molecular Beacon BLAST in Xenbase

chr	hit	Score	E-value	Identities	Length	Query strand	Hit strand	chr position	Name	Axonal reads
1	chr4S	1	31,9	2	17/17 (100%)	17	+	chr4S:84409591-84409607	pre-miR-181a-1	Yes
	2	30,1	7	16/16 (100%)	16	+	-	chr4S:79095178-79095163		No
	3	30,1	7	16/16 (100%)	16	+	+	chr4S:86435217-86435232	intron of ivsn1abp.S	No
2	chr3L	1	31,9	2	17/17 (100%)	17	+	chr3L:111609451-111609467		No
	2	30,1	7	19/21 (90%)	21	+	+	chr3L:89499322-89499342		No
3	chr2S	1	31,9	2	17/17 (100%)	17	+	chr2S:95381069-95381085		No
	2	30,1	7	16/16 (100%)	16	+	-	chr2S:105454301-105454286		No
4	chr2L	1	31,9	2	17/17 (100%)	17	+	chr2L:36241555-36241571		No
	2	30,1	7	16/16 (100%)	16	+	-	chr2L:77055047-77055032	intron of cask.L	No
5	chr8L	1	30,1	7	16/16 (100%)	16	+	chr8L:83301470-83301485	intron of numb.L	No
6	chr7L	1	30,1	7	16/16 (100%)	16	+	chr7L:20191991-20192006	intron of exoc5.L	No
	2	30,1	7	19/21 (90%)	21	+	+	chr7L:49937355-49937375	5'UTR of slc18a3.L	No
7	chr5S	1	30,1	7	16/16 (100%)	16	+	chr5S:81176673-81176688	intron of dlgap2.S	No
	2	30,1	7	16/16 (100%)	16	+	-	chr5S:126438407-126438392	intron of flkbp1b.S	No
8	chr4L	1	30,1	7	16/16 (100%)	16	+	chr4L:105418314-105418329	intron of ivsn1abp.L	No
9	chr1S	1	30,1	7	16/16 (100%)	16	+	chr1S:172192521-172192506		No

Molecular Beacon BLAST in Xenbase BLAST of Molecular Beacon sequence against the *Xenopus laevis* genome (version 9.1) using the blastn-DNA query to DNA database tool available at Xenbase (xenbase.org). The absence of RNA expression of matching genome regions was confirmed using RNA-sequencing of axonal transcriptome. Abbreviations: chr, chromosome; hit, sequential number of hits for each chromosome; chr position, exact chromosome position used as reference for checking match in the axonal seq data; Name, corresponding transcript name of the chromosome location (if reported); Axonal reads, check for absence (no) or presence (yes) of axonal reads in the region matching with MB predicted off-target.

Figure 5.1: Molecular Beacon (MB)



Molecular Beacon (MB) schematics (A) Schematic of molecular beacon (MB), pre-miR-181a-1 and their hybridization complex. (B) Schematic of thermal denaturation profile of the MB, in which the fluorescence signal is recorded as a function of temperature, both in absence (solid line) and presence (dashed line) of a target. Note that at the working temperature (20°C - 30°C) the fluorescence signal is due only to hybridization between MB and the target sequence.

levels of pre-miR-181a-1 in eye samples verifying the KD of the pre-miRNA.

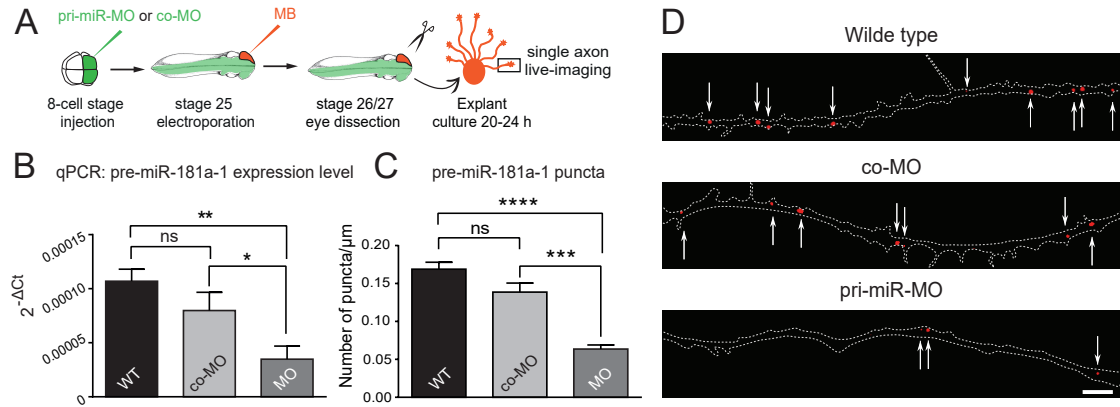
Pri-miR-MO induced a significant 54.37 ± 12.54 % average decrease of pre-miR-181a-1 levels compared to control MO (co-MO) (Figure 5.2 B). Consistently, the number of MB puncta in axons was significantly decreased by 58.45 ± 5.04 % on average within axons in pri-miR-MO vs co-MO treated embryos (Figure 5.2 C, D). No significant differences between WT and co-MO was observed (Figure 5.2). Other *in vitro* and *ex vivo* tests were performed to validate MB specificity. However, since I did not personally contribute to collecting those data, they are not presented in this thesis work.

5.2 Pre-miR-181a-1 trafficked along axons

We next characterized pre-miR-181a-1 trafficking dynamics in RGC axons by live imaging following targeted electroporation of MB or cy3-labeled pre-miR-181a-1 into retinal cells (Figure 5.4 A, Methods 3.2.9). MB-labeled pre-miR-181a-1 puncta were detected throughout the entire length of growing RGC axons and accumulated within the central domain of growth cones (star, Figure 5.4 B), confirming axonal translocation of endogenous pre-miR-181a-1 to the growth cone. Time-lapse images were continuously acquired at 7-10 frames per second. These acquisitions were quantitatively analysed by the transformation of movies into kymographs (Figure 5.4 C, Methods 3.5.3). Kymographs show puncta's movements in space and time (Figure 5.4), and the slope of each segment plotted is the speed of the puncta in that axonal portion. To characterize pre-miRNA transport behavior, puncta's velocity was calculated by arithmetically averaging the speeds of all its segmental components.

No difference was observed between anterograde and retrograde average velocity for

Figure 5.2: Molecular Beacon (MB) specificity



Molecular Beacon (MB) specificity (A) Schematic representation of the experimental protocol. Morpholinos were microinjected at 8-cell stage, followed by MB electroporation at stage 25. Electroporated eyes were then dissected and culture for single axon live-imaging. Concentrations used: MB (5 μM), co-MO (250 μM), pri-miR-MO (250 μM). (B) Quantification of the expression levels of pre-miR-181a-1 using the $2^{(-\Delta C_t)}$ method and U6 as normalizer from small total RNA fraction (< 150 nt). (C) Total number of MB puncta normalized to axon length (μm). (D) Representative axons. MB puncta are indicated (white arrow). Axons is delineated by the dashed lines. Values are mean \pm SEM. Statistics: * $p < 0.05$, ** $p < 0.01$, *** $p < 0.001$ and **** $p < 0.0001$. (B) Data were normally distributed (Shapiro-Wilk test), one-way ANOVA followed by Tukey's multiple comparison post-hoc test, $n=3$, 3 independent experiments. (C) Data were not normally distributed (Shapiro-Wilk test), Kruskal Wallis followed by Dunn's multiple comparison post-hoc test. Total numbers of puncta analyzed (n): 928 (WT); 226 (MO); 208 (co-MO); from 61 axons (WT); 15 axons (co-MO); 35 axons (MO); 4 independent experiments. In each independent experiment embryos are derived from a different fertilized frog. Abbreviations: MB, molecular beacon; co-MO, control morpholino; pri-miR-MO, morpholino blocking pre-miR-181a-1 processing by targeting the Drosha cleavage site; ns, not significant. Scale bars: 5 μm .

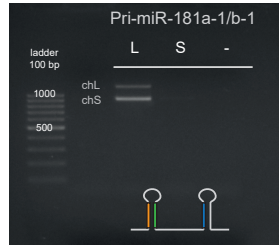
puncta slower than 0.5 $\mu\text{m/s}$ (< 0.2 $\mu\text{m/s}$: antero: $0.066 \pm 0.007 \mu\text{m/s}$; retro: $0.084 \pm 0.008 \mu\text{m/s}$; 0.2-0.5 $\mu\text{m/s}$: antero: $0.33 \pm 0.02 \mu\text{m/s}$; retro: $0.32 \pm 0.01 \mu\text{m/s}$).

However, fast (> 0.5 $\mu\text{m/s}$) anterogradely moving puncta were on average significantly faster than their retrograde counterpart (antero: $1.79 \pm 0.08 \mu\text{m/s}$ vs retro: $1.16 \pm 0.06 \mu\text{m/s}$) (Figure 5.5 A).

Within axons, molecular motors kinesins and dyneins are known to actively move cargos anterogradely and retrogradely, respectively, with a velocity of least at 0.5 $\mu\text{m/s}$ (Maday et al., 2014). Contrary to the highly processive unidirectional motility of kinesins, dynein makes frequent back and side steps (Maday et al., 2014). The slower pre-miRNA retrograde transport that we observe at speeds above 0.5 $\mu\text{m/s}$ may thus be due to dynein's unique property.

By dividing all puncta into categories according to their velocities, the most represented category is the one of fast puncta movements (> 0.5 $\mu\text{m/s}$) with 47% of puncta for endogenous MB-labeled pre-miR-181a-1, and 54% for the exogenous ones (Figure 5.5 B).

Figure 5.3: Pri-miR-181a-1/b-1 absence in small RNA fraction



Small and large RNA fractions separation RT-PCR performed on RNA small and large fractions extracted from pri-miR-MO microinjected eyes, confirming the presence of pri-miR-181a-1/b-1 in the large fraction only. The two bands correspond to the two *Xenopus* isoforms in the two chromosomes, the higher ch 4L, the lower ch 4S. Abbreviations: L, large RNA fraction; S, small RNA fraction; -, no template control of the PCR.

5.3 Endogenous pre-miR-181a-1 is actively transported toward the growth cones

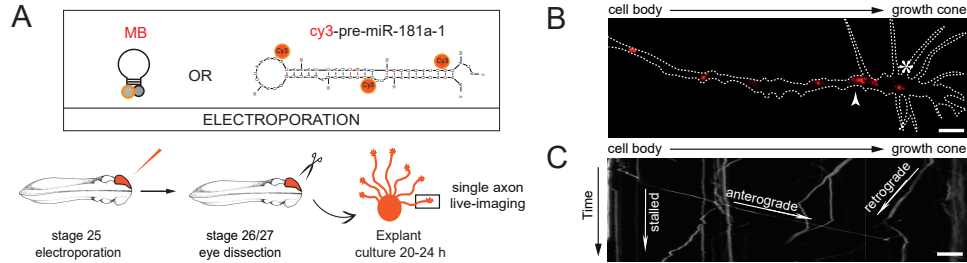
To address whether moving pre-miRNAs were driven by an active transport or instead, assumed a diffusive behavior, we performed mean square displacement (MSD) analysis (see Methods 3.5.4 for details and equations used). The MSD data were fitted with an anomalous diffusion model (Otero et al., 2014), Eq (3.7). Trajectories were conservatively classified as actively driven ($\alpha > 1.5$), diffusive ($0.9 < \alpha < 1.1$) or confined ($\alpha < 0.5$) depending on the value of the exponent obtained from the fitting of Eq (3.7) to the MSD data (Otero et al., 2014).

We calculated $\alpha = 1.78$ (endogenous) and $\alpha = 1.79$ (exogenous) (Figure 5.6 A), suggesting that moving pre-miRNAs were overall actively trafficked along axons. We analysed the α distribution of individual moving particles and detected different motion-type frequencies (Figure 5.6 B). The majority of particles assumed an active motion ($52.36 \pm 6.96\%$ for $\alpha > 1.5$) while we could also detect a small percentage of diffusive ($5.04 \pm 1.33\%$ for $0.9 < \alpha < 1.1$) and confined ($8.86 \pm 1.58\%$, $\alpha < 0.5$) particles (Figure 5.6 B).

Exogenous and endogenous pre-miRNAs appeared to behave similarly, since the computed α (Mann Whitney, p-value = 0.8797) (Figure 5.6 A) and α distribution (Figure 5.6 B) were not significantly different. To statistically compare the two fitting curves (Figure 5.6 A) an extra sum-of-square F-test was computed, specifically asking if the α value of the two datasets differed or not.

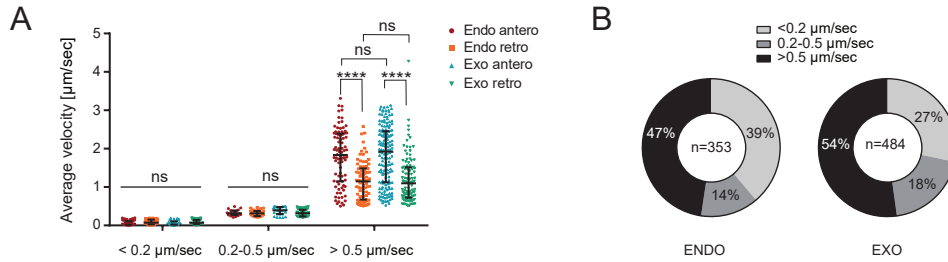
Together, these data suggest that the majority of pre-miRNAs exhibit an active, directed motion along the axon. To gain insight into the added biological value of this kind of active transport, I computed the diffusion coefficient D for diffusive moving particles (Methods 3.5.4, Eq (3.8) and Eq (3.9)). Considering that the displacement from the *Xenopus laevis* RGC cell body to the tip of the axon at this stage is $500\mu\text{m}$ (Turner-Bridger et al., 2018), diffusive pre-miRNA puncta would take $t=20$ days on average to reach the growth cone in great contrast with the two days required by *Xenopus laevis* RGC axons to navigate to

Figure 5.4: Pre-miR-181a-1 trafficking live imaging



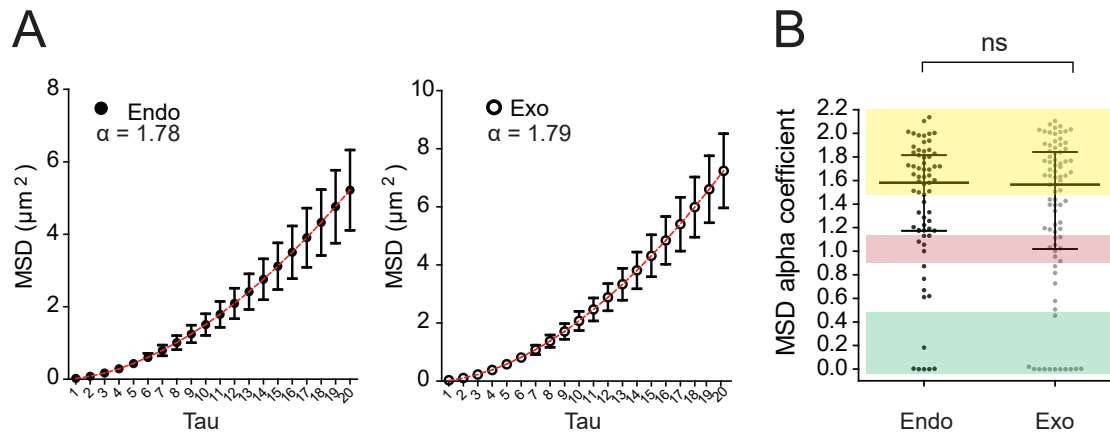
Endogenous and exogenous pre-miR-181a-1 trafficking live imaging (A) Schematic representation of the experimental paradigm. 5 μ M MB and 200 ng/ μ l cy3-pre-miR-181a-1 were electroporated. (B) Representative image of a single distal RGC axon from MB electroporated retina. Dashed white line delineates the axon. (C) Illustrative kymograph. Abbreviations: MB, molecular beacon. Scale bars: 5 μ m.

Figure 5.5: Pre-miR-181a-1 velocity categories



Endogenous and exogenous pre-miR-181a-1 puncta velocities (A) Average velocity of endo and exo puncta. Single dot corresponds to one puncta. (B) Pie plot with frequency distribution of the different velocities categories (in percentage) of MB (endo) and cy3-pre-miR-181a-1 (exo) puncta along the RGC axon shaft. Total number of analyzed particles (n): 353 (endo); 484 (exo). 3 (endo), 4 (exo) independent experiments. In each independent experiment embryos are derived from a different fertilized frog. Values are median with interquartile range. Statistics: **** $p < 0.0001$. Two way ANOVA followed by Tukey's multiple comparison post-hoc test. Abbreviations: ns, not significant; MB, molecular beacon; Endo, endogenous; Exo, exogenous.

Figure 5.6: MSD trafficking analysis



MSD trafficking analysis (A) MSD data for endo and exo tracked particles were fitted with an anomalous diffusion model and thus calculated (red). (B) MSD alpha coefficient distribution for each single endo and exo tracked particle. Yellow, particles actively driven ($\alpha > 1.5$); red, diffusive ($0.9 < \alpha < 1.1$); green, confined ($\alpha < 0.5$). Values are mean \pm SEM (A) or median with interquartile range (B). Total number of analyzed particles (n): 67 (endo); 82 (exo). 3 (endo), 4 (exo) independent experiments. In each independent experiment embryos are derived from a different fertilized frog. (B) Data are not normally distributed (Shapiro-Wilk test), two-tailed Mann Whitney test. Abbreviations: ns, not significant; Endo, endogenous (MB); Exo, exogenous (pre-miR-181a-1 labeled).

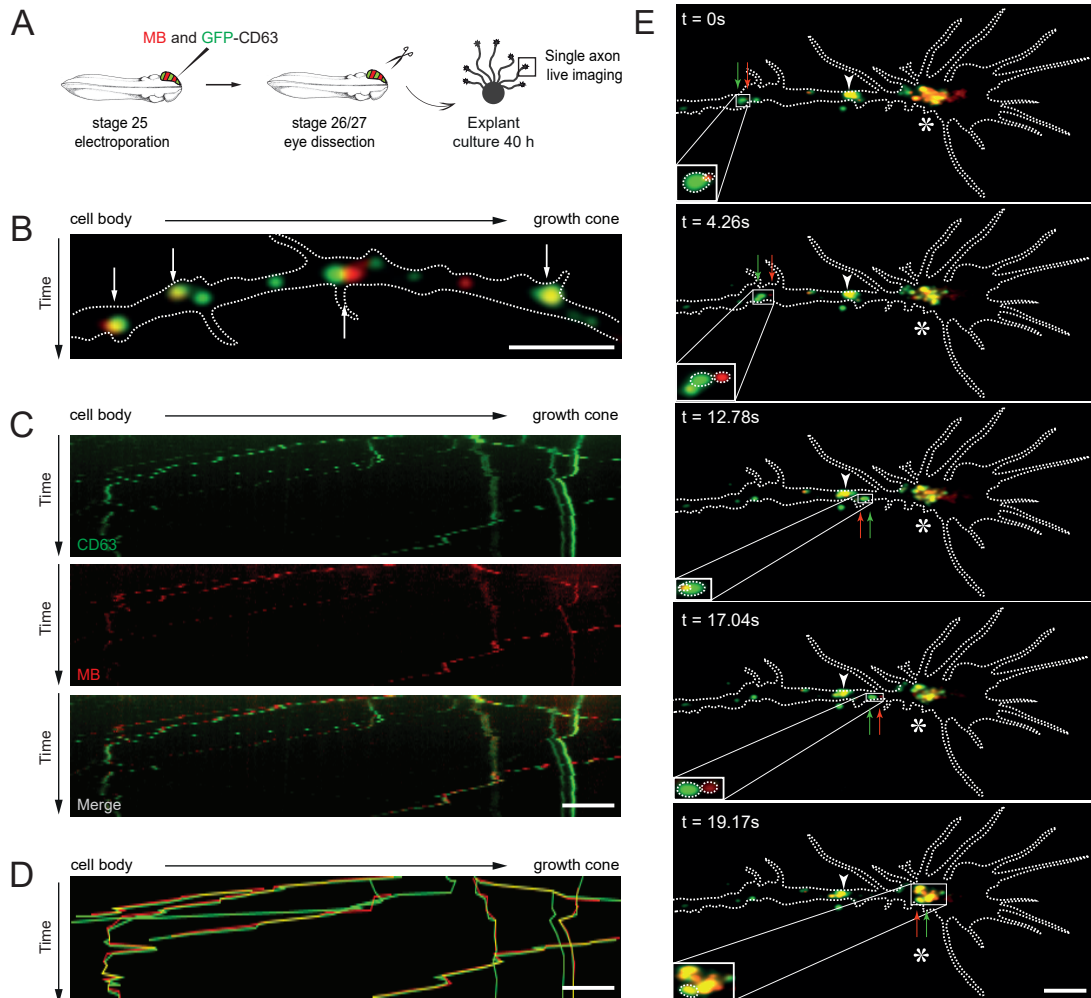
their main target (Holt, Harris, 1983). Collectively, these data suggest that pre-miRNAs do not accumulate in growth cones mostly due to diffusion. A contrario, they indicate that the majority of anterogradely displaced pre-miRNAs are actively transported to promptly reach the growth cone.

5.4 Endogenous pre-miR-181a-1 is transported on vesicles

In neurons, mRNAs are packaged within ribonucleoproteins (RNPs) and trafficked along microtubules (MT) to distal neurites and back (Bauer et al., 2017). Data not reported here, obtained by Antoneta Gavoci, demonstrated that pre-miR-181a-1 trafficking occurred along MT. In agreement with the literature on mRNA transport, pre-miRNAs may be dynamically trafficked as an RNP, as recent data on dendrites suggest (Bicker et al., 2013). However, mature miRNAs, miRNA-repressible mRNAs and components of the miRNA processing machinery associate with late endosomes and lysosomes (LE/Ly) in non-neuronal cells (Lee et al., 2009; Gibbins et al., 2009) and LE/Ly are detected in axons and growth cones (Falk et al., 2014; Konopacki et al., 2016). It is thus possible that pre-miRNAs adopt a non-canonical mode of transport within the axon shaft, associated with LE/Ly. We have here explored this latter possibility.

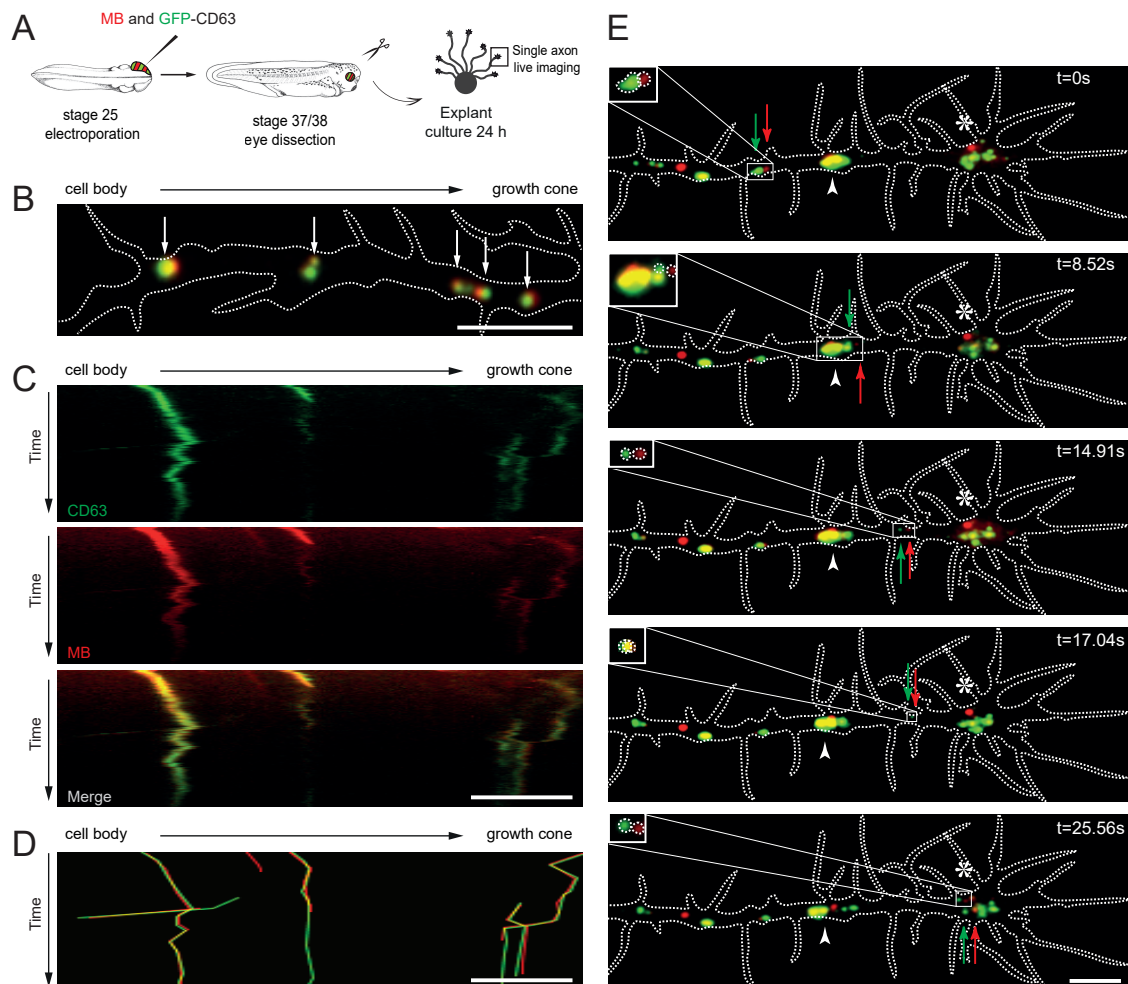
As a marker, we used CD63, a transmembrane protein enriched in this compartment

Figure 5.7: Pre-miRNAs are trafficked associated with vesicles - st26/27



Pre-miRNAs are trafficked associated with vesicles (A) Schematic of the experimental paradigm: $5 \mu\text{M}$ MB and $0.5 \mu\text{g}/\mu\text{l}$ pCS2-CD63-eGFP were co-electroporated at stage 25. Explants were cultured at stage 26/27 and imaged after 40 hours. (B) Representative axon where MB-labeled pre-miR-181a-1 (red) and CD63-GFP-labeled vesicles (green) are co-trafficked (white arrows). (C) Representative kymographs. (D) Composite kymograph shown in (C) where the individual traces were drawn and color coded. Yellow trajectories represent co-trafficking MB-labeled pre-miRNA (red) and CD63-GFP labeled vesicle (green). (E) Representative time-lapse depicting MB labeled pre-miR-181a-1 (red arrow) and CD63-GFP-positive vesicle (green arrow) co-trafficked along the axon shaft to the growth cone (delineated with dashed white lines) wrist (white arrowhead) and central domain (white star). Total number of counted puncta: 253 (MB+), 306 (CD63+). 22 axons, 5 independent experiments. In each independent experiment embryos are derived from a different fertilized frog. Abbreviations: CD63, CD63-GFP; MB, molecular beacon. Scale bars: $5 \mu\text{m}$.

Figure 5.8: Pre-miRNAs are trafficked associated with vesicles - st37/38



Pre-miRNAs are trafficked associated with vesicles (A) Schematic of the experimental paradigm: 5 μM MB and 0.5 $\mu\text{g}/\mu\text{l}$ pCS2-CD63-eGFP were co-electroporated at stage 25. Explants were cultured at stage 37/38 and imaged after 24 hours. (B) Representative axon where MB-labeled pre-miR-181a-1 (red) and CD63-GFP-labeled vesicles (green) are co-trafficked (white arrows). (C) Representative kymographs. (D) Composite kymograph shown in (C) where the individual traces were drawn and color coded. Yellow trajectories represent co-trafficking MB-labeled pre-miRNA (red) and CD63-GFP labeled vesicle (green). (E) Representative time-lapse depicting MB labeled pre-miR-181a-1 (red arrow) and CD63-GFP-positive vesicle (green arrow) co-trafficked along the axon shaft to the growth cone (delineated with dashed white lines) wrist (white arrowhead) and central domain (white star). Total number of puncta counted: 174 (MB+), 224 (CD63+). Data from 17 single axons from 5 independent experiments. In each independent experiment embryos are derived from a different fertilized frog. Abbreviations: CD63, CD63-GFP; MB, molecular beacon. Scale bars: 5 μm .

(Pols, Klumperman, 2009), fused to GFP. We first examined whether CD63-GFP- and MB-labeled pre-miRNA puncta were co-trafficked within single RGC axons following targeted eye electroporation (Figure 5.7 A). We detected that $71.37 \pm 4.07\%$ of MB-positive puncta were co-transported with CD63-GFP-labeled vesicle-like focal puncta and of these, an equal percentage moved anterogradely and retrogradely (Figure 5.7). Similar results were obtained when growth cones were cultured from older stage 37/38 embryos (#MB/CD63-GFP+: $73.58 \pm 4.77\%$) (Figure 5.8). These percentages appear quite high, considering that endogenous unlabeled vesicles present in these axons may mask the extent of co-trafficking. These results suggest that CD63-positive vesicles are, by and large, responsible for pre-miRNAs axonal transport. Remarkably, MB- and CD63-associated signal did not completely overlap (white arrows, Figure 5.7 B, 5.8 B), indicating that pre-miRNAs may not reside inside but may be tethered to vesicles.

We, subsequently, investigated whether pre-miRNAs are transported to growth cones by hitchhiking onto CD63-positive vesicles. We detected that numerous co-trafficked particles reached the growth cones and appeared to stall within the organelle-rich central domain (Dent, Gertler, 2003) (star, Figure 5.7 E, 5.8 E). We also observed a secondary storage point at the growth cone wrist, where MTs become bundled into dense parallel arrays (Bielas et al., 2007) in 70% of axons analyzed (arrowhead, Figure 5.7 E, 5.8 E).

Taken together, these results suggest that pre-miRNAs are transported tethered to vesicles to the growth cone central domain where they are stored.

5.5 Conclusions

The most abundant pre-miRNA among the ones validated in axons, pre-miR-181a-1, is actively trafficked towards the growth cone and stored at the wrist and in the central domain. Those two regions have a peculiar distribution of microtubules. Indeed, the central (C) domain is constituted by stable bundled microtubules that enter the growth cone from the axon shaft (Section 1.2), while the “wrist” represents the transition region between stabilized and dynamic microtubules (Dehmelt, Halpain, 2007). Therefore, pre-miR-181a-1 is trafficked along axon, reaching the “wrist” or the central domain, the two regions where a portion (wrist) or all the stable MT (C domain) finish and become dynamic MT. Those two regions might represent a strategic storage point before spreading the molecules in the growth cone region where needed.

The data presented in this Chapter demonstrate that the pre-miR-181a-1 trafficking is actively driven (Section 5.3) and that its trafficking could not be explained by diffusion only. Moreover, we observed that pre-miR-181a-1 is associated to vesicles in its travel along the axon (Section 5.4). NcRNAs trafficking docked on vesicles and the hitchhiking as trafficking model of pre-miRNAs in axons have never been shown before. Here, CD63-GFP has been used as vesicle marker, and it is a late endosome/lysosome marker enriched in MVBs. However, those data should be further characterized with other vesicles markers to really identify the type of vesicles mediating pre-miRNA trafficking (e.g. Rab4a/5c for early endosome, Rab7a for late endosomes, Rab11a/b for recycling endosome) (Falk et al., 2014; Cioni et al., 2019). Moreover, to further gain insight into hitchhiking as trafficking model it would be necessary to perform higher resolution imaging. In this way it would be possible to investigate whether the pre-miRNA really localized on the outer membrane

of those vesicles.

Nevertheless, the data we obtained already pointing to an intriguing possibility: pre-miRNAs may be transported docked to the outer vesicle and readily available to be directly processed at the right time and space at the axonal level.

6 Pre-miR-181a-1/a-2 local maturation in *Xenopus laevis* RGC axons upon Sema3A stimulation

Growth cones are sensory units that modulate and guide axons along their path to their target in response to cues. Pre-miRNAs are actively delivered to the growth cone (Chapter 5) where Dicer is also located (Chapter 4). These observations suggest that axonal pre-miRNAs may be locally processed into active mature miRNAs upon cue exposure thereby contributing to growth cone turning. Although exogenous double stranded RNA molecules designed to mimic endogenous small mature miRNAs (Ambion's Pre-miR miRNA Precursor Molecules) are known to lead to the increase in mature miRNA in axons upon transfection (Aschrafi et al., 2008; Kar et al., 2013), nothing is known about local processing of *bona fide* pre-miRNAs in axons.

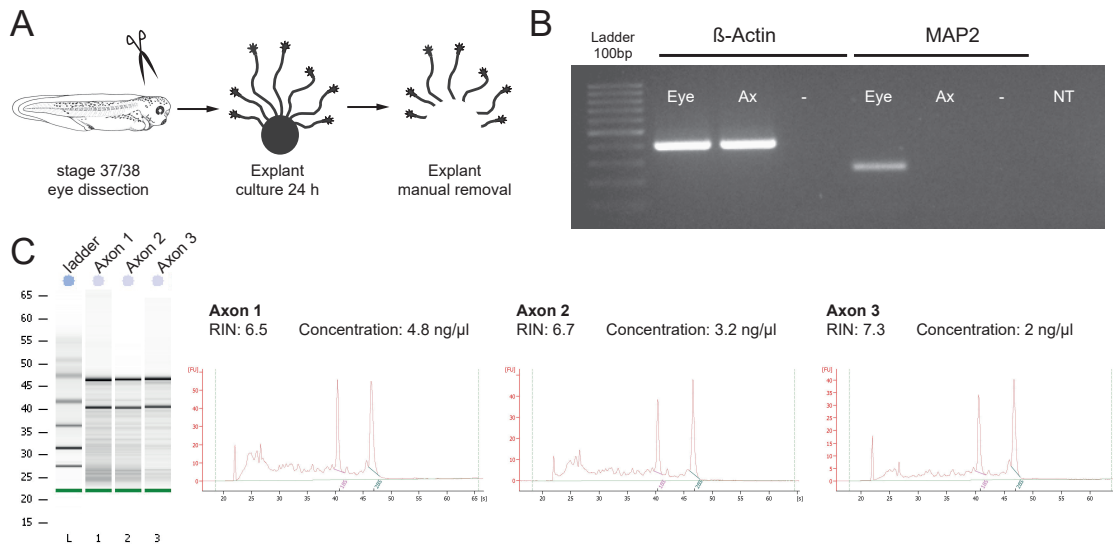
To address this, I used isolated axons. I chose this approach over other widely used methods (Kim, Jung, 2015; Wang, Bao, 2017), namely compartmentalized chambers, Boyden chambers, or LCM axons, because these latter tools cannot preclude communication between various neuronal compartments including axon-soma as they are still physically connected. Moreover, in the case of LCM, the axonal samples need to be fixed prior to microdissection, losing the possibility of having axons severed from the soma still able to respond to cue.

Therefore, to investigate the local processing of endogenous pre-miRNAs in axons, I first optimized an RGC axonal preparation to obtain live, pure isolated axons prepared by carefully dislodging and manually removing the entire explant from the culture (Method Section 3.2.4). Second, I established a qPCR method to investigate miRNA and pre-miRNA expression level changes (Method Section 3.3.5) and finally I exposed only the axonal compartment to specific guidance cues to investigate the local processing of those pre-miRNAs (Method Section 3.2.6).

6.1 Isolated axons preparation

Isolated axon sample collection was established for this thesis project. This kind of preparation yields pure axons that are devoid of the dendritic marker Map2 (Figure 6.1) and are, thus, not contaminated by the somatodendritic compartment. Moreover, the concentration of the collected RNA ranged from 1.5-5 ng/ μ L (depending on the axonal outgrowth and the number of explants per plate) and the RIN, an indication of RNA quality, span from 6 to 8 (Figure 6.1), indicating high yield and quality of the samples (see Methods 3.3.2). In my hands, the health of axons and growth cones is preserved with this approach and growth cones are responsive to cues and still able to grow and pathfind for at least 1.5 hour after the first severed explant (Figure 6.2).

Figure 6.1: Isolated axons purity and quality



Isolated axons purity and quality. (A) Isolated axons are obtained by manual removal of explants after 24 hour culture. (B) RT-PCR from RNA extracted from isolated axons or from stage 37/38 whole eyes. β -Actin mRNA is present both in eye and axons, while MAP2 mRNA is present only in eye, suggesting absence of dendritic material in the axonal samples. (C) Representative Bioanalyzer (Agilent Pico Kit) trace of isolated axonal samples. The two peaks correspond to the ribosomal mRNA 18 S and 28S, and the RIN is computed based on the integrity and intensity of those signals. Abbreviations: Ax, isolated axon; NT, no template RT negative control; -, no template PCR negative control; RIN, RNA integrity number.

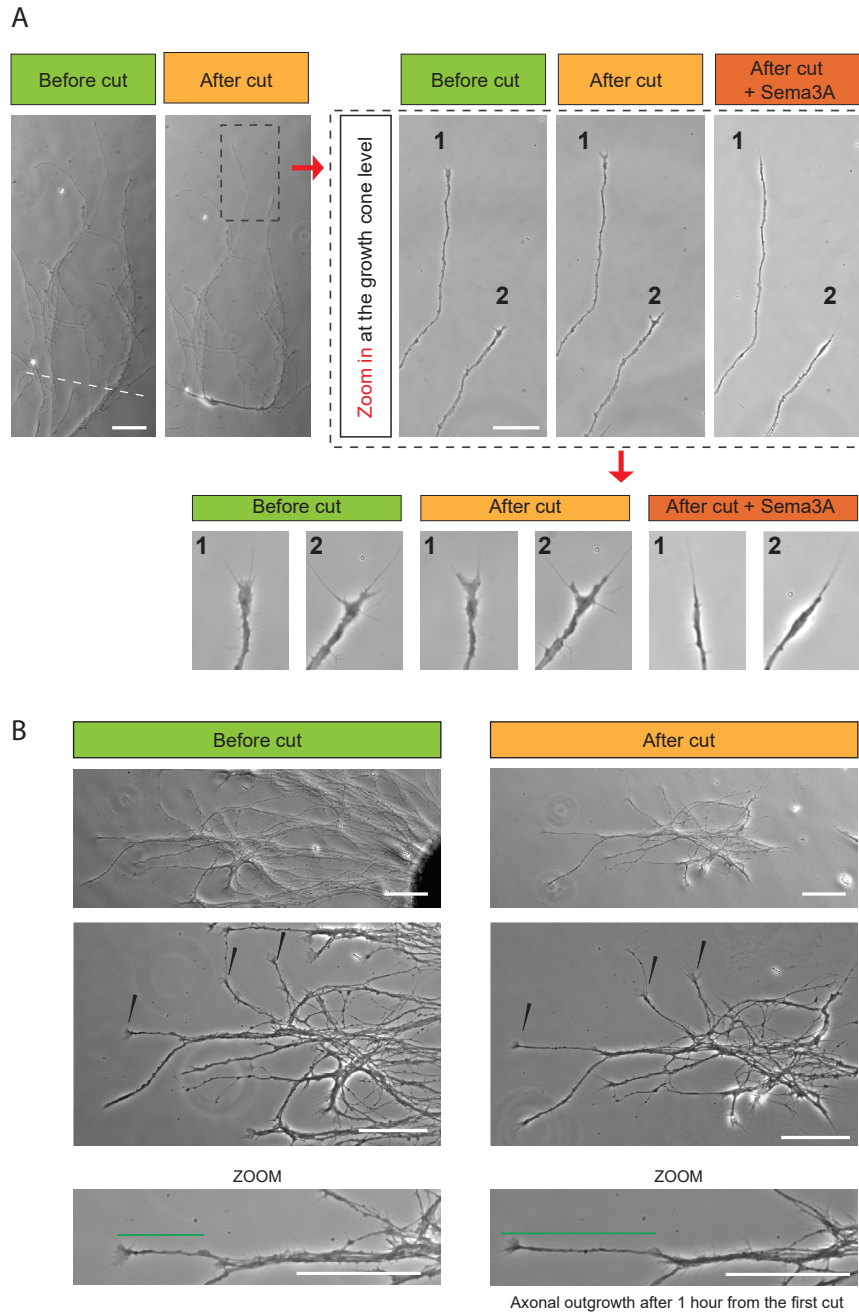
6.2 qPCR: assessment of pre-miRNA processing

I investigated the processing of the endogenous pre-miRNAs through RT-qPCR. After Dicer cleavage, the number of pre-miRNAs molecules will be reduced and the corresponding mature forms will increase (Figure 6.3). These changes in molecule levels can be captured by RT-qPCR. To investigate miRNAs expression levels, different already established kits and assays exist, and I chose the TaqMan miRNA assay, since it is considered the gold standard for miRNAs quantification (Methods Section 3.3.5).

However, there are no existing tools to specifically measure pre-miRNAs level. For this reason, I tested the miQ system (Benes et al., 2015), moving on to a standard SYBR qPCR approach because of obtained specificity issues with miQ in the first trials using RNA material from *Xenopus laevis*.

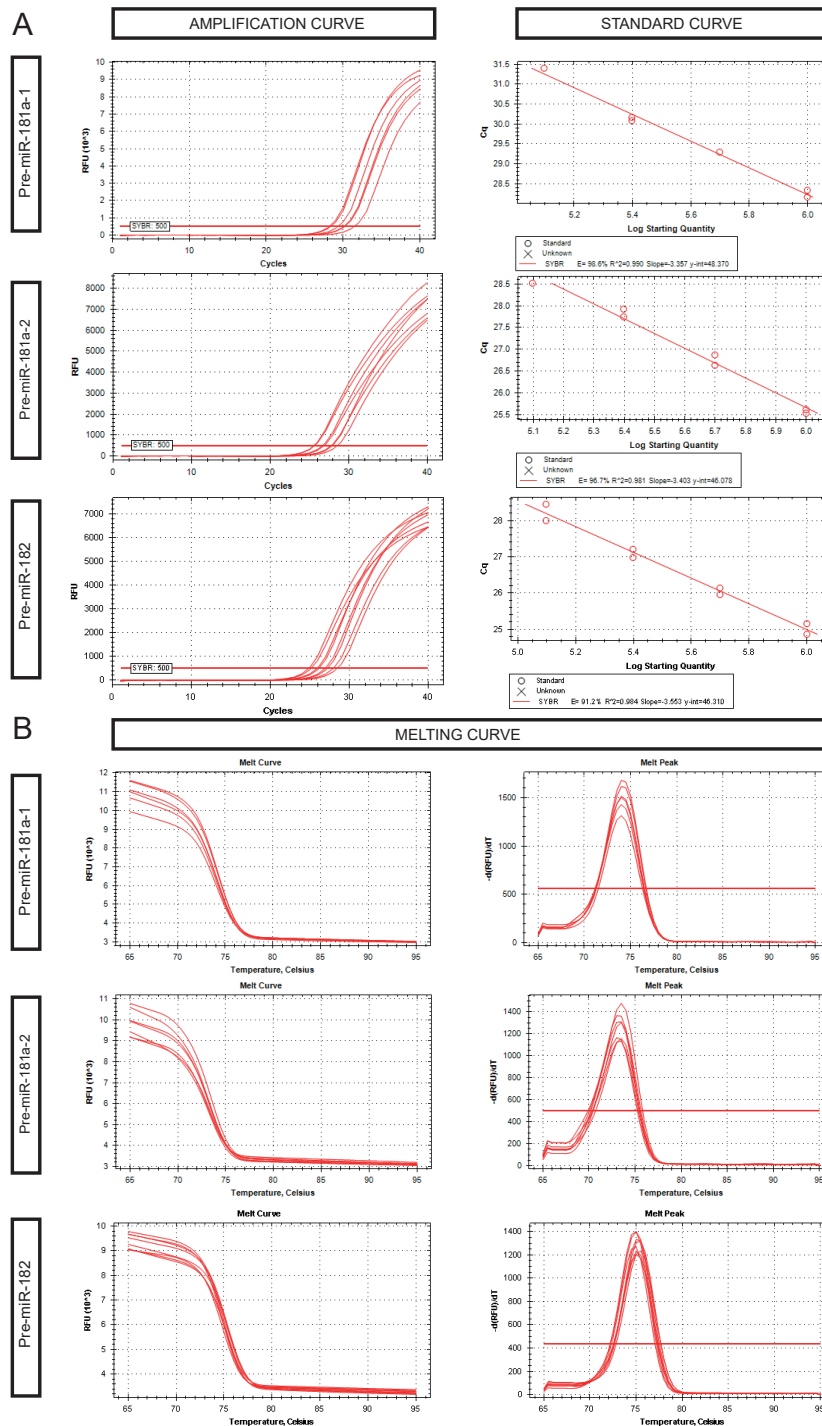
The efficiency and specificity of the new primers designed to measure pre-miR-181a-1, pre-miR-181a-2 and pre-miR-182 expression levels were investigated by running standard and melting curves (Figure 6.3), reagents and primers used are reported in Appendix B (Table B.1). Strong secondary structures (e.g. pre-miRNAs stem-loop) can affect the amplification efficiency, and it is critical to check this aspect to obtain reliable RT-qPCR

Figure 6.2: Isolated axon alive and responsiveness



Isolated axons. (A) Representative image of stage 37/38 RGC axons cultured for 24 hours, before and after explant removal. Zoom-in panels illustrate that growth cones (1 and 2) still adopt a stereotypical shape after removing the explant (“cut”) suggesting that axonal health is maintained. Axons also stay responsive to cues as demonstrated by Sema3A-induced collapse. (B) Representative image of stage 37/38 RGC axons cultured for 24 hours, before and after one hour from explant removal. Small black arrows indicate the growth cones still adopt a stereotypical shape after cut, and the zoomed panels show that axonal outgrowth is preserved after cut. Green line highlight the axonal movement. Scale bars: 50 μm (A left), 30 μm (A zoom-in panels, right; B).

Figure 6.3: Pre-miRNAs RT-qPCR primers efficiency and specificity



Pre-miRNAs RT-qPCR primers. (A) Amplification curves and corresponding standard curves for the three set of primers tested. Efficiency in the amplification of each pre-miRNA is reported in the small box under the standard curve plot. (B) Melting curve for the three set of primers tested. The fluorescence (RFU) with respect to the temperature is shown on the left column, while on the right the variation of fluorescence in time $-(RFU)/dT$ with respect to the temperature is depicted. Abbreviations: RFU, relative fluorescence units.

data (Bustin et al., 2009). All the newly designed primers showed an efficiency higher than 90% with an R^2 of the fitted standard curve between 0.99 and 1, indicating the suitability of these primer sets to being used for RT-qPCR (Figure 6.3).

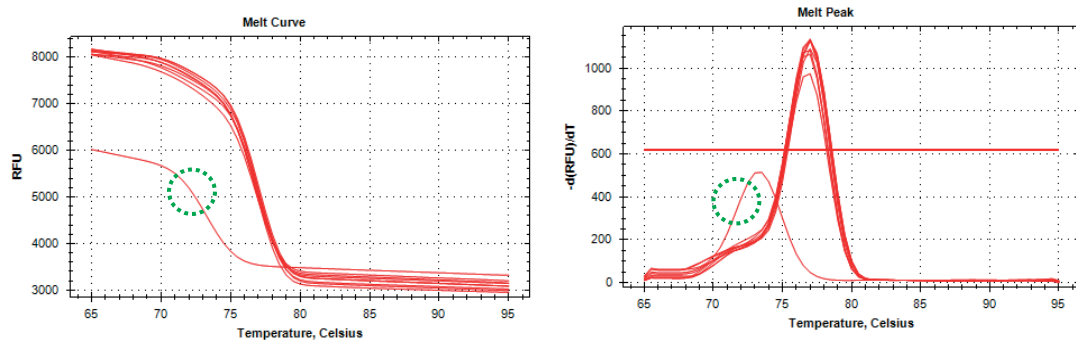
Melting curves are used to obtain a read out of primer specificity in qPCR experiments. As the temperature increase the DNA starts to denature and the intercalated SYBR signal drops (Figure 6.3 B, left). Differences in nucleotide composition of the amplicons, primers dimers and contaminants cause different denaturation curves, hence different melting curves are easily visualized. All the three new primer sets tested show a perfect single melting curve and peak at any dilution, demonstrating the specificity in amplicon population and the absence of primer dimers (Figure 6.3).

6.2.1 U6 as normalizer in axonal samples

Another critical aspect for RT-qPCR is the choice of normalizer. It should be an RNA present in *Xenopus laevis* RGC axons, and whose expression does not change under different experimental conditions, in our case, stimulated and unstimulated axons. The RNA used for normalization should reflect as much as possible the biochemical character of the molecules under study. Its extraction and quantification efficiency, as well as length and expression level, should be comparable to the RNA target (Gharbi et al., 2015).

The best choice for miRNAs normalization would be another miRNA with the characteristics just described. However, there are not known stable miRNA in axons that can be used as normalizer.

Figure 6.4: U6 primers melting curve



U6 primers melting curve (left) Fluorescence (RFU) with respect to the temperature; (right) melting peak plot as the variation of fluorescence in time $-(RFU)/dT$ with respect to the temperature. Green circles in both plot indicate primer dimers presence. Abbreviations: RFU, relative fluorescence units.

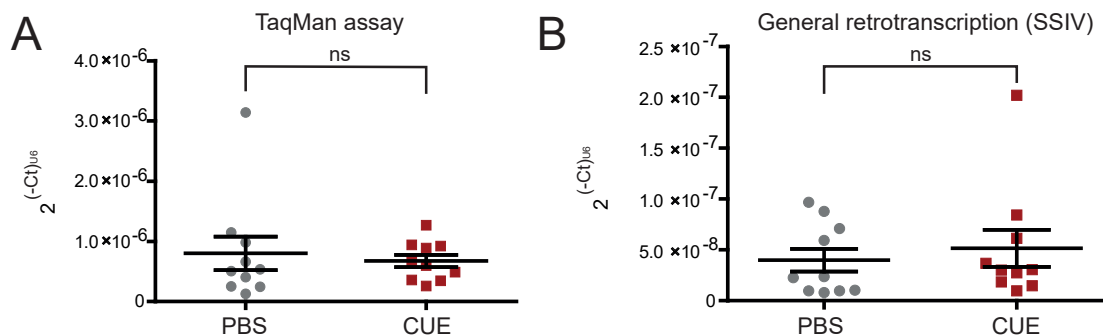
U6, a small non coding RNA, is a well-established normalizer for miRNA RT-qPCR from axons (Natera-Naranjo et al., 2010; Yang et al., 2014; Sun et al., 2014) and it has previously been used in our axonal model system (Bellon et al., 2017). U6 was used in this thesis work as normalizer for both miRNAs and pre-miRNAs with already established primer sets: TaqMan MicroRNA Assay #001973, to be matched for the miRNAs RT-qPCR, and

primers previously used (Zhao et al., 2011; Chai et al., 2015) for SYBR qPCR approach, to be used in pre-miRNAs experiments.

I checked by standard and melting curves the efficiency and specificity of those primers in our sample. I obtained an efficiency of 89.6 % with R^2 equal to 0.996, and a melting curve showing primer dimers (Figure 6.4 and Methods Section 3.5.1 for technical details). Primer dimer amplification curves came up at $Ct > 35$, and by diluting the primers to $2.5 \mu\text{M}$ final concentration, the primer dimer contribution appeared at $Ct > 37$ without affecting the amplification cycles of the sample. Therefore, even if those primers show a probability of interacting with each other, they still gave a good amplification efficiency ($\approx 90\%$) without interfering with sample amplification (all $Ct < 35$ in all the experiments run).

U6 stability was then checked for both TaqMan assay (used to investigate miRNAs) and SYBR assay after general retrotranscription with SSIV (approach used to study pre-miRNAs expression levels). U6 stability was investigated by comparing stimulated and unstimulated axons using $2^{(-Ct)}$ method (Schmittgen et al., 2008) (Figure 6.5). Stimulated and unstimulated axons do not significantly differ in term of U6 expression level, indicating that the small non coding U6-RNA is stable in our experimental conditions and it is suitable as normalizer in our cellular model, *Xenopus laevis* RGC axons (Figure 6.5).

Figure 6.5: U6 stability in RGC stimulated and unstimulated axons

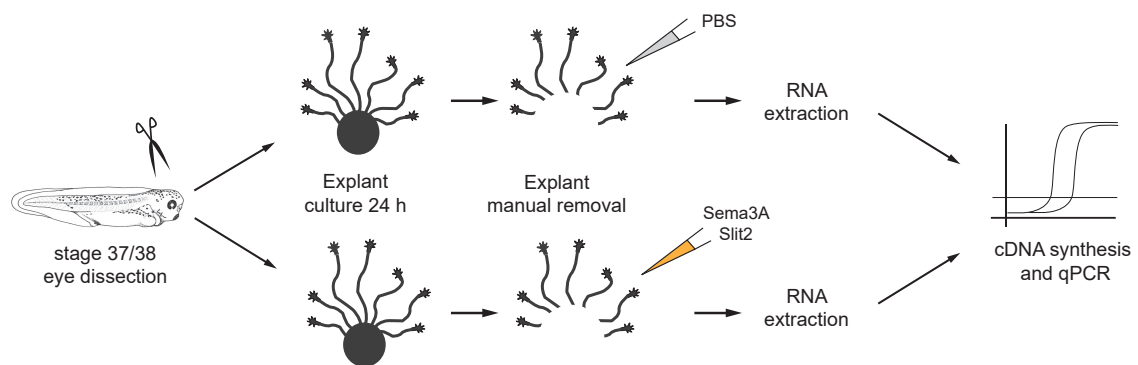


U6 stability in RGC stimulated and unstimulated axons (A) Investigation of TaqMan MicroRNA Assay U6 #001973 stability, quantifying its expression levels in unstimulated (PBS) or stimulated (CUE) using the $2^{(-Ct)}$ method. (B) Investigation of U6 stability in cDNA obtained by general retrotranscription, quantifying its expression levels in unstimulated (PBS) or stimulated (CUE) using the $2^{(-Ct)}$ method. Values are mean \pm SEM. Data were not normally distributed (Shapiro-Wilk test). Two-tailed Mann Whitney test, $n=10$ independent experiment, each n corresponds to a RT-qPCR experiment on axonal RNA derived from 40 explants per condition, in each independent experiment embryos are derived from a different fertilized frog. Exact p-value: 0.6842 (A); 0.4725 (B). Abbreviations: SSIV, SuperScript IV; ns, not significant.

6.3 Pre-miR-181a-1/a-2 maturation in RGC axons upon cue exposure

After setting up the sample preparation to obtain pure, live, responsive isolated axons (Section 6.1) and a reliable system to capture miRNA and pre-miRNA variations (Section 6.2), I investigated if a local maturation of miRNAs occurs upon cue stimulation (Figure 6.6).

Figure 6.6: Experimental paradigm

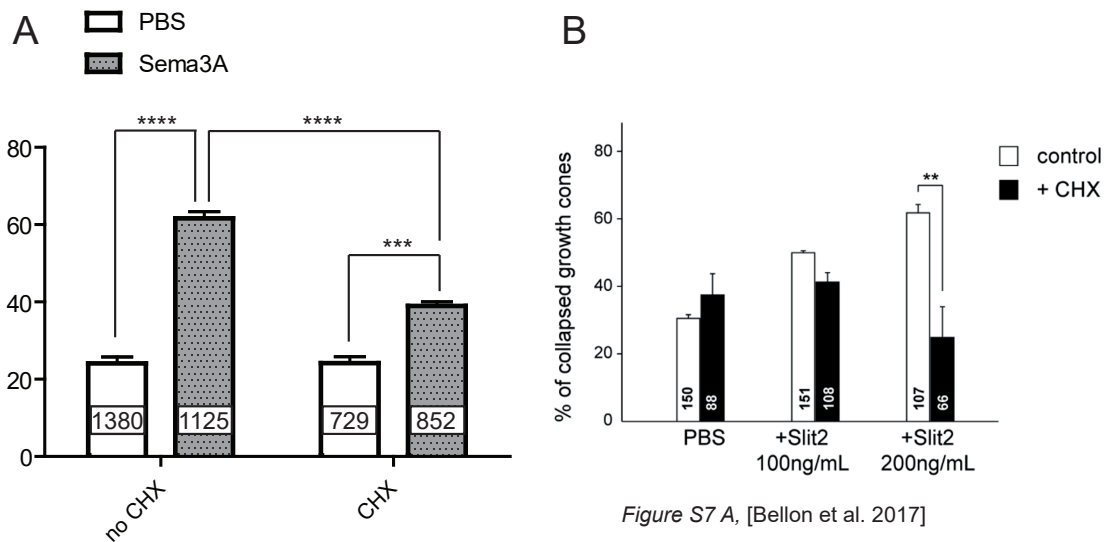


Schematic representation of the experimental paradigm. Stage 37/38 RGC axons cultured for 24 hours, explants were manually removed and axons expose to cue or PBS. Axonal RNA was extracted and miRNAs and pre-miRNAs levels were investigated through RT-qPCR. Sema3A and Slit2: 200 ng/mL.

The cue used were: Sema3A, and Slit2. Those cues are present at the optic tectum, the targeting RGC region (Wit de, Verhaagen, 2007). This choice was driven by experiments conducted in the lab by Archana Iyer, indicating an *in vivo* phenotype at the tectum level: misrouting RGC axons were observed when miR-181 maturation was blocked. The cue were used at a concentration inducing growth cone collapse in a protein synthesis dependency manner (Method Section 3.2.6).

Sema3A bath application induced a $61.22 \pm 2.18\%$ of axonal collapse, which significantly drop at $38.74 \pm 0.02\%$ by CHX incubation (Figure 6.7 A). Slit-2 was already tested through collapse previously (Bellon et al., 2017) (Figure 6.7 B). The final concentration used for both cues was 200 ng/mL.

Figure 6.7: Sema3A and Slit-2 collapse assay



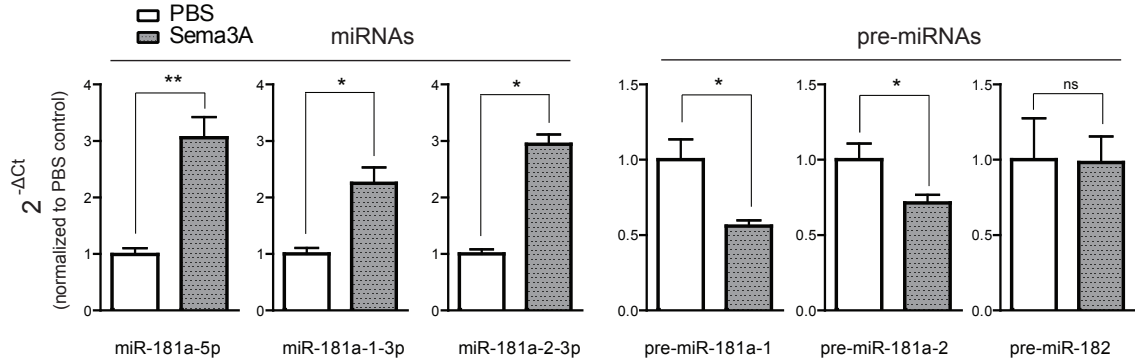
Sema3A and Slit-2 collapse assay (A) Frequency (in percentage) of collapsed growth cones from retinal explants stage 37/38 following a 10 min (200 ng/mL) Sema3A bath application (B) and from stage 35/36 following 10 min 100ng/mL or 200ng/mL Slit2 bath application. At 200 ng/mL a Slit2-induced PS dependent collapse was observed. 50 μ M cyclohexamide (CHX) was applied to block translation. Total number of counted growth cones is reported in the column. Figure (B) from (Bellon et al., 2017), original Figure number indicated in italics below the image. Values are mean \pm SEM. Statistics: * $p < 0.05$, ** $p < 0.01$, *** $p < 0.001$, **** $p < 0.0001$. (C) Two-way ANOVA followed by Tukey's multiple comparison post-hoc test, $n=4$ independent experiments, in each independent experiment embryos are derived from a different fertilized frog.

6.3.1 Sema3A stimulation

Following a Sema3A bath application of explants, I detected a significant increase in mature miR-181a-5p (+207.97%), miR-181a-1-3p (+124.98%) and miR-181a-2-3p (+194.21%) (Figure 6.8). I further measured a significant decrease in pre-miR-181a-1 (-44.07%) and pre-miR-181a-2 (-28.73%) but not in pre-miR-182 (-1.94%) (Figure 6.8).

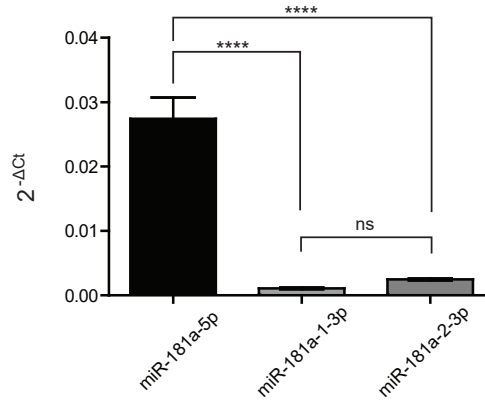
Of interest, miR-181a-5p levels were far higher than miR-181a-1-3p and miR-181a-2-3p (24.30 and 10.11 fold difference respectively) following Sema3A exposure (Figure 6.9), suggesting that the 3p forms are rapidly degraded and unlikely to be functional. Taken together, these results suggest that Sema3A triggers the processing of pre-miR-181a-1 and to some extent of pre-miR-181a-2 into mature miR-181a-5p, miR-181a-1-3p and miR-181a-2-3p.

Figure 6.8: miRNAs and pre-miRNAs level upon axonal Sema3A stimulation



RT-qPCR Quantification of miRNA and pre-miRNA expression levels using the $2^{(-\Delta Ct)}$ method and U6 as normalizer, upon a 10 min (200 ng/mL) Sema3A bath application. Data are normalized to PBS control. Values are mean \pm SEM. Statistics: * $p < 0.05$, ** $p < 0.01$, *** $p < 0.001$, **** $p < 0.0001$. Data were not normally distributed (Shapiro-Wilk test). Two-tailed Mann Whitney test, $n=3-4$ independent experiment. Each n corresponds to a RT-qPCR experiment on axonal RNA derived from 40 explants per condition, in each independent experiment embryos are derived from a different fertilized frog. Abbreviations: ns, not significant.

Figure 6.9: miRNAs relative abundance in RGC axons



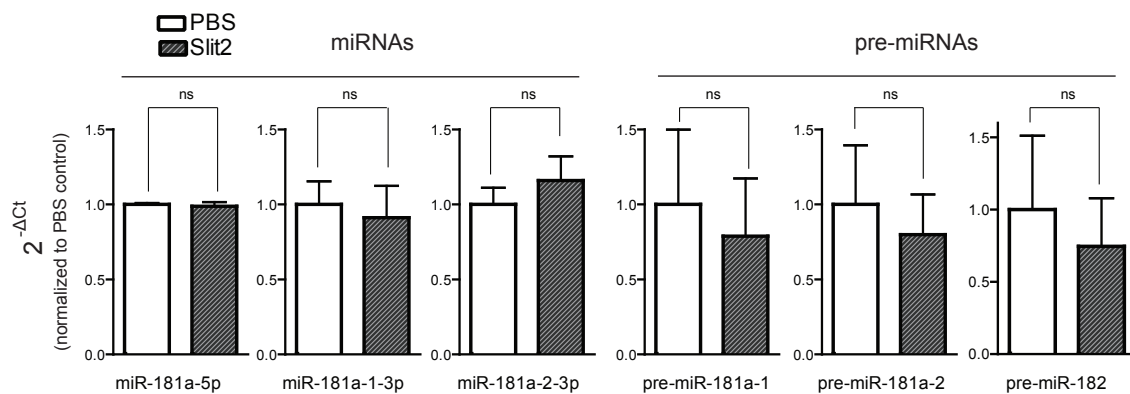
RT-qPCR Quantification of miRNA expression levels using the $2^{(-\Delta Ct)}$ method and U6 as normalizer, upon a 10 min (200 ng/mL) Sema3A bath application. Values are mean \pm SEM. Statistics: *** $p < 0.001$, **** $p < 0.0001$. Data were normally distributed (Shapiro-Wilk test). One-way ANOVA followed by Tukey's multiple comparison post-hoc test, $n=3-4$ independent experiments, each n corresponds to a RT-qPCR experiment on axonal RNA derived from 40 explants per condition, in each independent experiment embryos are derived from a different fertilized frog.

6.3.2 Slit2 stimulation

Additionally, Slit2 exposure did not significantly alter the levels of any of the tested miRNAs including miR-181a-5p (-1.26%), miR-181a-1-3p (-8.82%) and miR-181a-2-3p (+15.85%), and pre-miRNAs including pre-miR-181a-1 (-21.13%), pre-miR-181a-2 (-20.22%), pre-miR-182 (-25.45%) (Figure 6.10).

Slit-2 was shown to decrease miR-182 activity without degrading it (Bellon et al., 2017). It is noteworthy here that the corresponding pre-miR-182 is also not significantly deregulated upon cue exposure.

Figure 6.10: miRNAs and pre-miRNAs level upon axonal Slit2 stimulation



RT-qPCR Quantification of miRNA and pre-miRNA expression levels using the $2^{(-\Delta Ct)}$ method and U6 as normalizer, upon a 10 min (200 ng/mL) Slit2 bath application. Data are normalized to PBS control. Values are mean \pm SEM. Statistics: * $p < 0.05$, ** $p < 0.01$, *** $p < 0.001$, **** $p < 0.0001$. Data were not normally distributed (Shapiro-Wilk test). Two-tailed Mann Whitney test, $n = 3-4$ independent experiment. Each n corresponds to a RT-qPCR experiment on axonal RNA derived from 40 explants per condition, in each independent experiment embryos are derived from a different fertilized frog. Abbreviations: ns, not significant.

6.4 Conclusions

In this Chapter a pure axonal preparation was presented (Section 6.1). Exploiting this technique to isolate axons, pre-miRNA and miRNA expression levels were assessed by RT-qPCR (Section 6.2) to investigate the intriguing possibility of local processing of pre-miRNAs upon cue stimulation (Section 6.3).

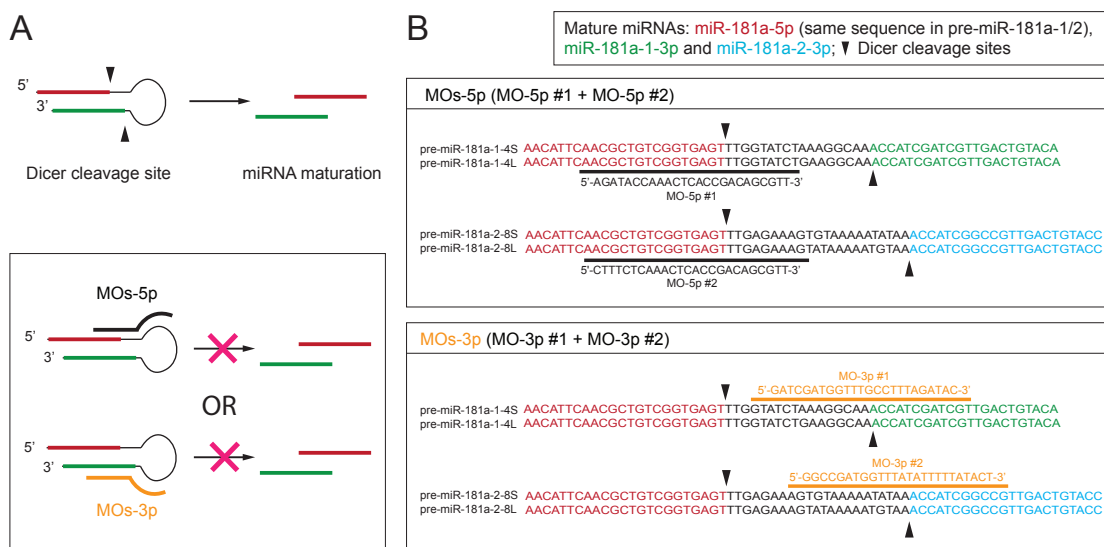
The mechanism unraveled is a pre-miRNA processing which is cue- and pre-miR- specific and occurs locally at the axonal level. Indeed, Slit-2 does not affect neither miRNA nor pre-miRNA expression levels while Sema3A induced specifically the processing of pre-miR-181a-1/a-2, but pre-miR-182 was not altered. An exogenous pre-miRNA was recently demonstrated to be processed in dendrites in response to glutamate (Sambandan et al., 2017), pointing to the exciting possibility that cue-induced local miRNA maturation may be a key mechanism across different compartments.

7 Newly generated miRNAs are important for growth cone steering ex vivo

Pre-miR-181a-1/a-2 are locally processed in retinal ganglion cells (RGC) axons upon Sema3A exposure: a local miRNAs production that is both pre-miRNA and cue specific (Chapter 6). These observations open new questions: “What is the role of the locally matured miRNAs?” “Is growth cone responsiveness dependent on this process generating mature miRNAs locally?”.

I thus explored whether newly generated miRNAs (NGmiRNAs) are important players in the modulation of growth cone behavior. If they are indeed crucial, then blocking their production should impair growth cone responsiveness to cues. To investigate this I used a loss of function approach, blocking miRNAs biogenesis by preventing Dicer-mediated cleavage with a mix of two morpholinos (MOs) complementary to the 5p (MOs-5p) or 3p (MOs-3p) Dicer cleavage site of both pre-miR-181a-1 and -2 (Figure 7.1).

Figure 7.1: Morpholinos blocking Dicer cleavage



Mixture morpholinos (A) Schematic of pre-miRNA maturation upon Dicer cleavage (A, top panel). Schematic of MOs-5p and MOs-3p targeting 5' and 3' pre-miRNA Dicer cleavage site respectively (A, bottom panel). (B) Exact MO targeting region within pre-miR-181a-1 and -2 derived from chromosomes 8, and 4, long (L) or short (S). Black arrowheads indicate Dicer cleavage sites.

First, miRNA maturation was blocked within the entire CNS using microinjection (performed by Antoneta Gavoci) to validate morpholinos efficiency (Section 7.1). In a second step, I then blocked miRNA maturation by axonal transfection of the morpholinos, blocking the miRNAs biogenesis right before axonal stimulation (Section 7.2). Hence, this approach leads to a miRNAs biogenesis regulation in a time and space specific manner.

7.1 MO design and validation

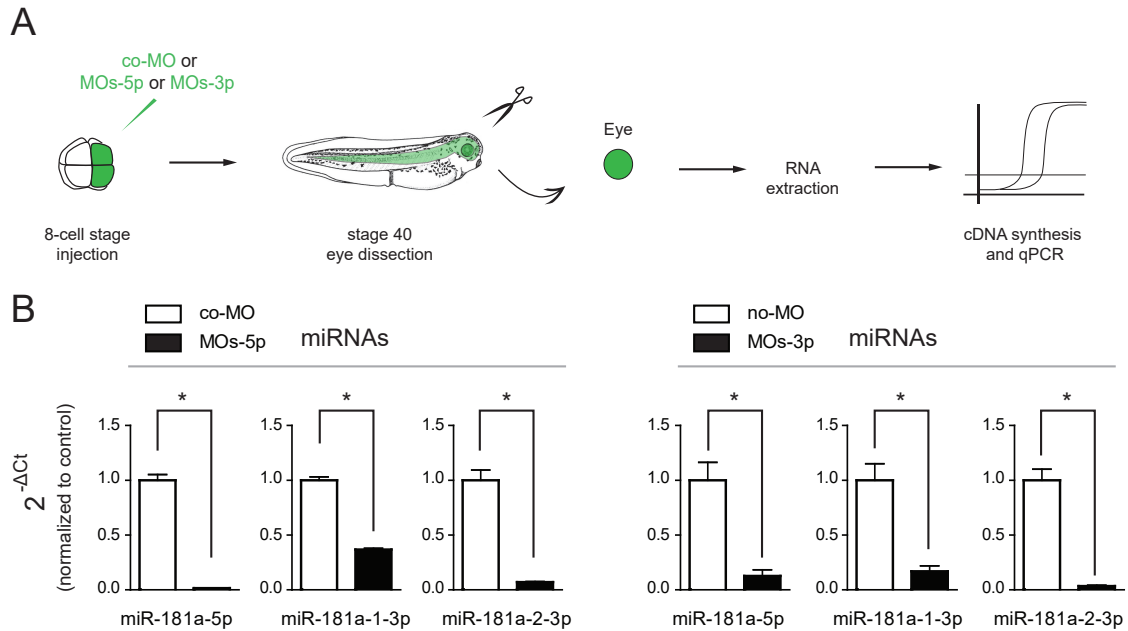
Morpholinos were designed to block pre-miR-181a-1/a-2 Dicer cleavage sites at the -5p (MOs-5p) or -3p side (MOs-3p) in both chromosomes (Figure 7.1 A). MOs-5p block the miR-181a maturation but they also recognize miR-181a-5p (but not with miR-181a-3ps) since their sequence is partially complementary to the mature isoform (69% overlap, Figure 7.1 B). Similarly MOs-3p is partly complementary to mature miR-181a-1-3p and miR-181a-2-3p but not with miR-181a-5p (54% overlap, Figure 7.1 B). We aimed for a decrease in miRNAs levels due to hybridization to the pre-miRNAs. Measuring miRNAs by PCR in the presence of antisense oligonucleotides might be challenging (Torres et al., 2011). Therefore, both cocktails were tested and the mature miRNAs not recognized by the MOs cocktails measured by RT-qPCR (e.g. miR-181a-3ps with MOs-5p and miR-181a-5p with MOs-3p, Figure 7.4).

Therefore, before investigating potential effects at the axonal level, I first established that the two MO cocktails successfully impair pre-miRNA processing *in vivo*. For this, Antoneta Gavoci microinjected MOs at the 8-cell stage into those cells fated to form the CNS, and I measured miRNA levels in stage 40 retinal extracts by RT-qPCR (Figure 7.2 A). As expected, MOs-5p and MOs-3p both lead to the strong reduction of mature miR-181a-5p (-98.41% [MOs-5p] and -87.36% [MOs-3p]), miR-181a-1-3p (-63.20% [MOs-5p] and -83.02% [MOs-3p]) and miR-181a-2-3p (-92.89% [MOs-5p] and -96.55% [MOs-3p]) (Figure 7.2 B), confirming that these MOs block miRNA biogenesis. Indeed, if the biogenesis was not impaired, then MOs-5p would not alter the levels of 3ps; and MOs-3p would not alter the levels of miR-181a-5p and this is not the case.

Through microinjection the pre-miR-181a-1/a-2 were blocked from the 8-cell stage, hence at stage 40 (1 week later) I expected to observe a strong knock-down of all the mature isoforms. However, to uncover the role of the locally matured miRNAs and the potential dependency of growth cone responsiveness on local pre-miRNA processing, a more specific axonal knock-down (KD) approach was selected. A KD at the cellular level of pre-miRNA processing would have been a major confounding. If an axonal KD of the process were observed with this approach, it would have been impossible to determine the cause. Impossible to distinguish if it was due to alteration of biogenesis in axons or in the cell body.

An efficient and rapid way to introduce molecules into the axonal compartment is required to achieve a specific axonal KD. Fabio Laprea and Archana Iyer tried different axonal transfection approaches using lipofectamine and Neuromag beads (Method Section 3.2.5). Based on their previous experiments, I selected the Neuromag approach due to its superior performance both in timing and efficiency to investigate the axonal role of NGmiRNA.

Figure 7.2: Morpholino validation: RT-qPCR microinjected MO and co-MO



Experimental paradigm for morpholino mixture validation (A) Stage 40 eyes, derived from either 150 μM MOs-5p or co-MO or 200 μM MOs-3p or co-MO microinjected embryos, were dissected and miRNAs expression levels investigated through RT-qPCR. (B) Quantification of the expression levels of miRNAs using the $2^{(-\Delta Ct)}$ method and U6 as normalizer, from stage 40 eyes, derived from either 150 μM MOs-5p or co-MO or 200 μM MOs-3p or co-MO microinjected embryos. Data are presented normalized to control. Values are mean \pm SEM. Statistics: * $p < 0.05$. Data were not normally distributed (Shapiro-Wilk test). Two-tailed Mann Whitney test. $n=4$ independent experiments, each n corresponds to a RT-qPCR experiment on RNA derived from 10 eyes, in each independent experiment embryos are derived from a different fertilized frog. Abbreviations: ns, non-significant.

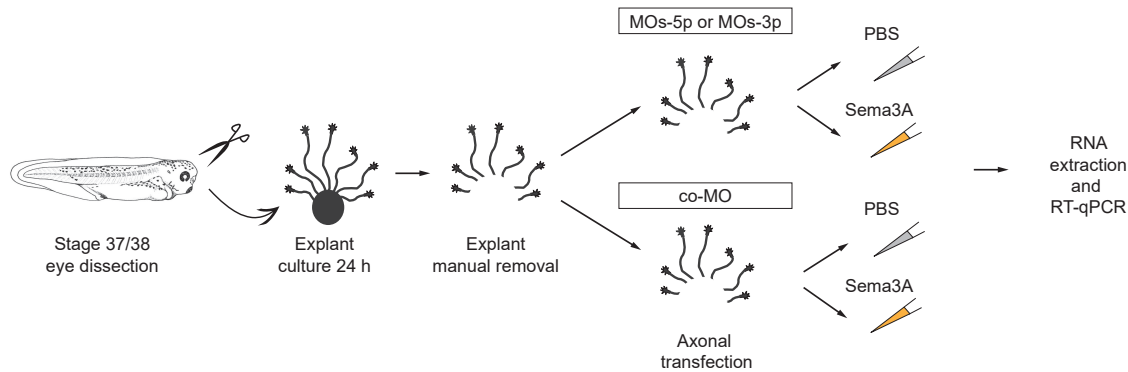
7.2 Axonal block of NGmiRNAs

Isolated axons survive in a healthy state for at least 1.5 hours (Method Section 3.2.4), thus it is essential to perform axonal transfection and stimulation within this timeframe to guarantee proper axon responsiveness.

I first assessed whether the MO cocktails prevented Sema3A-induced pre-miR-181a-1 and pre-miR-181a-2 processing in pure isolated axons *ex vivo* (Figure 7.3). Stage 37/38 isolated axons were transfected with MOs-5p or -3p, and subsequently bathed with Sema3A or PBS for 10 min (Figure 7.3). The level of the mature miRNA stemming from the strand opposite to that complementary to the MO was measured by TaqMan RT-qPCR (Figure 7.3). The amplification of the opposite strand was selected to avoid competition between the TaqMan probe and the MO for the mature miRNAs.

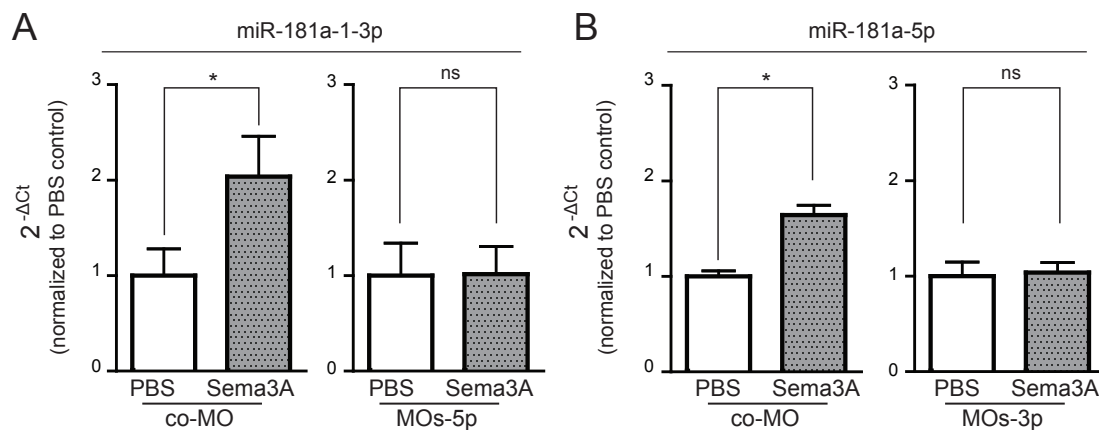
As expected, Sema3A induced a significant increase in axonal miR-181a-1-3p and -5p levels in co-MO transfected axons (+103.59 [3p]; +64.23 [5p]) indicative of pre-miRNA

Figure 7.3: MO and co-MO axonal transfection



Experimental paradigm for RT-qPCR on axonal transfected axons Stage 37/38 explants were cultured 24 hours and axons manually isolated by severing them from explants. Isolated axons were then transfected with 2 μ M MOs-5p, MOs-3p or co-MO, bathed 10 minutes with Sema3A 200 ng/mL or PBS 1x. miRNAs expression levels were assessed using RT-qPCR.

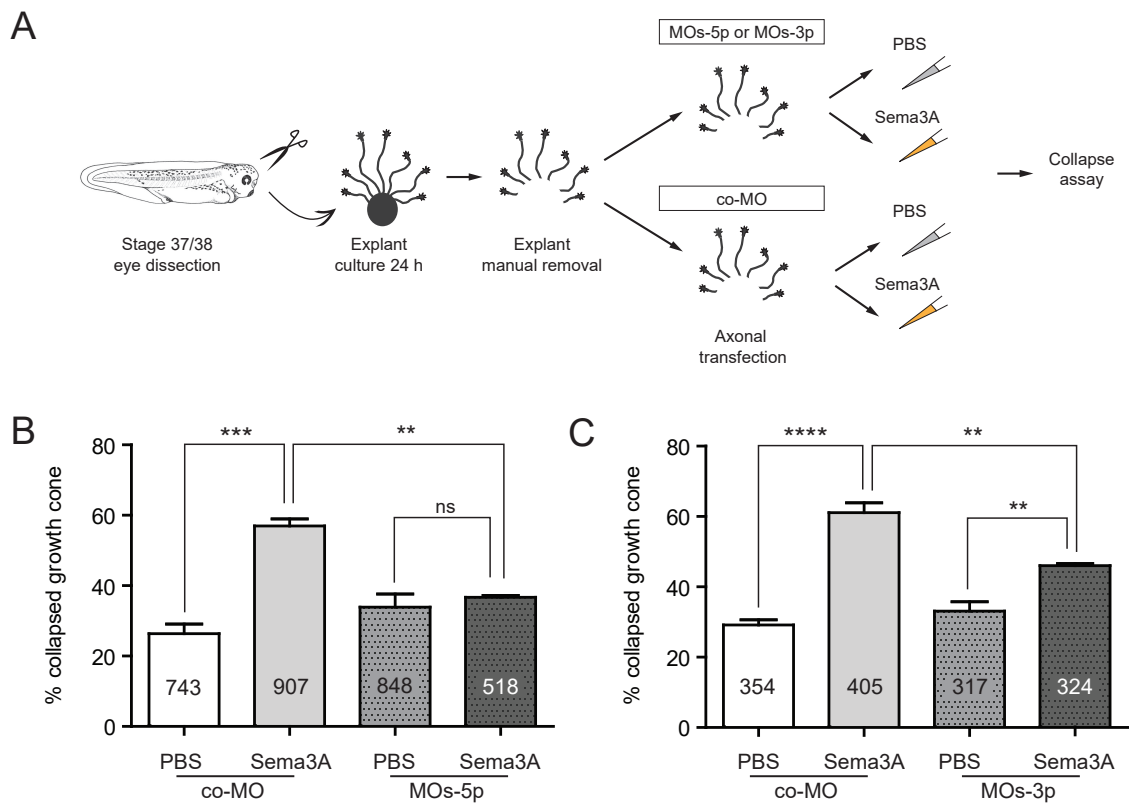
Figure 7.4: miRNAs expression levels in transfected axons



RT-qPCR: MO or co-MO transfected axons Quantification of the expression levels of miR-181a-1-3p (A) and miR-181a-5p (B) using the $2^{(-\Delta Ct)}$ method and U6 as normalizer, from axons transfected with 2 μ M MOs-5p, MOs-3p or co-MO, upon Sema3A bath application. Data are presented normalized to PBS control. $p < 0.05$. Data were not normally distributed (Shapiro-Wilk test). Two-tailed Mann Whitney test. (A) $n=4$; (B) $n=3$; independent experiments. Each n corresponds to a RT-qPCR experiment on axonal RNA derived from 20 explants per condition, in each independent experiment embryos are derived from a different fertilized frog. Abbreviations: ns, non-significant.

processing but not in MOs-5p and -3p transfected axons (+1.42 [3p]; +3.83 [5p]) (Figure 7.4). This indicates that the MOs block Dicer-induced pre-miRNA cleavage in axons and also confirms the specificity of Sema3A-induced pre-miR-181a-1 and pre-miR-181a-2 processing observed earlier.

Figure 7.5: Collapse assay blocking pre-miRNAs maturation



Collapse assay: MO or co-MO transfected axons (A) Experimental paradigm: stage 37/38 explants were cultured for 24 hours and axons were manually isolated by severing them from explants. Isolated axons were then transfected with 2 μ M MOs-5p, MOs-3p or co-MO, bathed 10 minutes with Sema3A 200 ng/mL or PBS 1x. Growth cone responsiveness to Sema3A was then investigated by collapse assay. (B,C) Frequency (in percentage) of collapsed growth cones from stage 37/38 embryos, following a 10 min (200 ng/mL) Sema3A bath application. 2 μ M MOs-5p (B) or 2 μ M MOs-3p (C) were used. The total number of counted growth cones is reported in the column. Values are mean \pm SEM. Statistics (B,C): ** $p < 0.01$, *** $p < 0.001$, **** $p < 0.0001$. Two-way ANOVA followed by Tukey's multiple comparison post-hoc test, $n=3$ independent experiments. Each n corresponds to an independent experiment on 16 cultured explants per condition, in each independent experiment embryos are derived from a different fertilized frog. Abbreviations: co-MO, control morpholino; MOs-3p and MOs-5p, morpholino mixture blocking Dicer cleavage, recognizing respectively the loop and -3p or -5p of pre-miR-181a-1/-2; ns, not significant.

7.2.1 Growth cone responsiveness to Sema3A is impaired when blocking NGmiRNAs

I then examined whether blocking pre-miRNAs processing, as above, impairs growth cone responsiveness to Sema3A. I employed a similar experimental paradigm except that this time I assessed growth cone behavior using collapse assay (Figure 7.5 A). The collapse assay is an *ex vivo* test on axons to investigate cue responsiveness (Campbell, Holt, 2001). When repellent cues are bath applied to axonal culture, the growth cones fully collapse (Method Section 3.2.7). Therefore, this assay can be used to investigate for proper or impaired axonal responsiveness to guidance cue *ex vivo*.

Sema3A induced growth cone collapse in isolated axons transfected with co-MO (Figure 7.5 B: 26.37 ± 2.76 % [PBS]; 56.97 ± 2.03 % [Sema3A]; Figure 7.5 C: 29.17 ± 1.43 % [PBS]; 61.13 ± 2.76 % [Sema3A] collapsed growth cones). In contrast, a significant reduction in Sema3A-induced collapse was observed in axons transfected with MOs-5p or -3p (MOs-5p (Figure 7.5 B): 33.89 ± 3.73 % [PBS]; 36.71 ± 0.53 % [Sema3A]; MOs-3p (Figure 7.5 C): 33.12 ± 2.67 % [PBS]; 46.04 ± 0.61 % [Sema3A] collapsed growth cones).

7.3 Conclusions

Sema3A induces growth cone collapse within 5-10 minutes (Campbell et al., 2001) and the specific axonal block of pre-miR-181a-1/a-2 maturation impaired severely the expected collapse response within the 10 minutes of the assay. This observation suggests that NGmiRNAs are crucial for Sema3A-mediated growth cone turning and steering and that the pre-miRNA processing occur in a short time-frame after cue exposure. Collectively, these data indicate that the local processing of pre-miR-181a-1/a-2 upon Sema3A is axonal-specific (Figure 7.4) and that NGmiRNAs upon cue exposure are required for growth cone responsiveness to Sema3A (Figure 7.5).

NGmiRNAs probably impinge on the Sema3A signaling pathway by targeting transcripts important for Sema3A-mediated growth cone turning. A silencing of specific mRNAs mediated by NGmiRNAs upon Sema3A adds another layer of regulation to the complexity of axon guidance response during brain wiring.

8 NGmiRNAs silence locally translated transcripts

Pre-miR-181a-1 and pre-miR-181a-2 are processed upon Sema3A exposure (Chapter 6) and blocking their maturation impairs Sema3A-mediated growth cone responsiveness (Chapter 7). Newly generated miRNAs (NGmiRNAs) may exert their regulatory function via several molecular mechanisms; they may 1) silence translationally active transcripts acting as a switch, 2) prevent translational onset of axonal mRNAs as a fail-safe mechanism to avoid spurious translation, or 3) degrade unneeded or unwanted transcripts to promote growth cone turning. We ruled out the latter possibility, since the combined processes of miRNA biogenesis and mRNA degradation are unlikely to occur within the time frame of cue stimulation (5-10 min). We thus explored the effect of NGmiRNAs on local translation.

8.1 Investigation of local axonal translation: polysome profiling

The first approach tested was polysome profiling, whereby mRNA is fractionated based on the number of associated ribosomes to capture the translation state of the sample (Figure 8.1 A). When an mRNA molecule is actively translated, it is engaged with multiple ribosomes, hence associated with polyribosomes (a.k.a. polysomes) and mRNAs which are translationally repressed are not engaged with polyribosomes (Sheets et al., 2010). Therefore, by polysome collection and profiling of the non associated and associated mRNAs, it is possible to obtain an overview of concurrent transcriptome and translato-
me changes through a combination of this technique with sequencing.

According to the different number of associated ribosomes to the mRNAs, after sample lysis, the actively translated transcripts are separated by centrifugation in a sucrose gradient from the not translated ones (Figure 8.1 A). The different fractions from the linear gradient are collected separately, and the UV absorption is measured for all of them, showing specific peaks in correspondence to 40S, 60S, 80S and polysomes (Figure 8.1 A, right). The intensity of the peak is proportional to the amount of RNA in that particular fraction. The single ribosomal subunits (40S, 60S) are the lightest, the first fractions in the sucrose gradient. These fractions are followed by the one containing monosomes (80S), in which a single ribosome is associated to the transcript. The heaviest fractions on the bottom part of the sucrose gradient, are the one following the 80S peak, where multiple ribosomes associated to mRNAs (Figure 8.1 A).

The possibility of capturing the translato-
me state *Xenopus laevis* axons through polysome profiling was tested in collaboration with Gabriella Viero and Marta Marchioretto (CNR, FBK Trento), who recently established a sucrose gradient based fractionation method for small sample sizes, similar to those found in axon samples (Bernabo et al., 2017).

For a successful polysome profiling in *Xenopus laevis* it is first crucial to identify the 80S peak position in the absorption profiling, because after this peak all the polysome-

containing fractions will be collected from the gradient (Figure 8.1 A). Secondly, it is important to investigate if the detection sensitivity of this technique enables me to capture translational changes at the axonal level.

The identification of the 80S peak was performed on whole embryos. When whole embryos were lysed and fractionated, a clear profile with 80S peak and polysomes was obtained compared to the negative control samples in which no *Xenopus laevis* lysate was loaded (Figure 8.1 B). Whole embryo profiles were used as reference to collect polysome fractions in other analysed samples (all fractions after the 80S peak). For the investigation of the sensitivity in polysomes detection, we have to take into account that polysome fractions from low concentrated samples or with low translational activity, may contain pg of RNA material, showing negligible absorption peaks not easy to be identify by eye. In those cases, all the fractions after the 80S peak are collected, and the RNA content in these polysome fractions measured with more sensitive technique (e.g. Picokit Bioanalyzer) before moving to further analysis (e.g. RNA-seq).

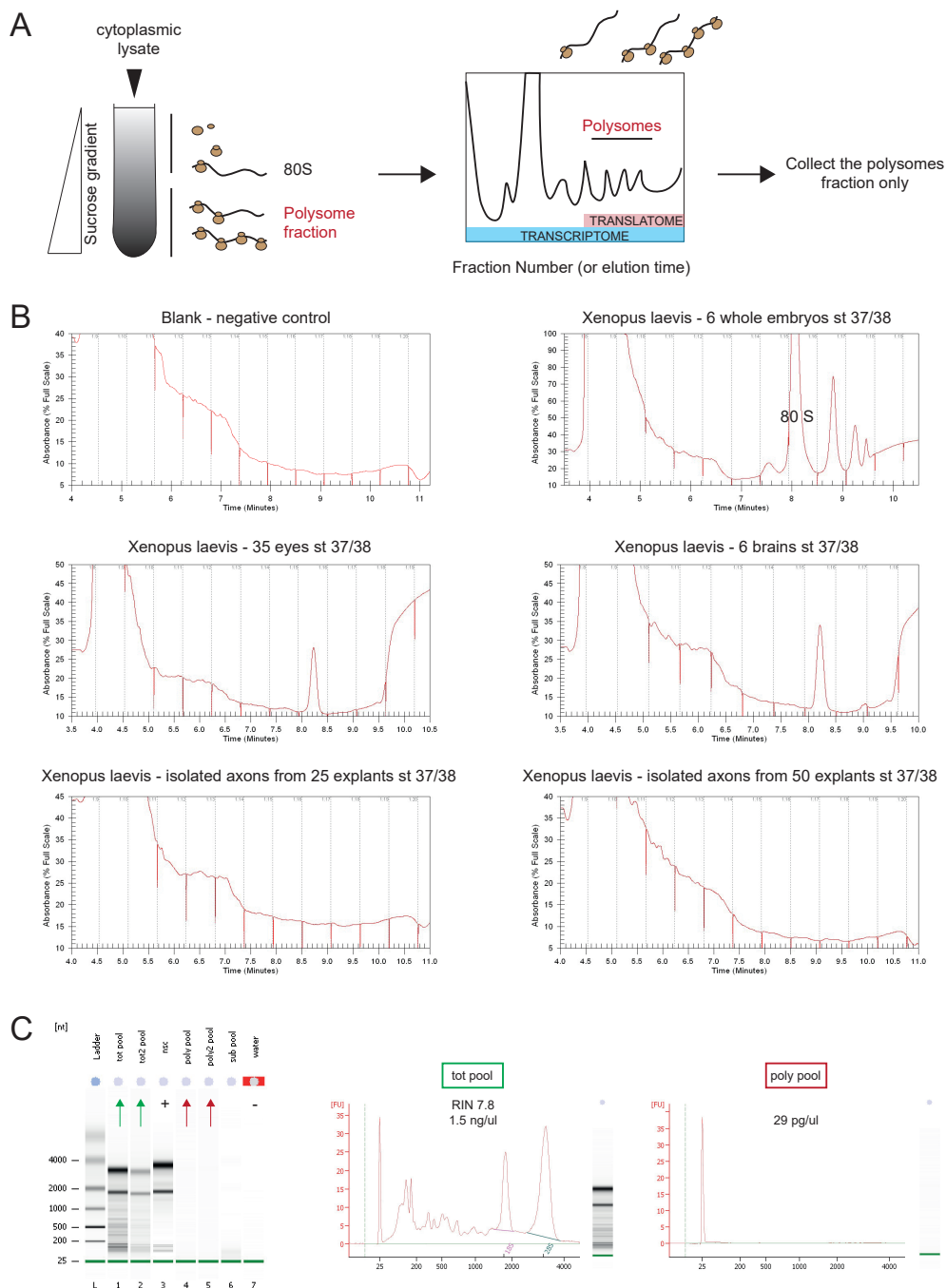
While eye and brain samples show a 80S peak, no signal was detected in the axonal samples (Figure 8.1 B). To better understand if the absence of the trace in axons was due to sensitivity of the technique or due to the complete loss of the sample during the lysis step, I prepared other isolated axonal samples and split them in two after lysis. One for direct RNA extraction, measuring the total RNA content and the other to perform polysome fractionation, investigating the amount of RNA in the polysome fractions (Figure 8.1 C).

Total RNA levels in whole axons was of good quality (RIN = 7.8, RIN = 8.6) and with concentrations ranging from 1.5 to 1 ng/ μ l (Bioanalyzer data, Figure 8.1 C). However, despite the quality and quantity of the total RNA extraction, indicating no RNA loss during the lysis step, no RNA was detected in the polysome fractions derived from axonal samples. This result indicates that even using the sucrose gradient optimized for small sample input, the sensitivity level required to detect polysomes in *Xenopus laevis* RGC isolated axons was not reached. To increase sensitivity, one should optimize other protocol steps before working with this model (e.g. cycloheximide concentration and incubation, improve samples' concentration after fractionation).

On the other hand, the lack of detected polysome fractions may be explained biologically. Indeed, it is still unknown how ribosomes mediating axonal translation are organized in RGC axons. Recently, β -Actin mRNA was shown to be docked and locally translated in RGC branches sites *in vivo* (Wong et al., 2017). Previous work in dendrites showed β -Actin accumulation in hotspots in hippocampal neurons *in vitro* (Yoon et al., 2016), contrasting with the broadly distributed pattern of newly synthesized β -Actin seen in *Xenopus laevis* RGC axonal growth cones in culture (Ströhl et al., 2017). The authors of this study suggested that these divergent Actin patterns, could be explained by either nascent protein accumulation, or the nature of translation by monosomes versus polysomes (Wong et al., 2017). Since there is no evidence of a polysome-based translation system in *Xenopus laevis* RGC axons, I cannot exclude the possibility that the observed absence of polysomes in axons (Figure 8.1), is a real biological results.

8.1 Investigation of local axonal translation: polysome profiling

Figure 8.1: *Xenopus laevis* polysomes fractionation



***Xenopus laevis* polysomes fractionation** (A) Schematic of cytoplasmic lysate separation in a sucrose gradient. The polysome fractions (active translated sample portion) are collected separately from the rest of mRNAs contained in the sample. (B) *Xenopus laevis* sample profiles after fractionation: blank, negative control where no lysate was loaded. Samples tested: whole embryos, eyes, brains, and axonal sample profiles. Note in whole embryos sample a saturation of 80S peak is present as clear polysome peaks are following the one derived from monosomes. (C) Bioanalyzer trace of axonal sample. Green arrows and box indicate total axonal RNA traces; red arrows and box indicate axonal RNA collected from the polysome fractions.

8.2 Investigation of local axonal translation: a candidate-driven approach

Polysome profiling represents a promising technique to capture the transcriptome and translome state in *Xenopus laevis* samples, however this approach appeared unsuitable for isolated axonal samples, in which the RNA starting amount is hugely limited. Moreover, it is still unknown if translation in axons relies on polysomes or monosomes. If polysomes are indeed part of the axonal translational machinery, further optimization with improved amounts of starting material would be necessary to obtain a working protocol.

Considering the limitation of working with low amounts of material, I moved towards a candidate-driven approach to investigate which mRNAs may be regulated by NGmiRNAs in axons. We observed pre-miR-181a-1 and pre-miR-181a-2 processing upon *Sema3A* exposure (Chapter 6), and a failure of the a proper *Sema3A* responsiveness by blocking this local maturation (Chapter 7). Since miR-181-5p was the highest in expression level upon *Sema3A* exposure (Figure 6.9), we aimed to identify those locally regulated miR-181-5p targets whose translation would be silenced upon *Sema3A* exposure and whose translation would be activated if miR-181-5p regulation is compromised.

As aforementioned, we hypothesized two possible regulatory mechanisms exerted by NGmiRNAs: 1) translational silencing of active transcripts, 2) prevention of unwanted transcripts translation. In both cases by studying the translation of selected miR-181-5p targets, in presence or absence of *Sema3A* stimulation, it would be possible to unravel the NGmiRNAs mechanism of action. Indeed, in the first case we expect to have a silencing of actively translated transcripts upon *Sema3A* exposure mediated by the miRNA, in the second case we expect to have a transcript not translated before stimulation, still silent after stimulation because of the pre-miRNAs processing, but translated after stimulation if NGmiRNAs were blocked.

8.2.1 miR-181-5p candidate selection

Stephanie Strohbuecker, a postdoc in the lab, identified putative direct targets of NG-miRNA miR-181a-5p by bioinformatics prediction analysis (Methods Section 3.6.3). We focused on miR-181a-5p since it is the most abundant axonal mature miRNAs derived from pre-miR-181a-1 and pre-miR-181a-2 upon *Sema3A* induced-biogenesis (Figure 6.9).

We first sequenced a pure axonal sample collected after manually severed 50 cultured explants (Method Section 3.2.4, 3.6.3). We then focused on the identification of miR-181 targets that were detected in those pure axons by RNA-seq using TargetScan 6 and the annotated *Xenopus laevis* 3'UTR sequences (Method Section 3.6.3).

Following total RNA-seq from stage 37/38 isolated axons, we shortlisted axonally expressed mRNAs that complied with the following criteria (Methods section 3.6.3): 1) to have a minimum 50 bp 3'UTR length, 2) to have at least one miR-181 miRNA responsive elements (MRE), 3) to be among the top 20 % of predicted targets (based on TargetScan's total context score), and 4) to also be predicted miR-181 targets in either human or mouse. The complete result of the prediction analysis is reported in Table 1 (bioRxiv 470393; doi: 10.1101/470393).

Since blocking NGmiRNA biogenesis impaired *Sema3A*-induced collapse (Figure 7.5), we inferred that under normal conditions, the NGmiRNA-induced silencing of candidate

8.2 Investigation of local axonal translation: a candidate-driven approach

Table 8.1: Predicted miR-181-5p targets - Reactome

Members of the axon guidance pathway (R-HSA-422475)									
Gene	TCS	# MRE	# MRE human	Hct	Hct name	# MRE mouse	Mct	Mct name	Axon FPKM
frs2.L	-0,428	2	3	yes	yes	1	yes	yes	9,0188002
tubb3.L	-0,349	2		no	no	2	yes	yes	3,1025396
itsn1.S	-0,324	2	2	yes	yes	2	yes	yes	12,265673
unc5a.L	-0,308	1	1	no	yes	1	yes	yes	1,1172835
pik3cb.S	-0,282	4	3	yes	yes	1	yes	yes	2,9717807
llcam.S	-0,275	1	1	yes	yes	1	yes	yes	2,0738562
myo10.2.S	-0,274	1	3	yes	no		no	no	8,2009463
rhob.S	-0,255	2		no	no	3	yes	yes	123,4081
myo9b.S	-0,249	2	1	yes	yes	5	yes	yes	11,523746
hvj.S	-0,243	3	1	yes	no	2	yes	no	1,8067957
pik3r1.S	-0,223	3	2	yes	yes	2	yes	yes	10,866924
arhgef28.S	-0,215	1		no	no	1	yes	yes	1,6891058
rpl27a.S	-0,205	1	6	yes	yes		no	no	207,02691
psma3.L	-0,198	1		no	no	1	yes	yes	10,531648
hsp90aa1.1.L	-0,193	1		no	no	1	yes	no	19,334686
ptprc.L	-0,187	1	1	no	yes	2	yes	yes	4,0718288
sptb.L	-0,186	1	3	yes	yes	1	yes	yes	56,611537
lypla2.L	-0,184	1	1	yes	yes		no	no	23,064262
mapk14.S	-0,162	2	7	yes	yes	1	yes	yes	14,403155
lypla2.S	-0,155	1	1	yes	yes		no	no	45,332993
frs2.S	-0,153	1	3	yes	yes	1	yes	yes	4,4768328

Members of the integrin cell surface interactions pathway (R-HSA-216083)									
Gene	TCS	# MRE	# MRE human	Hct	Hct name	# MRE mouse	Mct	Mct name	Axon FPKM
thbs1.L	-0,301	3	5	yes	yes	2	yes	yes	257,82862
fnb1.L	-0,189	2	3	yes	yes		no	no	1,2250878
col8a1.S	-0,185	1		no	no	1	yes	yes	2,1876266
itga6.S	-0,182	1	3	no	yes	1	yes	yes	1,4875861

miR-181 target identification in RGC *Xenopus laevis* isolated axons Predicted miR-181-5p targets, detectable within the axonal transcriptome, ranked by TotalContextScore (TCS). The final candidate selection is based on the 20% best ranked candidates which were conserved as targets in human and mice, filtered by the Reactome axon guidance pathway (R-HSA-422475) and the Reactome integrin cell surface interactions pathway (R-HSA-216083). Abbreviations: TCS, Total Context Score (Score from miR-181a-5p targets predicted using TargetScan 6); # MRE, number of miR-181a-5p Responsive Elements in *Xenopus laevis*; # MRE human, number of miR-181a-5p Responsive Elements in human; Hct, Human conserved target, miR-181 TargetScan targeting conserved in human based on entrez ID; Hct name, miR-181 TargetScan targeting conserved in human based on gene name; # MRE mouse, number of miR-181a-5p Responsive Elements in mice; Mct, Mice conserved target, miR-181 TargetScan targeting conserved in mice based on entrez ID; Mct name, miR-181 TargetScan targeting conserved in mice based on gene name; FPKM, fragments per kilobase of transcript per million mapped reads.

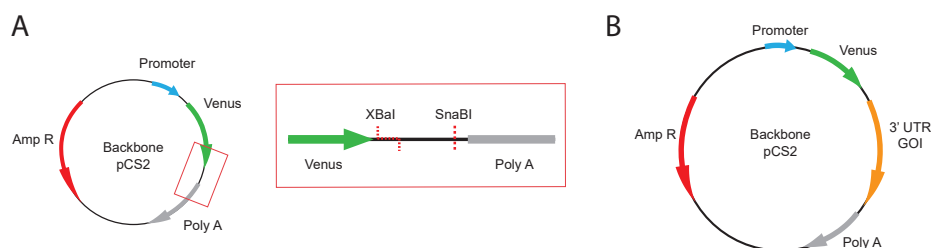
mRNAs would assist the collapse response. It could do so by supporting mechanisms involved in repulsive turning such as by impairing cytoskeleton polymerization, impairing cell adhesion to laminin and/or by enabling Sema3A signaling. We selected one representative miR-181 target candidate reflecting each of these three possibilities.

First, we chose to focus on tubulin beta 3 class III (TUBB3), a microtubule beta isotype needed for proper axon guidance and targeting (Poirier et al., 2010; Tischfield et al., 2010), and ranked second among the putative targets of the axon guidance Reactome pathway (R-HSA-422475) (Table 8.1). We also selected Thrombospondin 1 (THBS1), an adhesive glycoprotein mediating the interaction between cells and the extracellular matrix (Resovi et al., 2014) and the top ranked target among the members of the integrin cell surface interaction Reactome pathway (R-HSA-216083) (Table 8.1). Integrins are transmembrane receptors mediating axonal adhesion to laminin (Yamada, Sekiguchi, 2015). Finally, we selected amyloid beta precursor protein (APP) known to prevent Sema3A-induced collapse (Magdesian et al., 2011) with clinical relevance in neurodegenerative diseases (Roher et al., 2017).

8.3 Fluorescence recovery after photobleaching (FRAP) with Venus construct

We wanted to assess whether local translation of the three candidate mRNAs, TUBB3, THBS1 and APP, may be regulated by NGmiRNAs. I investigated this possibility using FRAP (fluorescence recovery after photobleaching) of a fast folding and fast bleaching translation reporter, Venus, carrying the 3'UTR of the genes of interest (Ströhl et al., 2017; Wong et al., 2017). *De novo* protein synthesis can be study using Venus reporter thanks to its properties. Indeed, as soon as Venus is translated the protein rapidly fold and fluorescence. Venus can also be fast bleached, using 488 nm laser, and its recovery in fluorescence indicate a local *de novo* protein synthesis (Ströhl et al., 2017; Wong et al., 2017).

Figure 8.2: Schematic of Venus plasmid



Schematic of Venus plasmid (A) Backbone plasmid: green arrows, Venus coding gene; gray arrow, Poly(A); red box, highlighting the region where the 3'UTR of interest was inserted. (A, right) Zoom on the region of insertion, showing XbaI (sticky ends) and SnaBI (blunt ends) digestion sites. (B) Schematic of the expected final vector.

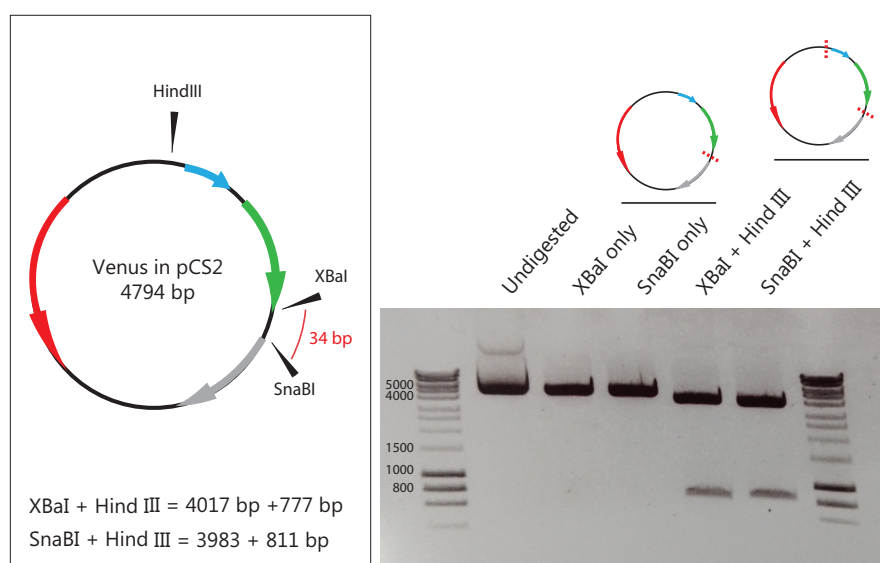
Therefore, Venus reporter was used to investigate axonal local protein synthesis (LPS) of the candidates of interest, by cloning the 3'UTR sequences of the selected candidates after the Venus coding part (Figure 8.2). The 3'UTR is the region containing the miRNAs responsive elements (MREs), miRNAs act by directly binding the MREs and regulating the translation of the mRNAs target. We therefore decided to insert in the Venus reporter the 3'UTR of the selected candidates to study the potential regulatory effect of miR-181a-5p on the translation of those transcripts using FRAP on RGC axons.

8.3.1 Venus plasmids cloning

To study local translation with Venus, the 3'UTR sequences of interest were inserted between the Venus coding sequence and the PolyA signal (Figure 8.2 and Method 3.4).

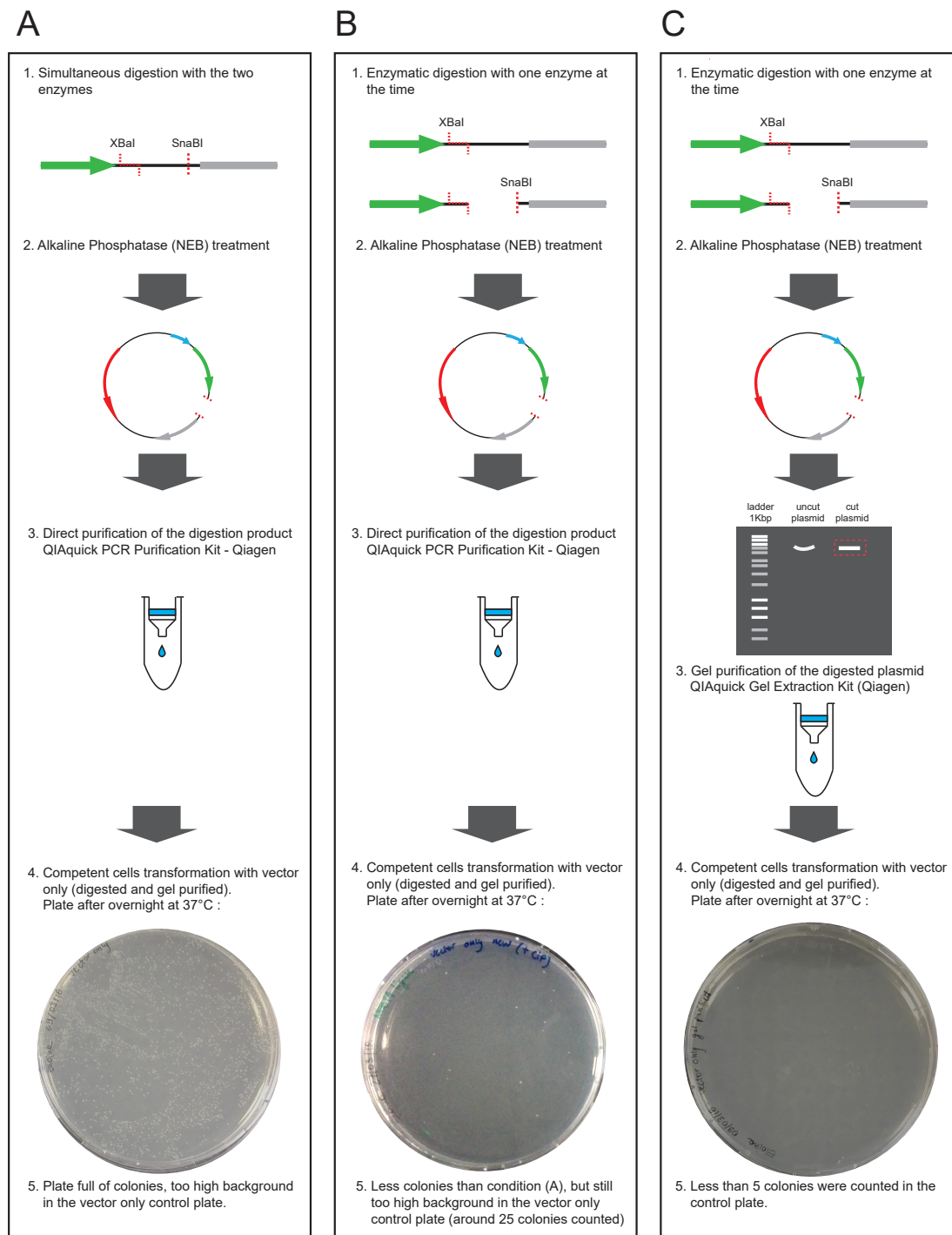
Plasmid digestion was performed with SnaBI (NEB) and XbaI (NEB) (Figure 8.2). The enzymes were tested separately to ensure proper functionality for both (Figure 8.3). This control was performed as both enzymes present possible limiting factors: SnaBI is a blunt end enzyme, and may result in an inefficient cut due to self-ligation; XbaI activity is blocked by dam methylation and the strain of competent cells used was not dam-negative (#C2987, NEB). However, the digestion test showed efficient cutting by both enzymes (Figure 8.3).

Figure 8.3: Control for enzymatic digestion



Control for enzymatic digestion Undigested plasmid was compared with digestion of XbaI and SnaBI alone digestion. Note that no higher bands are visible in the single enzyme digestion suggesting a linearization of the vector. Cut efficiency of XbaI and SnaBI was assessed by combination with a second enzyme (HindIII) checking for a double cut and not a linearization.

Figure 8.4: Background reduction of plasmid only transformation



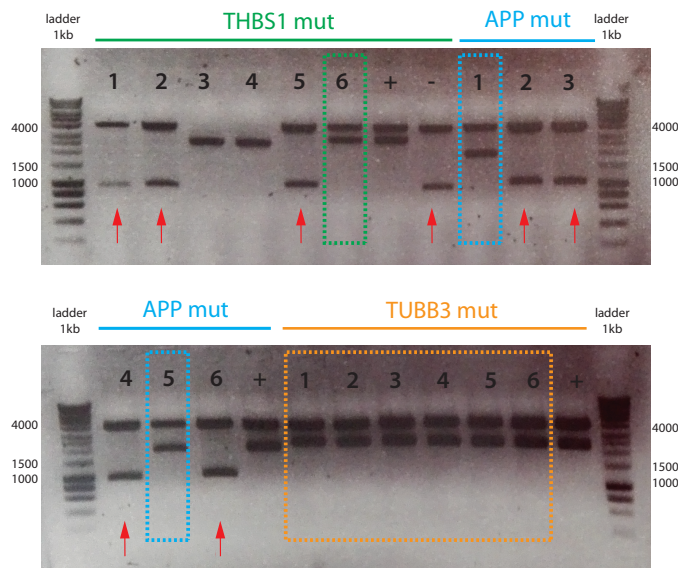
Enzyme digestion and plasmid purification protocols were further optimized regarding their timing and incubation. The goal was to decrease the background of plasmid transfection alone as much as possible (Figure 8.4). The plasmid alone if not digested or digested but self-ligated without the insert induces ampicillin resistance to the bacteria causing huge background transfection, and the higher the background the more difficult will be the selection of the colonies with the vector containing the insert of interest. Therefore, a transfection with the vector only after linearization was used as the control for the amount of background, and optimization were run to reduce it as much as possible (Figure 8.4). The protocol which produced the best result in terms of efficient enzymatic activity, high level of plasmid purification and low levels of vector self-ligation is shown in Figure 8.4 C.

The two cleavage sites are close to one another, and the double digestion was performed sequentially (XbaI first and SnaBI next) with increasing digestion efficiency. The increase in efficiency was probably due to competition avoidance between the two enzymes for the same space simultaneously. Gel purification instead of simple reaction purification after digestion, reduced the background in the control plate significantly. By purifying the whole reaction also undigested vector might be collected, while selectively cutting from the gel the band corresponding to the open vector and then purify it, drastically reduced the background in control plate (Figure 8.3). Moreover, to avoid self ligation of the digested plasmid an alkaline phosphatase treatment was used (CIP, NEB, Method Section 3.4.3). This enzyme catalyzes the dephosphorylation of the vector 5' and 3' ends, therefore preventing the re-ligation of the linearized plasmid before cloning.

As described in the Method Section 3.4, 3'UTR were amplified by PCR and mutated fragments were joint with overlapping-extension PCR (OE-PCR). After insertion of the 3'UTR (WT) or (MUT) through ligation, the transformed colonies were screened by enzymatic digestion to select those containing the insertion. By endonuclease digestion a different cleavage pattern was observed if the colonies were successfully transformed compare to the ones in which the fragment was not inserted (Figure 8.5). For this screening, different combinations of endonucleases (NEB) were used according to the 3'UTR (APP: Hind III HF and XbaI; THBS1: Hind III HF; TUBB3: Hind III HF).

Finally, the different pCS2-Venus-3'UTR plasmids (schematic in Figure 8.6) positive in the enzymatic digestion cleavage were further checked by sequencing before their *in vivo* use.

Figure 8.5: Colony screening through enzymatic digestion



Colony screening through enzymatic digestion Mutated 3'UTRs were inserted into pCS2-Venus plasmid. 6 colonies per gene were picked, grown and digested to check for insert presence. Red arrows indicate the cleavage pattern expected for an empty vector; colored boxes highlighted the positive clones for each mutated gene. The corresponding WT vector per each gene was used as positive control (+) for the expected cleavage pattern.

Figure 8.6: Schematic of Venus-3'UTR constructs

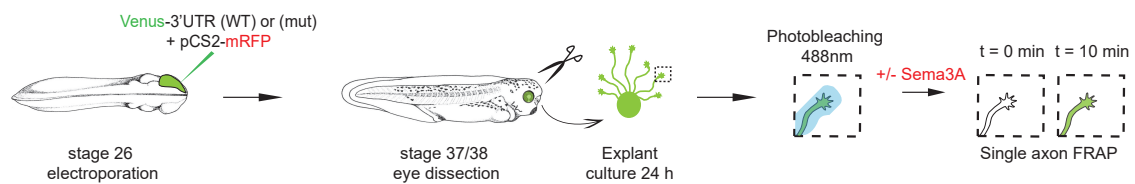


Schematic of Venus-3'UTR constructs Constructs used as reporters of axonal translation in FRAP experiments in which the 3'UTR of interest was cloned between the Venus coding sequence and the Poly(A) signal. Length of the 3'UTR is reported in brackets for each gene. Abbreviations: ACTB, β -Actin; bp, base pair; TUBB3, tubulin beta 3 class III; APP, Amyloid precursor protein; THBS1, Thrombospondin 1.

8.3.2 FRAP control: β -Actin

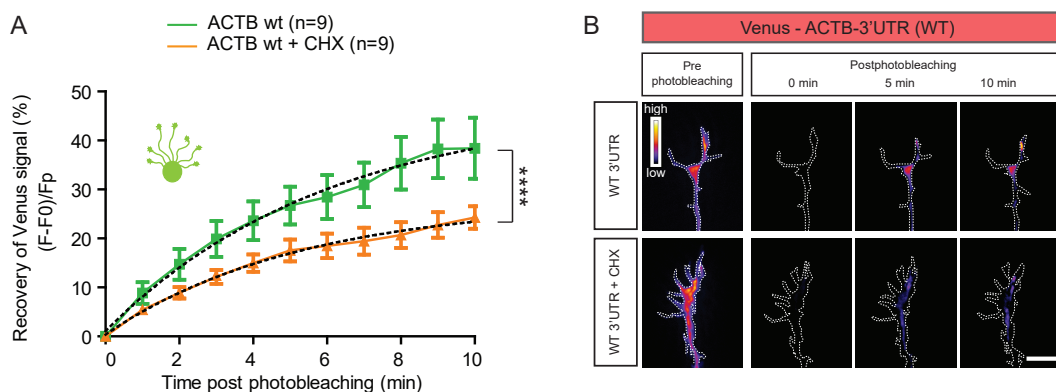
Before studying the local translation of the three candidate mRNAs of interest, I first tested that FRAP could be used successfully to measure LPS of a well-established axonal mRNA, β -Actin (ACTB). I conducted FRAP on *ex vivo* RGC growth cones following the targeted eye electroporation of Venus-ACTB-3'UTR construct and mRFP as a general cell marker (the general experimental paradigm is reported in Figure 8.7).

Figure 8.7: FRAP: experimental paradigm



Axonal *ex vivo* FRAP: experimental paradigm Stage 26 embryos were electroporated with Venus plasmid, to investigate translational regulation, and mRFP as axonal counterstaining. Eyes were dissected at stage 37/38 and cultured for 24 hours. Single axon FRAP was performed with or without Sema3A exposure. Plasmid concentrations used: 1 $\mu\text{g}/\mu\text{l}$ of pCS2+mRFP; 0.7 $\mu\text{g}/\mu\text{l}$ of pCS2+Venus-no 3'UTR/pCS2+Venus-3'UTR of interest.

Figure 8.8: FRAP: axonal *ex vivo* ACTB-3'UTR regulation



FRAP *ex vivo* ACTB-3'UTR (A) Quantification (in percentage) of the axonal fluorescence recovery after photobleaching (FRAP) of Venus-ACTB-3'UTR constructs *ex vivo*, whole explants. The translational blocker cyclohexamide (CHX) was bath applied at 100 μM . (B) Representative growth cones depicting Venus fluorescence intensity as a heatmap. Values are mean \pm SEM. Statistics: **** $p < 0.0001$. Dashed black lines represent least squares fits to a single-exponential decay equation. Differences among fitting curves were tested using an extra sum-of-square F test. Numbers of single axons analyzed are reported between brackets (n of the statistical test). 3 independent experiments, in each embryos are derived from a different fertilized frog. Abbreviations: ACTB, β -Actin. Scale bar: 10 μm .

I observed a rapid $38.28 \pm 5.98\%$ fluorescence recovery at 10 min in growth cones expressing Venus-ACTB-3'UTR and a significant lower recovery $22.75 \pm 2.61\%$ when 100 μM cycloheximide (CHX), a translational blocker, was applied (Figure 8.8). These results show that FRAP of Venus-3'UTR constructs can be used to analyze local translation regulation of transcripts in growth cones.

8.3.3 TUBB3 is locally translated in axons and inhibited by Sema3A exposure

I then sought to examine the *de novo* synthesis of TUBB3 using the Venus-TUBB3-3'UTR construct (Figure 8.6). Growth cones expressing Venus alone (no 3'UTR) displayed a minimal amount of recovery within 10 min post-photobleaching ($13.24 \pm 1.22\%$). This corresponds to diffusion of Venus from adjacent, non-bleached regions to the bleached growth cone (Wong et al., 2017). The entire axon in the field of view of the microscope is bleached, however from the adjacent region non-bleached the already folded Venus proteins can move into the bleached area due to diffusion, and contribute to an increase in fluorescence recovery. Venus alone (no 3'UTR) reporter was used to evaluate the contribution of diffusion, using it as a baseline to investigate LPS occurrence

Compared to Venus-no-3'UTR control, Venus-TUBB3-3'UTR expressing growth cones exhibited rapid recovery within this 10 min-time frame ($21.85 \pm 2.30\%$) (Figure 8.9 A,B). Sema3A exposure suppressed the fluorescence recovery in Venus-TUBB3-3'UTR growth cones to levels similar to Venus alone ($12.32 \pm 1.81\%$ at 10 min) (Figure 8.9 A,B).

These data suggest that TUBB3 is rapidly synthesized in growth cones and that Sema3A prevents local translation of TUBB3.

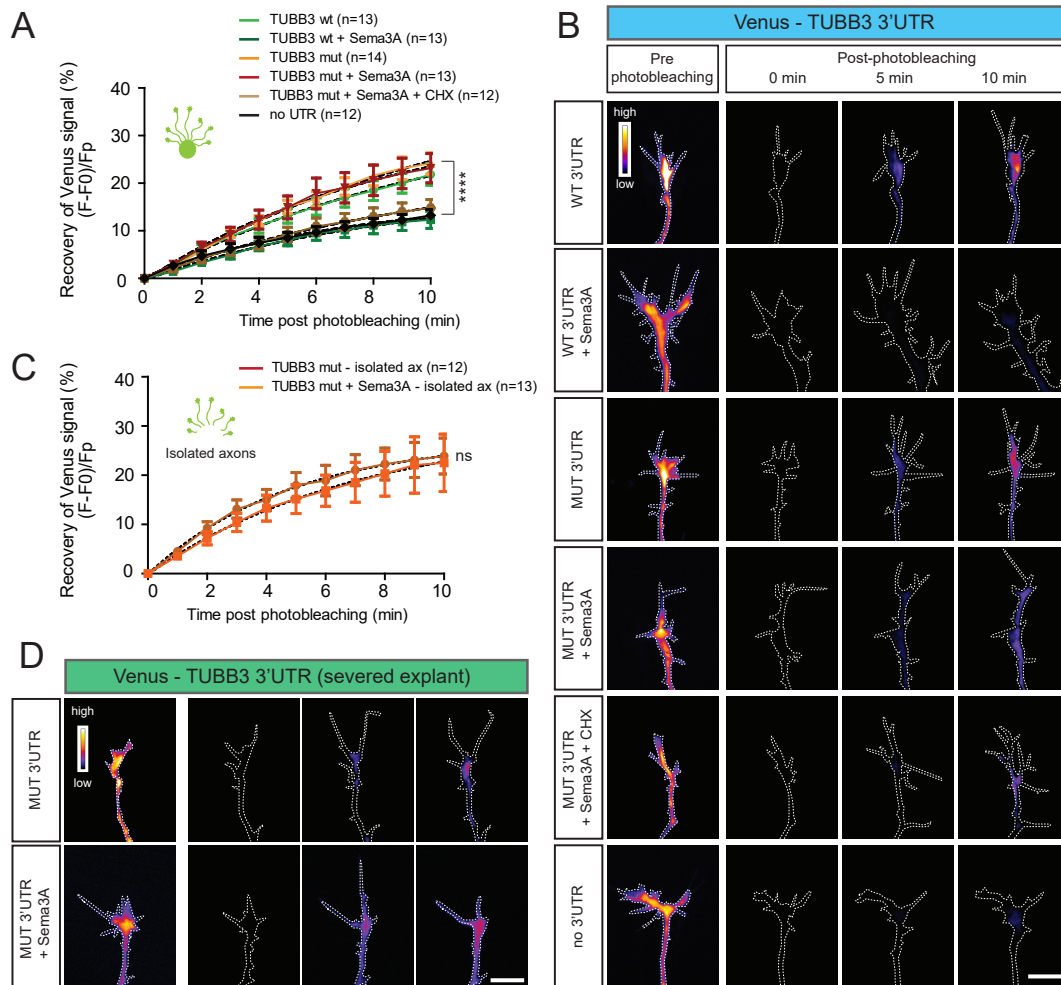
8.3.4 Sema3A inhibition of TUBB3 axonal translation is mediated by NGmiRNAs

Next, I tested the role of mature miRNAs in mediating Sema3A-induced repression of TUBB3. To this end, I mutated the two miR-181a-5p MREs within TUBB3 3'UTR(mut) to decouple Sema3A-induced miRNA maturation from mRNA binding and silencing (Figure 8.6). Mutating TUBB3 3'UTR did not affect fluorescence recovery in basal conditions ($24.14 \pm 2.23\%$ at 10 min) compared to WT ($21.85 \pm 2.30\%$ at 10 min) indicating that mature miRNAs do not regulate constitutive TUBB3 expression in distal axons (Figure 8.9 A, B). Furthermore, upon Sema3A exposure, fluorescence recovery in growth cones expressing Venus-TUBB3-3'UTR(mut) ($23.15 \pm 3.08\%$ at 10 min) was significantly higher than that of growth cones expressing Venus-TUBB3-3'UTR(WT) ($12.32 \pm 1.81\%$ at 10 min), and similar to that observed for Venus-TUBB3-3'UTR(mut) without Sema3A ($24.14 \pm 2.23\%$ at 10 min) (Figure 8.9 A, B).

Taken together with the previous data showing that Sema3A triggers pre-miRNA processing (Chapter 6), this FRAP results further indicate that TUBB3 local translation is repressed via miRNA activity upon growth cone exposure to Sema3A. CHX abolished the recovery of Venus-TUBB3-3'UTR(mut) expressing growth cones bathed with Sema3A ($14.77 \pm 1.79\%$ at 10 min) (Figure 8.9 A,B), indicating that TUBB3(mut) is still translated even in the presence of Sema3A and, therefore, that it is not repressed in the absence of mature miRNAs regulation.

Similar results were obtained when isolated axons were used (Venus-TUBB3-3'UTR(mut))

Figure 8.9: FRAP: axonal *ex vivo* TUBB3-3'UTR regulation

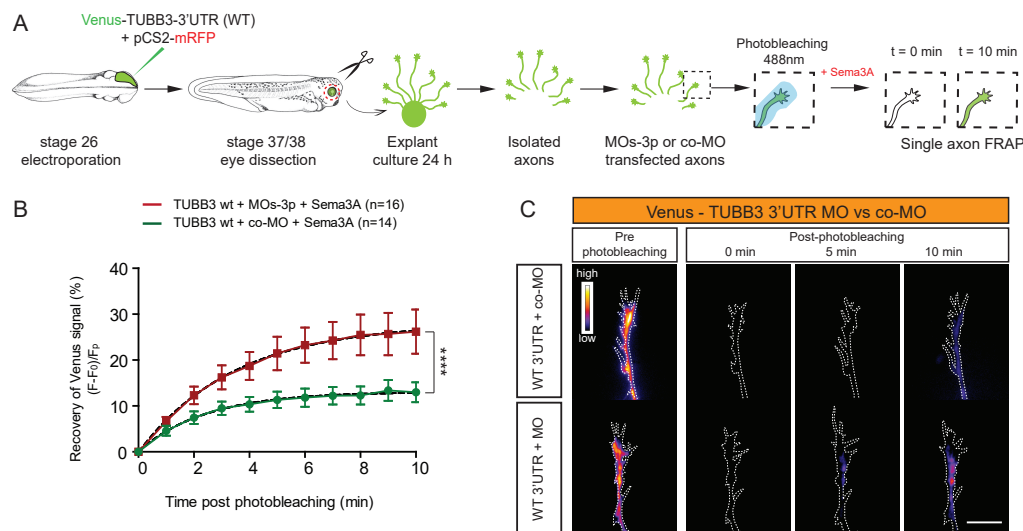


FRAP *ex vivo* TUBB3-3'UTR (A,C) Quantification (in percentage) of the axonal fluorescence recovery after photobleaching (FRAP) of Venus-TUBB3-3'UTR constructs *ex vivo*: whole explants (A), or isolated axons (C). 200 ng/ml Sema3A was bath applied with or without 100 μ M cycloheximide (CHX, a translational blocker). (B,D) Representative growth cones depicting Venus fluorescence intensity as a heatmap. Values are mean \pm SEM. Statistics: **** $p < 0.0001$. Dashed black lines represent least squares fits to a single-exponential decay equation. Differences among fitting curves were tested using an extra sum-of-square F test. Numbers of single axons analyzed are reported between brackets (n of the statistical test). 5 (A), 4 (C) independent experiments. In each independent experiment embryos are derived from a different fertilized frog. Abbreviations: TUBB3, tubulin beta 3 class III; ns, not significant. Scale bar: 10 μ m.

[no Sema3A]: $23.90 \pm 3.66\%$; Venus-TUBB3-3'UTR(mut) [+Sema3A]: $22.52 \pm 5.83\%$ at 10 min) (Figure 8.9 C, D).

The data presented so far shows that TUBB3 translation is down-regulated via Sema3A activated miRNAs, and I have previously shown that Sema3A triggers miRNA maturation (Chapter 6). Therefore, we wanted to confirm that Sema3A-triggered miRNA maturation is the *bona fide* cause of TUBB3 repression. To investigate this link, I interfered with the biogenesis of NGmiRNAs prior to FRAP. I transfected isolated axons with co-MO or MOs-3p that block the processing of pre-miRNAs (Figure 8.10 A, morpholino schematic reported in Figure 7.1). Upon Sema3A exposure, growth cones expressing Venus-TUBB3-3'UTR(WT) exhibited a significantly higher recovery when transfected with MOs-3p ($26.20 \pm 4.82\%$ at 10 min) compared to those transfected with co-MO ($12.98 \pm 2.17\%$ at 10 min) (Figure 8.10 B,C). This indicates that NGmiRNAs mediate Sema3A-induced translational silencing of TUBB3 locally within axons.

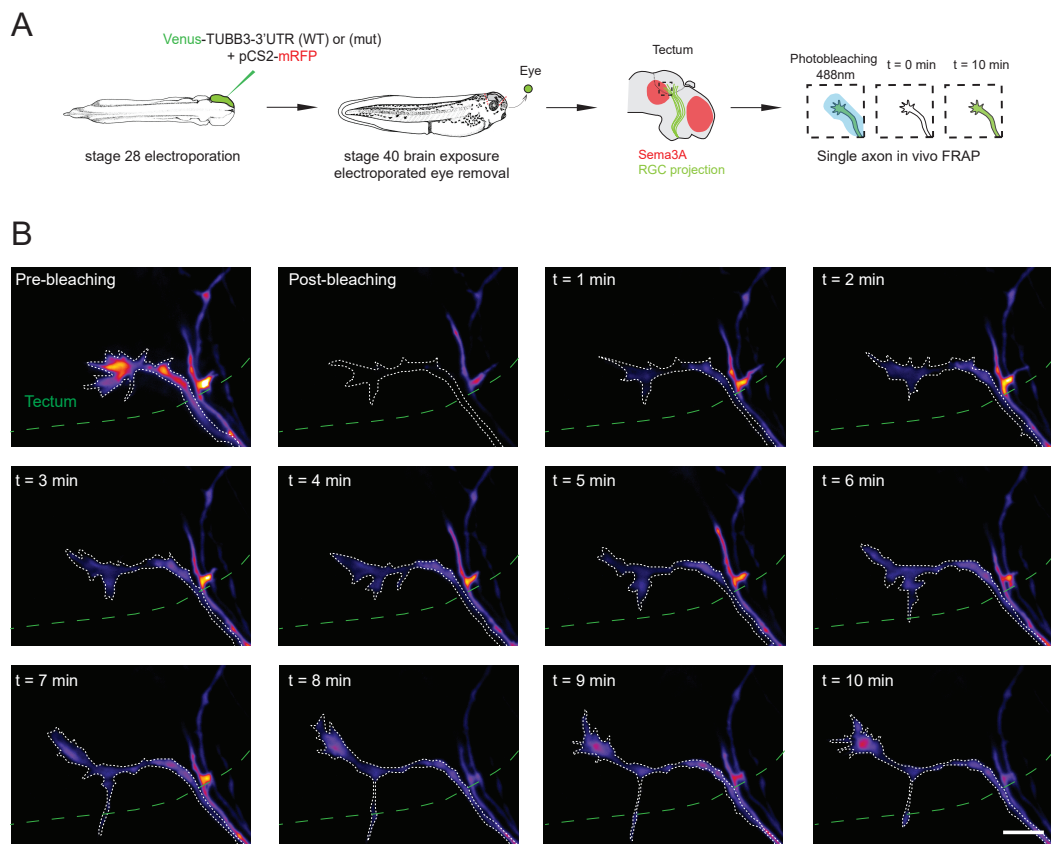
Figure 8.10: FRAP: axonal *ex vivo* TUBB3-3'UTR regulation MO and co-MO



FRAP *ex vivo* TUBB3-3'UTR-WT in transfected axons (A) Experimental paradigm. Stage 26 embryos were electroporated with $0.7 \mu\text{g}/\mu\text{l}$ of pCS2+Venus-TUBB3-3'UTR (WT), to investigate translational regulation, and $1 \mu\text{g}/\mu\text{l}$ of pCS2+mRFP as axonal counterstaining. Axons were transfected with $2 \mu\text{M}$ control morpholino (co-MO) or $2 \mu\text{M}$ MOs-3p. (B) Quantification (in percentage) of the axonal fluorescence recovery after photobleaching (FRAP) of Venus-TUBB3-3'UTR-(WT) constructs *ex vivo* isolated and transfected axons. 200 ng/ml Sema3A was bath applied. (C) Representative growth cones depicting Venus fluorescence intensity as a heatmap. Values are mean \pm SEM. Statistics: **** $p < 0.0001$. Dashed black lines represent least squares fits to a single-exponential decay equation. Differences among fitting curves were tested using an extra sum-of-square F test. Numbers of single axons analyzed are reported between brackets (n of the statistical test). 3 independent experiments. In each independent experiment embryos are derived from a different fertilized frog. Abbreviations: TUBB3, tubulin beta 3 class III; co-MO, control morpholino; MOs-3p, morpholino mixture blocking Dicer cleavage, recognizing loop and 3p of pre-miR-181a-1/-2. Scale bar: $10 \mu\text{m}$.

8.3.5 TUBB3 local translation regulation by NGmiRNAs in vivo

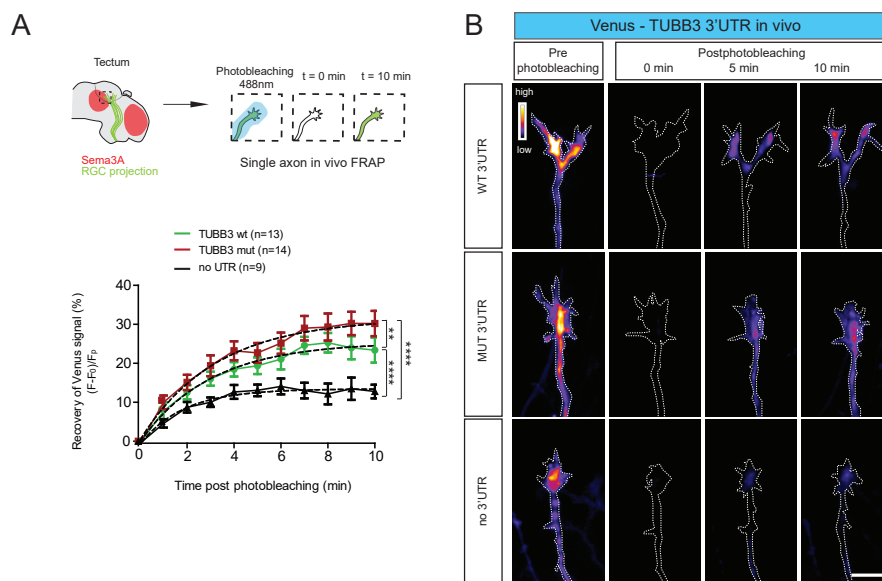
I then investigated whether mature miRNAs control TUBB3 expression in RGC axons *in vivo*. For this, I expressed Venus-TUBB3-3'UTR (WT or mut) and mRFP in RGC using retinal electroporation and performed *in vivo* FRAP on RGC distal axons within the tectum in the vicinity of Sema3A-expressing territories (Figure 8.11). The electroporated eye was removed to avoid diffusion of confounding soma-derived, Venus-tagged proteins into the axons (Figure 8.11 A).

Figure 8.11: *In vivo* axonal pathfinding at the boundaries of the optic tectum

FRAP *in vivo* (A) Experimental paradigm. Stage 28 embryos were electroporated with $0.7 \mu\text{g}/\mu\text{l}$ of pCS2+Venus-TUBB3-3'UTR, to investigate translational regulation, and $1 \mu\text{g}/\mu\text{l}$ of pCS2+mRFP as axonal counterstaining. Whole embryos with exposed brain were used. The electroporated eye was removed prior to mounting the embryo to eliminate somatic contribution. The red area on the brain schematic indicate Sema3A expressing territories. Axons in the vicinity of tectal Sema3A expression territories were selected for FRAP analysis. (B) Representative growth cones depicting Venus fluorescence intensity as a heatmap at the tectum boundaries (dashed green line), entering the Sema3A expressing region. Pre-photobleaching and post-photobleaching (from minute 1 to 10). Abbreviations: TUBB3, tubulin beta 3 class III. Scale bar: $10 \mu\text{m}$.

Growth cones expressing Venus alone displayed low levels of signal recovery ($15.07 \pm 2.36\%$ at 10 min) following photobleaching. By contrast, growth cones expressing Venus-TUBB3-3'UTR(WT) displayed a rapid fluorescence recovery reaching $24.13 \pm 2.96\%$ at 10 min. This indicates that TUBB3 is locally translated *in vivo* within the RGC targeting region. When growth cones expressed Venus-TUBB3-3'UTR(mut) instead, fluorescence recovery was significantly increased ($30.72 \pm 2.23\%$ at 10 min) (Figure 8.12 B,C).

Figure 8.12: FRAP: axonal *in vivo* TUBB3-3'UTR regulation



FRAP *in vivo* TUBB3-3'UTR-(WT) and (mut) (A) Quantification (in percentage) of the axonal fluorescence recovery after photobleaching (FRAP) of Venus-TUBB3-3'UTR constructs *in vivo*. (B) Representative growth cones depicting Venus fluorescence intensity as a heatmap. Values are mean \pm SEM. Statistics: ** $p < 0.01$ and **** $p < 0.0001$. Dashed black lines represent least squares fits to a single-exponential decay equation. Differences among fitting curves were tested using an extra sum-of-square F test. Numbers of single axons analyzed are reported between brackets (n of the statistical test). 3 independent experiments. In each independent experiment embryos are derived from a different fertilized frog. Abbreviations: TUBB3, tubulin beta 3 class III. Scale bar: 10 μm .

8.3.6 APP is locally translated in axons and inhibited by Sema3A exposure

Finally, I assessed whether Sema3A-induced NGmiRNAs modulate the translation of APP and THBS1 (Figure 8.6). Fluorescence from Venus-APP-3'UTR expressing axons recovered following photobleaching ($21.47 \pm 2.35\%$ at 10 min), and this recovery was significantly impaired when growth cones were exposed to Sema3A ($13.20 \pm 2.25\%$ at 10 min) (Figure 8.13). This indicates that APP is locally translated in growth cones, and APP LPS is repressed by Sema3A. Since APP interferes with Sema3A-induced growth cone collapse (Magdesian et al., 2011), Sema3A may increase growth cone sensitivity to itself by controlling APP expression level.

I, next, tested whether mature miRNAs may be a key mediator in *Sema3A*-mediated repression of APP by mutating the MRE as above (Figure 8.6). Venus-APP-3'UTR(mut) expressing axons exhibited a fluorescence recovery ($12.74 \pm 1.87\%$ at 10 min) similar to that of WT 3'UTR ($13.20 \pm 2.25\%$ at 10 min) (Figure 8.13), suggesting that mature miR-181a-5p does not contribute to *Sema3A*-induced silencing of APP.

APP is a predicted target of miR-181-5p and it contains an MRE for it, however, APP is not downregulated by that miRNA. There are several possible explanations for this observation. The easiest is that APP is only a predicted target, not an experimentally validated one, and maybe simply not a real target. However, seed-pairing stability (SPS) between miRNA and MRE on the target, and the target-site abundance (TA) are influencing the strength in miRNA-target inhibition (Garcia et al., 2011) and it might be that miR-181-5p is actually targeting APP but in an inefficient way. APP has a single MRE for miR-181a-5p, hence it is not abundant in target-sites, and it is a 7 mer, which is a less strong site compare to an 8 mer. Also the context of the MRE is important and strong secondary structures on the 3'UTR may masking the binding site, competing with the miRNA, and also the nucleotide composition surrounding the MRE can influence the miRNA binding (Grimson et al., 2007). Another possible case scenario could also be that miR-181a-5p is actually targeting APP, but in this specific axonal context an RNA binding protein could interact with the transcript, stabilizing it or masking the MRE. Further investigation will need to better understand why APP, predicted target of miR-181-5p, is not downregulated by that miRNA.

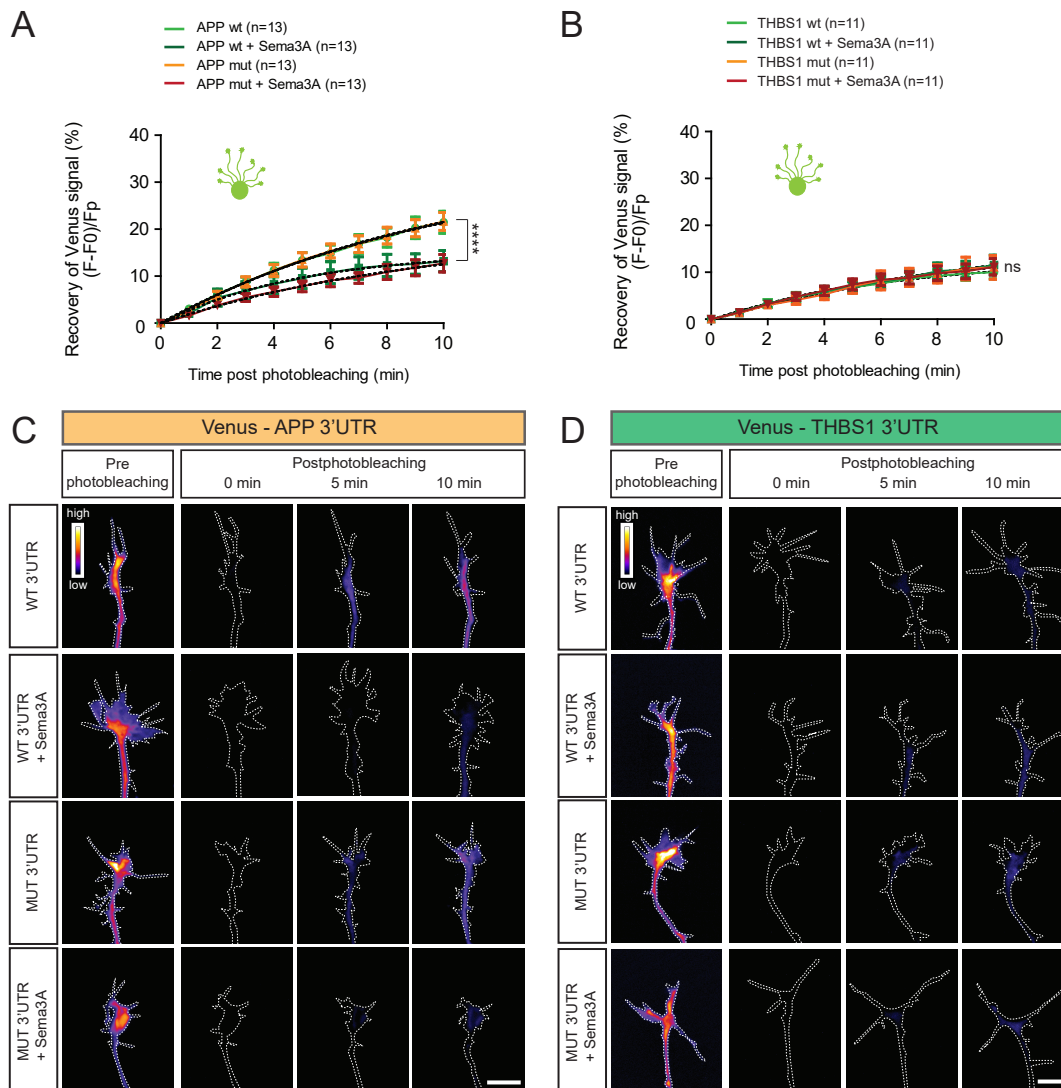
Nevertheless, the down-regulation of APP upon *Sema3A* exposure is a relevant observation, which open an intriguingly link between the guidance cue processing and a gene related to a neurological disease.

8.3.7 THBS1 is not translated in axons

Finally, I assessed by FRAP whether THBS1 translation is modulated by *Sema3A*-induced NGmiRNAs. THBS1 has 3 MREs on its 3'UTR for miR-181a-5p. Considering both target site abundance and the fact that cell adhesion is downregulated in response to repellent cue as *Sema3A* (Bechara et al., 2008), this transcript represents a promising candidate. As for the other candidates, Venus-THBS1-3'UTR(WT) and (mut) were electroporated at stage 26 in the eye primordia, eyes were dissected at stage 37/38 and culture 24 hours, then single axons were photobleached and Venus recovery was measure in the presence or absence of *Sema3A* (Figure 8.7).

Venus-THBS1-3'UTR(WT) expressing axons displayed similar recovery ($9.99 \pm 1.40\%$ at 10 min) compared to *Sema3A*-exposed WT axons ($11.54 \pm 2.11\%$ at 10 min) or when the three miR-181a-5p MREs within THBS1-3'UTR were mutated (mut) in the presence ($11.17 \pm 1.76\%$ at 10 min) or absence of *Sema3A* ($11.05 \pm 2.53\%$ at 10 min) (Figure 8.13). This suggests that THBS1 is not locally translated in axons, indicating that not all the axonal transcripts are actually locally translated in axons at a basal level, as already reported in the literature (Cagnetta et al., 2018).

THBS1 might be not translated at the specific embryonic stage under study, but being selectively synthesized before or after it. In our experimental condition THBS1 is neither basally translated nor translated upon *Sema3A*, but its expression might be switched on by others guidance cues.

Figure 8.13: FRAP: axonal *ex vivo* APP-3'UTR and THBS1-3'UTR regulation

FRAP *ex vivo* APP-3'UTR and THBS1-3'UTR (A,B) Quantification (in percentage) of the axonal fluorescence recovery after photobleaching (FRAP) of Venus-3'UTR constructs *ex vivo*, whole explants. 200 ng/ml Sema3A was bath applied. (C,D) Representative growth cones depicting Venus fluorescence intensity as a heatmap. Values are mean \pm SEM. Statistics: **** $p < 0.0001$. Dashed black lines represent least squares fits to a single-exponential decay equation. Differences among fitting curves were tested using an extra sum-of-square F test. Numbers of single axons analyzed are reported between brackets (n of the statistical test). 5 (A), 4 (B) independent experiments. In each independent experiment embryos are derived from a different fertilized frog. Abbreviations: APP, Amyloid precursor protein; THBS1, Thrombospondin 1; ns, not significant. Scale bar: 10 μ m.

8.4 Conclusions

Using FRAP with Venus constructs to study local translation of specific candidate in axons, I unraveled that both TUBB3 and APP undergo basal translation in axons and are downregulated upon Sema3A exposure (Figure 8.9, 8.13 A). For TUBB3, this downregulation is mediated by the local production of miR-181a-5p upon cue exposure (Figure 8.10). Even though APP-regulation is not miR-181-dependent, the link between a guidance cue exposure and the local translation of a well-established Alzheimer's disease gene is noteworthy. This observation opens the door to studies on how guidance cues may act in neurological disease context. Not all the studied candidates were locally translated at the axonal level, indeed THBS1 was not showing FRAP recovery (Figure 8.13 B).

At the beginning of this Chapter we hypothesized three possible regulatory mechanisms exerted by newly generated miRNAs (NGmiRNAs). First, NGmiRNAs degrade unwanted transcripts, but we actually exclude this possibility considering the time frame of cue stimulation (5-10 min). Second, NGmiRNAs silence actively translated transcripts, and this hypothesis has proved to be correct. Indeed, TUBB3 undergoes basal translation and is silenced by miR-181-5p upon Sema3A exposure. Third, NGmiRNAs prevent the translational onset of unwanted axonal mRNAs. If THBS1-WT had not been translated under Sema3A stimulus, but THBS1-MUT had been, this hypothesis would have proved to be correct. However, considering our results, we can not state that NGmiRNAs play this role too, at least in the case of THBS1.

Taken together, these results demonstrate that Sema3A inhibits basal translation of key molecules. They further reveal that NGmiRNAs are a major component of the Sema3A signaling pathway that are required for the repression of specific, translationally active transcripts within growth cones, thereby acting as a switch.

9 General discussion

The presented results reveal that inactive pre-miRNAs are actively transported to local sites for miRNA biogenesis and function, similarly to the subcellular translocation and subsequent local translation of silent mRNAs into functional proteins. At the growth cone, cue-induced newly generated miRNAs (NGmiRNAs) impinge on local protein production by inhibiting basal local protein synthesis (LPS) of their target mRNAs thereby contributing to changing growth cone direction. This type of ncRNA-based signaling pathway constitutes an additional regulatory layer that warrants the high degree of precision required for brain wiring. Indeed, this study shows the importance of subcompartmentalization and delocalization of miRNA function as a way to increase the specificity in time and space of LPS in axons.

9.1 Different pre-miRNAs and miRNAs distribution in subcellular compartments

miR-182 has been shown to be present in RGC soma and axons, however this miRNA exerts its function at the axonal level only (Bellon et al., 2017) (Appendix A). This observation suggests a local function specifically at the axonal level for this regulatory molecule, despite its wider spread distribution. It might be that miR-182 is active preferentially in RGC axons, because the targets of this miRNA are transported towards and accumulated to the axonal compartment. Circular RNA (circRNA) are ncRNA characterized by a closed loop structure without 5' or 3' end, neither a polyA tail (Zheng et al., 2016). They are highly expressed in brain (Rybak-Wolf et al., 2015) and several papers show circRNA acting as sponges of miRNAs (Hansen et al., 2013; Zheng et al., 2016; Zhao et al., 2016). CircRNA might contain several binding sites for miRNAs and therefore they are able to sponge them, competing with the endogenous miRNA target. The final effect of this sponging circRNA function is a decrease in the normal miRNAs role of target translation inhibition, without a miRNAs degradation. Therefore, it could be that at the soma level miR-182 is sponged by a circular RNA (circRNA) and thus inactivated. Another possibility is that soma-enriched RNA binding proteins might compete for the same binding sites making miR-182 action less efficient.

We can also speculate that the same regulatory molecule that in axons relieves miR-182 inhibition from Cofilin-1 without degradation of the miRNA is also active at the soma level and its action in counteracting miR-182 might be more prominent in the soma. Why miR-182 is preferentially active in axons remain to be elucidated. Further investigations are needed to uncover how and why the same ncRNA molecule has different function in different compartment in the same cells.

miR-182 axonal function (Bellon et al., 2017) is not the only intriguing data pointing to different subcellular miRNAs distribution and function presented in this thesis. Indeed,

pre-miR-181-a-1/a-2 were identified in axons by RNA-seq, while pre-miR-181-b-1/b-2 were absent (Figure 4.7). Some mature miRNAs deriving from those pre-miRNAs share the seed sequence, the sequence recognizing the 3'UTR target. This sharing in regulatory sequence by miRNAs of the same family, suggest a redundancy in functionality. However, considering the different distribution in the pre-miRNA molecules, the redundancy model in regulation functions appear to be limited. Why should pre-miRNAs with common seed regulatory sequence in the mature forms begin differently distributed in cellular compartments if their targets are exactly the same? Probably this different distribution has regulatory roles beyond the shared seed sequences by miRNAs of the same family.

I observed that pre-miR-181a-1 is more abundant than pre-miR-181a-2 in RGC axons, while the opposite distribution is observed in whole eye (Figure 4.11). Moreover, also the mature form deriving from those different pre-miRNAs have different relative abundance in the axonal compartment: miR-181-5p is more present than the relative -3p forms (Figure 6.9). Pre-miR-181a-1 and pre-miR-181-a-2 are highly different in their loop structure (Figure 4.9). This difference might leads to different mechanisms in the trafficking of those molecules, potentially explaining how they are differently distributed in the cells. It has been shown that pre-miR-134 is trafficked to hippocampal neurons and at synapses within the dendritic compartment through recognition in its loop sequence by the RNA binding protein DHX36 (Bicker et al., 2013). It is possible that pre-miR-181a-1 is more likely trafficked towards the growth cone than pre-miR-181a-2 because of motif contained in the loop sequence. Apart from a trafficking regulation of those molecules, the different distribution of those pre-miRNAs can have another biological consequence. Pre-miR-181a-1 and pre-miR-181-a-2 have identical -5p mature form, but the -3p are not identical in sequence and target different mRNAs- (Figure 4.9). It is conceivable that pre-miRNA distribution leads to a delocalization of -3p function in subcompartment (Figure 6.9).

Finally, another totally unexplored possibility is that the loop sequence of the pre-miRNAs have a regulatory function *per se*. Interestingly, it has been shown for members of the miR-181 family a specific function due to their loop sequence and not mature form (Liu et al., 2008). In particular, Liu and colleagues, observed that mir-181a-1, but not mir-181c, despite their identical -5p mature form, promotes CD4 and CD8 double-positive (DP) T cell development when ectopically expressed in thymic progenitor cells (Liu et al., 2008). They showed that this difference in mir-181a-1 and mir-181c function in DP cell development resides in the pre-miRNA loop nucleotides, investigating the loop functions by mutating it specially (Liu et al., 2008). Few years later, the same research group, showed that pri-let-7 has a direct function in target repression through its loop sequence even in the absence of a properly processed mature let-7 (Trujillo et al., 2010). Collectively, those data raised the possibility that pri- and pre-miRNAs have direct roles in target recognition and repression *per se*, through their loop sequence. How this is working mechanistically is not yet described.

In summary, pre-miRNA loop region might have a function *per se* (Liu et al., 2008; Trujillo et al., 2010). We observed a different distribution of pre-miRNAs in *Xenopus* RGC subcompartments and it might be interesting to investigate if it is due to specific regulatory roles in the pre-miRNAs loop sequence exerted at the axonal level. As previously reported, pre-miRNAs loop can regulate the activity of other miRNAs gene (Liu et al., 2008). We can hypothesized that after pre-miR-181a-1/a-2 processing in RGC axons, the loop sequence directly regulates other pre-miRNAs processing at the axonal level, or interferes with other

miRNAs loading in the RISC complex by RNA complementarity.

A second hypothesis could be that the pre-miRNA loop might recognize another RNA. The loop is the single stranded portion of the hairpin which might be recognized by other sequences by complementarity. RNA-RNA interaction might be important for recruitment in granules, or other complexes (Van Treeck, Parker, 2018). Intriguingly, it has been recently shown that oskar 3'UTR contains stem-loop structures, promoting dimerization with other oskar molecules, and that the dimerization is needed for the correct localization of the RNA in *Drosophila* oocytes (Jambor et al., 2011). Similarly, the loop in the pre-miRNAs could dimerize with other RNAs mediating the localization closer to where its function is needed, or in granules to be stored/transported in sub-regions, or avoiding the processing until a specific signal.

9.2 Subcompartmentalization of miRNA biogenesis

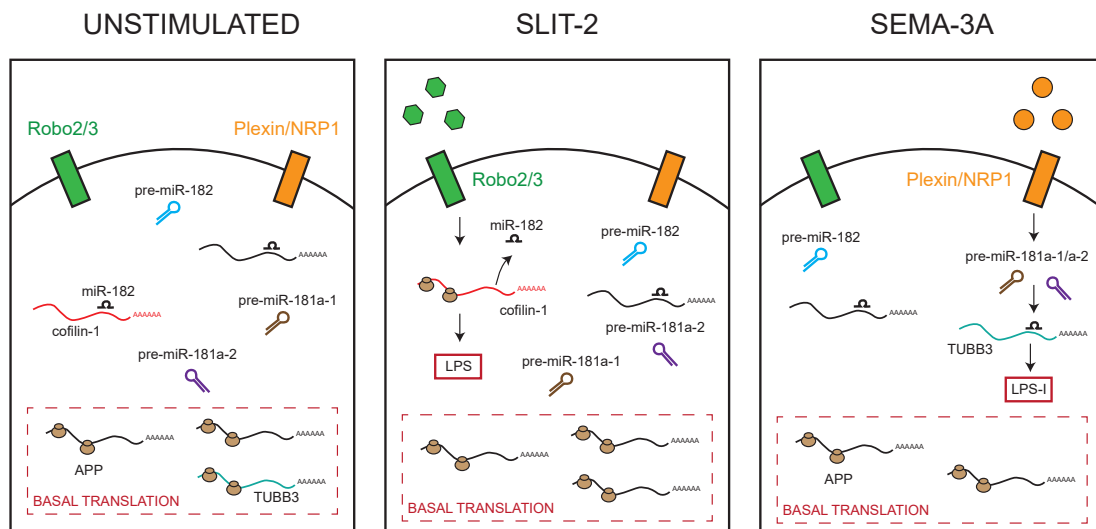
Upon translocation to distal axons pre-miRNAs are stored within growth cones and processed into mature, active miRNAs on demand. Axonal subcompartmentalization of miRNA biogenesis presents several key advantages. First, sequences within the pre-miRNA, such as the loop region, would allow the evolutionary acquisition of distinct and putative targeting motifs (Bicker et al., 2013; Smalheiser, 2008) which would otherwise not easily fit within the much shorter 22 nt mature miRNA sequence. These motifs would subsequently aid the translocation of pre-miRNAs to specific subcellular compartments. Second, the transport of inactive precursors would avoid spurious activity along the transport route until the proper processing machinery - and signal - is encountered at the growth cone. This would constitute a fail-safe mechanism to compartmentalize signaling events at the right time, i.e. upon cue exposure, and at the right place, i.e. not only within the growth cone but perhaps within growth cone subdomains closest to the cue. Finally, pre-miRNAs would be readily available for immediate use by the growth cone on demand, contrary to mature miRNAs which would need to be transported from the soma to the distal axon activated locally. Overall, local processing of miRNAs into NGmiRNAs would be beneficial to the cell. Impaired pre-miRNA trafficking and concomitant local action of NGmiRNAs may be a hitherto overlooked etiological factor of neurodegenerative diseases.

9.2.1 Pre-miRNAs versus miRNAs

The axonal mRNA repertoire is vast, it differs among developmental stages (Zivraj et al., 2010), and only a specific subset of those mRNAs are translated upon certain stimuli (Cagnetta et al., 2018). However, the regulators of protein synthesis of these specific mRNA subgroups in space and time are still largely unknown. miRNAs are one of the described molecules through which certain mRNAs are kept silent until newly synthesized proteins are needed (Bellon et al., 2017) or during their transport towards the axonal compartment to avoid ectopic protein expression (Wang et al., 2015a). In these examples miRNAs silence mRNA until the axon receives a specific stimulus (e.g. Slit-2 or NGF, respectively). My observations on the locally processing of pre-miRNAs go in the opposite direction of local protein synthesis (LPS) regulation. Indeed, upon cue-stimulation, newly generated miRNAs (NGmiRNAs) target mRNAs undergoing basal translation. On this line, there is another example of a cue-induced silencing of a transcript mediated by miR-

NAs. BDNF stimulation increases miR-9 expression, which downregulates Map1B protein expression, and therefore promotes branching (Dajas-Bailador et al., 2012). Therefore, a combination of already cue-activated miRNAs and NGmiRNAs gate translation of the correct subset of mRNAs at the axonal level. They do so by acting as silencers until a specific signal is received on the other hand (miRNAs), and on the other hand (NGmiRNAs) acting as an off-switch by inhibiting basal translation of mRNAs no longer required under specific cellular conditions both enabling regulation in time and space, as well as under basal and stimulated conditions (Figure 9.1).

Figure 9.1: NGmiRNAs and miRNAs control of LPS in unstimulated and stimulated axons



LPS and LPS-I regulation by miRNAs and NGmiRNAs Among mRNAs axonal repertoire, some mRNAs undergo basal translation in unstimulated and stimulated condition. Specific guidance cues inhibit miRNAs silencing therefore inducing local protein synthesis (Slit-2, miR-182, cofilin-1, (Bellon et al., 2017)). Other guidance cues cause the local maturation of pre-miRNAs, triggering the inhibition of basally translated mRNAs (Sema3A, pre-miR-181a-1/a-2, TUBB3, (Corradi et al., 2018)). Abbreviations: NGmiRNAs, newly generated miRNAs; LPS, local protein synthesis; LPS-I, local protein synthesis inhibition; TUBB3, tubulin beta 3 class III; APP, Amyloid precursor protein.

The requirement of LPS for proper axonal responsiveness to cues is well established (Campbell, Holt, 2001; Wu et al., 2005). Furthermore, different guidance cues not only induce the expression of a subset of RNAs, but also reduce another subset (Cagnetta et al., 2018). Collectively those data demonstrate that LPS and LPS inhibition (LPS-I) are coupled in order to fine tune the translatoome state in axons, and I found that pre-miRNAs are key participants in the regulation of this process.

The regulation via NGmiRNAs may be shared by different cellular compartments and cellular models, as pre-miRNA processing was recently shown in CA1 of the rat hippocampus dendrites (Sambandan et al., 2017) and in this work in *Xenopus* RGC axons.

9.3 Delocalization of miRNA biogenesis by pre-miRNAs trafficking

Transport of mRNA as a means to delocalize genetic material is well described. While emerging evidence strongly suggests that ncRNAs, and in particular miRNAs are differentially distributed in subcellular compartments (Iyer et al., 2014; Kye et al., 2007; Lugli et al., 2008; Natera-Naranjo et al., 2010), mechanisms leading to the compartmentalization of ncRNAs are largely unexplored. Here we show that pre-miRNAs are actively transported to the growth cone, docked on vesicles.

9.3.1 miRNAs are transported actively to the growth cone

Molecular beacon (MB) was recently adopted to investigate mRNA trafficking in living cells including in *Xenopus* RGC axons (Turner-Bridger et al., 2018). In our lab, this tool was established to follow endogenous trafficking of pre-miRNAs. Some data of the validation tests, those to which I personally contributed, were presented in this thesis (Section 5.1).

Using MB we tracked for the first time, endogenous trafficking of pre-miRNA molecules. Recent studies have provided great insight into axonal mRNA trafficking (Leung et al., 2018; Turner-Bridger et al., 2018). Many components of pre-miRNA dynamics that we report here resemble those of mRNA in axons (e.g. bidirectional trafficking and faster anterograde than retrograde transport). Maximal velocities and average speed of active particles (~ 0.8 - $1.1 \mu\text{m/s}$ (Turner-Bridger et al., 2018) vs $\sim 1 \mu\text{m/s}$ ($0.972 \pm 0.08 \mu\text{m/s}$ (endo); $1.064 \pm 0.08 \mu\text{m/s}$ (exo) [mean speed \pm SEM] our work) are also comparable (Leung et al., 2018; Turner-Bridger et al., 2018). In contrast to our study, the dominant mRNA trajectories previously measured (Turner-Bridger et al., 2018) were confined and diffusive, with only a small proportion being directed, while the majority of particles we detected adopted an overall active and directed trajectory. This disparity in motion type frequencies could have a technical explanation, or reflect actual biological differences. Indeed, we employed an MSD analysis of overall trajectories limited to moving particles, over a short temporal frame, while Turner-Bridger and collaborators used a bespoke analysis pipeline of segmental trajectories of all particles (Turner-Bridger et al., 2018). Alternatively, there may be *bona fide* biological differences in transport dynamics between mRNAs and pre-miRNAs. In axons mRNA can be reused for multiple rounds of translation while pre-miRNA cannot be re-utilized, after they have been processed. It is thus tempting to speculate that a constant supply of fresh pre-miRNAs may therefore be required to replenish the growth cone pre-miRNA storage. Since pre-miRNA diffusion to the growth cone would, on average, take 20 days, rapid active transport would be required to match the ever-changing demands of fast elongating axons.

9.3.2 miRNAs are transported to the growth cone on vesicles

We provide evidences demonstrating that pre-miRNA molecules are co-trafficked with vesicles. What is the nature of these vesicles? Several lines of evidence support the notion that pre-miRNAs are trafficked and stored in close association with late endosome/lysosome (LE/Ly). First, the vast majority (71-74 %, depending on the stage under study) of

pre-miRNA puncta are co-trafficked along axons coupled to CD63-GFP-positive vesicles. CD63 is a small integral protein belonging to the tetraspanin superfamily (Charrin et al., 2014). While CD63 is found in the exocytic pathway and on the cell surface, like most transmembrane proteins, it is predominantly detected within LE/Ly (Pols, Klumperman, 2009). Second, markers of LE/Ly are chiefly located at the central domain within the growth cone, similar to where pre-miRNA and CD63-GFP positive vesicles are detected. In contrast, markers for early and recycling endosomes are found within the growth cone peripheral domain and filopodia in embryonic *Xenopus* RGC (Falk et al., 2014; Konopacki et al., 2016) where pre-miRNA/CD63-GFP were rarely observed (Figure 5.7, 5.8). Third, pre-miRNAs were detected in close proximity to CD63-positive vesicles. miRNAs, components of miRISC such as Ago2 and GW182, and miRNA-repressible mRNA associate with LE/Ly membranes in non-neuronal cells (Gibbins et al., 2009; Lee et al., 2009). GW-182, for example is juxtaposed to the outer limiting membrane of LE/Ly within the cytosol (Lee et al., 2009). Overall, our data suggest that pre-miRNAs are transported, tethered to the outer membrane of LE/Ly, to growth cones for subsequent storage. Pre-miRNAs are therefore not destined to be shipped to the extracellular milieu via exosomes but to act within axons.

Our results contrast with a previous report that documented an association of exogenous pre-miRNAs (pre-miR-338 in rat SCGs) with mitochondria in axons (Vargas et al., 2016). Although we cannot rule out that pre-miR-181a-1 is linked to this organelle in small percentages or in addition to LE/Ly, this difference might be attributed to several factors including the type of miRNA and/or neuron under study. In contrast to Kaplan's group which investigated PNS axons, we examined here CNS axons here. Intriguingly, non-canonical hitchhiking onto membrane-bound vehicles such as ER, early endosomes, COPI and secretory vesicles has been described for a small subset of cargoes to achieve subcellular motility (Salogiannis, Reck-Peterson, 2017). In particular, mRNAs in fungi were found to translocate docked to cytoplasmic surface endosomes (Baumann et al., 2012). This suggests that the pre-miRNA mode of trafficking belongs to an ancient and evolutionary conserved transport system that spans across species and subcellular compartments.

Intriguingly, it has been recently published that endosomes work as platform for local protein synthesis (LPS) in *Xenopus* RGC axons (Cioni et al., 2019). This might be extremely relevant for our studying, supporting a model of local processing of pre-miR-181a-1 on late endosomes coupling with the LPS and LPS-I on those vesicles and the selection of miRNAs gating which mRNAs should be translated.

9.4 Basal translation

A vastly accepted view posits that local axonal translation is triggered by stimuli, either by chemotropic and maturation cues during development or under injury conditions in adults (Batista, Hengst, 2016; Jung et al., 2012; Rangaraju et al., 2017). For instance, *Sema3A* induces the synthesis of proteins that elicit cytoskeletal remodeling and steering (Campbell, Holt, 2001; Wu et al., 2005). Here, however, the basal translation of APP, TUBB3 and β -Actin has been reported in individual axons elongating *ex vivo* on laminin substrate in absence of chemotropic and trophic cues. This is in agreement with several studies that have documented the basal translation of specific transcripts (Batista et al.,

2017; Eng et al., 1999; Preitner et al., 2014; Taylor et al., 2013). A recent report furthermore revealed widescale protein synthesis that occurs in isolated unstimulated *Xenopus laevis* axons within minutes (Cagnetta et al., 2018). These newly synthesized proteins represent one third of the total axonal proteome suggesting the existence of an unsuspected rich and complex basal translatoome.

9.4.1 Basal local protein translation of TUBB3 is silenced by Sema3A-induced NGmiRNAs

While the induction of global translation by chemotropic cues is well established, very little is known about the fate of the basal translatoome upon cue exposure. Here, using single axon FRAP of Venus translational reporter constructs, we reveal that Sema3A rapidly suppresses the basal translation of TUBB3 and APP *ex vivo*. This is in line with two other studies that have also measured cue-induced decreases in the translation of specific molecules in distal axons (Cagnetta et al., 2018; Yao et al., 2006).

Overall, it is conceivable that two cue-activated pathways may co-exist in parallel to regulate the expression of two separate sets of proteins: a dominant pathway eliciting a burst of LPS and a secondary pathway inducing a trough of LPS or LPS inhibition (LPS-I). Both cue-induced LPS and LPS-I may ultimately lead to cytoskeleton remodeling and changes in growth cone behavior. LPS-I may be used as an alternative to proteasome degradation, which is not systematically employed for cue-mediated growth cone response (Campbell et al., 2001). One key unresolved question is how cues inhibit basal LPS in axons. In this thesis work, a series of evidence demonstrating that cue-induced LPS-I is mediated by NGmiRNAs has been provided.

Using single axon FRAP of Venus-TUBB3-3'UTR constructs, we show that a cue-induced miRNA silences TUBB3 translation locally and that this effect is not due to a generic activation of miRNAs but to the cue-induced local biogenesis of miRNAs. Overall, the data collected suggest that an RNA-based signaling pathway exists, composed of mRNA and NGmiRNAs, two serially connected components of the same regulatory circuit. In response to cue, NGmiRNAs impinge on basal LPS of mRNAs to induce LPS-I. LPS and LPS-I are thereby coupled and co-ordinately regulated by NGmiRNAs acting on 3'UTR regulatory motifs.

This coupling may generate a crucial leverage point for repellent cues to quickly and accurately adjust the desired level of individual proteins, including tubulin isoforms, within growth cones. Since Sema3A-induced growth cone turning does not depend on proteome degradation, contrary to other cues such as Netrin-1 (Campbell et al., 2001), this RNA-based mechanism may be crucial to regulate rapid changes in protein expression in response to specific repellents. To a large extent, this type of RNA-based signaling would allow to tightly control the rate and type of protein production for cytoskeletal remodeling, and thereby confer a higher order of regulatory potential to ensure the exquisite precision required for brain wiring.

What is the biological implication of the NGmiRNAs-triggered LPS-to-LPS-I switch for axon development? We uncover that this switch mediates cue-induced growth cone steering. We reveal that Sema3A triggers growth cone collapse response *ex vivo* through NGmiRNAs. NGmiRNAs, in turn, silence TUBB3 mRNA translation upon Sema3A exposure *ex vivo* and in the vicinity of Sema3A-expressing territories *in vivo*. Taken together,

these data suggest that Sema3A-induced NGmiRNAs lead to the silencing of MT tubulin isotype TUBB3, MT depolymerization, and ultimately, growth cone steering. Collectively, our data thus support a model whereby Sema3A-produced NGmiRNAs elicit a rapid shift in axon behavior from axon elongation supported by basal TUBB3 LPS, to growth cone collapse prompted by TUBB3 LPS-I (Figure 10.1). According to this model, blocking NGmiRNA production prevents Sema3A-induced LPS-I of TUBB3 leading to the persistent production of TUBB3 and the maintenance of MT throughout the growth cone. As a consequence, growth cones fail to collapse *ex vivo* consistent with the phenotype that was observed.

9.5 Impact of the study

Several novel aspects which may be of interest for different research fields were described in this thesis project. My data reveal the axonal presence of pre-miRNAs, their active trafficking towards the growth cone, their maturation upon cue exposure and their role in regulating growth cone steering. For the first time I show a pre-miRNA's crucial function in the process of axon guidance, revealing new important aspects for the field of developmental neurobiology. Moreover, gaining insights into molecular mechanisms involved in the establishment of fully functional neuronal circuits is relevant for research in neurodegeneration and other brain pathologies, or in neuronal recovery after injury.

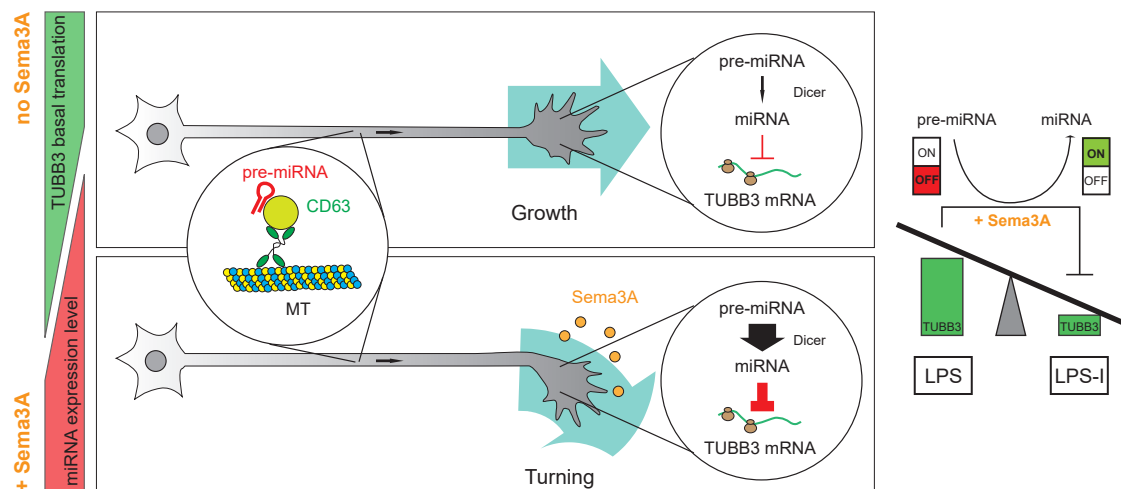
Local activation of pre-miRNAs was never observed in axons before, adding spatial specificity to miRNAs regulatory action. Indeed, as mRNAs can be viewed as a pool of inactive protein precursors, pre-miRNAs can be defined as a pool of inactive mature miRNAs. What is biological added value of delocalizing pre-miRNAs instead of mRNAs? It is conceivable that pre-miRNA delocalization avoids ectopic action of the mature active forms confining their regulation in time and space. This notion is not only relevant for the RNA biology field, in all its applications including the clinical ones (Lambert et al., 2015; Nagaraj et al., 2015) and ncRNA biology. It is also of interested for molecular biologists studying the regulatory mechanisms of local protein synthesis, and neurobiologists, particularly focused on compartmentalized functions in highly polarized cells as neurons.

Moreover, I show an axonal basal translation of APP and TUBB3, which is down-regulated upon cue-exposure, thereby providing a link between axon guidance cues and clinically relevant genes (Roher et al., 2017; Tischfield et al., 2010). This observation opens new questions regarding the role of basal translation in axons at specific developmental stages, and also in neuronal pathological states, an aspect so far unknown.

10 Summary and future perspectives

In this study it has been shown that pre-miR-181a-1 is actively transported, tethered to CD63-positive vesicles along axons to the growth cone central domain using a novel approach based on Molecular Beacon (MB). Sema3A bath application of isolated axons leads to the processing of pre-miR-181a-1 and pre-miR-181a-2 into mature miRNAs in a cue and pre-miRNA-specific manner. These mature miRNAs are important for growth cone collapse *ex vivo*. Mechanistically, cue-induced NGmiRNAs silence the basal translation of a specific transcript, TUBB3, at the growth cone *ex vivo* and *in vivo*. Collectively, the findings are consistent with a model in which pre-miRNAs are de-localized to and stored within growth cones in an inactive form. Upon cue exposure, they are rapidly processed into active miRNAs to inhibit the basal local translation of transcripts, thereby ensuring accurate axon trajectories.

Figure 10.1: Proposed model



Proposed model Pre-miR-181a-1 is transported along RGC axons tethered to CD63-positive vesicles. Under non-stimulated conditions TUBB3 undergoes basal translation in the axonal compartment. Upon Sema3A exposure, pre-miR-181a-1 and pre-miR-181a-2 are locally processed and the expression level of the concomitant newly generated miRNAs increase locally within the growth cone. miR-181a-5p, the predominant mature miRNA generated from pre-miR-181a-1 and pre-miR-181a-2, targets TUBB3, thereby silencing protein synthesis through LPS inhibition (LPS-I).

10.1 Future perspectives

Overall this thesis work contributed on one hand to clarify molecular regulatory mechanisms during brain wiring, using *Xenopus* RGC axons as model system, on the other hand to open new questions based on the collected data.

Dicer axonal localization during development While Dicer axonal localization was already reported, here I show for the first time the different distribution in axons of this enzyme according to the developmental stage (Chapter 4). At which stage Dicer start to be localized in RGC axons? Is it depending on the pathfinding state of axons (e.i. navigation vs targeting)? Which is the biological meaning of Dicer localization in axon at specific developmental point? It is possible to speculate that the more the growing tip of the axon gets far from the soma, the more a local presence of Dicer protein is needed and axons cannot rely only on trafficking from the soma of already matured miRNAs. This might explain why at the RGC target region in P0 Dicer is present in RGC axons, but not at earlier stage (i.e. E13.5), closer to the retina (Chapter 4).

In order to address these questions in mice, two aspects should be ameliorated in the experimental design compare to what has been presented in Chapter 4: first of all, a specific labeling of RGC axons would be crucial to really characterize Dicer localization in sub-compartment, and second, more than two developmental stages would have to be considered. A specific axonal label would enable to easily study Dicer throughout the optic tract at any stage, without limiting the observations only to specific structures such as ONH, chiasm or SC. A screening on more stages will be helpful in the characterization of the distribution of this enzyme at different pathfinding state of RGC axons.

A specific RGC axons labeling could be obtained by crossing our mice line FLAG-HA₂-Dicer mice (Much et al., 2016) with a line inducing Cre expression specifically in RGC cells under Pax6 promoter (Marquardt et al., 2001). Such a mice line would make possible to study Dicer localization specifically in RGC compartment by immuno-labeling of Dicer in its *in vivo* context at different developmental stages or even by dissecting RGC axonal compartment (i.e. optic nerve, chiasm, brain target region) and performed western blot using anti-HA antibody. However, creating new mice line is not a straightforward process and it is time consuming. A possible alternative way to specifically label RGC axons and study Dicer localization in this compartment would be to combine DiI injection (Soares, Mason, 2015) and immuno on FLAG-HA₂-Dicer mice, such an approach is less time consuming, but technically challenging. Indeed, the permeabilization step needed for immuno-labeling might be not fully compatible with DiI (Holmqvist et al., 1992). DiI might exit the axonal compartment during the permeabilization step and the specificity in the axonal stain impaired. Another possibility would be to move to an *ex vivo* system, culturing RGC axons. This approach would enable to characterized Dicer localization even at the growth cone level, but it would not be possible to study this at many developmental stages nor in mice neither in *Xenopus* and the *in vivo* information would be lost.

Pre-miRNAs abundance in axons In Chapter 4, differences in pre-miRNAs abundance and sub-distribution in axons was observed. In the thesis discussion (Chapter 9) I dedicated a section on this topic (9.1) formulating possible hypotheses on the biological role of this distribution. Indeed, also this observation open many questions and possible new

regulatory mechanisms. Why pre-miRNAs of the same family, with identical mature forms are differently distributed in the same cell? Does the loop sequence play regulatory unknown function, which are sub-compartment specific?

By RT-qPCR pre-miRNAs relative abundance could be investigated both in RGC axons and soma. A limitation in a direct comparison of pre-miRNA levels among different sub-cellular compartments through RT-qPCR is the selection of an appropriate normalizer (see also 6.2.1). However, a possible way to overcome this limitation is to study relative abundance through droplet digital PCR (ddPCR) or RNA sequencing. ddPCR does not need a normalizer since it relies on an absolute quantification (Hindson et al., 2013) and it has been recently used for pre-miRNAs amplification (Bill et al., 2016). While the selection of a single stable normalizer is not needed for RNA-seq data since they are usually normalized on library size, counts, distribution or average expression of the measured molecules (Evans et al., 2017).

A part from a study on the different distribution of pre-miRNAs in neuronal cell sub-compartments, it would be interesting to characterize the biological function of this different distribution. In order to unravel whether different pre-miRNAs of the same family might have a specific and different role in axons a series of loss-of-function experiments could be run. A possible approach is to selectively knock down with morpholinos one pre-miRNAs isoforms at the time of pre-miRNAs belonging to the same family (e.g. pre-miR-181a-1 and pre-miR-181a-2) and for instance study the biological effect using a collapse assay as read-out (see Section 1.2.4). Is the axonal responsiveness depending on a single pre-miRNA of the family? Then, by specific mutation on the part that differ between the two isoforms (e.g. loop and 3p mature forms) a further characterization of the motif involved in the regulation mechanism under study can be further investigated. What is the motif needed for axonal trafficking and processing? By testing different mutation on labeled molecules, it would be possible to check for trafficking and processing impairment of the specific isoform.

Pre-miRNAs trafficked on vesicles NcRNAs trafficking docked on vesicles was never observed before. What is the nature of those vesicles? What is the advantage of such a trafficking instead of RNPs? Is the pre-miRNA transported linked to the outer limiting membrane of the vesicle and directly processed there? An entire section in the discussion chapter is dedicated to hypothesis formulation linked to pre-miRNAs trafficking (Section 9.3.2). A unique marker for a vesicle type does not exist, thus to better characterize the nature of those vesicles other markers apart from CD63 might be used. RAB proteins are located on vesicles, and some of them are specific for a subset of vesicle-type (e.g. Rab4a/5c for early endosome, Rab7a for late endosomes, Rab11a/b for recycling endosome) (Falk et al., 2014; Cioni et al., 2019). Therefore, in order to better describe the nature of those vesicles, it would be interesting to perform trafficking experiments labeling the vesicles not only with CD63-GFP but also RABs fluorescence labeled protein.

A possible advantage of pre-miRNAs trafficked docked on vesicles outer membranes might be an accessible way of transport, a way to have the molecule ready for processing. This outer membrane localization of the pre-miRNA might be confirmed with higher resolution microscope approaches compare to what shown in Figures 5.7 and 5.8. MVB vesicles are typical around 400-500 nm in diameter (Gruenberg, Stenmark, 2004), and the resolution of the light microscope is limited by Abbe's Law to 200-250nm in xy axis

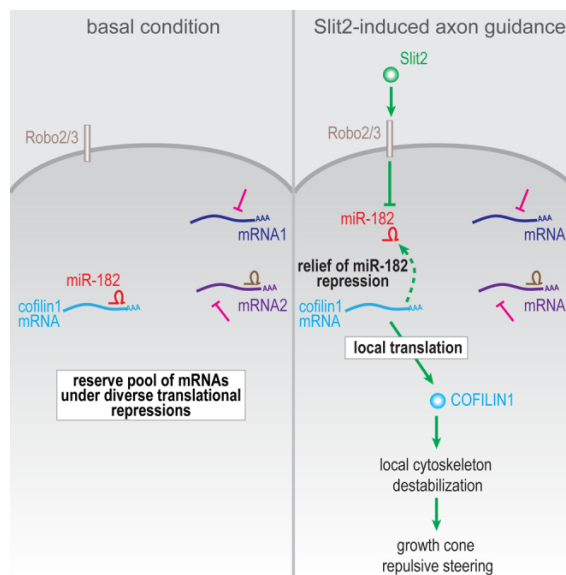
and 500-700nm in the z (Wegel et al., 2016). Super resolution microscopy can resolved much better the localization of the pre-miR-181a-1 in respect to the vesicle. Structured Illumination Microscopy (SIM) gives rise to a two-fold increase in resolution compare to light microscopy and STimulated Emission Depletion (STED) enables to go down to 50 nm lateral resolution (Wegel et al., 2016).

All these are some of the new questions opened by this research work, and future perspective are not missing. Santiago Ramon y Cajal defined the brain as a world consisting of a number of unexplored continents and great stretches of unknown territory. The brain is still a mystery, and every new result, makes us add a piece of knowledge and move to another unknown territory.

A miR-182 regulates Slit2-mediated axon guidance by modulating Cofilin-1 LPS

Local protein synthesis (LPS) is an important mechanism to regulate the specific translatome state during axon guidance (Section 1.4), and miRNAs are key regulators of axonal LPS (Section 1.5). However, how specific mRNAs are selected to be translated upon cue-stimulation in axons is not fully unraveled. We provided the first evidence of miRNAs role in mRNAs selection: miR-182 gates Cofilin-1 translation upon Slit2 stimulation (Bellon et al., 2017). In this work, small RNA-seq analysis shows a rich repertoire of miRNAs at the RGC axonal level, with miR-182 as the most abundant in this compartment. We found that down-regulation of miR-182 causes axon targeting defects *in vivo* and impairs *ex vivo* and *in vivo* the growth cone responsiveness to Slit2 repellent cue. miR-182 regulates the expression of Cofilin-1, protein inducing F-actin depolymerization, silencing it at basal condition. Slit2 relieves miR-182 repression, allowing Cofilin-1 translation and therefore, growth cone repulsion (Figure A.1, graphical abstract of the paper). Those data show for the first time how a miRNA upon cue-stimulation reversibly gates the translation of specific mRNAs.

Figure A.1: MiR-182 reversibly gates Cofilin-1 translation upon Slit2 stimulation



A.1 My contributions in the paper

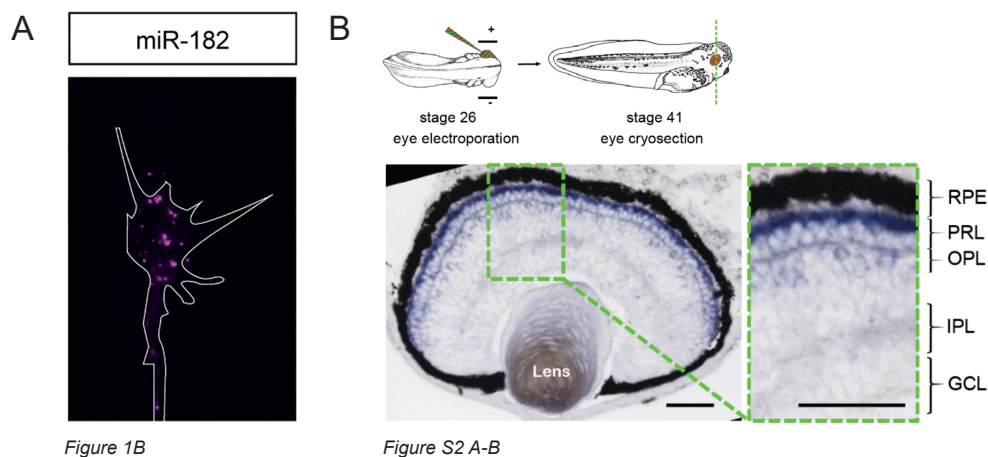
I contributed to this work by investigating specific questions:

1. Why is miR-182 absent from RGC soma in the ganglion cell layer (GCL) by in situ hybridization (ISH) while it is present in growth cone? Is this due to the limitation of the technique sensitivity? In other words, is miR-182 detectable in RGC soma with a more sensitive technique?
2. Is miR-182 enriched in axons?
3. Is miR-182 activity preferentially occurring in RGC axons as opposed to soma?

I therefore organized this Appendix in question, the experimental approach we have chosen to answer, and the data I generated to answer to it.

Is miR-182 present in RGC soma? *In situ hybridization* data clearly showed miR-182 presence at the growth cone level in RGC axons (Figure A.2 A), while in RGC cell body no signal was detected with the same technique (Figure A.2 B). Generally, a molecule present in the axonal compartment is also present at the soma level of the same cell type. We therefore wanted to investigate more these puzzling results.

Figure A.2: miR-182 ISH: RGC axons and soma



miR-182 presence (A) Fluorescent ISH on stage 35/36 RGC GCs cultured in vitro for 24 hr (B) Representative images of endogenous miR-182 distribution detected by in situ hybridization on stage 40 retinal section. Figures from (Bellon et al., 2017), original Figure number indicated in italics below the image. Abbreviations: ISH, in situ hybridization; GCL, ganglion cell layer; INL, inner nuclear layer; IPL, inner plexiform layer; OPL, outer plexiform layer; PRL, photoreceptor layer; RPE, retinal pigmented epithelium. Scale bars: 5 μm (A), 50 μm (B).

We decided to investigate miR-182 presence in RGC soma, by specifically selecting this axonal compartment by laser capture microdissection (LCM), and then measuring the miRNA expression level by RT-qPCR, an extremely sensitive technique. The qPCR product was loaded on a gel, to check for the proper miR-182 length (Figure A.3 A). The visualized band corresponded to miR-182 expected size, and the amplification curves clearly showed miR-182 presence in RGC soma LCM (Figure A.3).

Figure A.3: miR-182 traces in laser captured RGC layer

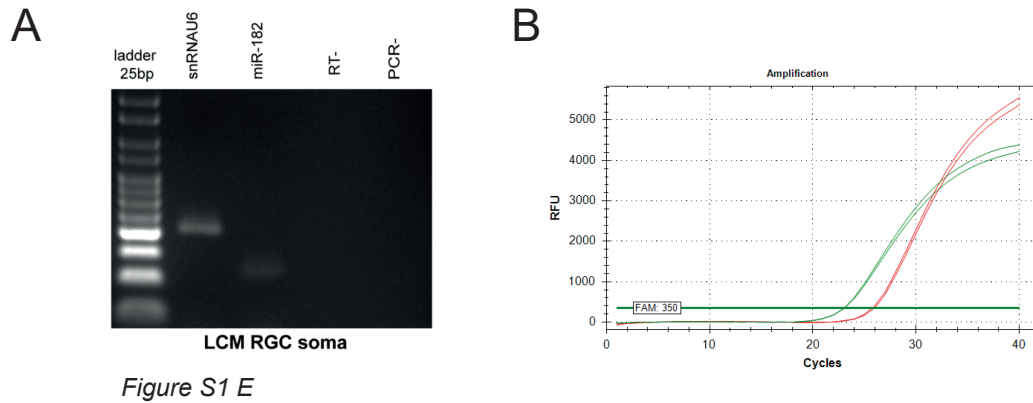


Figure S1 E

miR-182 presence in RGC soma (A) Illustrative gel showing TaqMan RT-qPCR performed on RNA extracted from laser captured RGC layer detecting traces of miR-182 in RGC soma. RNA-U6 was used as a positive control. Figure (A) from (Bellon et al., 2017), original Figure number indicated in italics below the image. (B) Representative RT-qPCR amplification curves of U6 (green) and miR-182 (red) of RGC soma sample. All Ct are below 35. Abbreviations: RT-, RT no template negative control; PCR-, PCR no template negative control; RFU, relative fluorescence units.

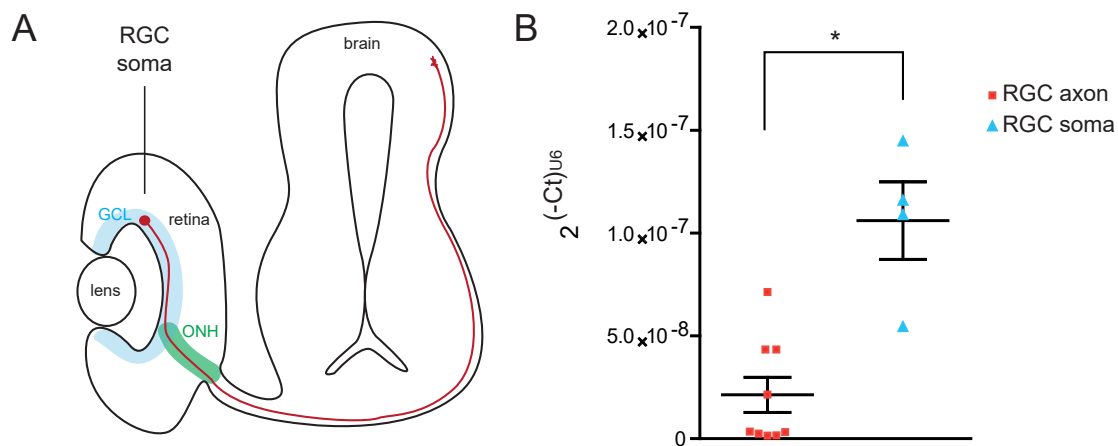
Is miR-182 enriched in axons? miR-182 was identified in RGC axons by sequencing, and its presence confirmed by *in situ hybridization* (ISH) and by RT-qPCR (Bellon et al., 2017). miR-182 was not visible by ISH on sections at the soma level (Figure A.2 B), but detectable by RT-qPCR (Figure A.3), suggesting an enrichment in miR-182 at the axonal level.

We therefore decided to investigate miR-182 expression changes in the two compartments by RT-qPCR, encountering however a big limitation: the use of U6 as normalizer (for details see Method Section 3.5.1).

Axons were collected through LCM after explants culture (Figure A.7 G), while RGC soma were isolated through LCM on sections (schematic showing GCL on section is reported in Figure A.4 A). We investigated the suitability of U6 as normalizer to compare these two compartments with the $2^{(-Ct)}$ method (Method Section 3.5.1). U6 resulted to be 62.15% less in axons compare to RGC soma, which is consistent with the fact that soma layer contained the nuclei, and has expected U6 levels higher than these found in axons

(Figure A.4). This high difference between U6 level in axons and soma RGC does not make U6 suitable as normalizer for RT-qPCR data. So far, a characterized and validated gene, present and stable in both compartment is not known.

Figure A.4: U6 is not a suitable normalizer to compare soma and axonal samples



U6 stability among RGC compartments (A) Cross section of *Xenopus laevis* retina and brain. A single RGC axons projection is depicted from axogenesis to stage 39/40 when axons reach the final target, the optic tectum. RGC soma are in the retina layer GCL indicated in blue. (B) Investigation of U6 stability in cDNA obtained from RGC soma and axons using the $2^{(-Ct)}$ method. Values are mean \pm SEM. Statistics: * $p < 0.05$. Data were not normally distributed (Shapiro-Wilk test). Two-tailed Mann Whitney test, $n=9$ (axons) $n=4$ (soma) independent experiment. Abbreviations: GCL, ganglion cell layer; RGC, retinal ganglion cells.

Without the possibility of a direct comparison between the two compartments by RT-qPCR, we decided to change the technical approach, capturing the level of miR-182 activity instead of its expression level. In order to do that, a sensor plasmid was created and validated in our lab by Simone Bridi (Figure A.6 A).

This Sensor expresses destabilized GFP (dGFP) under the translational control region of 3'UTR containing three sequences complementary to miR-182. mCherry was used as internal control with the same plasmid, and scramble sequences instead of miR-182 complementary sequences were inserted in the control-Sensor (Figure A.6 A).

miR-182 Sensor was electroporated at stage 26, cultured at stage 40 and axons were then laser captured. I validated the presence of the Sensor at the axonal level by PCR (Figure A.5). To avoid detecting the parent plasmid, DNaseI treatment was carried out and RT was performed using oligo(dT). Presence of these two transcripts in axons indicates that Sensor construct is suitable to assess local activity of miR-182 in axons.

Figure A.5: miR-182 sensor in axons

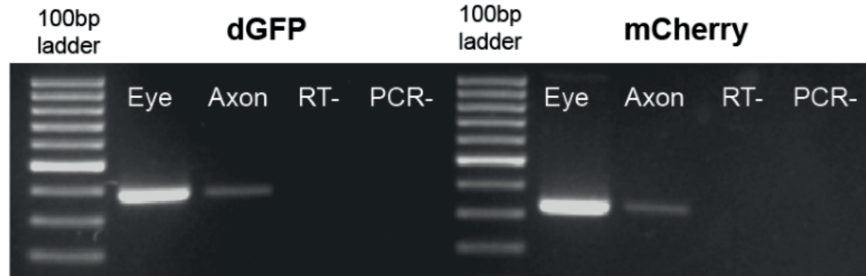


Figure S2 F

miR-182 sensor in axons Illustrative gel following RT-PCR of dGFP and mCherry mRNAs on electroporated eye, collected at stage 37/38, and RGC axon collected by LCM from stage 40. Figure from (Bellon et al., 2017), original Figure number indicated in italics below the image. Abbreviations: RT-, RT no template negative control; PCR-, PCR no template negative control.

Is miR-182 activity RGC-axon enriched? After verifying miR-182 Sensor axonal presence (Figure A.5) we used it to investigate whether miR-182 has an enriched activity in RGC axons compare to soma.

I contributed to this piece of work by performing acquisitions on cryosectioned explants from electroporated embryos, capturing the retinal ganglion cell layer (RGCL) and photoreceptor (PR) layer (Figure A.6 D,E,G). miR-182 is known to be functional in photoreceptors (Busskamp et al., 2014; Xu et al., 2013) and abundant in *Xenopus laevis* sections (Figure A.2 B), hence PRs were used as positive control for the Sensor function. The Sensor or control-Sensor were electroporated into the eye primordia at stage 26, and the comparison of the dGFP/mCherry was computed at stage 41 retinas, by quantification of the fluorescence signal in the layer of interest. dGFP/mCherry ratio from miR-182-Sensor, but not from control-Sensor, was significantly decreased in PRs ($-73.3\% \pm 0.04\%$), showing the ability of the Sensor of capturing miR-182 activity where the miR is highly expressed (Figure A.6 E,G).

Intriguingly, the quantification of dGFP/mCherry in the two compartments (RGC soma and axons) revealed that while the control-Sensor was not changing, the ratio of miR-182-Sensor was significantly decrease in RGC axons ($-31\% \pm 8.1\%$) but not in RGC soma ($+33.4\% \pm 0.11\%$).

Collectively those data show that miR-182 is specifically active in the axonal compartment of RGCs and not at the soma level, confirming an enrichment in miR-182 activity at the axonal growth cones level (Figure A.6).

The last part of my contribution in this paper, related to miR-182 activity, has been to reproduce the experiment upon Slit2 exposure (Figure A.7 I) and validating the purity of the axonal samples used (Figure A.7 H). miR-182 upon Slit2 exposure relieves its repression on Cofilin-1 mRNA (Figure A.1), we hypothesized a degradation of miR-182 upon Slit2 exposure and we investigated this possibility through RT-qPCR. This data, collected first by Sara Longhi, and further validated by me, show that Slit2 does not cause

Figure A.6: miR-182 is active and enriched in RGC axons

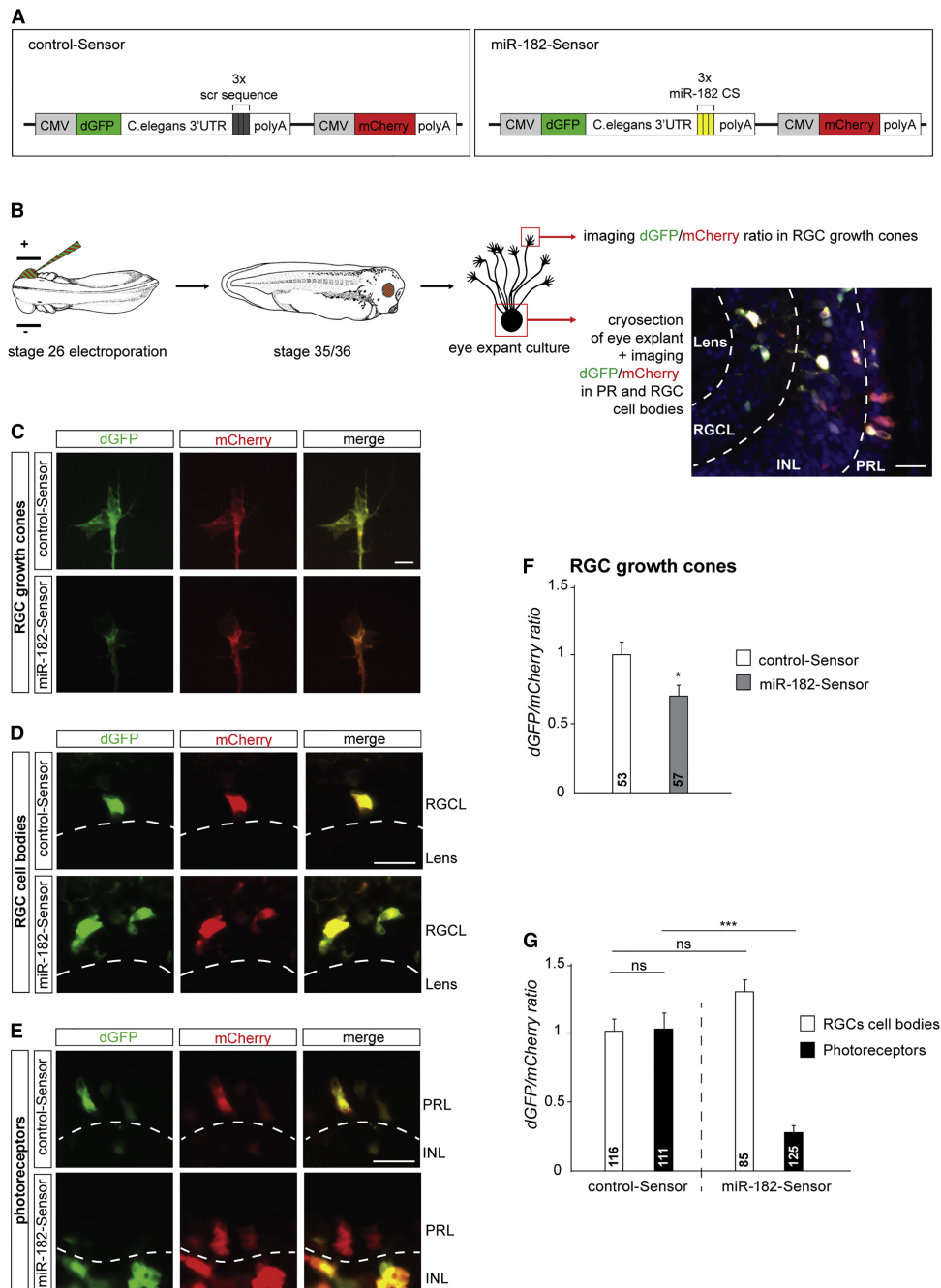
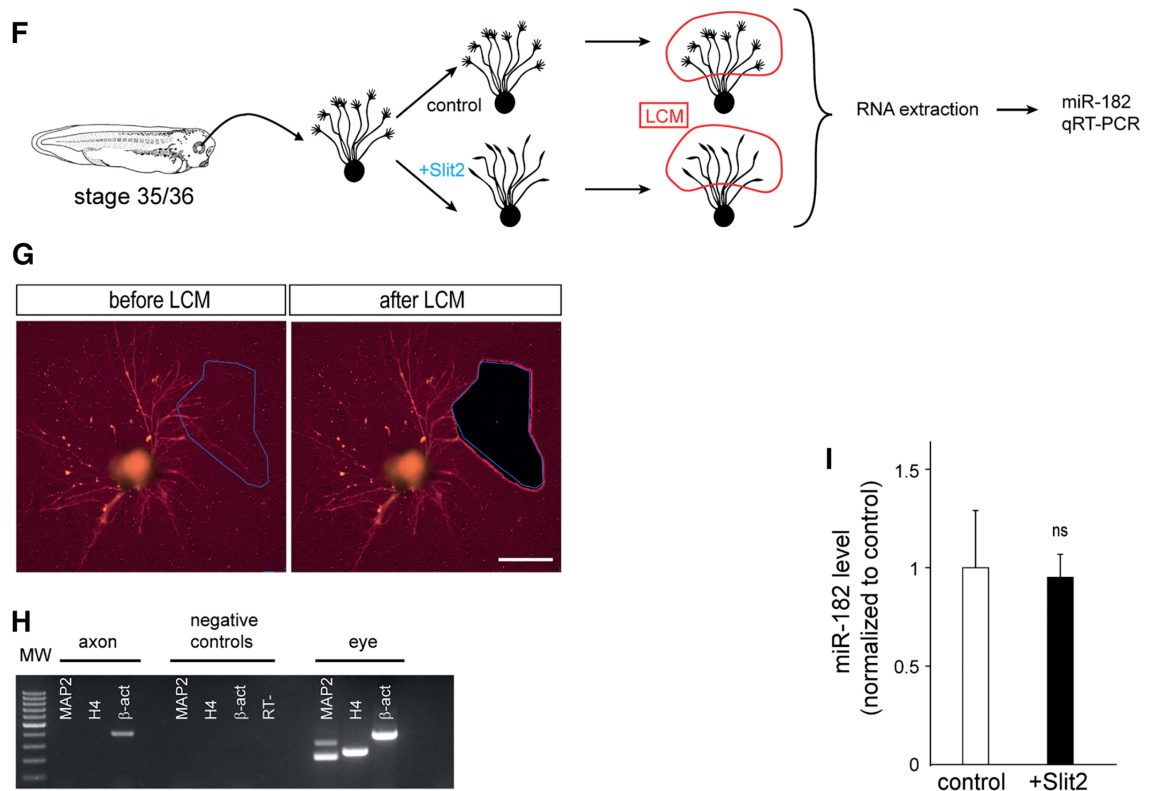


Figure 2 (Bellon et al., 2017) (A) Sensor construct design. (B) Schematic representation of the experimental protocol. (C–E) Illustrative images of RGC GCs (C), RGC soma (D), or PRs (E) following retinal electroporation of control-Sensor or miR-182-Sensor. Clear examples of dGFP/mCherry ratio decrease are shown in (C) and (E). (F and G) Quantification of the dGFP/mCherry ratio at the RGC GCs, soma, or PRs. Values are mean \pm SEM. Mann-Whitney test (F) and two-way ANOVA followed by Tukey post hoc test (G), $p < 0.05$, $p < 0.0001$. Abbreviations: ns, non significant; CMV, cytomegalovirus promoter; CS, complementary sequence; dGFP, destabilized GFP; INL, inner nuclear layer; PRL, photoreceptor layer; RGCL, retinal ganglion cell layer. Scale bars: 20 μ m (B, D, and E) and 5 μ m (C).

miR-182 degradation (Figure A.7 I). All the laser captured axonal samples used were pure: showing the presence of β -actin mRNA and the absence of MAP2, a dendritic marker, and histone H4, a nuclear marker mRNAs (Figure A.7 H).

Figure A.7: Slit2 Inhibits miR-182 activity in RGC axons without decay



Portion of Figure 7 (Bellon et al., 2017) (F) Schematic representation of the experimental paradigm. Stage 35/36 retinal explants were cultured for 24 hours, and then Slit2 or vehicle were bath applied for 10 minutes. (G) Illustrative images of explants and axons before and after LCM. (H) Illustrative gel of RT-PCR reaction for β -actin (β -act), MAP2, and histone H4 (H4) mRNA from cultured axons collected from stage 37/38 by LCM. In MAP2, H4, and β -act negative controls, PCR template was omitted. (I) Quantification of miR-182 by the Ct method in LCM axons. Values are mean \pm SEM. Mann-Whitney test, $p < 0.05$. Abbreviations: ns, nonsignificant; LCM, laser capture microdissection; RT, RT no template negative control. Scale bars: 200 μ m (G).

A.2 Conclusions

In Bellon et al. 2017, we showed for the first time that miRNAs gate the specificity in mRNAs translation upon cue exposure, reversibly release the inhibition on specific mRNAs allowing their translation. A mechanism of mRNAs selection in the vast repertoire of mRNAs present at the axonal level, gating in time and space the translation of the right molecule.

I personally contributed in showing that miR-182 activity in RGCs is axonal specific, despite its presence at the soma level of the same cell. I then validated that in pure axonal preparation, Slit2 is not decreasing miR-182 expression level, suggesting that the cue is rapidly lifting miR-182-mediated repression of cofilin-1 but without degrading it.

B Primers, oligos and reagents table

Table B.1: Primers and oligo list

PRIMERS (genotyping, axonal purity test, pre-miRNAs PCR and RT-qPCR)

Oligo Name	Ta	Sequence (5'-3')	Used for
Dicer HA Fw	60	AAGAAACACTGGATGATTGAAAAGC	mice genotyping
Dicer HA Rv	60	AAGAAAGGACCCATTGGTGAGG	mice genotyping
MAP2 Fw	60	CACGTACTCCTGGAACACCC	axonal purity test
MAP2 Rv	60	TGGAACCACAACGAGACTGA	axonal purity test
H4 Fw	60	GGCAAAGGAGGAAAAGGACT	axonal purity test
H4 Rv	60	GAGAGCGTACACCACATCCA	axonal purity test
ACTB Fw	60	CGTAAGGACCTCTATGCCAA	axonal purity test
ACTB Rv	60	TGCATTGATGACCATACAGTG	axonal purity test
U6 Fw	60	CTCGCTTCGGCAGCACA	pre-miRNAs PCR
U6 Rv	60	AACGCTTCACGAATTTGCGT	pre-miRNAs PCR
pre-miR-181a-1/a-2 Fw	60	GAACATTCAACGCTGTCCGGT	pre-miRNAs PCR
pre-miR-181a-2 Rv	60	TCAACGGCCGATGGTTTACA	pre-miRNAs PCR
pre-miR-181a-1-4L Rv	60	GATCGATGGTTTGCCTTCAGA	pre-miRNAs PCR
pre-miR-181a-1 4S Rv	60	ACGATCGATGGTTTGCCTTTAG	pre-miRNAs PCR
pre-miR-182 Fw	60	TGGCAATGGTAGAACTCACAC	pre-miRNAs PCR
pre-miR-182 Rv	60	GCAAGTCTAGAACCACCGGAT	pre-miRNAs PCR

CLONING (primers for PCR amplification of the 3'UTR of interest: wild type and mutated fragments)

Oligo Name	Ta	Sequence (5'-3')	3'UTR
APP Fw	66	GTACAAGTAATCTAGACCCCGGGAGCCTCT CGAATC	WT
APP Rv	66	CATGTCTGGATCTACGTACTAATTTTCAACCA GCTGGGCAC	WT
TUBB3 Fw	68	GTACAAGTAATCTAGAAGGAACCACTGCAAA GCCAGAG	WT
TUBB3 Rv	68	GTATCTTATCATGTCTGGATCTACGTATAAAA TACAGTACTCTGTCATCTGAACCTGTGC	WT
THBS1 Fw	55	CGGCATGGACGAGCTGTACAAGTAATCTAGA TCCAGAAGTTCTTCATTCCATG	WT
THBS1 Rv	55	GTATCTTATCATGTCTGGATCTACGTATCTTA TGTTTTTAATAGTTTATTTTTTTTATATTTTAC	WT
APP Fw	68	GTACAAGTAATCTAGACCCCGGGAGCCTC TCGAATC	MUT frg1
APP 1mut Rv	68	CTTTACAGTACACAAAACTCCTATTGATAA TGTCGTGGAAAGAGGGAAATGTTAAGAG	MUT frg1
APP 2mut Fw	66	CCACGACATTATCAATAGGAGTTTTTGTGTAC TGTAAGAGTTTAGCTGTCTCTTAACTACTTGC	MUT frg2
APP Rv	66	CATGTCTGGATCTACGTACTAATTTTCAACCA GCTGGGCAC	MUT frg2
TUBB3 Fw	67	GTACAAGTAATCTAGAAGGAACCACTGCAAA GCCAGAG	MUT frg1
TUBB3 1mut Rv	67	GCCTCACTCCTACATGTTGAACAGCAGGAAGT	MUT frg1

B Primers, oligos and reagents table

TUBB3 2mut Fw	63	TTATTTATTTAAAAATAAATAATCCAG TAAACTTCCTGCTGTTCAACATGTAGGAGTG	MUT frg2
TUBB3 2mut Rv	63	AGGCTTTTTTCTAATTATGGAACAGGC GGATTATATTTATGTACGTGTCTATATCAAC	MUT frg2
TUBB3 3mut Fw	67	ACAGACTCAAACCTCTATATATGC GAGTCTGTGTTGATATAGACACGTACATAAATA	MUT frg3
TUBB3 Rv	67	TAATCCTTTATCTATTCAGCTATCAACTTTG GTATCTTATCATGTCTGGATCTACGTATAAAA	MUT frg3
THBS1 Fw	64	TACAGTACTCTGTCTGTAACCTGTGC CGGCATGGACGAGCTGTACAAGTAATCTAGAT	MUT frg1
THBS1 1mut Rv	64	CCAGAAGTTCTTCATTCCATG GCTACATCTACAGCCTACCACTCCTTAGTACT	MUT frg1
THBS1 2mut Fw	63	CTGGAGATTCCAGGTCCTCTC GAATCTCCAGAGTACTAAGGAGTGGTAGGCTG	MUT frg2
THBS1 2mut Rv	63	TAGATGTAGCTCCCGCTG CACACACACACACACGTGCCGTGTCTAATACT	MUT frg2
THBS1 3mut Fw	56	C'TTTTAAAGGCAGTAATATATATAACCCAAC C'TTTAAAAGAGTATTAGACACGGCACGTGTGTG	MUT frg3
THBS1 Rv	56	TGTGTGTGTTTTCGTGTGGGGAGAGAGAG GTATCTTATCATGTCTGGATCTACGTATCTTAT	MUT frg3
THBS1 Q5 Fw	60	GTTTTTAATAGTTTATTTTTTTTATATTTTAC ATTCCATAGACACTAAGAGGATGTGATCGCAC	MUT Q5
THBS1 Q5 Rv	60	GAAGAACTTCTGGATCTAGATTACTTGTACA GCTC	MUT Q5

LIST OF MORPHOLINOS (MOs) - Gene tools (GT)

Name	Vendor	Sequence (5'-3') all 3' Fluorescein	Used
MO-5p # 1	GT	AGATACCAAACCTCACCGACAGCGTT	in MOs-5p cocktail
MO-5p # 2	GT	C'TTTCTCAAACCTCACCGACAGCGTT	in MOs-5p cocktail
MO-3p # 1	GT	GATCGATGGTTTGCCTTTAGATAC	in MOs-3p cocktail
MO-3p # 2	GT	GGCCGATGGTTTATATTTTTTATACT	in MOs-3p cocktail
Pri-miR-MO	GT	ATTGCCGTAATGTACAGTCAACGAT	block pre-miR-181a-1 Drosha cleavage
Standard control	GT	CCTCTTACCTCAGTTACAATTTATA	co-MO 25 nt
Custom control	GT	GTGTAACACGTCTATACGCCCA	co-MO 22 nt

Molecular Beacon (MB)

Name	Vendor	Sequence (5'-3') F:cy3, Q: BHQ2	Used
MB	Eurogentec	CAUUGCCUUUAGAUAACCAAUG	live imaging

TaqMan MicroRNA Assay - Thermo Fisher Scientific (TFS)

miRNA name	Vendor	Catalog and assay number	Used for
miR-181a-5p	TFS	Cat# 4427975; 000480	miRNA RT-qPCR
miR-181a-1-3p	TFS	Cat# 4440886; 004367	miRNA RT-qPCR
miR-181a-2-3p	TFS	Cat# 4440886; 005555	miRNA RT-qPCR
snU6	TFS	Cat# 4427975; 001973	miRNA RT-qPCR
hsa-miR-182	TFS	Cat# 4427975; 000597	miRNA RT-qPCR

Abbreviations: Ta, primers annealing temperature; frg, fragments (mutated fragments joint through overlapping extension PCR - OE-PCR); Fw, forward; Rv, reverse; MO, morpholino; co-MO, control morpholino; MUT, mutated miR-181a-5p responsive element; MUT Q5, mutated by Q5 mutagenesis kit (NEB); TUBB3, tubulin beta 3 class III; APP, Amyloid precursor protein; THBS1, Thrombospondin 1.

Table B.2: Reagents list

Name	Manufacturer	Catalog Number
Normal PCR (genotyping, axonal purity, pre-miRNA presence in axon)		
Go Taq G2HotStart Polymerase	Promega	M740B
MgCl ₂	Promega	A351H
5X Green Go Taq Flexi Buffer	Promega	M891A
Water, molecular biology reagent	Sigma-Aldrich	W4502
Genotyping (sample preparation, DNA extraction)		
Proteinase K	Ambion	AM2548
Tris-HCl, Trizma hydrochloride	Sigma-Aldrich	T5941
Ethylene diaminetetraacetic acid (EDTA)	ACS reagent, Sigma-Aldrich	E9884
Sodium Chloride (NaCl)	Sigma-Aldrich	S7653
Sodiumlaurylsulfate (SDS 1%)	ACS reagent, Sigma-Aldrich	436143
Phenol:Chloroform:Isoamyl Alcohol	Invitrogen ThermoScientific	15593031
Sodium Acetate (NaOAc)	Sigma-Aldrich	S2889
Isopropanol	Sigma-Aldrich	I9516
Nucleospin PCR & gel clean up	Carlo Erba Reagents	740.609.250
RNase H (Ribonuclease H)	NEB	M0297S
Gel electrophoresis		
Atlas ClearSight DNA Stain	Bioatlas	BH40501
Agarose	Sigma-Aldrich	A9539
Gene Ruler 100 bp ladder	Thermo Fisher Scientific	SM0241
Gene Ruler 1kb DNA Ladder Plus	Thermo Fisher Scientific	SM1331
HyperLadder 25bp	Bioline	BIO-33057
6 x DNA Loading Dye	Thermo Fisher Scientific	R0611
TAE buffer 50X 1L	Euroclone	EMR064001
10X TBE BUFFER 1000 ML	Ambion (Life Technologies)	AM9863
SYBR Gold Nucleic Acid Gel Stain	Life technologies	S11494
Retrotranscription and qPCR		
Single Cell RNA Purification Kit	Norgen Biotek	51800
Total RNA Purification Micro Kit	Norgen Biotek	35300
RNase-Free DNase I Kit	Norgen Biotek	25710
SPLIT RNA extraction kit	Lexogen	008.48
SuperScript IV Reverse Transcriptase	Thermo Fisher Scientific	18090050
RNase Inhibitor, Human Placenta	New England Biolabs (NEB)	M0307L
Random Hexamers 100 M	Euroclone	EMR428200
dNTP Mix 10mM/1ML	Euroclone	EMR416001
RNase Zap	Ambion (Life Technologies)	AM9782
TaqMan MicroRNA Reverse Transcription Kit	Thermo Fisher Scientific	4366596
Power SYBR Green, PCR Master Mix	Thermo Fisher Scientific	4367659
TaqMan Universal Master Mix II, no UNG 1x5mL	Thermo Fisher Scientific	4440040
Water, molecular biology reagent	Sigma-Aldrich	W4502
IHC Reagents		
NGS, Goat Serum	Gibco	16210072
70% Ethanol pure	Carlo Erba Reagents	308771
Triton X-100	Fisher Chemical	T/3751/08
PBS pH 7.4 (10X)	Gibco	70011-036
D(+)-Sucrose	ACS reagent	424500050
Sodium citrate tribasic dihydrate	ACS reagent	S4641- 1KG

B Primers, oligos and reagents table

TO-PRO-3 Iodide	Molecular Probes	T3605
ProLong Gold AntifadeMountant without DAPI	Molecular Probes	P36930
Tissue Freezing Medium (OCT)	Leica	381480
Superfrost Plus Microscope Slides	Thermo Fisher Scientific	4951PLUS4
Alexa Fluor 488 conjugate	Life technologies	A11070
Alexa Fluor 594 conjugate	Life technologies	A11020
Dicer Antibody (H-212)	Santa Cruz Biotechnology	sc-30226
Anti-Neurofilament (3A10)	DSHB	3A10-c
HA-probe antibody (Y-11)	Santa Cruz Biotechnology	sc-805

Organoculture

NeuroMag Transfection Reagent	OZ Biosciences	NM50200
Laminin	Sigma-Aldrich	L2020-1MG
Poly-L-lysine hydrobromide	Sigma-Aldrich	P1274-25MG
Antibiotic-Antimycotic (100X) - PSF	Thermo Fisher Scientific	15240062
Leibovitz's L-15 Medium	Thermo Fisher Scientific	11415049
MS222	Sigma-Aldrich	A5040
PFA (paraformaldehyde)	Sigma-Aldrich	
50 mm Dish — 14 mm Glass Diameter	MatTek	P50G-1.5-14-F
50 mm Dish — 30 mm Glass Diameter	MatTek	P50G-1.5-30-F
Round Cover Slips 12mm	Bellco Glass	1943-10012A
POL membrane 0.9 um	Leica	1150591
Sema3A	R&D System	1250-S3-025
Slit2	R&D System	5444-SL-050
Netrin-1	R&D System	1109-N1-025
BSA	Sigma-Aldrich	A7906-10G

C Recipes and reagent preparation

C.1 IHC

Heat inactivation goat serum (HIGS) Goat Serum stock 100 mL (Gibco) was incubated for 30 minutes in a 56°C water bath previously warmed sterilized water. After 30 minutes, the bottle was removed from the water and the external part was cleaned with EtOH 70%. 510 µl aliquots were prepared in autoclaved 1.5 ml tubes and stored at -20°C.

1x PBS	10x PBS in milliQ water
4% PFA	16% PFA in 1x PBS
30% sucrose	sucrose in 1x PBS
10% Triton	Triton x-100 diluted in milliQ water
1x TPBS	PBS 1x with 0.1% Triton
10% HIGS	100% HIGS in TPBS 1x
5% HIGS	10% NGS in TPBS 1x
Sodium citrate 0.01 M pH 6	Tri-sodium citrate in distilled water and successively add HCl to adjust the pH. Store at room temperature for maximum one month.

C.2 Organoculture

Poly-L-Lysine Poly-L-Lysine (PLL) stock is a 1 mg/mL solution in milliQ water, aliquoted and stored at -20°C. PLL stock is thawed at room temperature and an intermediate dilution of 100 µg/mL in milliQ is prepared and stored at 4°C for maximum two weeks. The plates are coated with a final working dilution of 10 µg/mL the day of the usage (3 hours PLL) or the day before (overnight PLL).

MBS buffer Autoclaved 0.1x Modified Barths saline is diluted in double distillate water ddH₂O pH 7.5 and prepared as a 10x stock. MBS 10x: 88 mM NaCl, 1 mM KCl, 0.82 mM MgSO₄, 2.4 mM NaHCO₃, 10 mM HEPES, 0.33 mM Ca(NO₃)₂, 0.41 mM CaCl₂.

Organoculture solutions All the following stock solutions for organoculture were prepared under the hood in sterile condition. The pH was adjusted with NaOH 1M to range between 7.6 and 7.8. All the medium were filtered by vacuum application and stored at 4°C.

0.1X MMR + PSF	5 mL PSF, 5 mL MMR 10x, top up to 500 mL with autoclaved milliQ water
L-15 60% + PSF	300 mL L-15, 5 mL PSF, top up to 500 mL with autoclaved milliQ water
L-15 60% + PSF + MS222	300 mL L-15, 5 mL PSF, 150 mg MS222, top up to 500 mL with autoclaved milliQ water

Bibliography

- Akhmanova Anna, Steinmetz Michel O.* Tracking the ends: a dynamic protein network controls the fate of microtubule tips // *Nature Reviews Molecular Cell Biology*. 2008. 9, 4. 309.
- Andreassi Catia, Luisier Raphaelle, Crerar Hamish, Franke Sasja, Luscombe Nicholas M, Cuda Giovanni, Gaspari Marco, Riccio Antonella.* 3' UTR cleavage of transcripts localized in axons of sympathetic neurons // *BioRxiv*. 2019. 170100.
- Andreassi Catia, Riccio Antonella.* To localize or not to localize: mRNA fate is in 3' UTR ends // *Trends in Cell Biology*. 2009. 19, 9. 465–474.
- Andreassi Catia, Zimmermann Carola, Mitter Richard, Fusco Salvatore, De Vita Serena, Saiardi Adolfo, Riccio Antonella.* An NGF-responsive element targets myo-inositol monophosphatase-1 mRNA to sympathetic neuron axons // *Nature Neuroscience*. 2010. 13, 3. 291.
- Arthur Ashley L, Yang Sihui Z, Abellana Allison, Wildonger Jill.* Dendrite arborization requires the dynein cofactor NudE // *J Cell Sci*. 2015. jcs–170316.
- Aschrafi Armaz, Kar Amar N, Natera-Naranjo Orlangie, MacGibeny Margaret A, Gioio Anthony E, Kaplan Barry B.* MicroRNA-338 regulates the axonal expression of multiple nuclear-encoded mitochondrial mRNAs encoding subunits of the oxidative phosphorylation machinery // *Cellular and Molecular Life Sciences*. 2012. 69, 23. 4017–4027.
- Aschrafi Armaz, Schwechter Azik D, Mameza Marie G, Natera-Naranjo Orlangie, Gioio Anthony E, Kaplan Barry B.* MicroRNA-338 regulates local cytochrome c oxidase IV mRNA levels and oxidative phosphorylation in the axons of sympathetic neurons // *Journal of Neuroscience*. 2008. 28, 47. 12581–12590.
- Augsburger Adela, Schuchardt Anita, Hoskins Sally, Dodd Jane, Butler Samantha.* BMPs as mediators of roof plate repulsion of commissural neurons // *Neuron*. 1999. 24, 1. 127–141.
- Baek Daehyun, Villén Judit, Shin Chanseok, Camargo Fernando D, Gygi Steven P, Bartel David P.* The impact of microRNAs on protein output // *Nature*. 2008. 455, 7209. 64.
- Bartel David P.* MicroRNAs: genomics, biogenesis, mechanism, and function // *Cell*. 2004. 116, 2. 281–297.
- Bartel David P.* Metazoan MicroRNAs // *Cell*. 2018. 173, 1. 20–51.
- Bashaw Greg J, Goodman Corey S.* Chimeric axon guidance receptors: the cytoplasmic domains of slit and netrin receptors specify attraction versus repulsion // *Cell*. 1999. 97, 7. 917–926.
- Bassell Gary J, Zhang Honglai, Byrd Anne L, Femino Andrea M, Singer Robert H, Taneja Krishan L, Lifshitz Lawrence M, Herman Ira M, Kosik Kenneth S.* Sorting of β -actin mRNA and protein to neurites and growth cones in culture // *The Journal of Neuroscience*. 1998. 18, 1. 251–265.
- Batista Andreia FR, Martínez José C, Hengst Ulrich.* Intra-axonal synthesis of SNAP25 is required for the formation of presynaptic terminals // *Cell Reports*. 2017. 20, 13. 3085–3098.
- Batista Andreia Filipa Rodrigues, Hengst Ulrich.* Intra-axonal protein synthesis in development and beyond // *International Journal of Developmental Neuroscience*. 2016. 55. 140–149.
- Baudet Marie-Laure, Zivraj Krishna H, Abreu-Goodger Cei, Muldal Alistair, Armisen Javier, Blenkiron Cherie, Goldstein Leonard D, Miska Eric A, Holt Christine E.* miR-124 acts through CoREST to control onset of Sema3A sensitivity in navigating retinal growth cones // *Nature Neuroscience*. 2012. 15, 1. 29–38.
- Bauer Karl E, Kiebler Michael A, Segura Inmaculada.* Visualizing RNA granule transport and translation in living neurons // *Methods*. 2017. 126. 177–185.
- Baumann Sebastian, Pohlmann Thomas, Jungbluth Marc, Brachmann Andreas, Feldbrügge Michael.* Kinesin-3 and dynein mediate microtubule-dependent co-transport of mRNPs and endosomes // *J Cell Sci*. 2012. jcs–101212.

Bibliography

- Bechara Ahmad, Nawabi Homaira, Moret Frédéric, Yaron Avraham, Weaver Eli, Bozon Muriel, Abouzeid Karima, Guan Jun-Lin, Tessier-Lavigne Marc, Lemmon Vance, others . FAK–MAPK-dependent adhesion disassembly downstream of L1 contributes to semaphorin3A-induced collapse // *The EMBO Journal*. 2008. 27, 11. 1549–1562.
- Bellon Anaïs, Iyer Archana, Bridi Simone, Lee Flora CY, Ovando-Vazquez Cesare, Corradi Eloina, Longhi Sara, Rocuzzo Michela, Strohbuecker Stephanie, Naik Sindhu, others . miR-182 regulates Slit2-mediated axon guidance by modulating the local translation of a specific mRNA // *Cell Reports*. 2017. 18, 5. 1171–1186.
- Ben-Yaakov Keren, Dagan Shachar Y, Segal-Ruder Yael, Shalem Ophir, Vuppalanchi Deepika, Willis Dianna E, Yudin Dmitry, Rishal Ida, Rother Franziska, Bader Michael, others . Axonal transcription factors signal retrogradely in lesioned peripheral nerve // *The EMBO Journal*. 2012. 31, 6. 1350–1363.
- Benes Vladimír, Collier Paul, Kordes Claus, Stolte Jens, Rausch Tobias, Muckentaler Martina U, Häussinger Dieter, Castoldi Mirco. Identification of cytokine-induced modulation of microRNA expression and secretion as measured by a novel microRNA specific qPCR assay // *Scientific Reports*. 2015. 5. 11590.
- Bernabo Paola, Tebaldi Toma, Groen Ewout JN, Lane Fiona M, Perenthaler Elena, Mattedi Francesca, Newbery Helen J, Zhou Haiyan, Zuccotti Paola, Potrich Valentina, others . In vivo transcriptome profiling in spinal muscular atrophy reveals a role for SMN protein in ribosome biology // *Cell Reports*. 2017. 21, 4. 953–965.
- Bicker Silvia, Khudayberdiev Sharof, Weiß Kerstin, Zocher Kathleen, Baumeister Stefan, Schratt Gerhard. The DEAH-box helicase DHX36 mediates dendritic localization of the neuronal precursor-microRNA-134 // *Genes & Development*. 2013. 27, 9. 991–996.
- Bielas Stephanie L, Serneo Finley F, Chechlacz Magdalena, Deerinck Thomas J, Perkins Guy A, Allen Patrick B, Ellisman Mark H, Gleeson Joseph G. Spinophilin facilitates dephosphorylation of doublecortin by PP1 to mediate microtubule bundling at the axonal wrist // *Cell*. 2007. 129, 3. 579–591.
- Bill Marius, Jentzsch Madlen, Schulz Julia, Schubert Karoline, Grimm Juliane, Schmalbrock Laura Katharina, Bonifacio Lynn Baquiran, Beinicke Stefanie, Haentschel Janine, Poenisch Wolfram, others . Absolute Quantification of Pre-microRNA-155 Copy Numbers By Digital Droplet PCR Identifies Acute Myeloid Leukemia (AML) Patients with Adverse Outcome // *Blood*. 2016. 128. 1698.
- Boese Amrit S, Saba Reuben, Campbell Kristyn, Majer Anna, Medina Sarah, Burton Lynn, Booth Timothy F, Chong Patrick, Westmacott Garrett, Dutta Sucharita M, others . MicroRNA abundance is altered in synaptoneuroosomes during prion disease // *Molecular and Cellular Neuroscience*. 2016. 71. 13–24.
- Bovolenta P, Mason Carol. Growth cone morphology varies with position in the developing mouse visual pathway from retina to first targets // *Journal of Neuroscience*. 1987. 7, 5. 1447–1460.
- Bullmore Ed, Barnes Anna, Bassett Danielle S, Fornito Alex, Kitzbichler Manfred, Meunier David, Suckling John. Generic aspects of complexity in brain imaging data and other biological systems // *Neuroimage*. 2009. 47, 3. 1125–1134.
- Busskamp Volker, Krol Jacek, Nelidova Dasha, Daum Janine, Szikra Tamas, Tsuda Ben, Jüttner Josephine, Farrow Karl, Scherf Brigitte Gross, Alvarez Claudia Patricia Patino, others . miRNAs 182 and 183 are necessary to maintain adult cone photoreceptor outer segments and visual function // *Neuron*. 2014. 83, 3. 586–600.
- Bustin Stephen A, Benes Vladimír, Garson Jeremy A, Hellemans Jan, Huggett Jim, Kubista Mikael, Mueller Reinhold, Nolan Tania, Pfaffl Michael W, Shipley Gregory L, others . The MIQE guidelines: minimum information for publication of quantitative real-time PCR experiments // *Clinical Chemistry*. 2009. 55, 4. 611–622.
- Butler Samantha J, Tear Guy. Getting axons onto the right path: the role of transcription factors in axon guidance // *Development*. 2007. 134, 3. 439–448.
- Cagnetta Roberta, Frese Christian K, Shigeoka Toshiaki, Krijgsveld Jeroen, Holt Christine E. Rapid cue-specific remodeling of the nascent axonal proteome // *Neuron*. 2018. 99, 1. 29–46.
- Cai Xuezhong, Hagedorn Curt H, Cullen Bryan R. Human microRNAs are processed from capped, polyadenylated transcripts that can also function as mRNAs // *RNA*. 2004. 10, 12. 1957–1966.
- Cajal Santiago Ramon. A quelle époque apparaissent les expansions des cellules nerveuses de la moëlle épinière du poulet? 1890.
- Campbell Douglas S, Holt Christine E. Chemotropic responses of retinal growth cones mediated by rapid local protein synthesis and degradation // *Neuron*. 2001. 32, 6. 1013–1026.

- Campbell Douglas S, Regan Aoife G, Lopez Juanita S, Tannahill David, Harris William A, Holt Christine E. Semaphorin 3A elicits stage-dependent collapse, turning, and branching in *Xenopus* retinal growth cones // *Journal of Neuroscience*. 2001. 21, 21. 8538–8547.
- Carcea Ioana, Ma'ayan Avi, Mesias Roxana, Sepulveda Bryan, Salton Stephen R, Benson Deanna L. Flotillin-mediated endocytic events dictate cell type-specific responses to semaphorin 3A // *Journal of Neuroscience*. 2010. 30, 45. 15317–15329.
- Cederquist Gustav Y, Luchniak Anna, Tischfield Max A, Peeva Maya, Song Yuyu, Menezes Manoj P, Chan Wai-Man, Andrews Caroline, Chew Sheena, Jamieson Robyn V, others . An inherited TUBB2B mutation alters a kinesin-binding site and causes polymicrogyria, CFEOM and axon dysinnervation // *Human Molecular Genetics*. 2012. 21, 26. 5484–5499.
- Chai Jie, Wang Shan, Han Dali, Dong Wei, Xie Chao, Guo Hongliang. MicroRNA-455 inhibits proliferation and invasion of colorectal cancer by targeting RAF proto-oncogene serine/threonine-protein kinase // *Tumor Biology*. 2015. 36, 2. 1313–1321.
- Challacombe Jean F, Snow Diane M, Letourneau Paul C. Role of the cytoskeleton in growth cone motility and axonal elongation // *Seminars in Neuroscience*. 8, 2. 1996. 67–80.
- Charrin Stéphanie, Jouannet Stéphanie, Boucheix Claude, Rubinstein Eric. Tetraspanins at a glance // *J Cell Sci*. 2014. 127, 17. 3641–3648.
- Chédotal Alain, Richards Linda J. Wiring the brain: the biology of neuronal guidance // *Cold Spring Harbor Perspectives in Biology*. 2010. 2, 6. a001917.
- Chen Chyi-Ying A, Shyu Ann-Bin. AU-rich elements: characterization and importance in mRNA degradation // *Trends in Biochemical Sciences*. 1995. 20, 11. 465–470.
- Chen Zhe, Gore Bryan B, Long Hua, Ma Le, Tessier-Lavigne Marc. Alternative splicing of the Robo3 axon guidance receptor governs the midline switch from attraction to repulsion // *Neuron*. 2008. 58, 3. 325–332.
- Chendrimada Thimmaiah P, Gregory Richard I, Kumaraswamy Easwari, Norman Jessica, Cooch Neil, Nishikura Kazuko, Shiekhattar Ramin. TRBP recruits the Dicer complex to Ago2 for microRNA processing and gene silencing // *Nature*. 2005. 436, 7051. 740.
- Cheng Hwai-Jong, Nakamoto Masaru, Bergemann Andrew D, Flanagan John G. Complementary gradients in expression and binding of ELF-1 and Mek4 in development of the topographic retinotectal projection map // *Cell*. 1995. 82, 3. 371–381.
- Cifuentes Daniel, Xue Huiling, Taylor David W, Patnode Heather, Mishima Yuichiro, Cheloufi Sihem, Ma Enbo, Mane Shrikant, Hannon Gregory J, Lawson Nathan, others . A novel miRNA processing pathway independent of Dicer requires Argonaute2 catalytic activity // *Science*. 2010. 1190809.
- Cioni Jean-Michel, Koppers Max, Holt Christine E. Molecular control of local translation in axon development and maintenance // *Current Opinion in Neurobiology*. 2018. 51. 86–94.
- Cioni Jean-Michel, Lin Julie Qiaojin, Holtermann Anne V, Koppers Max, Jakobs Maximilian AH, Azizi Afnan, Turner-Bridger Benita, Shigeoka Toshiaki, Franze Kristian, Harris William A, others . Late Endosomes Act as mRNA Translation Platforms and Sustain Mitochondria in Axons // *Cell*. 2019.
- Colamarino Sophia A, Tessier-Lavigne Marc. The axonal chemoattractant netrin-1 is also a chemorepellent for trochlear motor axons // *Cell*. 1995. 81, 4. 621–629.
- Colello RJ, Guillery RW. The early development of retinal ganglion cells with uncrossed axons in the mouse: retinal position and axonal course // *Development*. 1990. 108, 3. 515–523.
- Comazzetto Stefano, Di Giacomo Monica, Rasmussen Kasper Dindler, Much Christian, Azzi Chiara, Perlas Emerald, Morgan Marcos, O'Carroll Dónal. Oligoasthenoteratozoospermia and infertility in mice deficient for miR-34b/c and miR-449 loci // *PLoS Genet*. 2014. 10, 10. e1004597.
- Corradi Eloina, Gavoci Antoneta, Strohbuecker Stephanie, Rocuzzo Michela, Dalla Costa Irene, Iyer Archana, Bridi Simone, Rodriguez Gabriela Santoz, Abreu-Goodger Cei, Baudet Marie-Laure. Precursor miRNAs are trafficked along axons associated with vesicles and locally processed to regulate growth cone steering // *BioRxiv*. 2018. 470393.

Bibliography

- Cosker Katharina E, Fenstermacher Sara J, Pazyra-Murphy Maria F, Elliott Hunter L, Segal Rosalind A.* The RNA-binding protein SFPQ orchestrates an RNA regulon to promote axon viability // *Nature Neuroscience*. 2016. 19, 5. 690.
- Cox Llewellyn J, Hengst Ulrich, Gurskaya Nadya G, Lukyanov Konstantin A, Jaffrey Samie R.* Intra-axonal translation and retrograde trafficking of CREB promotes neuronal survival // *Nature Cell Biology*. 2008. 10, 2. 149–159.
- Craig Ann Marie, Banker Gary.* Neuronal polarity // *Annual Review of Neuroscience*. 1994. 17, 1. 267–310.
- Dajas-Bailador Federico, Bonev Boyan, Garcez Patricia, Stanley Peter, Guillemot Francois, Papalopulu Nancy.* microRNA-9 regulates axon extension and branching by targeting Map1b in mouse cortical neurons // *Nature Neuroscience*. 2012. 15, 5. 697–699.
- Dalva Matthew B, Takasu Mari A, Lin Michael Z, Shamah Steven M, Hu Linda, Gale Nicholas W, Greenberg Michael E.* EphB receptors interact with NMDA receptors and regulate excitatory synapse formation // *Cell*. 2000. 103, 6. 945–956.
- Dang Puneet, Smythe Elizabeth, Furley Andrew JW.* TAG1 regulates the endocytic trafficking and signaling of the semaphorin3A receptor complex // *Journal of Neuroscience*. 2012. 32, 30. 10370–10382.
- Davis Lauren, Dou PING, DeWit Marcia, Kater Stanley B.* Protein synthesis within neuronal growth cones // *Journal of Neuroscience*. 1992. 12, 12. 4867–4877.
- Deglincerti Alessia, Jaffrey Samie R.* Insights into the roles of local translation from the axonal transcriptome // *Open Biology*. 2012. 2, 6. 120079.
- Deglincerti Alessia, Liu Yaobin, Colak Dilek, Hengst Ulrich, Xu Guoqiang, Jaffrey Samie R.* Coupled local translation and degradation regulate growth cone collapse // *Nature Communications*. 2015. 6.
- Dehmelt Leif, Halpain Shelley.* Neurite outgrowth: a flick of the wrist // *Current Biology*. 2007. 17, 15. R611–R614.
- Denoulet Philippe, Eddé Bernard, Gros François.* Differential expression of several neurospecific β -tubulin mRNAs in the mouse brain during development // *Gene*. 1986. 50, 1-3. 289–297.
- Dent Erik W, Gertler Frank B.* Cytoskeletal dynamics and transport in growth cone motility and axon guidance // *Neuron*. 2003. 40, 2. 209–227.
- Dent Erik W, Gupton Stephanie L, Gertler Frank B.* The growth cone cytoskeleton in axon outgrowth and guidance // *Cold Spring Harbor Perspectives in Biology*. 2011. 3, 3. a001800.
- Dickson Barry J.* Molecular mechanisms of axon guidance // *Science*. 2002. 298, 5600. 1959–1964.
- Dingwell Kevin S, Holt Christine E, Harris William A.* The multiple decisions made by growth cones of RGCs as they navigate from the retina to the tectum in *Xenopus* embryos // *Journal of Neurobiology*. 2000. 44, 2. 246–259.
- Dräger Ursula C.* Birth dates of retinal ganglion cells giving rise to the crossed and uncrossed optic projections in the mouse // *Proc. R. Soc. Lond. B*. 1985. 224, 1234. 57–77.
- Ebert Margaret S, Sharp Phillip A.* Emerging roles for natural microRNA sponges // *Current Biology*. 2010. 20, 19. R858–R861.
- Eickholt Britta J, Walsh Frank S, Doherty Patrick.* An inactive pool of GSK-3 at the leading edge of growth cones is implicated in Semaphorin 3A signaling // *The Journal of Cell Biology*. 2002. 157, 2. 211–217.
- Eng Hubert, Lund Karen, Campenot Robert B.* Synthesis of β -tubulin, actin, and other proteins in axons of sympathetic neurons in compartmented cultures // *Journal of Neuroscience*. 1999. 19, 1. 1–9.
- Engelke Martin F, Burckhardt Christoph J, Morf Matthias K, Greber Urs F.* The dynactin complex enhances the speed of microtubule-dependent motions of adenovirus both towards and away from the nucleus // *Viruses*. 2011. 3, 3. 233–253.
- Erdogan Burcu, Ebbert Patrick T, Lowery Laura Anne.* Using *Xenopus laevis* retinal and spinal neurons to study mechanisms of axon guidance in vivo and in vitro // *Seminars in Cell & Developmental Biology*. 51. 2016. 64–72.
- Erskine Lynda, Herrera Eloisa.* Connecting the retina to the brain // *ASN Neuro*. 2014. 6, 6. 1759091414562107.

- Erskine Lynda, Williams Scott E, Brose Katja, Kidd Thomas, Rachel Rivka A, Goodman Corey S, Tessier-Lavigne Marc, Mason Carol A.* Retinal ganglion cell axon guidance in the mouse optic chiasm: expression and function of robo and slits // *Journal of Neuroscience*. 2000. 20, 13. 4975–4982.
- Evans Ciaran, Hardin Johanna, Stoebel Daniel M.* Selecting between-sample RNA-Seq normalization methods from the perspective of their assumptions // *Briefings in Bioinformatics*. 2017. 19, 5. 776–792.
- Fabregat Antonio, Sidiropoulos Konstantinos, Garapati Phani, Gillespie Marc, Hausmann Kerstin, Haw Robin, Jassal Bijay, Jupe Steven, Korninger Florian, McKay Sheldon, others .* The reactome pathway knowledgebase // *Nucleic Acids Research*. 2015. 44, D1. D481–D487.
- Falk Julien, Drinjakovic Jovana, Leung Kin Mei, Dwivedy Asha, Regan Aoife G, Piper Michael, Holt Christine E.* Electroporation of cDNA/Morpholinos to targeted areas of embryonic CNS in *Xenopus* // *BMC Developmental Biology*. 2007. 7, 1. 107.
- Falk Julien, Konopacki Filip A, Zivraj Krishna H, Holt Christine E.* Rab5 and Rab4 regulate axon elongation in the *Xenopus* visual system // *Journal of Neuroscience*. 2014. 34, 2. 373–391.
- Fawcett James W.* Growth-cone collapse: too much of a good thing? // *Trends in Neurosciences*. 1993. 16, 5. 165–167.
- Fleige Simone, Walf Vanessa, Huch Silvia, Prgomet Christian, Sehm Julia, Pfaffl Michael W.* Comparison of relative mRNA quantification models and the impact of RNA integrity in quantitative real-time RT-PCR // *Biotechnology Letters*. 2006. 28, 19. 1601–1613.
- Fukata Yuko, Itoh Tomohiko J, Kimura Toshihide, Ménager Céline, Nishimura Takashi, Shiromizu Takashi, Watanabe Hiroyasu, Inagaki Naoyuki, Iwamatsu Akihiro, Hotani Hirokazu, others .* CRMP-2 binds to tubulin heterodimers to promote microtubule assembly // *Nature Cell Biology*. 2002. 4, 8. 583.
- Gallo Gianluca, Letourneau Paul C.* Regulation of growth cone actin filaments by guidance cues // *Journal of Neurobiology*. 2004. 58, 1. 92–102.
- Garcia David M, Baek Daehyun, Shin Chanseok, Bell George W, Grimson Andrew, Bartel David P.* Weak seed-pairing stability and high target-site abundance decrease the proficiency of *lscy-6* and other microRNAs // *Nature Structural & Molecular Biology*. 2011. 18, 10. 1139.
- Georgi Sean A, Reh Thomas A.* Dicer is required for the transition from early to late progenitor state in the developing mouse retina // *Journal of Neuroscience*. 2010. 30, 11. 4048–4061.
- Geraldo Sara, Gordon-Weeks Phillip R.* Cytoskeletal dynamics in growth-cone steering // *Journal of Cell Science*. 2009. 122, 20. 3595–3604.
- Gershoni Emek Noga, Altman Topaz, Ionescu Ariel, Costa Christopher, Gradus-Pery Tal, Willis Dianna E, Perlson Eran.* Localization of RNAi machinery to axonal branch points and growth cones is facilitated by mitochondria and is disrupted in ALS // *Frontiers in Molecular Neuroscience*. 2018. 11. 311.
- Gharbi Sedigheh, Shamsara Mehdi, Khateri Shahriar, Soroush Mohammad Reza, Ghorbanmehr Nassim, Tavallaei Mahmood, Nourani Mohammad Reza, Mowla Seyed Javad.* Identification of reliable reference genes for quantification of microRNAs in serum samples of sulfur mustard-exposed veterans // *Cell Journal (Yakhteh)*. 2015. 17, 3. 494.
- Gibbins Derrick J, Ciaudo Constance, Erhardt Mathieu, Voinnet Olivier.* Multivesicular bodies associate with components of miRNA effector complexes and modulate miRNA activity // *Nature Cell Biology*. 2009. 11, 9. 1143.
- Giraldez Antonio J, Cinalli Ryan M, Glasner Margaret E, Enright Anton J, Thomson J Michael, Baskerville Scott, Hammond Scott M, Bartel David P, Schier Alexander F.* MicroRNAs regulate brain morphogenesis in zebrafish // *Science*. 2005. 308, 5723. 833–838.
- Godement Pierre, Salaün Josselyne, Imbert Michel.* Prenatal and postnatal development of retinogeniculate and retinocollicular projections in the mouse // *Journal of Comparative Neurology*. 1984. 230, 4. 552–575.
- Goldberg Daniel J, Burmeister Donald W.* Stages in axon formation: observations of growth of *Aplysia* axons in culture using video-enhanced contrast-differential interference contrast microscopy // *The Journal of Cell Biology*. 1986. 103, 5. 1921–1931.

Bibliography

- Gomez Timothy M, Letourneau Paul C. Actin dynamics in growth cone motility and navigation // *Journal of Neurochemistry*. 2014. 129, 2. 221–234.
- Gordon-Weeks Phillip R. Microtubules and growth cone function // *Journal of Neurobiology*. 2004. 58, 1. 70–83.
- Gorovoy Matvey, Niu Jiaxin, Bernard Ora, Profirovic Jasmina, Minshall Richard, Neamu Radu, Voyno-Yasenetskaya Tatyana. LIM kinase 1 coordinates microtubule stability and actin polymerization in human endothelial cells // *Journal of Biological Chemistry*. 2005. 280, 28. 26533–26542.
- Grimson Andrew, Farh Kyle Kai-How, Johnston Wendy K, Garrett-Engele Philip, Lim Lee P, Bartel David P. MicroRNA targeting specificity in mammals: determinants beyond seed pairing // *Molecular Cell*. 2007. 27, 1. 91–105.
- Gruenberg Jean, Stenmark Harald. The biogenesis of multivesicular endosomes // *Nature Reviews Molecular Cell Biology*. 2004. 5, 4. 317.
- Gu Chenghua, Rodriguez E Rene, Reimert Dorothy V, Shu Tianzhi, Fritsch Bernd, Richards Linda J, Kolodkin Alex L, Ginty David D. Neuropilin-1 conveys semaphorin and VEGF signaling during neural and cardiovascular development // *Developmental Cell*. 2003. 5, 1. 45–57.
- Gumy Laura F, Yeo Giles SH, Tung Yi-Chun Loraine, Zivraj Krishna H, Willis Dianna, Coppola Giovanni, Lam Brian YH, Twiss Jeffery L, Holt Christine E, Fawcett James W. Transcriptome analysis of embryonic and adult sensory axons reveals changes in mRNA repertoire localization // *RNA*. 2011. 17, 1. 85–98.
- Gwizdek Carole, Bertrand Edouard, Dargemont Catherine, Lefebvre Jean-Claude, Blanchard Jean-Marie, Singer Robert H, Doglio Alain. Terminal minihelix, a novel RNA motif that directs polymerase III transcripts to the cell cytoplasm. Terminal minihelix and RNA export // *Journal of Biological Chemistry*. 2001. 276, 28. 25910–25918.
- Ha Minju, Kim V Narry. Regulation of microRNA biogenesis // *Nature Reviews Molecular Cell Biology*. 2014. 15, 8. 509–524.
- Hall Alan. Rho GTPases and the actin cytoskeleton // *Science*. 1998. 279, 5350. 509–514.
- Hammond Jennetta W, Cai Dawen, Verhey Kristen J. Tubulin modifications and their cellular functions // *Current Opinion in Cell Biology*. 2008. 20, 1. 71–76.
- Han F, Huo Y, Huang C-J, Chen C-L, Ye J. MicroRNA-30b promotes axon outgrowth of retinal ganglion cells by inhibiting Semaphorin3A expression // *Brain Research*. 2015. 1611. 65–73.
- Han Liang, Wen Zhezeng, Lynn Rachel C, Baudet Marie-Laure, Holt Christine E, Sasaki Yukio, Bassell Gary J, Zheng James Q. Regulation of chemotropic guidance of nerve growth cones by microRNA // *Molecular Brain*. 2011. 4, 1. 40.
- Hancock Melissa L, Preitner Nicolas, Quan Jie, Flanagan John G. MicroRNA-132 is enriched in developing axons, locally regulates Ras1 mRNA, and promotes axon extension // *The Journal of Neuroscience*. 2014. 34, 1. 66–78.
- Hankenson F Claire, Garzel Laura M, Fischer David D, Nolan Bonnie, Hankenson Kurt D. Evaluation of tail biopsy collection in laboratory mice (*Mus musculus*): vertebral ossification, DNA quantity, and acute behavioral responses // *Journal of the American Association for Laboratory Animal Science*. 2008. 47, 6. 10–18.
- Hansel Christian, Linden David J. Long-term depression of the cerebellar climbing fiber–Purkinje neuron synapse // *Neuron*. 2000. 26, 2. 473–482.
- Hansen Thomas B, Jensen Trine I, Clausen Bettina H, Bramsen Jesper B, Finsen Bente, Damgaard Christian K, Kjems Jørgen. Natural RNA circles function as efficient microRNA sponges // *Nature*. 2013. 495, 7441. 384.
- Harrison Ross Granville. The outgrowth of the nerve fiber as a mode of protoplasmic movement // *Journal of Experimental Zoology*. 1910. 9, 4. 787–846.
- Hata Akiko, Lieberman Judy. Dysregulation of microRNA biogenesis and gene silencing in cancer // *Sci. Signal*. 2015. 8, 368. re3–re3.
- He Lin, Hannon Gregory J. MicroRNAs: small RNAs with a big role in gene regulation // *Nature Reviews Genetics*. 2004. 5, 7. 522–531.
- Hedgecock Edward M, Culotti Joseph G, Hall David H. The unc-5, unc-6, and unc-40 genes guide circumferential migrations of pioneer axons and mesodermal cells on the epidermis in *C. elegans* // *Neuron*. 1990. 4, 1. 61–85.

- Hengst Ulrich, Cox Llewellyn J, Macosko Evan Z, Jaffrey Samie R.* Functional and selective RNA interference in developing axons and growth cones // *The Journal of Neuroscience*. 2006. 26, 21. 5727–5732.
- Hengst Ulrich, Deglincerti Alessia, Kim Hyung Joon, Jeon Noo Li, Jaffrey Samie R.* Axonal elongation triggered by stimulus-induced local translation of a polarity complex protein // *Nature Cell Biology*. 2009. 11, 8. 1024–1030.
- Heumüller-Klug Sabine, Sticht Carsten, Kaiser Karin, Wink Elwira, Hagl Cornelia, Wessel Lucas, Schäfer Karl-Herbert.* Degradation of intestinal mRNA: a matter of treatment // *World Journal of Gastroenterology*. 2015. 21, 12. 3499.
- Hewel Martijn P van den, Kahn René S.* Abnormal brain wiring as a pathogenetic mechanism in schizophrenia // *Biological Psychiatry*. 2011. 70, 12. 1107–1108.
- Hindges Robert, McLaughlin Todd, Genoud Nicolas, Henkemeyer Mark, O’Leary Dennis DM.* EphB forward signaling controls directional branch extension and arborization required for dorsal-ventral retinotopic mapping // *Neuron*. 2002. 35, 3. 475–487.
- Hindson Christopher M, Chevillet John R, Briggs Hilary A, Gallichotte Emily N, Ruf Ingrid K, Hindson Benjamin J, Vessella Robert L, Tewari Muneesh.* Absolute quantification by droplet digital PCR versus analog real-time PCR // *Nature Methods*. 2013. 10, 10. 1003.
- Hirokawa Nobutaka, Niwa Shinsuke, Tanaka Yosuke.* Molecular motors in neurons: transport mechanisms and roles in brain function, development, and disease // *Neuron*. 2010. 68, 4. 610–638.
- Holmqvist Bo I, Ostholm Thomas, Ekström Peter.* Dil tracing in combination with immunocytochemistry for analysis of connectivities and chemoarchitectonics of specific neural systems in a teleost, the Atlantic salmon // *Journal of Neuroscience Methods*. 1992. 42, 1-2. 45–63.
- Holt Christine E.* Does timing of axon outgrowth influence initial retinotectal topography in *Xenopus*? // *Journal of Neuroscience*. 1984. 4, 4. 1130–1152.
- Holt Christine E, Harris William A.* Order in the initial retinotectal map in *Xenopus*: a new technique for labelling growing nerve fibres // *Nature*. 1983. 301, 5896. 150.
- Horio Tetsuya, Murata Takashi.* The role of dynamic instability in microtubule organization // *Frontiers in Plant Science*. 2014. 5. 511.
- Hornberg Hanna Kristina, Holt Christine.* RNA-binding proteins and translational regulation in axons and growth cones // *Frontiers in Neuroscience*. 2013. 7. 81.
- Hoskins SALLY G, Grobstein PAUL.* Development of the ipsilateral retinothalamic projection in the frog *Xenopus laevis*. III. The role of thyroxine // *Journal of Neuroscience*. 1985. 5, 4. 930–940.
- Houng Shen-Yi Bruce, Huang Yong, Ptáček Louis, Fu Ying-Hui.* Understanding the role of dicer in astrocyte development // *PloS One*. 2015. 10, 5. e0126667.
- Hsieh Jenny.* Orchestrating transcriptional control of adult neurogenesis // *Genes & Development*. 2012. 26, 10. 1010–1021.
- Hughes Arthur.* The development of the neural tube of the chick embryo. A study with the ultraviolet microscope // *Journal of Embryology and Experimental Morphology*. 1955. 3, 4. 305–325.
- Iida Atsumi, Shinoe Toru, Baba Yukihiro, Mano Hiroyuki, Watanabe Sumiko.* Dicer plays essential roles for retinal development by regulation of survival and differentiation // *Investigative Ophthalmology & Visual Science*. 2011. 52, 6. 3008–3017.
- Iyer Archana N, Bellon Anaïs, Baudet Marie-Laure.* microRNAs in axon guidance // *Frontiers in Cellular Neuroscience*. 2014. 8.
- Jambor Helena, Brunel Christine, Ephrussi Anne.* Dimerization of oskar 3’ UTRs promotes hitchhiking for RNA localization in the *Drosophila* oocyte // *RNA*. 2011. 17, 12. 2049–2057.
- Jeffery Glen, Erskine Lynda.* Variations in the architecture and development of the vertebrate optic chiasm // *Progress in Retinal and Eye Research*. 2005. 24, 6. 721–753.
- Jiang YUAN QING, Oblinger Monica M.* Differential regulation of beta III and other tubulin genes during peripheral and central neuron development // *Journal of Cell Science*. 1992. 103, 3. 643–651.

Bibliography

- Jin Zhao, Strittmatter Stephen M.* Rac1 mediates collapsin-1-induced growth cone collapse // *Journal of Neuroscience*. 1997. 17, 16. 6256–6263.
- Jones Matthew R, Quinton Lee J, Blahna Matthew T, Neilson Joel R, Fu Suneng, Ivanov Alexander R, Wolf Dieter A, Mizgerd Joseph P.* Zcchc11-dependent uridylation of microRNA directs cytokine expression // *Nature Cell Biology*. 2009. 11, 9. 1157–1163.
- Joshi Harish C, Cleveland Don W.* Diversity among tubulin subunits: toward what functional end? // *Cell Motility and The Cytoskeleton*. 1990. 16, 3. 159–163.
- Jung Hosung, Yoon Byung C, Holt Christine E.* Axonal mRNA localization and local protein synthesis in nervous system assembly, maintenance and repair // *Nature Reviews Neuroscience*. 2012. 13, 5. 308.
- Kar Amar N, MacGibeny Margaret A, Gervasi Noreen M, Gioio Anthony E, Kaplan Barry B.* Intra-axonal synthesis of eukaryotic translation initiation factors regulates local protein synthesis and axon growth in rat sympathetic neurons // *Journal of Neuroscience*. 2013. 33, 17. 7165–7174.
- Katoh Takayuki, Sakaguchi Yuriko, Miyauchi Kenjiyo, Suzuki Takeo, Kashiwabara Shin-ichi, Baba Tadashi, Suzuki Tsutomu.* Selective stabilization of mammalian microRNAs by 3' adenylation mediated by the cytoplasmic poly (A) polymerase GLD-2 // *Genes & Development*. 2009. 23, 4. 433–438.
- Katsetos Christos D, Herman Mary M, Mörk Sverre J.* Class III β -tubulin in human development and cancer // *Cell Motility and The Cytoskeleton*. 2003. 55, 2. 77–96.
- Kim Eunjin, Jung Hosung.* Local protein synthesis in neuronal axons: why and how we study // *BMB Reports*. 2015. 48, 3. 139.
- Kim Hak Hee, Kim Paul, Phay Monichan, Yoo Soonmoon.* Identification of precursor microRNAs within distal axons of sensory neuron // *Journal of Neurochemistry*. 2015.
- Kislauskis Edward H, Singer Robert H.* Determinants of mRNA localization // *Current Opinion in Cell Biology*. 1992. 4, 6. 975–978.
- Klitschar M, Neuherber F.* Evaluation of an alkaline lysis method for the extraction of DNA from whole blood and forensic stains for STR analysis // *Journal of Forensic Science*. 2000. 45, 3. 669–673.
- Knabbe Johannes, Nassal Joris Paul, Verhage Matthijs, Kuner Thomas.* Secretory vesicle trafficking in awake and anesthetized mice: differential speeds in axons versus synapses // *The Journal of Physiology*. 2018.
- Knobel Karla M, Jorgensen Erik M, Bastiani Michael J.* Growth cones stall and collapse during axon outgrowth in *Caenorhabditis elegans* // *Development*. 1999. 126, 20. 4489–4498.
- Knowles Roger B, Sabry James H, Martone Maryann E, Deerinck Thomas J, Ellisman Mark H, Bassell Gary J, Kosik Kenneth S.* Translocation of RNA granules in living neurons // *Journal of Neuroscience*. 1996. 16, 24. 7812–7820.
- Konopacki Filip A, Wong Hovy Ho-Wai, Dwivedy Asha, Bellon Anaïs, Blower Michael D, Holt Christine E.* ESCRT-II controls retinal axon growth by regulating DCC receptor levels and local protein synthesis // *Open Biology*. 2016. 6, 4. 150218.
- Korbo Lise, Andersen Birgitte Bo, Ladefoged Ole, Møller Arne.* Total numbers of various cell types in rat cerebellar cortex estimated using an unbiased stereological method // *Brain Research*. 1993. 609, 1-2. 262–268.
- Koropouli Eleftheria, Kolodkin Alex L.* Semaphorins and the dynamic regulation of synapse assembly, refinement, and function // *Current Opinion in Neurobiology*. 2014. 27. 1–7.
- Kos Aron, Loohuis Nikkie Olde, Meinhardt Julia, Bokhoven Hans van, Kaplan Barry B, Martens Gerard J, Aschrafi Armaz.* MicroRNA-181 promotes synaptogenesis and attenuates axonal outgrowth in cortical neurons // *Cellular and Molecular Life Sciences*. 2016. 73, 18. 3555–3567.
- Krol Jacek, Busskamp Volker, Markiewicz Ilona, Stadler Michael B, Ribi Sebastian, Richter Jens, Duebel Jens, Bicker Silvia, Fehling Hans Jörg, Schübeler Dirk, others .* Characterizing light-regulated retinal microRNAs reveals rapid turnover as a common property of neuronal microRNAs // *Cell*. 2010. 141, 4. 618–631.
- Kundel Mitchell, Jones Kendrick J, Shin Chan Y, Wells David G.* Cytoplasmic polyadenylation element-binding protein regulates neurotrophin-3-dependent β -catenin mRNA translation in developing hippocampal neurons // *The Journal of Neuroscience*. 2009. 29, 43. 13630–13639.

- Kye Min-Jeong, Liu Tsunglin, Levy Sasha F, Xu Nan Lan, Groves Benjamin B, Bonneau Richard, Lao Kaigin, Kosik Kenneth S. Somatodendritic microRNAs identified by laser capture and multiplex RT-PCR // RNA. 2007.
- Lagos-Quintana Mariana, Rauhut Reinhard, Yalcin Abdullah, Meyer Jutta, Lendeckel Winfried, Tuschl Thomas. Identification of tissue-specific microRNAs from mouse // Current Biology. 2002. 12, 9. 735–739.
- Lambert Bernard, Meryet-Figuière Matthieu, Gauduchon Pascal, Vigneron Nicolas, Brotin Emilie, Poulain Laurent, Denoyelle Christophe. miRNAs as tools for tailoring personalized therapeutic strategies in ovarian carcinoma // RNA & DISEASE. 2015. 2, 2. 10–14800.
- Lanier Lorene M, Gertler Frank B. Actin cytoskeleton: thinking globally, actin' locally // Current Biology. 2000. 10, 18. R655–R657.
- Latremoliere Alban, Cheng Long, DeLisle Michelle, Wu Chen, Chew Sheena, Hutchinson Elizabeth B, Sheridan Andrew, Alexandre Chloe, Latremoliere Frederic, Sheu Shu-Hsien, others . Neuronal-Specific TUBB3 Is Not Required for Normal Neuronal Function but Is Essential for Timely Axon Regeneration // Cell Reports. 2018. 24, 7. 1865–1879.
- Leandro-García Luis J, Leskelä Susanna, Landa Iñigo, Montero-Conde Cristina, López-Jiménez Elena, Letón Rocío, Cascón Alberto, Robledo Mercedes, Rodríguez-Antona Cristina. Tumoral and tissue-specific expression of the major human β -tubulin isoforms // Cytoskeleton. 2010. 67, 4. 214–223.
- Lebrand Cecile, Dent Erik W, Strasser Geraldine A, Lanier Lorene M, Krause Matthias, Svitkina Tatyana M, Borisy Gary G, Gertler Frank B. Critical role of Ena/VASP proteins for filopodia formation in neurons and in function downstream of netrin-1 // Neuron. 2004. 42, 1. 37–49.
- Lee Yoontae, Ahn Chiyoung, Han Jinju, Choi Hyounjeong, Kim Jaekwang, Yim Jeongbin, Lee Junho, Provost Patrick, Rådmark Olof, Kim Sunyoung, others . The nuclear RNase III Drosha initiates microRNA processing // Nature. 2003. 425, 6956. 415–419.
- Lee Yoontae, Jeon Kipyoun, Lee Jun-Tae, Kim Sunyoung, Kim V Narry. MicroRNA maturation: stepwise processing and subcellular localization // The EMBO Journal. 2002. 21, 17. 4663–4670.
- Lee Young Sik, Pressman Sigal, Andress Arlise P, Kim Kevin, White Jamie L, Cassidy Justin J, Li Xin, Lubell Kim, Lim Do Hwan, Cho Ik Sang, others . Silencing by small RNAs is linked to endosomal trafficking // Nature Cell Biology. 2009. 11, 9. 1150.
- Leung Kin-Mei, Holt Christine E. Live visualization of protein synthesis in axonal growth cones by microinjection of photoconvertible Kaede into *Xenopus* embryos // Nature Protocols. 2008. 3, 8. 1318.
- Leung Kin-Mei, Horck Francisca PG van, Lin Andrew C, Allison Rachel, Standart Nancy, Holt Christine E. Asymmetrical β -actin mRNA translation in growth cones mediates attractive turning to netrin-1 // Nature Neuroscience. 2006. 9, 10. 1247–1256.
- Leung Kin-Mei, Lu Bo, Wong Hovy Ho-Wai, Lin Julie Qiaojin, Turner-Bridger Benita, Holt Christine E. Cue-polarized transport of β -actin mRNA depends on 3' UTR and microtubules in live growth cones // Frontiers in Cellular Neuroscience. 2018. 12.
- Li Chanxia, Sasaki Yukio, others . Fragile X mental retardation protein is involved in protein synthesis-dependent collapse of growth cones induced by semaphorin-3A // Frontiers in Neural Circuits. 2009. 3. 11.
- Li Tao, Wang Jingjing, Wang Hongkai, Yang Yujian, Wang Shouyu, Huang Nanxin, Wang Fei, Gao Xing, Niu Jianqin, Li Zhifang, others . The deletion of Dicer in mature myelinating glial cells causes progressive axonal degeneration but not overt demyelination in adult mice // Glia. 2018. 66, 9. 1960–1971.
- Lin Andrew C, Holt Christine E. Function and regulation of local axonal translation // Current Opinion in Neurobiology. 2008. 18, 1. 60–68.
- Liu Guofa, Dwyer Trisha. Microtubule dynamics in axon guidance // Neuroscience Bulletin. 2014. 30, 4. 569–583.
- Liu Gwen, Min Hyeyoung, Yue Sibiao, Chen Chang-Zheng. Pre-miRNA loop nucleotides control the distinct activities of mir-181a-1 and mir-181c in early T cell development // PloS One. 2008. 3, 10. e3592.
- Liu Janice, Wilson Steven, Reh Thomas. BMP receptor 1b is required for axon guidance and cell survival in the developing retina // Developmental Biology. 2003. 256, 1. 34–48.

Bibliography

- Lowery Laura Anne, Van Vector David. The trip of the tip: understanding the growth cone machinery // *Nature Reviews Molecular Cell Biology*. 2009. 10, 5. 332–343.
- Lugli Giovanni, Larson John, Martone Maryann E, Jones Ying, Smalheiser Neil R. Dicer and eIF2c are enriched at postsynaptic densities in adult mouse brain and are modified by neuronal activity in a calpain-dependent manner // *Journal of Neurochemistry*. 2005. 94, 4. 896–905.
- Lugli Giovanni, Torvik Vette I, Larson John, Smalheiser Neil R. Expression of microRNAs and their precursors in synaptic fractions of adult mouse forebrain // *Journal of Neurochemistry*. 2008. 106, 2. 650–661.
- Lund Elsebet, Güttinger Stephan, Calado Angelo, Dahlberg James E, Kutay Ulrike. Nuclear export of microRNA precursors // *Science*. 2004. 303, 5654. 95–98.
- Lyuksyutova Anna I, Lu Chin-Chun, Milanesio Nancy, King Leslie A, Guo Nini, Wang Yanshu, Nathans Jeremy, Tessier-Lavigne Marc, Zou Yimin. Anterior-posterior guidance of commissural axons by Wnt-frizzled signaling // *Science*. 2003. 302, 5652. 1984–1988.
- Maday Sandra, Twelvetrees Alison E, Moughamian Armen J, Holzbaur Erika LF. Axonal transport: cargo-specific mechanisms of motility and regulation // *Neuron*. 2014. 84, 2. 292–309.
- Magdesian Margaret H, Gralle Matthias, Guerreiro Luiz H, Beltrão Paulo José I, Carvalho Milena MVF, Santos Luís Eduardo da S, Mello Fernando G de, Reis Ricardo AM, Ferreira Sérgio T. Secreted human amyloid precursor protein binds semaphorin 3a and prevents semaphorin-induced growth cone collapse // *PloS One*. 2011. 6, 7. e22857.
- Maness Patricia F, Schachner Melitta. Neural recognition molecules of the immunoglobulin superfamily: signaling transducers of axon guidance and neuronal migration // *Nature Neuroscience*. 2007. 10, 1. 19–26.
- Marler Katharine J, Suetterlin Philipp, Dopplapudi Asha, Rubikaite Aine, Adnan Jihad, Maiorano Nicola A, Lowe Andrew S, Thompson Ian D, Pathania Manav, Bordey Angelique, Fulga Tudor, Van Vector David L., Hindges Robert, Drescher Uwe. BDNF promotes axon branching of retinal ganglion cells via miRNA-132 and p250GAP // *Journal of Neuroscience*. 2014. 34, 3. 969–979.
- Marquardt Till, Ashery-Padan Ruth, Andrejewski Nicole, Scardigli Raffaella, Guillemot Francois, Gruss Peter. Pax6 is required for the multipotent state of retinal progenitor cells // *Cell*. 2001. 105, 1. 43–55.
- Martin Kelsey C, Ephrussi Anne. mRNA localization: gene expression in the spatial dimension // *Cell*. 2009. 136, 4. 719–730.
- Mason Carol, Erskine Lynda. Growth cone form, behavior, and interactions in vivo: retinal axon pathfinding as a model // *Journal of Neurobiology*. 2000. 44, 2. 260–270.
- Mattson MP, Dou P, Kater SB. Outgrowth-regulating actions of glutamate in isolated hippocampal pyramidal neurons // *The Journal of Neuroscience*. 1988. 8, 6. 2087–2100.
- McFarlane Sarah, Lom Barbara. The *Xenopus* retinal ganglion cell as a model neuron to study the establishment of neuronal connectivity // *Developmental Neurobiology*. 2012. 72, 4. 520–536.
- McKean Paul G, Vaughan Sue, Gull Keith. The extended tubulin superfamily // *Journal of Cell Science*. 2001. 114, 15. 2723–2733.
- McLaughlin Todd, Hindges Robert, OLeary Dennis DM. Regulation of axial patterning of the retina and its topographic mapping in the brain // *Current Opinion in Neurobiology*. 2003. 13, 1. 57–69.
- Menesini Chen MG, Chen JS, Levi-Montalcini R. Sympathetic nerve fibers ingrowth in the central nervous system of neonatal rodent upon intracerebral NGF injections // *Archives Italiennes de Biologie*. 1978. 116, 1. 53–84.
- Ming Guo-li, Song Hong-jun, Berninger Benedikt, Holt Christine E, Tessier-Lavigne Marc, Poo Mu-ming. cAMP-dependent growth cone guidance by netrin-1 // *Neuron*. 1997. 19, 6. 1225–1235.
- Much Christian, Auchynnikava Tania, Pavlinic Dinko, Buness Andreas, Rappsilber Juri, Benes Vladimir, Allshire Robin, OCarroll Dónal. Endogenous mouse Dicer is an exclusively cytoplasmic protein // *PLoS Genetics*. 2016. 12, 6. e1006095.
- Nagaraj Anil Belur, Joseph Peronne, DiFeo Analisa. miRNAs as prognostic and therapeutic tools in epithelial ovarian cancer // *Biomarkers in Medicine*. 2015. 9, 3. 241–257.

- Nangle MR, Keast JR.* Semaphorin 3A inhibits growth of adult sympathetic and parasympathetic neurones via distinct cyclic nucleotide signalling pathways // *British journal of Pharmacology*. 2011. 162, 5. 1083–1095.
- Natera-Naranjo Orlangie, Aschrafi Armaz, Gioio Anthony E, Kaplan Barry B.* Identification and quantitative analyses of microRNAs located in the distal axons of sympathetic neurons // *RNA*. 2010.
- Nichol Robert H, Hagen Kate M, Lumbard Derek C, Dent Erik W, Gómez Timothy M.* Guidance of axons by local coupling of retrograde flow to point contact adhesions // *Journal of Neuroscience*. 2016. 36, 7. 2267–2282.
- Nieuwkoop Pieter D, Faber Jacob.* Normal table of *Xenopus laevis* (Daudin): A Systematical and Chronological Survey of the Development from the Fertilized Egg till the end of Metamorphosis. 1994.
- Nishiyama Makoto, Hoshino Akemi, Tsai Lily, Henley John R, Goshima Yoshio, Tessier-Lavigne Marc, Poo Muming, Hong Kyonsoo.* Cyclic AMP/GMP-dependent modulation of Ca²⁺ channels sets the polarity of nerve growth-cone turning // *Nature*. 2003. 423, 6943. 990.
- Okada Ami, Charron Frédéric, Morin Steves, Shin David S, Wong Karen, Fabre Pierre J, Tessier-Lavigne Marc, McConnell Susan K.* Boc is a receptor for sonic hedgehog in the guidance of commissural axons // *Nature*. 2006. 444, 7117. 369–373.
- Otero Maria G, Alloatti Matías, Cromberg Lucas E, Almenar-Queralt Angels, Encalada Sandra E, Devoto Victorio M Pozo, Bruno Luciana, Goldstein Laurence SB, Falzone Tomás L.* Fast axonal transport of the proteasome complex depends on membrane interaction and molecular motor function // *J Cell Sci*. 2014. jcs–140780.
- Panda Dulal, Miller Herbert P, Banerjee Asok, Luduena Richard F, Wilson Leslie.* Microtubule dynamics in vitro are regulated by the tubulin isotype composition // *Proceedings of the National Academy of Sciences*. 1994. 91, 24. 11358–11362.
- Pelt J van, Uylings MA Corner HBM, Silva FH Lopes da.* Initial tract formation in the vertebrate brain // *The Self-organizing Brain: From Growth Cones to Functional Networks*. 1994. 102. 79.
- Pinter Rita, Hindges Robert.* Perturbations of microRNA function in mouse dicer mutants produce retinal defects and lead to aberrant axon pathfinding at the optic chiasm // *PLoS One*. 2010. 5, 4. e10021–e10021.
- Piper Michael, Anderson Richard, Dwivedy Asha, Weigl Christine, Van Horck Francis, Leung Kin Mei, Cogill Emily, Holt Christine.* Signaling mechanisms underlying Slit2-induced collapse of *Xenopus* retinal growth cones // *Neuron*. 2006. 49, 2. 215–228.
- Piper Michael, Horck Francis van, Holt Christine.* The role of cyclic nucleotides in axon guidance // *Axon Growth and Guidance*. 2007. 134–143.
- Piper Michael, Salih Saif, Weigl Christine, Holt Christine E, Harris William A.* Endocytosis-dependent desensitization and protein synthesis-dependent resensitization in retinal growth cone adaptation // *Nature Neuroscience*. 2005. 8, 2. 179–186.
- Poirier Karine, Saillour Yoann, Bahi-Buisson Nadia, Jaglin Xavier H, Fallet-Bianco Catherine, Nabbout Rima, Castelnaud-Ptakhine Laetitia, Roubertie Agathe, Attie-Bitach Tania, Desguerre Isabelle, Genevieve David, Barnerias Christine, Keren Boris, Lebrun Nicolas, Boddaert Nathalie, Encha-Razavi Frecht, Chelly Jamel.* Mutations in the neuronal β -tubulin subunit TUBB3 result in malformation of cortical development and neuronal migration defects // *Human Molecular Genetics*. 2010. 19, 22. 4462–4473.
- Pollerberg GE, Thelen K, Theiss MO, Hochlehnert BC.* The role of cell adhesion molecules for navigating axons: density matters // *Mechanisms of Development*. 2013. 130, 6-8. 359–372.
- Pols Maaike S, Klumperman Judith.* Trafficking and function of the tetraspanin CD63 // *Experimental Cell Research*. 2009. 315, 9. 1584–1592.
- Preitner Nicolas, Quan Jie, Nowakowski Dan W, Hancock Melissa L, Shi Jianhua, Tcherkezian Joseph, Young-Pearse Tracy L, Flanagan John G.* APC is an RNA-binding protein, and its interactome provides a link to neural development and microtubule assembly // *Cell*. 2014. 158, 2. 368–382.
- Pritchett Kathleen, Corrow Dorcas, Stockwell Jason, Smith Abigail.* Euthanasia of neonatal mice with carbon dioxide // *Comparative Medicine*. 2005. 55, 3. 275–281.
- Rangaraju Vidhya, Dieck Susanne tom, Schuman Erin M.* Local translation in neuronal compartments: how local is local? // *EMBO Reports*. 2017. 18, 5. 693–711.

Bibliography

- Rangaraju Vidhya, Lauterbach Marcel, Schuman Erin M. Spatially stable mitochondrial compartments fuel local translation during plasticity // *Cell*. 2019. 176, 1-2. 73–84.
- Raper Jonathan, Mason Carol. Cellular strategies of axonal pathfinding // *Cold Spring Harbor Perspectives in Biology*. 2010. a001933.
- Raper Jonathan A. Semaphorins and their receptors in vertebrates and invertebrates // *Current Opinion in Neurobiology*. 2000. 10, 1. 88–94.
- Reh Thomas A, Hindges Robert. MicroRNAs in Retinal Development // *Annual Review of Vision Science*. 2018. 0.
- Reinhart Brenda J, Slack Frank J, Basson Michael, Pasquinelli Amy E, Bettinger Jill C, Rougvie Ann E, Horvitz H Robert, Ruvkun Gary. The 21-nucleotide let-7 RNA regulates developmental timing in *Caenorhabditis elegans* // *Nature*. 2000. 403, 6772. 901–906.
- Resovi Andrea, Pinessi Denise, Chiorino Giovanna, Tarabozetti Giulia. Current understanding of the thrombospondin-1 interactome // *Matrix Biology*. 2014. 37. 83–91.
- Riccio Antonella. Dynamic epigenetic regulation in neurons: enzymes, stimuli and signaling pathways // *Nature Neuroscience*. 2010. 13, 11. 1330.
- Riccio Antonella. RNA targeting and translation in axons // *Science*. 2018. 359, 6382. 1331–1332.
- Riccio Antonella, Andreassi Catia, Crerar Hamish. Post-transcriptional processing of mRNA in neurons: the vestiges of the RNA world drive transcriptome diversity // *Frontiers in Molecular Neuroscience*. 2018. 11. 304.
- Roher Alex E, Kokjohn Tyler A, Clarke Steven G, Sierks Michael R, Maarouf Chera L, Serrano Geidy E, Sabbagh Marwan S, Beach Thomas G. APP/A β structural diversity and Alzheimer's disease pathogenesis // *Neurochemistry International*. 2017. 110. 1–13.
- Rohm Beate, Ottmeyer Angelika, Lohrum Marion, Püschel Andreas W. Plexin/neuropilin complexes mediate repulsion by the axonal guidance signal semaphorin 3A // *Mechanisms of Development*. 2000. 93, 1-2. 95–104.
- Roine Ulrika, Roine Timo, Salmi Juha, Wendt Taina Nieminen-von, Tani Pekka, Leppämäki Sami, Rintahaka Pertti, Caeyenberghs Karen, Leemans Alexander, Sams Mikko. Abnormal wiring of the connectome in adults with high-functioning autism spectrum disorder // *Molecular Autism*. 2015. 6, 1. 1.
- Roy Subhojit, Coffee Pilar, Smith George, Liem Ronald KH, Brady Scott T, Black Mark M. Neurofilaments are transported rapidly but intermittently in axons: implications for slow axonal transport // *Journal of Neuroscience*. 2000. 20, 18. 6849–6861.
- Rüegger Stefan, Großhans Helge. MicroRNA turnover: when, how, and why // *Trends in Biochemical Sciences*. 2012. 37, 10. 436–446.
- Rupaimoole Rajesha, Slack Frank J. MicroRNA therapeutics: towards a new era for the management of cancer and other diseases // *Nature Reviews Drug Discovery*. 2017. 16, 3. 203.
- Ruthardt Nadia, Lamb Don C, Bräuchle Christoph. Single-particle tracking as a quantitative microscopy-based approach to unravel cell entry mechanisms of viruses and pharmaceutical nanoparticles // *Molecular Therapy*. 2011. 19, 7. 1199–1211.
- Rybak-Wolf Agnieszka, Stottmeister Christin, Glazar Petar, Jens Marvin, Pino Natalia, Giusti Sebastian, Hanan Mor, Behm Mikaela, Bartok Osnat, Ashwal-Fluss Reut, others. Circular RNAs in the mammalian brain are highly abundant, conserved, and dynamically expressed // *Molecular Cell*. 2015. 58, 5. 870–885.
- Sabry James H, O'Connor Timothy P, Evans Louise, Toroian-Raymond Alma, Kirschner Marc, Bentley David. Microtubule behavior during guidance of pioneer neuron growth cones in situ // *The Journal of Cell Biology*. 1991. 115, 2. 381–395.
- Salazar Juan J, Ramírez Ana I, De Hoz Rosa, Salobar-García Elena, Rojas Pilar, Fernández-Albarral José A, López-Cuenca Inés, Rojas Blanca, Triviño Alberto, Ramírez José M. Anatomy of the Human Optic Nerve: Structure and Function // *Optic Nerve*. 2018.
- Salogiannis John, Reck-Peterson Samara L. Hitchhiking: a non-canonical mode of microtubule-based transport // *Trends in Cell Biology*. 2017. 27, 2. 141–150.

- Sambandan Sivakumar, Akbalik Güney, Kochen Lisa, Rinne Jennifer, Kahlstatt Josefina, Glock Caspar, Tushev Georgi, Alvarez-Castelao Beatriz, Heckel Alexander, Schuman Erin M.* Activity-dependent spatially localized miRNA maturation in neuronal dendrites // *Science*. 2017. 355, 6325. 634–637.
- Sambrook Joseph, Russell David W.* Purification of nucleic acids by extraction with phenol: chloroform // *Cold Spring Harbor Protocols*. 2006. 2006, 1. pdb-prot4455.
- Santangelo Philip, Nitin Nitin, LaConte Leslie, Woolums Amelia, Bao Gang.* Live-cell characterization and analysis of a clinical isolate of bovine respiratory syncytial virus, using molecular beacons // *Journal of Virology*. 2006. 80, 2. 682–688.
- Sanz Elisenda, Yang Linghai, Su Thomas, Morris David R, McKnight G Stanley, Amieux Paul S.* Cell-type-specific isolation of ribosome-associated mRNA from complex tissues // *Proceedings of the National Academy of Sciences*. 2009. 106, 33. 13939–13944.
- Sasaki Yukio, Gross Christina, Xing Lei, Goshima Yoshio, Bassell Gary J.* Identification of axon-enriched MicroRNAs localized to growth cones of cortical neurons // *Developmental Neurobiology*. 2014. 74, 3. 397–406.
- Scalia F.* The optic pathway of the frog: Nuclear organization and connections // *Frog Neurobiology*. 1976. 386–406.
- Schaefer Andrew W, Schoonderwoert Vincent Th G, Ji Lin, Medeiros Nelson, Danuser Gaudenz, Forscher Paul.* Coordination of actin filament and microtubule dynamics during neurite outgrowth // *Developmental Cell*. 2008. 15, 1. 146–162.
- Schmidt Eric F, Strittmatter Stephen M.* The CRMP family of proteins and their role in Sema3A signaling // *Semaphorins: Receptor and Intracellular Signaling Mechanisms*. 2007. 1–11.
- Schmittgen Thomas D, Lee Eun Joo, Jiang Jinmai, Sarkar Anasuya, Yang Liuqing, Elton Terry S, Chen Caifu.* Real-time PCR quantification of precursor and mature microRNA // *Methods*. 2008. 44, 1. 31–38.
- Sethi Prerna, Lukiw Walter J.* Micro-RNA abundance and stability in human brain: specific alterations in Alzheimer's disease temporal lobe neocortex // *Neuroscience Letters*. 2009. 459, 2. 100–104.
- Sheets MD, Fritz B, Hartley RS, Zhang Y.* Polyribosome analysis for investigating mRNA translation in *Xenopus* oocytes, eggs and embryos // *Methods*. 2010. 51, 1. 152–156.
- Sheller Rebecca A, Bittner George D.* Maintenance and synthesis of proteins for an anucleate axon // *Brain Research*. 1992. 580, 1-2. 68–80.
- Shewan D, Dwivedy A, Anderson R, Holt CE.* Age-related changes underlie switch in netrin-1 responsiveness as growth cones advance along visual pathway // *Nature Neuroscience*. 2002. 5, 10. 955–962.
- Shibata Mikihito, Nakao Hiromi, Kiyonari Hiroshi, Abe Takaya, Aizawa Shinichi.* MicroRNA-9 regulates neurogenesis in mouse telencephalon by targeting multiple transcription factors // *The Journal of Neuroscience*. 2011. 31, 9. 3407–3422.
- Shigeoka Toshiaki, Jung Hosung, Jung Jane, Turner-Bridger Benita, Ohk Jiyeon, Lin Julie Qiaojin, Amieux Paul S, Holt Christine E.* Dynamic axonal translation in developing and mature visual circuits // *Cell*. 2016. 166, 1. 181–192.
- Shigeoka Toshiaki, Koppers Max, Wong Hovy Ho-Wai, Lin Julie Qiaojin, Dwivedy Asha, Freitas Nascimento Janaina de, Cagnetta Roberta, Tartwijk Francesca van, Strohl Florian, Cioni Jean-Michel, others .* On-site ribosome remodeling by locally synthesized ribosomal proteins in axons // *BioRxiv*. 2018. 500033.
- Smalheiser Neil R.* Regulation of mammalian microRNA processing and function by cellular signaling and subcellular localization // *Biochimica et Biophysica Acta (BBA)-Gene Regulatory Mechanisms*. 2008. 1779, 11. 678–681.
- Soares Célia A, Mason Carol A.* Transient ipsilateral retinal ganglion cell projections to the brain: Extent, targeting, and disappearance // *Developmental Neurobiology*. 2015. 75, 12. 1385–1401.
- Song Hong-jun, Ming Guo-li, He Zhigang, Lehmann Maxime, McKerracher Lisa, Tessier-Lavigne Marc, Poo Mu-ming.* Conversion of neuronal growth cone responses from repulsion to attraction by cyclic nucleotides // *Science*. 1998. 281, 5382. 1515–1518.
- Song Hong-jun, Ming Guo-li, Poo Mu-ming.* cAMP-induced switching in turning direction of nerve growth cones // *Nature*. 1997. 388, 6639. 275–279.

Bibliography

- Song Hong-jun, Poo Mu-ming.* Signal transduction underlying growth cone guidance by diffusible factors // *Current Opinion in Neurobiology.* 1999. 9, 3. 355–363.
- Speidel Carl Caskey.* Adjustments of Nerve Endings: Harvey Lecture, January 16, 1941 // *Bulletin of the New York Academy of Medicine.* 1941. 18, 10. 625.
- Starega-Roslan Julia, Koscianska Edyta, Kozlowski Piotr, Krzyzosiak Wlodzimierz J.* The role of the precursor structure in the biogenesis of microRNA // *Cellular and Molecular Life Sciences.* 2011. 68, 17. 2859.
- Steward Oswald, Levy WILLIAM B.* Preferential localization of polyribosomes under the base of dendritic spines in granule cells of the dentate gyrus // *Journal of Neuroscience.* 1982. 2, 3. 284–291.
- Strittmatter Stephen M, Fishman Mark C.* The neuronal growth cone as a specialized transduction system // *Bioessays.* 1991. 13, 3. 127–134.
- Ströhl Florian, Lin Julie Qiaojin, Laine Romain F, Wong Hovy Ho-Wai, Urbančič Vasja, Cagnetta Roberta, Holt Christine E, Kaminski Clemens F.* Single molecule translation imaging visualizes the dynamics of local β -actin synthesis in retinal axons // *Scientific Reports.* 2017. 7, 1. 709.
- Sun Ting-yi, Chen Xiao-rui, Liu Zi-long, Zhao Li-li, Jiang Yong-xiang, Qu Guo-qiang, Wang Rong-shuai, Huang Si-zhe, Liu Liang.* Expression profiling of microRNAs in hippocampus of rats following traumatic brain injury // *Journal of Huazhong University of Science and Technology.* 2014. 34, 4. 548–553.
- Takahashi Takuya, Fournier Alyson, Nakamura Fumio, Wang Li-Hsien, Murakami Yasunori, Kalb Robert G, Fujisawa Hajime, Strittmatter Stephen M.* Plexin-neuropilin-1 complexes form functional semaphorin-3A receptors // *Cell.* 1999. 99, 1. 59–69.
- Tamagnone Luca, Artigiani Stefania, Chen Hang, He Zhigang, Ming Guo-li, Song Hong-jun, Chedotal Alain, Winberg Margaret L, Goodman Corey S, Poo Mu-ming, others .* Plexins are a large family of receptors for transmembrane, secreted, and GPI-anchored semaphorins in vertebrates // *Cell.* 1999. 99, 1. 71–80.
- Tanaka Elly M, Kirschner Marc W.* Microtubule behavior in the growth cones of living neurons during axon elongation // *The Journal of Cell Biology.* 1991. 115, 2. 345–363.
- Tao Jifang, Wu Hao, Lin Quan, Wei Weizheng, Lu Xiao-Hong, Cantle Jeffrey P, Ao Yan, Olsen Richard W, Yang X William, Mody Istvan, others .* Deletion of astroglial Dicer causes non-cell-autonomous neuronal dysfunction and degeneration // *Journal of Neuroscience.* 2011. 31, 22. 8306–8319.
- Taylor Anne M, Berchtold Nicole C, Perreau Victoria M, Tu Christina H, Jeon Noo Li, Cotman Carl W.* Axonal mRNA in uninjured and regenerating cortical mammalian axons // *The Journal of Neuroscience.* 2009. 29, 15. 4697–4707.
- Taylor Anne Marion, Wu Jason, Tai Hwan-Ching, Schuman Erin M.* Axonal translation of β -catenin regulates synaptic vesicle dynamics // *Journal of Neuroscience.* 2013. 33, 13. 5584–5589.
- Tehrani Shandiz, Delf R Katherine, Cepurna William O, Davis Lauren, Johnson Elaine C, Morrison John C.* In vivo small molecule delivery to the optic nerve in a rodent model // *Scientific Reports.* 2018. 8, 1. 4453.
- Tennyson Virginia M.* The fine structure of the axon and growth cone of the dorsal root neuroblast of the rabbit embryo // *The Journal of Cell Biology.* 1970. 44, 1. 62–79.
- Terenzio Marco, Koley Sandip, Samra Nitzan, Rishal Ida, Zhao Qian, Sahoo Pabitra K, Urisman Anatoly, Marvaldi Letizia, Osés-Prieto Juan A, Forester Craig, others .* Locally translated mTOR controls axonal local translation in nerve injury // *Science.* 2018. 359, 6382. 1416–1421.
- Tessier-Lavigne Marc, Goodman Corey S.* The molecular biology of axon guidance // *Science.* 1996. 274, 5290. 1123–1133.
- Thelen Karsten, Maier Bettina, Faber Marc, Albrecht Christian, Fischer Paulina, Pollerberg G Elisabeth.* Translation of the cell adhesion molecule ALCAM in axonal growth cones-regulation and functional importance // *Journal of Cell Science.* 2012. 125, 4. 1003–1014.
- Tinevez Jean-Yves, Perry Nick, Schindelin Johannes, Hoopes Genevieve M, Reynolds Gregory D, Laplantine Emmanuel, Bednarek Sebastian Y, Shorte Spencer L, Eliceiri Kevin W.* TrackMate: An open and extensible platform for single-particle tracking // *Methods.* 2017. 115. 80–90.

- Tischfield Max A, Baris Hagit N, Wu Chen, Rudolph Guenther, Van Maldergem Lionel, He Wei, Chan Wai-Man, Andrews Caroline, Demer Joseph L, Robertson Richard L, others* . Human TUBB3 mutations perturb microtubule dynamics, kinesin interactions, and axon guidance // *Cell*. 2010. 140, 1. 74–87.
- Tojima Takuro, Kamiguchi Hiroyuki*. Exocytic and endocytic membrane trafficking in axon development // *Development, Growth & Differentiation*. 2015. 57, 4. 291–304.
- Torres Adrian G, Fabani Martin M, Vigorito Elena, Gait Michael J*. MicroRNA fate upon targeting with anti-miRNA oligonucleotides as revealed by an improved Northern-blot-based method for miRNA detection // *RNA*. 2011. 17, 5. 933–943.
- Toyofuku Toshihiko, Yoshida Junko, Sugimoto Tamiko, Zhang Hong, Kumanogoh Atsushi, Hori Masatsugu, Kikutani Hitoshi*. FARP2 triggers signals for Sema3A-mediated axonal repulsion // *Nature Neuroscience*. 2005. 8, 12. 1712.
- Tran Tracy S, Rubio Maria E, Clem Roger L, Johnson Dontais, Case Lauren, Tessier-Lavigne Marc, Huganir Richard L, Ginty David D, Kolodkin Alex L*. Secreted semaphorins control spine distribution and morphogenesis in the postnatal CNS // *Nature*. 2009. 462, 7276. 1065.
- Trujillo Robin Deis, Yue Si-Biao, Tang Yujie, O'gorman William E, Chen Chang-Zheng*. The potential functions of primary microRNAs in target recognition and repression // *The EMBO Journal*. 2010. 29, 19. 3272–3285.
- Turner-Bridger Benita, Jakobs Maximillian, Muresan Leila, Wong Hovy Ho-Wai, Franze Kristian, Harris William A, Holt Christine E*. Single-molecule analysis of endogenous β -actin mRNA trafficking reveals a mechanism for compartmentalized mRNA localization in axons // *Proceedings of the National Academy of Sciences*. 2018. 115, 41. E9697–E9706.
- Turner Laura J, Nicholls Sarah, Hall Alan*. The activity of the plexin-A1 receptor is regulated by Rac // *Journal of Biological Chemistry*. 2004. 279, 32. 33199–33205.
- Tuttle Rebecca, O'Leary Dennis DM*. Neurotrophins rapidly modulate growth cone response to the axon guidance molecule, collapsin-1 // *Molecular and Cellular Neuroscience*. 1998. 11, 1. 1–8.
- Unsain Nicolas, Bordenave Martin D, Martinez Gaby F, Sami Jalil, Bilderling Catalina, Barabas Federico M, Masullo Luciano A, Johnstone Aaron D, Barker Philip A, Mariano Bisbal, others* . Remodeling of the actin/spectrin membrane-associated periodic skeleton, growth cone collapse and F-actin decrease during axonal degeneration // *Scientific Reports*. 2018. 8, 1. 3007.
- Van Battum Eljo Y, Brignani Sara, Pasterkamp R Jeroen*. Axon guidance proteins in neurological disorders // *The Lancet Neurology*. 2015. 14, 5. 532–546.
- Van J Minnen, Bergman JJ, Van ER Kesteren, Smit AB, Geraerts WP, Lukowiak K, Hasan SU, Syed NI*. De novo protein synthesis in isolated axons of identified neurons. // *Neuroscience*. 1997. 80, 1. 1–7.
- Van Treeck Briana, Parker Roy*. Emerging roles for intermolecular RNA-RNA interactions in RNP assemblies // *Cell*. 2018. 174, 4. 791–802.
- Vargas Jose Norberto S, Kar Amar N, Kowalak Jeffrey A, Gale Jenna R, Aschrafi Armaz, Chen Cai-Yun, Gioio Anthony E, Kaplan Barry B*. Axonal localization and mitochondrial association of precursor microRNA 338 // *Cellular and Molecular Life Sciences*. 2016. 73, 22. 4327–4340.
- Verhey Kristen J, Gaertig Jacek*. The tubulin code // *Cell Cycle*. 2007. 6, 17. 2152–2160.
- Vicente Rita, Noël Danièle, Pers Yves-Marie, Apparailly Florence, Jorgensen Christian*. Deregulation and therapeutic potential of microRNAs in arthritic diseases // *Nature Reviews Rheumatology*. 2016. 12, 4. 211.
- Wahl Siegfried, Barth Holger, Ciossek Thomas, Aktories Klaus, Mueller Bernhard K*. Ephrin-A5 induces collapse of growth cones by activating Rho and Rho kinase // *The Journal of Cell Biology*. 2000. 149, 2. 263–270.
- Wang Bin, Bao Lan*. Axonal microRNAs: localization, function and regulatory mechanism during axon development // *Journal of Molecular Cell Biology*. 2017. 9, 2. 82–90.
- Wang Bin, Pan Lin, Wei Manyi, Wang Qiong, Liu Wen-Wen, Wang Nuoxin, Jiang Xing-Yu, Zhang Xu, Bao Lan*. FMRP-mediated axonal delivery of miR-181d regulates axon elongation by locally targeting Map1b and Calm1 // *Cell Reports*. 2015a. 13, 12. 2794–2807.

Bibliography

- Wang Hongjun, Tao Tao, Yan Wei, Feng Yan, Wang Yongzhi, Cai Jinguan, You Yongping, Jiang Tao, Jiang Chuanlu. Upregulation of miR-181s reverses mesenchymal transition by targeting KPNA4 in glioblastoma // *Scientific Reports*. 2015b. 5. 13072.
- Wang Lei, Ho Chung-liang, Sun Dongming, Liem Ronald KH, Brown Anthony. Rapid movement of axonal neurofilaments interrupted by prolonged pauses // *Nature Cell Biology*. 2000. 2, 3. 137.
- Watkins Simon. Immunohistochemistry // *Current Protocols in Molecular Biology*. 1995. 31, 1. 14–6.
- Wegel Eva, Göhler Antonia, Lagerholm B Christoffer, Wainman Alan, Uphoff Stephan, Kaufmann Rainer, Dobbie Ian M. Imaging cellular structures in super-resolution with SIM, STED and Localisation Microscopy: A practical comparison // *Scientific Reports*. 2016. 6. 27290.
- Wessells NK, Spooner BS, Ash JF, Bradley MO, Luduena MA, Taylor EL, Wrenn JT, Yamada KM. Microfilaments in cellular and developmental processes // *Science*. 1971. 171, 3967. 135–143.
- Wightman Bruce, Ha Ilho, Ruvkun Gary. Posttranscriptional regulation of the heterochronic gene *lin-14* by *lin-4* mediates temporal pattern formation in *C. elegans* // *Cell*. 1993. 75, 5. 855–862.
- Wilkinson David G. Multiple roles of EPH receptors and ephrins in neural development // *Nature Reviews Neuroscience*. 2001. 2, 3. 155–164.
- Williams Emma J, Furness Josie, Walsh Frank S, Doherty Patrick. Activation of the FGF receptor underlies neurite outgrowth stimulated by L1, N-CAM, and N-cadherin // *Neuron*. 1994. 13, 3. 583–594.
- Willis Dianna E, Niekerk Erna A van, Sasaki Yukio, Mesngon Mariano, Merianda Tanuja T, Williams Gervan G, Kendall Marvin, Smith Deanna S, Bassell Gary J, Twiss Jeffery L. Extracellular stimuli specifically regulate localized levels of individual neuronal mRNAs // *The Journal of Cell Biology*. 2007. 178, 6. 965–980.
- Wit Joris de, Verhaagen Joost. Proteoglycans as modulators of axon guidance cue function // *Semaphorins: receptor and intracellular signaling mechanisms*. 2007. 73–89.
- Wolszon LR, Gao WQ, Passani MB, Macagno ER. Growth cone” collapse” in vivo: are inhibitory interactions mediated by gap junctions? // *Journal of Neuroscience*. 1994. 14, 3. 999–1010.
- Wong Hovy Ho-Wai, Lin Julie Qiaojin, Ströhl Florian, Roque Cláudio Gouveia, Cioni Jean-Michel, Cagnetta Roberta, Turner-Bridger Benita, Laine Romain F, Harris William A, Kaminski Clemens F, others . RNA docking and local translation regulate site-specific axon remodeling in vivo // *Neuron*. 2017. 95, 4. 852–868.
- Wu Karen Y, Hengst Ulrich, Cox Llewellyn J, Macosko Evan Z, Jeromin Andreas, Urquhart Erica R, Jaffrey Samie R. Local translation of RhoA regulates growth cone collapse // *Nature*. 2005. 436, 7053. 1020–1024.
- Xu Shunbin, Lumayag Stephen, Corbett Nicola, Wahlin Karl, Turturro Sanja, Larsen Peter, Valle David, Zack Donald, Nicholson Daniel, Cowan Colleen. Inactivation of the miR-183/96/182 Cluster Results In Photoreceptor Postnatal Developmental Arrest and Synaptic Defects, Leading to Retinal Dysfunction and Degeneration // *Investigative Ophthalmology & Visual Science*. 2013. 54, 15. 3725–3725.
- Yamada Kenneth M, Spooner Brian S, Wessells Norman K. Axon growth: roles of microfilaments and microtubules // *Proceedings of the National Academy of Sciences*. 1970. 66, 4. 1206–1212.
- Yamada Masashi, Sekiguchi Kiyotoshi. Molecular basis of Laminin–Integrin Interactions // *Current Topics in Membranes*. 76. 2015. 197–229.
- Yang Xiaolin, Yang Qinyan, Wang Xiaobin, Luo Chunqiong, Wan Yunqiang, Li Jiali, Liu Kezhi, Zhou Min, Zhang Chunxiang. MicroRNA expression profile and functional analysis reveal that miR-206 is a critical novel gene for the expression of BDNF induced by ketamine // *Neuromolecular Medicine*. 2014. 16, 3. 594–605.
- Yao Bing, La Lan B, Chen Ying-Chi, Chang Lung-Ji, Chan Edward KL. Defining a new role of GW182 in maintaining miRNA stability // *EMBO Reports*. 2012. 13, 12. 1102–1108.
- Yao Jiaqi, Sasaki Yukio, Wen Zhexing, Bassell Gary J, Zheng James Q. An essential role for β -actin mRNA localization and translation in Ca²⁺-dependent growth cone guidance // *Nature Neuroscience*. 2006. 9, 10. 1265.
- Yaron Avraham, Zheng Binhai. Navigating their way to the clinic: emerging roles for axon guidance molecules in neurological disorders and injury // *Developmental Neurobiology*. 2007. 67, 9. 1216–1231.

- Yekta Soraya, Shih I-hung, Bartel David P.* MicroRNA-directed cleavage of HOXB8 mRNA // *Science*. 2004. 304, 5670. 594–596.
- Yoon Young J, Wu Bin, Buxbaum Adina R, Das Sulagna, Tsai Albert, English Brian P, Grimm Jonathan B, Lavis Luke D, Singer Robert H.* Glutamate-induced RNA localization and translation in neurons // *Proceedings of the National Academy of Sciences*. 2016. 113, 44. E6877–E6886.
- Yoshimura Takeshi, Kawano Yoji, Arimura Nariko, Kawabata Saeko, Kikuchi Akira, Kaibuchi Kozo.* GSK-3 β regulates phosphorylation of CRMP-2 and neuronal polarity // *Cell*. 2005. 120, 1. 137–149.
- Zampa Federico, Bicker Silvia, Schratt Gerhard.* Activity-dependent pre-miR-134 dendritic localization is required for hippocampal neuron dendritogenesis // *Frontiers in Molecular Neuroscience*. 2018. 11.
- Zanata Silvio M, Hovatta Iris, Rohm Beate, Püschel Andreas W.* Antagonistic effects of Rnd1 and RhoD GTPases regulate receptor activity in Semaphorin 3A-induced cytoskeletal collapse // *Journal of Neuroscience*. 2002. 22, 2. 471–477.
- Zhang Yi, Ueno Yuji, Liu Xian Shuang, Buller Benjamin, Wang Xinli, Chopp Michael, Zhang Zheng Gang.* The microRNA-17–92 cluster enhances axonal outgrowth in embryonic cortical neurons // *The Journal of Neuroscience*. 2013. 33, 16. 6885–6894.
- Zhao Huijie, Zhu Lei, Jin Yujuan, Ji Hongbin, Yan Xiumin, Zhu Xueliang.* miR-375 is highly expressed and possibly transactivated by achaete-scute complex homolog 1 in small-cell lung cancer cells // *Acta Biochim Biophys Sin*. 2011. 44, 2. 177–182.
- Zhao Yuhai, Alexandrov Peter, Jaber Vivian, Lukiw Walter.* Deficiency in the ubiquitin conjugating enzyme UBE2A in Alzheimers disease (AD) is linked to deficits in a natural circular miRNA-7 sponge (circRNA; ciRS-7) // *Genes*. 2016. 7, 12. 116.
- Zheng Qiupeng, Bao Chunyang, Guo Weijie, Li Shuyi, Chen Jie, Chen Bing, Luo Yanting, Lyu Dongbin, Li Yan, Shi Guohai, others .* Circular RNA profiling reveals an abundant circHIPK3 that regulates cell growth by sponging multiple miRNAs // *Nature Communications*. 2016. 7. 11215.
- Zivraj Krishna H, Tung Yi Chun Loraine, Piper Michael, Gumy Laura, Fawcett James W, Yeo Giles SH, Holt Christine E.* Subcellular profiling reveals distinct and developmentally regulated repertoire of growth cone mRNAs // *The Journal of Neuroscience*. 2010. 30, 46. 15464–15478.
- Zou Yan, Chiu Hui, Domenger Dorothée, Chuang Chiou-Fen, Chang Chieh.* The lin-4 microRNA targets the LIN-14 transcription factor to inhibit netrin-mediated axon attraction // *Science Signaling*. 2012. 5, 228. ra43.
- Zou Yan, Chiu Hui, Zinovyeva Anna, Ambros Victor, Chuang Chiou-Fen, Chang Chieh.* Developmental decline in neuronal regeneration by the progressive change of two intrinsic timers // *Science*. 2013. 340, 6130. 372–376.
- Zou Yimin.* Wnt signaling in axon guidance // *Trends in Neurosciences*. 2004. 27, 9. 528–532.
- Zou Yimin, Lyuksytova Anna I.* Morphogens as conserved axon guidance cues // *Current Opinion in Neurobiology*. 2007. 17, 1. 22–28.

List of Tables

1.1	Guidance cue and receptors	10
1.2	Roles of local axonal mRNA translation	19
1.3	miRNAs involve in axon guidance	26
1.4	miRNAs found enriched in axons and growth cone profiling during axonal development	27
3.1	Culture support - PLL, laminin, cultural medium volume	44
3.2	RNA input and cDNA dilutions	49
3.3	Software and Algorithms	56
5.1	Molecular Beacon BLAST in Xenbase	73
8.1	Predicted miR-181-5p targets - Reactome	103
B.1	Primers and oligo list	139
B.2	Reagents list	141

List of Figures

1.1	Growth cone structure	3
1.2	Stage of growth cone progression.	4
1.3	Growth cone advance	5
1.4	Major families of cell-adhesion molecules (CAMs)	9
1.5	Growth cone guidance cues	11
1.6	Signal transduction	14
1.7	Local translation of axonal mRNA	20
1.8	miRNA biogenesis	22
1.9	miRNAs seed sequence	23
1.10	RGC journey in <i>Xenopus laevis</i> and <i>Mus musculus</i> animal model	29
1.11	<i>Xenopus laevis</i> stages and guidance cues	31
1.12	<i>Xenopus laevis</i> manipulation	33
3.1	Dicer schematic	39
3.2	Organoculture protocol	43
4.1	Dicer and Ago2 in <i>Xenopus laevis</i> growth cone	59
4.2	FLAG-HA ₂ -Dicer mice genotyping	60
4.3	Cytoplasmic Dicer localization in E13.5 retina	60
4.4	Bleedthrough absence in the imaging settings	61
4.5	Dicer localization in E13.5 and P0 mice	62
4.6	Dicer localization in P0 mice	63
4.7	List of candidate axonal pre-miRNAs	64
4.8	Pre-miRNAs' presence in pure RGC axons	65
4.9	Schematic and sequence of pre-miR-181a-1/a-2 locus	66
4.10	Pri-miRNA absence in axon	67
4.11	miRNAs precursors relative abundance	68
5.1	Molecular Beacon (MB)	74
5.2	Molecular Beacon (MB) specificity	75
5.3	Pri-miR-181a-1/b-1 absence in small RNA fraction	76
5.4	Pre-miR-181a-1 trafficking live imaging	77
5.5	Pre-miR-181a-1 velocity categories	77
5.6	MSD trafficking analysis	78
5.7	Pre-miRNAs are trafficked associated with vesicles - st26/27	79
5.8	Pre-miRNAs are trafficked associated with vesicles - st37/38	80
6.1	Isolated axons purity and quality	84
6.2	Isolated axon alive and responsiveness	85
6.3	Pre-miRNAs RT-qPCR primers efficiency and specificity	86
6.4	U6 primers melting curve	87
6.5	U6 stability in RGC stimulated and unstimulated axons	88
6.6	Experimental paradigm	89
6.7	Sema3A and Slit-2 collapse assay	90
6.8	miRNAs and pre-miRNAs level upon axonal Sema3A stimulation	91
6.9	miRNAs relative abundancy in RGC axons	91
6.10	miRNAs and pre-miRNAs level upon axonal Slit2 stimulation	92
7.1	Morpholinos blocking Dicer cleavage	93
7.2	Morpholino validation: RT-qPCR microinjected MO and co-MO	95
7.3	MO and co-MO axonal transfection	96
7.4	miRNAs expression levels in transfected axons	96
7.5	Collapse assay blocking pre-miRNAs maturation	97
8.1	<i>Xenopus laevis</i> polysomes fractionation	101
8.2	Schematic of Venus plasmid	104
8.3	Control for enzymatic digestion	105

List of Figures

8.4	Background reduction of plasmid only transformation	106
8.5	Colony screening through enzymatic digestion	108
8.6	Schematic of Venus-3'UTR constructs	108
8.7	FRAP: experimental paradigm	109
8.8	FRAP: axonal <i>ex vivo</i> ACTB-3'UTR regulation	109
8.9	FRAP: axonal <i>ex vivo</i> TUBB3-3'UTR regulation	111
8.10	FRAP: axonal <i>ex vivo</i> TUBB3-3'UTR regulation MO and co-MO	112
8.11	<i>In vivo</i> axonal pathfinding at the boundaries of the optic tectum	113
8.12	FRAP: axonal <i>in vivo</i> TUBB3-3'UTR regulation	114
8.13	FRAP: axonal <i>ex vivo</i> APP-3'UTR and THBS1-3'UTR regulation	116
9.1	NGmiRNAs and miRNAs control of LPS in unstimulated and stimulated axons	122
10.1	Proposed model	127
A.1	MiR-182 reversibly gates Cofilin-1 translation upon Slit2 stimulation	131
A.2	miR-182 ISH: RGC axons and soma	132
A.3	miR-182 traces in laser captured RGC layer	133
A.4	U6 is not a suitable normalizer to compare soma and axonal samples	134
A.5	miR-182 sensor in axons	135
A.6	miR-182 is active and enriched in RGC axons	136
A.7	Slit2 Inhibits miR-182 activity in RGC axons without decay	137